ASICS: STRUCTURE, FUNCTION, AND PHARMACOLOGY

EDITED BY: Enrique Soto, Candice Askwith, Osvaldo D. Uchitel, Chih-Cheng Chen and David MacLean

PUBLISHED IN: Frontiers in Cellular Neuroscience, Frontiers in Physiology and Frontiers in Behavioral Neuroscience

frontiers Research Topics

ISSN 1664-8714
ISBN 978-2-88974-550-0
DOI 10.3389/978-2-88974-550-0

About Frontiers

Frontiers is more than just an open-access publisher of scholarly articles: it is a pioneering approach to the world of academia, radically improving the way scholarly research is managed. The grand vision of Frontiers is a world where all people have an equal opportunity to seek, share and generate knowledge. Frontiers provides immediate and permanent online open access to all its publications, but this alone is not enough to realize our grand goals.

Frontiers Journal Series

The Frontiers Journal Series is a multi-tier and interdisciplinary set of open-access, online journals, promising a paradigm shift from the current review, selection and dissemination processes in academic publishing. All Frontiers journals are driven by researchers for researchers; therefore, they constitute a service to the scholarly community. At the same time, the Frontiers Journal Series operates on a revolutionary invention, the tiered publishing system, initially addressing specific communities of scholars, and gradually climbing up to broader public understanding, thus serving the interests of the lay society, too.

Dedication to Quality

Each Frontiers article is a landmark of the highest quality, thanks to genuinely collaborative interactions between authors and review editors, who include some of the world's best academicians. Research must be certified by peers before entering a stream of knowledge that may eventually reach the public - and shape society; therefore, Frontiers only applies the most rigorous and unbiased reviews.
Frontiers revolutionizes research publishing by freely delivering the most outstanding research, evaluated with no bias from both the academic and social point of view. By applying the most advanced information technologies, Frontiers is catapulting scholarly publishing into a new generation.

What are Frontiers Research Topics?

Frontiers Research Topics are very popular trademarks of the Frontiers Journals Series: they are collections of at least ten articles, all centered on a particular subject. With their unique mix of varied contributions from Original Research to Review Articles, Frontiers Research Topics unify the most influential researchers, the latest key findings and historical advances in a hot research area! Find out more on how to host your own Frontiers Research Topic or contribute to one as an author by contacting the Frontiers Editorial Office: frontiersin.org/about/contact

ASICS: STRUCTURE, FUNCTION, AND PHARMACOLOGY

Topic Editors:
Enrique Soto, Meritorious Autonomous University of Puebla, Mexico
Candice Askwith, The Ohio State Universitys, United States
Osvaldo D. Uchitel, University of Buenos Aires, Argentina
Chih-Cheng Chen, Academia Sinica, Taiwan
David MacLean, University of Rochester, United States

Citation: Soto, E., Askwith, C., Uchitel, O. D., Chen, C.-C., MacLean, D., eds. (2022). ASICs: Structure, Function, and Pharmacology. Lausanne: Frontiers Media SA.
doi: 10.3389/978-2-88974-550-0

Table of Contents

frontiers in Physiology

EDITORIAL
published: 31 January 2022
doi: 10.3389/fphys.2022.831830

Editorial: ASICs: Structure, Function, and Pharmacology

David M. MacLean[1] *and Enrique Soto*[2]*

[1] Department of Pharmacology & Physiology, University of Rochester Medical Center, Rochester, NY, United States, [2] Instituto de Fisiología, Benemérita Universidad Autónoma de Puebla, Puebla, Mexico

Keywords: ASIC, fear conditioning, desensitization, amiloride, pain, immune activation, glioblastoma, cell signaling

Editorial on the Research Topic

ASICs: Structure, Function, and Pharmacology

The receptor for protons was first reported by Krishtal and Pidoplichko in the early 1980s (Krishtal and Pidoplichko, 1980, 1981). This serendipitous discovery, and the concept of a proton-sensing channel in general, remained controversial for some time (Krishtal, 2015). Eventually, the cloning of ASIC1a clearly established that acid-sensing ion channels exist and ushered in a new era of investigation (Waldmann et al., 1997). In short order, additional ASICs subunits were cloned (or identified) allowing detailed biophysical and physiological work to commence in earnest. These early studies characterized the acid evoked currents from ASICs, established the ionic selectivity and inhibition by amiloride, and ultimately granted ASICs full "citizenship" as proton gated Na^+ selective channels.

Subsequent to the cloning of ASICs, more selective pharmacological agents such as Psalmotoxin and APETx2 were identified, knockout mice were generated and the first ASIC structure was solved. All of these landmarks spurred the field forward, opening new avenues of inquiry and expanding our knowledge of the physiological and pathophysiological roles these channels play. This expansion of ASIC research is clearly reflected in the literature. A Pubmed search for (https://pubmed.ncbi.nlm.nih.gov/) "Acid Sensing Ionic Channels" either in the title, the abstract or the key words, within the years 1980–2021, shows a clear increase in published papers using this term (**Figure 1**). The first use was in 1997 in a paper by Waldmann et al. (1997), and the number of papers peaked in 2015 with 70 and has remained around 60 or so per year (**Figure 1**).

The articles collected in this Research Topic reflect the increasing diversity of the field and the myriad roles played by ASICs. These papers range from basic structural mechanism of desensitization and pharmacological interactions on to ASIC participation in processes such as immune cell activation, sensory coding, fear conditioning and pathological processes such as neoplastic cell migration, epilepsy, and neurodegenerative processes.

This collection features four reviews covering the understudied role of ASICs in the immune system (Foster et al.), in the physiopathology of neurodegenerative processes (Mango and Nisticó), the contribution of ASIC1 to migration of human malignant glioblastoma cells (Shah et al.), and in nociceptive sensory coding (Paéz et al.).

ASICs activate and desensitize quickly. In fact, the original report of proton-gated currents developed a specific method for fast perfusion to resolve these currents (Krishtal and Pidoplichko, 1980; Krishtal, 2015). Despite high resolution structures in multiple functional states, the precise sequence of molecular motions linking the resting or open states with the desensitized state is unclear. Rook et al. focus on this problem of ASIC desensitization and recovery using channel mutagenesis, fast perfusion electrophysiology, and molecular dynamics (Rook et al.). The authors examined the role of the β11/β12 linker that previous observations have shown may be critical for

Edited and reviewed by:
Christoph Fahlke, Julich Research Center, Helmholtz Association of German Research Centres (HZ), Germany

***Correspondence:**
Enrique Soto
esoto24@gmail.com

Specialty section:
This article was submitted to Membrane Physiology and Membrane Biophysics, a section of the journal Frontiers in Physiology

Received: *08 December 2021*
Accepted: *03 January 2022*
Published: *31 January 2022*

Citation:
MacLean DM and Soto E (2022) Editorial: ASICs: Structure, Function, and Pharmacology. Front. Physiol. 13:831830. doi: 10.3389/fphys.2022.831830

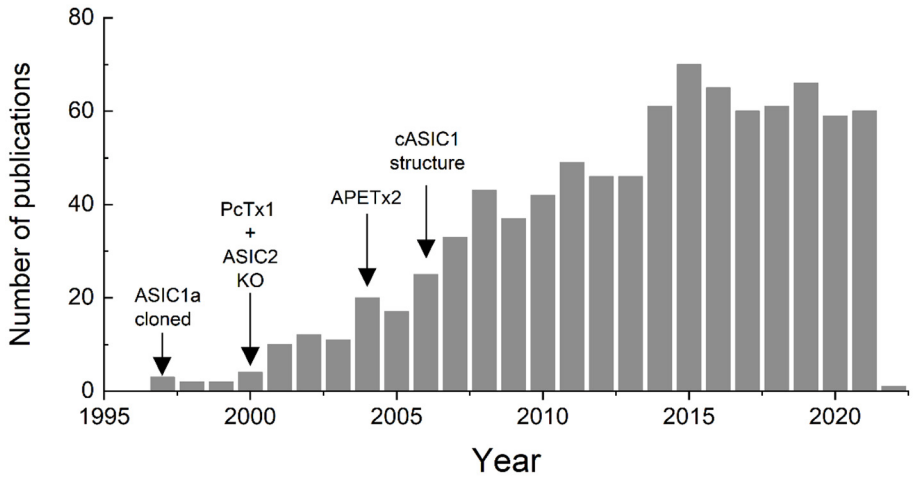

FIGURE 1 | Number of papers published since 1997 in which the term "acid sensing ionic channel" is included in the title, abstract or key words, according to a search performed in Pubmed.

controlling desensitization and recovery of ASIC1 (Rook et al., 2020). They find this linker to be highly sensitive to even small mutations while also uncovering new electrostatic interactions that control desensitized state stability.

Amiloride is a critically useful molecule in the study of the ASICS. While generally used as an ASIC blocker, amiloride can produce potentiation of ASIC responses under certain conditions. The molecular mechanism for this paradoxical effect is unclear. In the work by Matasic et al. the authors used detailed electrophysiological investigation of amiloride effects on ASIC3. They find the potentiating effects largely occur at more alkaline conditions and seem to depend on the presence of external Ca^{2+}. Further, they show that disrupting the purported amiloride binding site (G445C) reduces both the inhibitory and potentiating actions, suggesting amiloride exerts these complex actions partly through a shared site.

The role of ASICs in memory consolidation has been a significant subject of research in the field. Fear memories consolidation and retrieval are essential in defining animal behavior. CO_2 inhalation increases the lability of fear memories during retrieval in mice and this process depends on ASIC1a. In the paper by Taugher et al. the authors report that 10% CO_2 inhalation soon after fear acquisition increased cued and context fear memory. The effect of CO_2 was time-dependent (time window of 1–4 h after fear acquisition). CO_2 inhalation did not alter fear memory in ASIC1a-/- mice thus indicating that ASIC1a activation by acidosis induced by neuronal hyperactivity may enhance memory.

The study by Neuhof et al. found that ASICs, particularly ASIC1a, are expressed in a human mesencephalic cell line (LUHMES) with characteristics of dopaminergic neurons. Using a combination of PCR, Western blot, patch-clamp, and fluorescence imaging techniques, the authors found that ASIC1a is mainly expressed in these neurons and that its blockade reduced neurite outgrowth in developing LUHMES cells. The work is relevant for the understanding of the role of ASIC1a in human pathologies such as Parkinson disease.

An emerging topic of interest is the intracellular signaling cascades activated by ASICs. To gain insight into this question, Salinas et al. investigated how mouse, rat, and human ASIC1a might trigger intracellular signaling via by proton or non-proton stimuli. Using either acidic pH or ASIC-activating toxins at neutral pH (ie. MitTx), they found pERK stimulation to be greater using non-proton activation than by the pH stimulus. Further, this effect was completely absent in ASIC1a knockout mice.

A final paper by Alijevic et al. addresses a particular mystery in the ASIC field. ASICs are activated by rapid pH drops and quickly desensitize essentially completely, with negligible residual current. These channels are clearly implicated in ischemic stroke yet under those conditions the pH changes are likely to be gradual. In prior work, this team used slow pH ramps to better approximate the pathophysiological course of pH change (Alijevic et al., 2020). They found that pH ramps of intermediate speed were best at promoting neuronal spiking. Here they extend this work to mimic the high extracellular K^+ and low Ca^{2+} expected during ischemia. Under such conditions, the number of action potentials and the firing time increased strongly with acidification accompanied by a change to higher K^+ and lower Ca^{2+} concentrations. Interestingly the phenomenon was also expressed in ASIC1 knockout mice suggesting other channels may be involved.

It has been more than 40 years since a receptor for protons was first reported. We have come a long way from doubting the existence of proton-gated channels to now having multiple knockout mice, structures, and some pharmacological tools. ASIC research appears in a steady-state or "normal phase" of science in which questions, both big and small, are answered without enormous shifts in understanding (e.g.,

questioning the existence of the channel itself) (Kuhn, 1970). Some of the remaining big problems include what is the "typical" pH stimulus experienced by a neuronal ASIC? What role do these channels play in the progression of various neuropathological process or pathology in other tissues? And can we leverage our growing knowledge of ASIC biology to inform real world therapeutic options? Addressing these and other problems will weave the role of ASICs into the great tangle of functional relationships between ion channels, transporters, membrane receptors, and messenger molecules that determine cellular excitability, behavior, and pathophysiology. We expect this collection of papers will further contribute to potentiate the ASIC research progress and understanding of the specific role of ASICs in physiology, pathology, and pharmaceutical potential.

AUTHOR CONTRIBUTIONS

All authors listed have made a substantial, direct, and intellectual contribution to the work and approved it for publication.

FUNDING

ES work was supported by grant from Consejo Nacional de Ciencia y Tecnología (CONACyT), Fronteras de la Ciencia grant No. 1544.

REFERENCES

Alijevic, O., Bignucolo, O., Hichri, E., Peng, Z., Kucera, J. P., and Kellenberger, S. (2020). Slowing of the time course of acidification decreases the acid-sensing ion channel 1a current amplitude and modulates action potential firing in neurons. *Front. Cell. Neurosc.* 14:41. doi: 10.3389/fncel.2020.00041

Krishtal, O. (2015). Receptor for protons: first observations on acid sensing ion channels. *Neuropharmacology* 94, 4–8. doi: 10.1016/j.neuropharm.2014.12.014

Krishtal, O. A., and Pidoplichko, V. I. (1980). A receptor for protons in the nerve cell membrane. *Neuroscience* 5, 2325–2327 doi: 10.1016/0306-4522(80)90149-9

Krishtal, O. A., and Pidoplichko, V. I. (1981). Receptor for protons in the membrane of sensory neurons. *Brain Res.* 214, 150–154. doi: 10.1016/0006-8993(81)90446-7

Kuhn, T. S. (1970). *The Structure of Scientific Revolutions*. 2nd Ed. London: The University of Chicago Press.

Rook, M. L., Williamson, A., Lueck, J. D., Musgaard, M., and Maclean, D. M. (2020). beta11-12 linker isomerization governs Acid-sensing ion channel desensitization and recovery. *Elife* 9:e51111. doi: 10.7554/eLife.51111

Waldmann, R., Champigny, G., Bassilana, F., Heurteaux, C., and Lazdunski, M. (1997). A proton-gated cation channel involved in acid-sensing. *Nature* 386:173. doi: 10.1038/386173a0

Conflict of Interest: The authors declare that the research was conducted in the absence of any commercial or financial relationships that could be construed as a potential conflict of interest.

Publisher's Note: All claims expressed in this article are solely those of the authors and do not necessarily represent those of their affiliated organizations, or those of the publisher, the editors and the reviewers. Any product that may be evaluated in this article, or claim that may be made by its manufacturer, is not guaranteed or endorsed by the publisher.

frontiers in Cellular Neuroscience

ORIGINAL RESEARCH
published: 27 April 2021
doi: 10.3389/fncel.2021.668008

Large Acid-Evoked Currents, Mediated by ASIC1a, Accompany Differentiation in Human Dopaminergic Neurons

Andreas Neuhof[1,2†], Yuemin Tian[1†], Anna Reska[1], Björn H. Falkenburger[2‡] and Stefan Gründer[1*‡]*

[1]Department of Neurology, Institute of Physiology, RWTH Aachen University, Aachen, Germany, [2]Department of Neurology, RWTH Aachen University, Aachen, Germany

OPEN ACCESS

Edited by:
Enrique Soto,
Meritorious Autonomous University of Puebla, Mexico

Reviewed by:
John Wemmie,
The University of Iowa, United States
Zhigang Xiong,
Morehouse School of Medicine, United States

***Correspondence:**
Björn H. Falkenburger
bjoern.falkenburger@dzne.de
Stefan Gründer
sgruender@ukaachen.de

†These authors have contributed equally to this work and share first authorship

‡These authors have contributed equally to this work and share senior authorship

Specialty section:
This article was submitted to Cellular Neurophysiology, a section of the journal Frontiers in Cellular Neuroscience

Received: 15 February 2021
Accepted: 06 April 2021
Published: 27 April 2021

Citation:
Neuhof A, Tian Y, Reska A, Falkenburger BH and Gründer S (2021) Large Acid-Evoked Currents, Mediated by ASIC1a, Accompany Differentiation in Human Dopaminergic Neurons. Front. Cell. Neurosci. 15:668008. doi: 10.3389/fncel.2021.668008

Acid-sensing ion channels (ASICs) are proton-gated Na^+ channels. They contribute to synaptic transmission, neuronal differentiation and neurodegeneration. ASICs have been mainly characterized in neurons from mice or rats and our knowledge of their properties in human neurons is scarce. Here, we functionally characterized ASICs in differentiating LUHMES cells, a human mesencephalic cell line with characteristics of dopaminergic neurons. We find that LUHMES cells express functional ASICs, predominantly homomeric ASIC1a. Expression starts early during differentiation with a striking surge in current amplitude at days 4–6 of differentiation, a time point where—based on published data—LUHMES cells start expressing synaptic markers. Peak ASIC expression therefore coincides with a critical period of LUHMES cell differentiation. It was associated with increased excitability, but not paralleled by an increase in ASIC1 mRNA or protein. In differentiating as well as in terminally differentiated LUHMES cells, ASIC activation by slight acidification elicited large currents, action potentials and a rise in cytosolic Ca^{2+}. Applying the ASIC pore blocker diminazene during differentiation reduced the length of neurites, consistent with the hypothesis that ASICs play a critical role in LUHMES cell differentiation. In summary, our study establishes LUHMES cells as a valuable model to study the role of ASICs for neuronal differentiation and potentially also cell death in a human cell line.

Keywords: acid-sensing ion channel, neuronal differentiation, LUHMES cells, dopaminergic neuron differentiation, Ca^{2+} imaging, midbrain

Abbreviations: ASIC, acid-sensing ion channel; CNS, central nervous system; LUHMES, Lund human mesencephalic; GAPDH, glyceraldehyde 3-phosphate dehydrogenase; mRNA, messenger RNA; qPCR, quantitative polymerase chain reaction; PcTx1, psalmotoxin 1; AP, action potential; Ca_V, voltage-gated Ca^{2+} channel; SNc, substantia nigra pars compacta; PD, Parkinson's disease.

INTRODUCTION

Acid-sensing ion channels (ASICs) are proton-gated Na^+ channels (Gründer, 2020). Among the six main ASIC subtypes, ASIC1a and ASIC2a are particularly highly expressed in the central nervous system (CNS) of rodents (Price et al., 1996; García-Añoveros et al., 1997; Lingueglia et al., 1997; Waldmann et al., 1997). ASICs are trimers and most functional channels in the rodent CNS are either ASIC1a homomers or heteromers of ASIC1a with ASIC2a or ASIC2b (Baron et al., 2002, 2008; Askwith et al., 2004; Chu et al., 2004; Wu et al., 2004; Li et al., 2010b). Because synaptic vesicles have acidic pH, ASICs contribute to synaptic transmission at excitatory synapses (Du et al., 2014; Kreple et al., 2014; Gonzalez-Inchauspe et al., 2017). Accordingly, ASIC1 is enriched in brain regions with strong excitatory input (Wemmie et al., 2003). Transient activation of ASICs, thus, modulates synaptic transmission. In addition, ASIC1 was shown to modulate the density of dendritic spines (Zha et al., 2006) and neuronal differentiation *in vitro* (O'Bryant et al., 2016). Prolonged activation of ASICs occurs in the course of ischemic stroke or inflammation and contributes to cell death in these conditions (Friese et al., 2007; Xiong et al., 2012; Wang et al., 2015; Chassagnon et al., 2017).

Most of these findings were obtained in mice or rats, and our knowledge about ASICs in the human nervous system is much more limited. In human brain, the main ASIC transcript is ASIC1a (Hoagland et al., 2010; Delaunay et al., 2012) and ASICs in human cortical neurons are predominantly homomeric ASIC1a (Li et al., 2010a). A more detailed characterization of ASICs in human neurons is clearly necessary to better understand their role in synaptic transmission, neuronal maturation and neurodegeneration in humans.

The LUHMES cell line is a subclone of the human mesenencephalic-derived cell line MESC2.10 (Lotharius et al., 2005), which was obtained by transforming committed neural precursor cells with the oncogene myc. LUHMES cells are therefore proliferating in standard medium. When myc expression is repressed by adding tetracycline, they differentiate into post-mitotic neurons (Lotharius et al., 2002). One particular advantage of LUHMES cells is the very high conversion rate (>99%) into a uniform post-mitotic population of excitable dopaminergic neurons (Scholz et al., 2011). Dopaminergic neurons of the midbrain through their projections to the striatum are essential for motor control and reward-based learning. Loss of dopaminergic neurons in the substantia nigra pars compacta (SNc) leads to Parkinson's disease (PD). Because differentiated LUHMES cells share many characteristics with dopaminergic neurons of the SNc, they constitute a valuable model to study cellular mechanisms of neuronal differentiation, neurodegeneration (Lotharius et al., 2005) and reward-based learning.

In this study, we functionally characterized ASICs during differentiation of LUHMES cells. We found that homomeric ASIC1a is the main ASIC of LUHMES cells and found a striking transient increase of functional ASIC1a during the first week of differentiation. Activation of ASICs induced action potentials and intracellular Ca^{2+} signals and blocking ASICs reduced the length of neurites. Our study establishes LUHMES cells as a model to study ASICs in a human cell line and suggests that ASICs contribute to maturation of LUHMES cells.

MATERIALS AND METHODS

Cell Culture

LUHMES cells were grown at 37 °C in a humidified atmosphere with 5% of CO_2. For proliferation, they were cultivated in Nunclon cell culture flasks (Thermo Fisher Scientific, Waltham, MA, USA) in Advanced DMEM/F12 medium supplemented with 2 mM L-Glu, 1× N2-supplement (Thermo Fisher Scientific, Waltham, MA, USA) and 40 μg/ml FGF, as previously described (Scholz et al., 2011). Cells were splitted 1:10 or 1:5 every 3–4 days.

To convert LUHMES cells into post-mitotic neurons, a 2-step differentiation protocol was used (Scholz et al., 2011). On day 0 (d0), the medium was exchanged by the differentiation medium: advanced DMEM/F12 medium with 2 mM L-Glu, 1 ×N2-supplement, 1 mM dibutyryl-cAMP, 1 μg/ml tetracycline and 2 ng/ml GDNF. Cells were either directly seeded in the desired density (d3 or earlier) or they were splitted on d3 and then seeded in the desired density. Depending on the experiments, cells were grown either on Nunclon cell culture dishes or on cover slips. Flasks and dishes were coated with 50 μg/μl poly-L-ornithin and 1 μg/μl fibronectin; cover slips were coated with 10 μg/μl poly-L-ornithin and 10 μg/μl laminin.

For quantification of neurite lengths, diminazene (Sigma–Aldrich; Munich, Germany) was dissolved in DMSO and added in a final concentration of 10 μM to differentiation medium; differentiation medium containing DMSO without diminazene served as a control. The same cultures from two independent differentiations were used to determine neurite outgrowth across days.

Reverse Transcription–Quantitative Real Time PCR (qPCR)

For isolation of RNA, LUHMES cells were grown on cell culture dishes with differentiation medium or, as a control, in normal proliferation medium. On d2–d7 and additionally on d10, total RNA was isolated using RNeasy minikit (Qiagen, Venlo, The Netherlands). Concentration and quality of the RNA was measured using a NanoDrop 2000c spectrophotometer (Thermo Fisher Scientific, Waltham, MA, USA). RNAs with a 260 nm/280 nm ratio >2.00 and a 260 nm/230 nm ratio >1.80 were used for reverse transcription. First-strand cDNA was synthesized from 1 μg total RNA using QuantiTect Reverse Transcription Kit (Qiagen), yielding 20 μl cDNA. All kits were used according to manufacturer's instructions. Contamination with genomic DNA was controlled by RT-PCR using intron-spanning primers for the reference gene glyceraldehyde-3-phosphate dehydrogenase (*GAPDH*).

For qPCR, hydrolysis probes (TaqMan probes) for *GAPDH*, *ASIC1a* and *ASIC2* were ordered from Applied Biosystems (the assay identification numbers are Hs02758991_g1, Hs00952807_m1, Hs00153756_m1). Each reaction, containing 1 μl cDNA, 1 μl TaqMan Gene Expression Assay and 5 μl

of two times Rotor-Gene Probe PCR Master Mix (Qiagen), was performed in triplicates; a sample without cDNA served as negative control. qPCR was performed in a Rotor-Gene Q (Qiagen), starting with a long denaturation phase (10 min, 95°C), followed by 40 cycles with denaturation (15 s, 95°C) and annealing/elongation (60 s, 60°C/72°C). Experiments were repeated with RNA from two independent cell batches and analyzed using the ΔCt method. Efficiency of each probe was determined by a standard curve and was close to 100%. Results are reported as relative levels of *ASIC*/*GAPDH* mRNA.

Immunoblotting

LUHMES cells were lysed with RIPA buffer (25 mM Tris-Cl pH 7.6, 0.1% SDS, 150 mM NaCl, 1% Triton-X-100, 1% sodium deoxycholate, 1% PMSF, and 1% proteinase inhibitor cocktail; Roche). Proteins were quantified using a kit (Micro BCA; Thermo Fisher Scientific, Waltham, MA, USA) and the same amount of protein was separated by SDS-PAGE (10%). Proteins were transferred to PVDF membranes (Roche, Mannheim, Germany), and probed overnight at 4°C with the following primary antibodies: mouse monoclonal anti-ASIC1 (1:1,000 dilution, NeuroMab #75-277) and mouse monoclonal anti-acetylated tubulin (1:5,000 dilution, Sigma–Aldrich #T7451). The anti-ASIC1 antibody was derived against a fusion protein from the cytoplasmic C-terminus of mouse ASIC1; 65 of the 67 amino acids of this fusion protein are identical in human ASIC1. It was validated by NeuroMab in immunoblots from ASIC1 knock-out tissue. Blots were visualized using secondary HRP-conjugated anti-rabbit (Invitrogen #UB280570) or anti-mouse antibodies (1:10,000 dilution, Invitrogen #2122350) and Super Signal West Pico Chemiluminescent Substrate (Thermo Fisher Scientific, Waltham, MA, USA). Bands of the expected size were quantified using ImageJ, and density for ASIC1a was normalized to tubulin.

Electrophysiology

Electrodes with a resistance of 5–10 MΩ were pulled from borosilicate glass with a DMZ-Universal Puller (Zeitz Instruments GmbH, Martinsried, Germany). Electrodes were filled with an intracellular solution containing 10 mM NaCl, 10 mM KCl, 25 mM HEPES, 70 mM K-Gluconate, 10 mM EGTA and 1 mM $MgCl_2$; pH was adjusted to 7.25 with tetramethylammonium hydroxide (TMAOH) solution. The extracellular solution in the bath chamber contained 100 mM NaCl, 5.4 mM KCl, 10 mM HEPES or MES, 2 mM $CaCl_2$ and 1 mM $MgCl_2$; pH was adjusted with TMAOH. Whole cell currents were recorded using a patch-clamp amplifier (Axopatch 200B), the Axon-CNS (Digidata 1440A) and Clampex software (Molecular Devices). Data were filtered at 1 kHz with low-pass filter, and stored continuously on a computer hard disc and analyzed using pCLAMP software. For voltage clamp, the membrane voltage was clamped to −70 mV, and the sampling rate was 4 kHz. PcTx1 was purchased from Smartox biotechnology. For current clamp, the membrane current was clamped to 0 pA for the gap free protocol. For measurements of the rheobase, ten long (1 s) depolarizing current pulses (increments of 1, 2, 5, or 10 pA) were delivered; data was sampled at a rate of 20 kHz.

Ca^{2+} Imaging

For cell fluorescence measurements, LUHMES cells grown on glass coverslips were mounted in a cell chamber and perfused with bath solution at room temperature. Fluorescence was measured continuously on an inverted microscope (IX71, Olympus, Chromaphor) using a Fluar 20×/0.75 objective (Olympus) and Till Vision real-time imaging software (Till Photonics). Cells were loaded for 15 min at 37°C with 2 μM Fura-2-AM (Molecular Probes) in bath solution. Fura-2 was excited at 340/380 nm, and the emission was recorded between 470 and 550 nm using a sensicam CCD camera (PCO imaging). Acquisition and data analysis were done using Till Vision software. Amiloride and nimodipine were purchased from Sigma–Aldrich.

Data Analysis

To analyze the expression of functional ASICs, the peak current elicited by pH 6.0 was divided by the electrical capacity to obtain the current density. The time constant τ_{des} was determined by fitting a single exponential function to the current decay using the software Igor Pro (WaveMetrics, Tigard, OR, USA). The concentration-response curve in **Figure 3** was obtained by a fit to a Hill function:

$$I = \frac{1}{\left(1 + \left(\frac{[H^+]}{EC_{50}}\right)^H\right)}$$

where I is the current, $[H^+]$ is the proton concentration, EC_{50} is the concentration at which 50% of the maximal current is obtained, and H is the Hill coefficient (GraphPad Prism).

Ca^{2+} signals elicited by acidic pH were quantified by subtracting the baseline values at 340/380 nm before application of acidic pH from the peak values during application of acidic pH. For application of inhibitors (nimodipine or amiloride, or no additional treatment as control), Ca^{2+} signals during application of the inhibitor were normalized to the Ca^{2+} signals before application of the inhibitor (3rd/2nd peak).

Data are reported as mean ± SD, except for the data in **Figure 3A**, which are reported as mean ± SEM, to indicate the precision of the data points used to draw the graph. Statistical analyses were conducted with Prism 7.0 (GraphPad Software, San Diego, CA, USA). Normal distribution of each dataset was tested using the D'Agostino–Pearson omnibus K2 test. For data, which was normally distributed according to the omnibus K2 test, we used two-tailed paired or unpaired Student's *t*-test, as appropriate, when comparing two groups and a one-way or two-way analysis of variance (ANOVA), followed by Tukey's multiple comparison test, when comparing more than two groups. For data, which was not normally distributed according to the omnibus K2 test, we either used a Mann–Whitney test (two groups) or a Kruskal–Wallis test followed by Dunn's multiple comparison test (more than two groups). Data, which were categorized in two classes (AP vs. no AP), was analyzed using Fisher's exact text. $p \leq 0.05$ was considered as significant.

The total length of neurites of single cells was determined on d1–d5 using the plugin IC Neuron of the application IC Capture (The Imaging Source, Bremen, Germany).

RESULTS

ASIC1a mRNA Is the Predominant ASIC Transcript in LUHMES Cells

The *ASIC1* gene codes for ASIC1a and ASIC1b and *ASIC2* for ASIC2a and ASIC2b, respectively. Expression levels of *ASIC1* variant a (*ASIC1a*) and *ASIC2* were determined during differentiation of LUHMES cells by quantitative real time PCR (qPCR; **Figure 1A**). For *ASIC2*, we used primers that detect mRNAs for variant a (ASIC2a) and for variant b (ASIC2b). Nevertheless, at any time point, expression of *ASIC2* was much lower (60- to >1,000-fold) than that of *ASIC1a*, indicating that *ASIC1a* mRNA was the primary ASIC transcript in these cells. The average expression of *ASIC1a* rose by <10-fold during differentiation of LUHMES cells. Expression of ASIC1a protein in LUHMES cells was confirmed by Western blot analysis (**Figure 1B**). ASIC1a abundance was about 2-fold higher after 3 days of differentiation (d3) compared with undifferentiated LUHMES cells (d0), but there was no further increase with longer time in differentiation medium and the difference was not statistically significant (p = 0.09, one-way ANOVA).

ASIC Current Amplitude Peaks on Day 6 of LUHMES Cell Differentiation Into Neurons

We then determined the expression of functional ASICs in LUHMES cells during differentiation using the whole cell patch clamp technique. We activated ASICs by a pH drop from 7.4 to 6.0. In proliferating LUHMES cells on d0, which have already a definite neuronal commitment (Scholz et al., 2011), ASIC current density was very small (<10 pA/pF; n = 3). Peak current density strongly increased from d3 to d4 and d5 (increase from 59.6 pA/pF on d3 to 158.6 pA/pF on d5; $p < 0.001$; t-test; **Figure 2**). During the next 5 days, peak current density decreased again to its initial levels. Thus, there was a striking, transient surge in ASIC peak current density during the first 5 days of differentiation, which was only partially mirrored by the mRNA and protein expression levels (**Figure 1**). ASIC currents had a

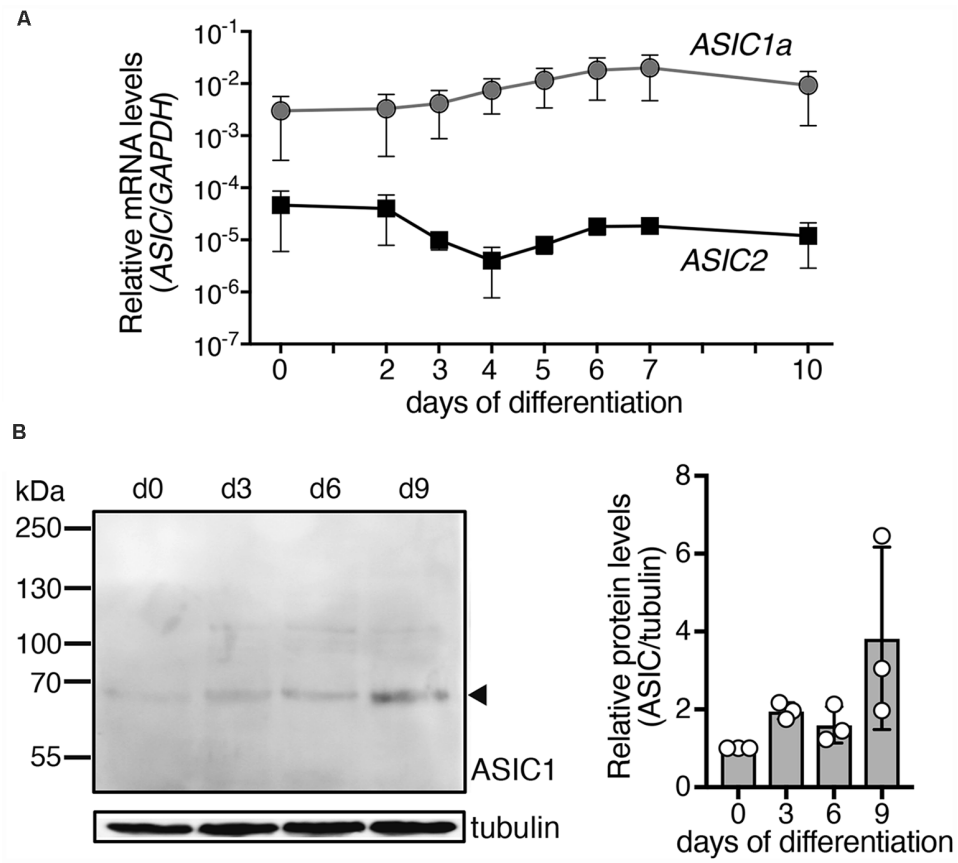

FIGURE 1 | Expression of *ASIC1a* and *ASIC2* mRNAs and ASIC1a protein during differentiation of LUHMES cells into post-mitotic neurons. **(A)** Expression of ASIC mRNA was quantified using quantitative real time PCR and was normalized to the housekeeping gene glyceraldehyde 3-phosphate dehydrogenase (*GAPDH*), n = 2. Note that errors bars have different length above and below of the data points, because of the logarithmic scale of the y axis. **(B)** Left, representative Western blot showing expression of ASIC1 protein in LUHMES cells; tubulin was used as control. Right, summary of three Western blots; expression was normalized to tubulin and to d0.

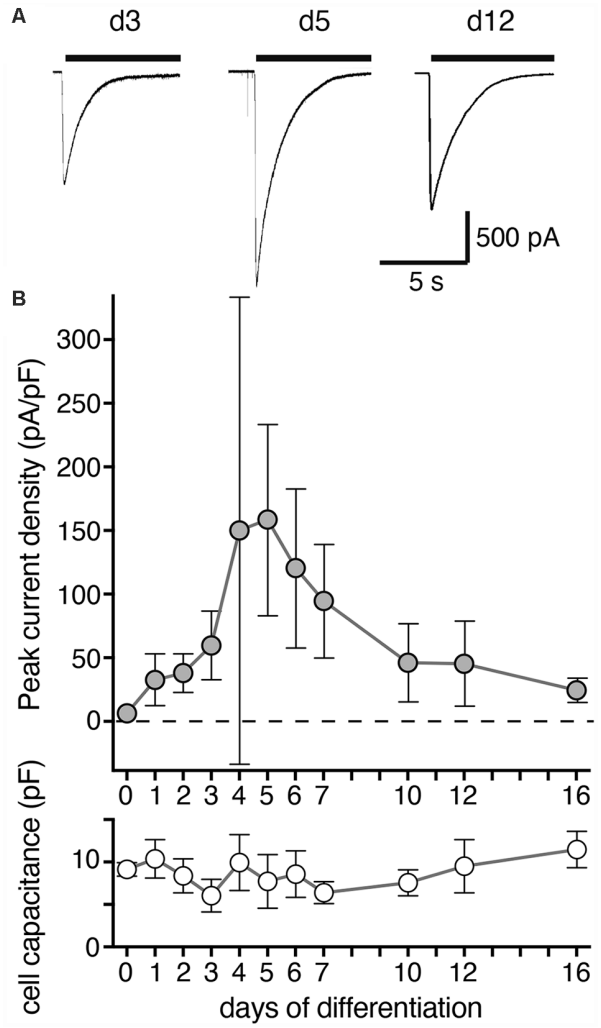

FIGURE 2 | Density of ASIC peak currents during differentiation of LUHMES cells into post-mitotic neurons. **(A)** Representative current traces from d3, d5 and d12. ASIC currents were elicited by a drop in pH from 7.4 to 6.0 and cells analyzed by whole cell patch-clamp. **(B)** Summary of current density and cell capacitance for different days of differentiation as indicated (mean ± SD; n = 4–12 from two independent experiments). Note that the current density on d4 was highly variable and not normally distributed with some cells having a small density like on d3 and others a large density like on d5. Current amplitude ranged from 36 to 3,603 pA for individual cells on different days of differentiation.

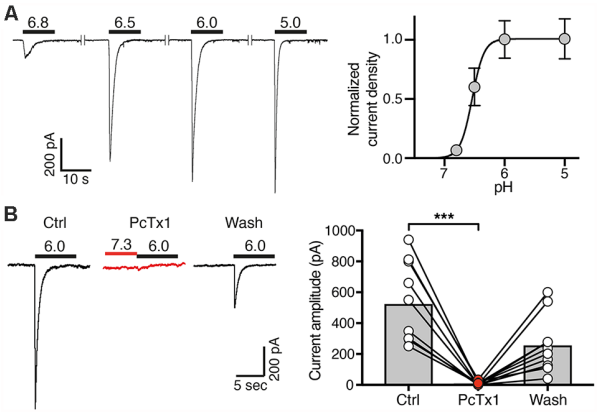

FIGURE 3 | Concentration-response curve and PcTx1 sensitivity of ASICs in post-mitotic LUHMES cells. **(A)** Cells were cultivated in differentiation medium for 6 days and were then analyzed by whole cell patch-clamp in voltage clamp mode. Left, representative ASIC currents elicited by transient pH changes from pH 7.4 to values between 6.8 and 5.0 for 10 s. For recovery of ASICs, cells were washed with a solution of pH 7.4 for 30 s. Right, concentration response curve. Currents were normalized to the current at pH 5.0, which had a density of 120 pA/pF. Line represents a fit to the Hill function. n = 11 cells from two independent experiments. **(B)** PcTx1 sensitivity of ASICs on d4–d8. Left, representative whole cell current traces, each elicited by a 10 s-pulse of pH 6 from conditioning pH 7.3. Traces were acquired before, during and after application of 30 nM PcTx1 for 2 min. Right, summary of peak current amplitude before, during and after PcTx1 application. n = 10. ***p = 0.0001 (paired t-test).

large amplitude, with a mean amplitude of 1,084 ± 479 pA (mean ± SD) on d5.

Homomeric ASIC1a Is the Predominant Functional ASIC in LUHMES Cells

Next, we determined the ASIC current amplitude at d4–d7 at different pH values, revealing half-maximal activation at pH 6.6 ± 0.1 on d4 (mean ± SD; n = 12), at pH 6.5 ± 0.2 on d5 (n = 11), at pH 6.5 ± 0.1 on d6 (n = 11) and at pH 6.6 ± 0.1 on d7 (n = 12) and saturating amplitudes at pH 6.0 (**Figure 3A**). This result strongly suggests that the highly proton-sensitive homomeric ASIC1a mediates the surge in ASIC current. Nearly complete inhibition of ASIC currents by PcTx1 (30 nM) at d4–d8 confirmed the presence of mainly homomeric ASIC1a in differentiating LUHMES cells (**Figure 3B**). Heteromeric ASIC1a/2b has similar functional properties as homomeric ASIC1a, including sensitivity to protons and to PcTx1 (Sherwood et al., 2011). Therefore, the presence of functional ASIC1a/2b in LUHMES cells cannot be excluded. Low expression of the *ASIC2* gene (**Figure 1A**), however, suggests low abundance of ASIC2b in LUHMES cells. In contrast, the presence of ASIC1a homomers in differentiating LUHMES cells would be consistent with the mRNA analysis (**Figure 1A**).

To determine whether heteromeric ASIC1a/2a is also present during differentiation, we measured peak currents elicited by pH 6.0 and by pH 5.0. While homomeric ASIC1a is already maximally activated by pH 6.0 or by slightly more acidic pH (Waldmann et al., 1997; Babini et al., 2002), current amplitudes of heteromeric ASIC1a/2a only saturate around pH 5.0 or at slightly more acidic pH (Bassilana et al., 1997; Bartoi et al., 2014; Joeres et al., 2016). Thus, a ratio of $I_{pH5.0}/I_{pH6.0}$ close to 1 is indicative of homomeric ASIC1a; the presence of ASIC2a should increase this value up to 2 for a pure heteromeric channel. In LUHMES cells, the $I_{pH5.0}/I_{pH6.0}$ was close to 1 on almost all days; only on d10 it was 1.5 ($p < 0.05$ compared to d1, d2, d3 and d6; Kruskal–Wallis test; **Figure 4A**).

As a further characteristic that differentiates between different ASIC subtypes, we determined the desensitization time constant τ_{des} after activation with pH 6.0. At pH 6.0, human ASIC1a desensitizes with a time constant τ_{des} of 1–2 s (Xu et al., 2018;

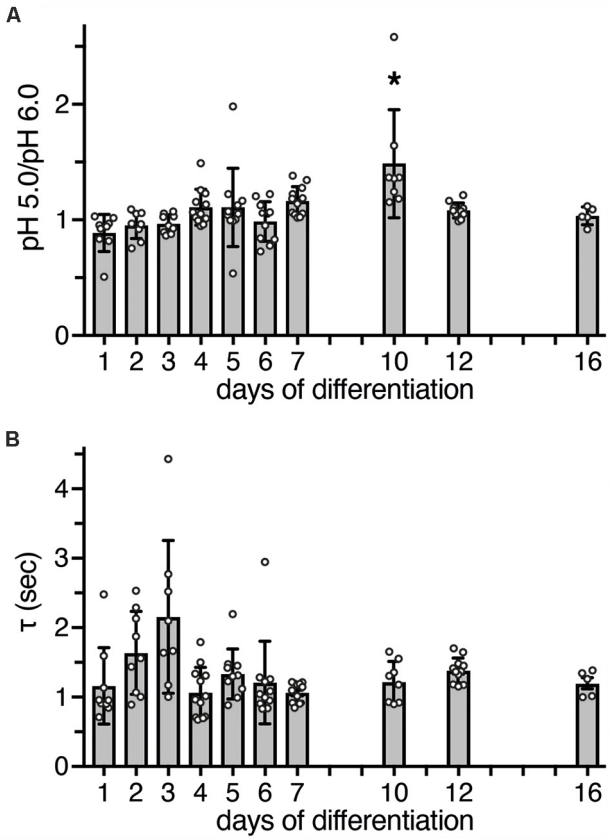

FIGURE 4 | Functional characteristics of ASIC currents *between* d1 *and* d16. **(A)** Bars represent the peak amplitude elicited by pH 5.0 divided by the peak amplitude elicited by pH 6.0. Currents were elicited by a pH drop from 7.4 to 6.0 or 5.0, respectively, for 10 s. The ratio at d10 was significantly different from d1 ($p < 0.0001$), d2 ($p = 0.001$), d3 ($p = 0.001$), and d6 ($p = 0.011$, Kruskal-Wallis test followed by Dunn's test). *$p < 0.05$. **(B)** Bars represent τ_{des} of ASIC currents at different days of differentiation; $p > 0.05$ on all days (Kruskal-Wallis test followed by Dunn's test). n = 5–12 from two independent experiments.

Vaithia et al., 2019). To our knowledge, the time constant of heteromeric human ASIC1a/2a has not yet been reported, but ASIC1a/2a from rodents desensitizes with a τ_{des} <1 s (Benson et al., 2002; Hattori et al., 2009). A time constant τ_{des} of ASIC currents in LUHMES cells could be well fitted with a single exponential function, suggesting a predominantly homogenous population of ASIC channels. Moreover, on all days, τ_{des} was similar and >1 s ($p > 0.05$, Kruskal-Wallis test; **Figure 4B**). Thus, although on d10 the ratio of $I_{pH5.0}/I_{pH6.0}$ was 1.5, the presence of a heteromeric ASIC1a/2a on d10 was not confirmed by the analysis of τ_{des}. Therefore, these results, collectively, suggest that ASIC currents were carried mainly by homomeric ASIC1a and perhaps ASIC1a/2b during the entire period of differentiation.

Activation of ASICs by Slight Acidification Elicits Action Potentials in LUHMES Cells

We next assessed excitability of undifferentiated LUHMES cells (d0) and of cells on d5–d7 or on d10. We stimulated the cells by applying 1 s-current pulses of increasing amplitude and monitored the membrane potential in current clamp mode. In undifferentiated cells (d0), even depolarizing close to 0 mV did not elicit an action potential (AP). In contrast, APs were readily elicited at d5 or later (**Figure 5A**). With longer time of differentiation, smaller current pulses were needed to reach threshold and elicit APs. The rheobase current decreased 2-fold from d5/d7 to d10 ($p = 0.02$; Mann–Whitney test), which can be explained by the less negative resting membrane potential (RMP) after longer differentiation ($p = 0.002$; Mann–Whitney test; **Figure 5B**). The proportion of cells, in which APs could be elicited, almost doubled from d5/d7 to d10 ($p = 0.23$, Fisher's exact test; **Figure 5C**). Spontaneous APs where not observed in any of the 22 cells on d5/d7, but we observed spontaneous APs in four out of nine cells on d10 ($p = 0.004$, Fisher's exact test), some of which occurred in bursts (**Figures 5D,E**). Taken together, although we did not systematically characterize excitability over the whole period of differentiation, these results suggest that excitability of LUHMES cells gradually increased during differentiation. This interpretation is in line with a previous study, which reported that current density of voltage-gated Na^+ channels gradually increases from d3 to d11, that approximately 40% of cells were spontaneously active up to d9, and that all cells generated spontaneous APs on d10–d12 (Scholz et al., 2011).

After examining general excitability, we next tested whether activation of ASICs was sufficient to reach threshold and elicit APs. Modest acidification to pH 6.8 indeed depolarized the membrane potential and elicited APs at both d6 and d10 (**Figure 5F**). The larger rheobase on d6 (**Figure 5B**) may be compensated for by the larger ASIC current density at this stage (**Figure 2**).

ASICs Are Involved in Neurite Outgrowth During LUHMES Cell Differentiation

The transient surge in ASIC current density during differentiation of LUHMES cells suggest their involvement in the differentiation process. Indeed, blocking ASICs was reported to reduce differentiation of NS20Y cells, a murine neuroblastoma-derived cell line (O'Bryant et al., 2016). To determine whether ASICs are involved in the differentiation of LUHMES cells, we applied the isoform-unselective ASIC pore blocker (Schmidt et al., 2017) diminazene (10 μm) during the first 5 days of differentiation and assessed the length of neurites as a measure for neuronal differentiation. In control cells, the length of neurites almost doubled from d1 to d5 (**Figure 6**). Neurite lengths of diminazene-treated cells were overall shorter than for control cells on all days investigated (**Figure 6**; $p < 0.001$, two-way ANOVA). Diminazene has, to our knowledge, not previously been tested on human ASICs, but the amino acids in the outer ion pore that are crucial for inhibition (Schmidt et al., 2017) are completely conserved in human ASICs, arguing that diminazene will also inhibit human ASICs. Although we cannot exclude that diminazene might also have other targets, this result supports the hypothesis that ASICs play an important role in neuronal development.

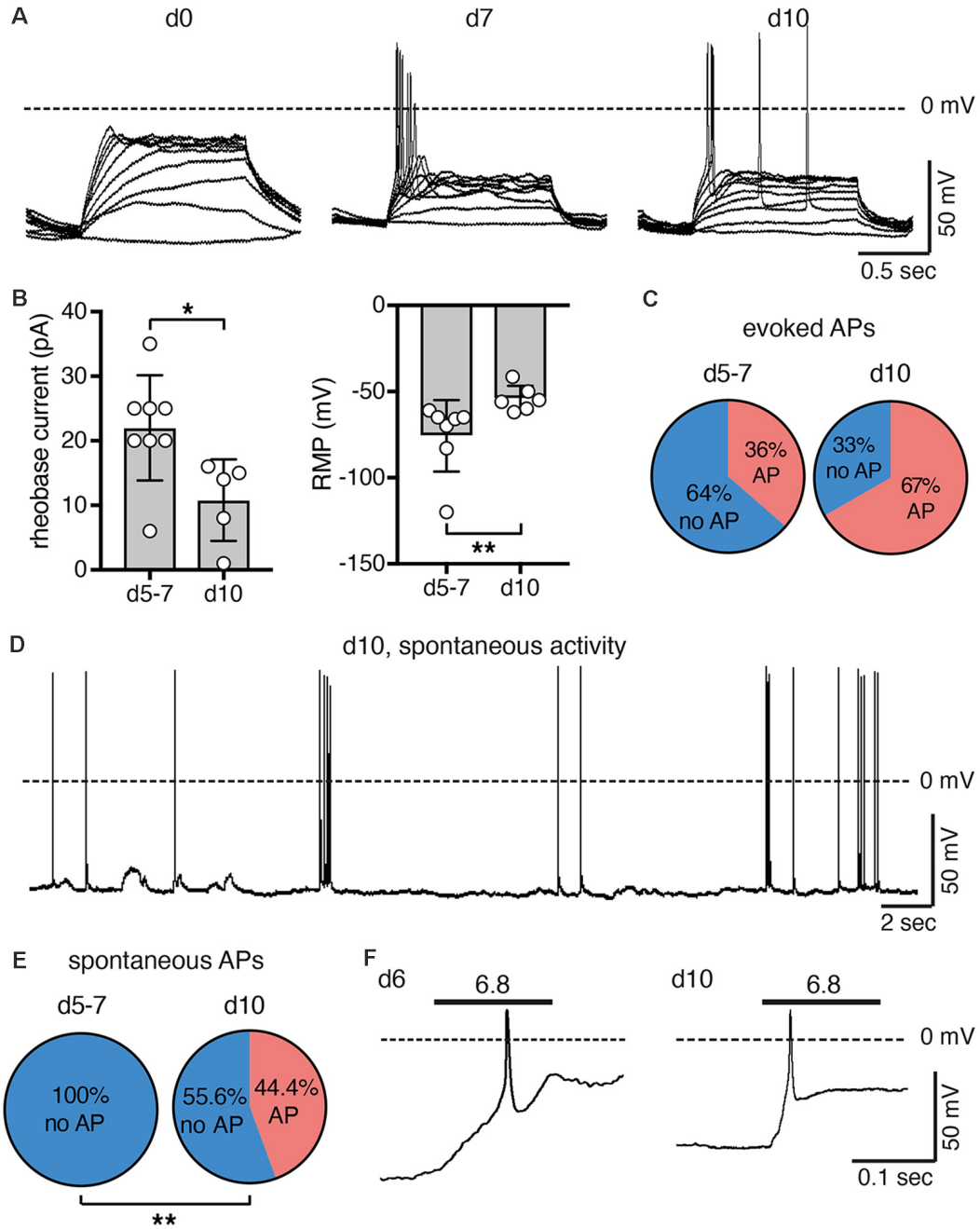

FIGURE 5 | Excitability of LUHMES cells during differentiation. **(A)** Representative current clamp recordings from LUHMES cells on d0, d7 and d10. Depolarizing step current pulses elicited APs only in differentiated LUHMES cells. **(B)** Summary of the rheobase and the resting membrane potential (RMP) at different times of differentiation (n = 5–8); *$p < 0.05$, **$p < 0.01$ (Mann-Whitney test). **(C)** Pie chart illustrating the proportion of cells, which responded with APs after pulse stimulation, at d5–d7 (8 out of 22 cells) and at d10 (six out of nine cells). **(D)** Example of spontaneous APs from LUHMES cells at d10. The trace is representative for four out of nine cells. **(E)** Pie chart illustrating the proportion of cells, which had spontaneous APs at d5–d7 and at d10. At d10, significantly more cells had spontaneous APs (p = 0.004, Fisher's exact test). **(F)** Examples of APs elicited by steps to pH 6.8 (n = 2 for each day).

ASIC Activation Elicits Ca^{2+} Signals in Differentiated LUHMES Cells

A rise in cytosolic Ca^{2+} is one of the main pathways by which excitation and excitability affect differentiation, morphology and degeneration. To determine whether ASICs could modulate differentiation of LUHMES cells through intracellular Ca^{2+}, we tested whether ASIC activation can induce a Ca^{2+} response in LUHMES cells. On d5 and d9, stimulation with pH 6.0 evoked a

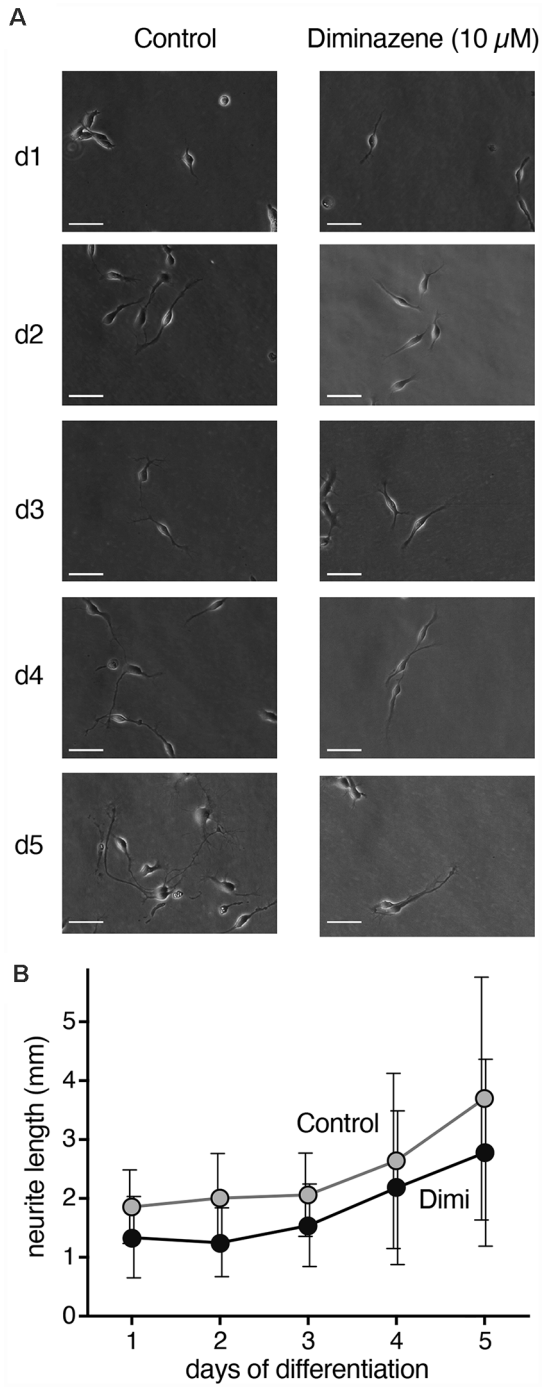

FIGURE 6 | Neurite length during differentiation of proliferating LUHMES cells into post-mitotic neurons. **(A)** Representative images of LUHMES cells at d1–d5, with and without incubation in diminazene (10 μM). **(B)** Quantification of the total length of neurites of single cells at d1–d5. Dimi, diminazene. *n* = 26–60 neurites from 12–24 different cells.

robust, transient Ca^{2+} signal (**Figure 7**), which would be expected if it was mediated by ASIC activation. The response gradually decreased upon repeated stimulation, which can be explained by tachyphylaxis of ASIC1a (Chen and Gründer, 2007). On both days, the isoform-unselective ASIC blocker amiloride almost completely inhibited the Ca^{2+} response ($p < 0.001$, two-way ANOVA; **Figure 7**). Although amiloride has other targets like Na^+/H^+ exchangers, this result suggests that the Ca^{2+} influx in LUHMES cells was indeed ASIC-dependent. To test whether the Ca^{2+} influx was through ASIC itself, or through activation of voltage-gated Ca^{2+} channels (Ca_V), we applied the L-type Ca_V blocker nimodipine. Nimodipine significantly reduced the Ca^{2+} influx induced by pH 6.0 on d9 ($p = 0.003$) but not on d5 (**Figure 7**). At d5, there were two outliers with unusually large Ca^{2+} signals (**Figure 7A**). Excluding them would reveal significantly reduced Ca^{2+} influx by nimodipine also at d5 ($p = 0.014$). On both d5 and d9, nimodipine reduced Ca^{2+}signals less strongly than amiloride ($p = 0.002$ at d5, $p = 0.0002$ when the outliers were removed; $p = 0.006$ at d9; p-values for the interaction *between* amiloride *and* nimodipine). Thus, although acidic pH-induced Ca^{2+} signals were at least on d9 partly through indirect activation of voltage-gated Ca^{2+} channels, the remaining Ca^{2+}might have entered the cell directly *via* ASIC1a.

DISCUSSION

Our results reveal expression of functional ASICs in human dopaminergic LUHMES cells, consistent with the previous description of ASICs in dopaminergic neurons of mouse midbrain slices (Pidoplichko and Dani, 2006), isolated neurons of the mouse substantia nigra pars compacta (SNc; Arias et al., 2008) and the human cell line SH-SY5Y, which is derived from a bone marrow biopsy of a patient with neuroblastoma, expresses dopaminergic markers and releases catecholamines (Xiong et al., 2012). Moreover, our results consistently suggest that homomeric ASIC1a is the main ASIC during the entire differentiation of LUHMES cells into postmitotic cells with neuronal characteristics; some contribution by heteromeric ASIC1a/2b can also not be excluded. First, qPCR revealed *a* >60-fold higher abundance of ASIC1a mRNA than ASIC2a and ASIC2b mRNA combined (**Figure 1A**). Second, apparent EC_{50} of this ASIC was pH 6.5 (**Figures 3A**, **4A**), indicative of highly proton-sensitive homomeric ASIC1a or ASIC3. Third, PcTx1, which at pH 7.4 specifically inhibits homomeric ASIC1a (Escoubas et al., 2000; Joeres et al., 2016), inhibited LUHMES cell ASICs almost completely (**Figure 3B**). Finally, τ_{des} was >1 s (**Figure 4B**), excluding heteromeric ASIC1a/2a as well as homomeric ASIC3. This is consistent with the characteristics of ASICs in mouse midbrain slices (Pidoplichko and Dani, 2006)—even though the apparent EC_{50} in these measurements was pH 5.5; homomeric ASIC1a was also shown to at least contribute to the currents in SH-SY5Y cells (Xiong et al., 2012).

LUHMES cells are human, dopaminergic cells that show neuron-like electrical properties and morphology (Lotharius et al., 2002; Scholz et al., 2011). They are derived from immortalized embryonic midbrain and show a very high conversion rate into dopaminergic neurons, which sets them apart from cells derived from human induced pluripotent stem cells (iPSC) where the rates of neuronal and dopaminergic phenotypes are typically much lower (Xi et al., 2012; Doi et al., 2014). Still, the phenotype of neurons is not only

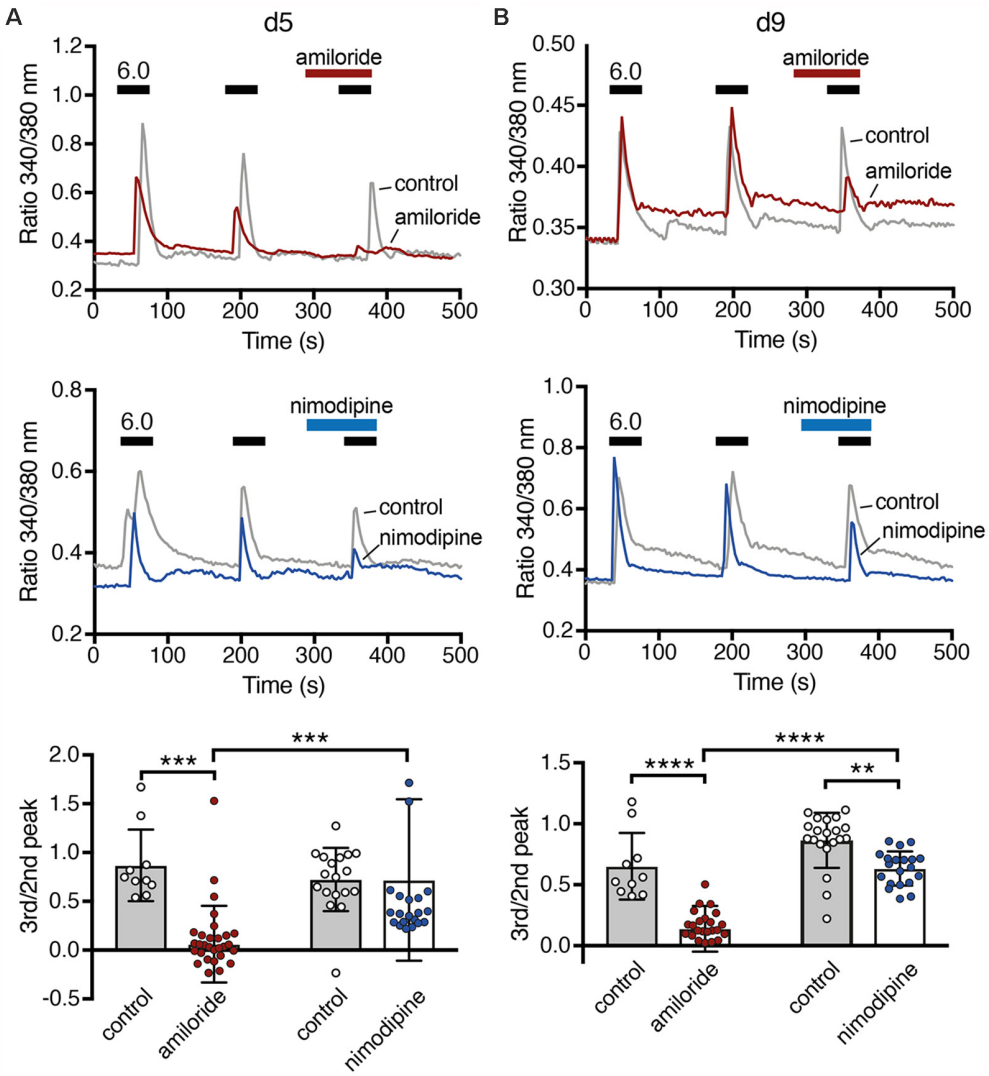

FIGURE 7 | Ca^{2+} responses of LUHMES cells after acidic stimulation. **(A)** Top, representative recordings of intracellular Ca^{2+} by Fura-2 in LUHMES cells at d5. Cells were repeatedly stimulated with pH 6 (black bars). For some cells, 100 μM amiloride was pre- and co-applied during the third stimulation (red bar). The gray trace represents the mean response of >10 control cells from one coverslip and the red trace of >10 cells from another coverslip exposed to amiloride. Middle, as for the top panel but with 10 μM nimodipine instead of amiloride. The blue trace is from cells exposed to nimodipine. Bottom, summary data. **(B)** As in **(A)** but for d9, $^{**}p < 0.01$, $^{***}p < 0.001$, $^{****}p < 0.0001$ (two-way ANOVA).

shaped by their origin, but also by their environment, and this environment is certainly different in the brain than in a culture dish. Furthermore, the human midbrain comprises at least two populations of dopaminergic neurons that are differentially affected in Parkinson's disease (Gibb and Lees, 1991; Dauer and Przedborski, 2003; Halliday et al., 2014). To our knowledge, LUHMES cells are the culture model that best model the population of dopaminergic SNc neurons that degenerate in PD, but they are still a model. Our conclusion that human midbrain dopaminergic neurons express functional ASICs, mainly homomeric ASIC1a, therefore needs to be confirmed by PCR and immunoblots from human mesencephalon.

Dopaminergic neurons of the midbrain receive excitatory input from the cortex and, because ASICs contribute to the postsynaptic current at excitatory synapses (Du et al., 2014; Kreple et al., 2014; Gonzalez-Inchauspe et al., 2017), it is conceivable that ASIC1a contributes to excitation of midbrain dopaminergic neurons. Accordingly, ASIC currents had a large amplitude in LUHMES cells (**Figure 2**) and activation of ASICs could elicit APs (**Figure 5**) and intracellular Ca^{2+} signals (**Figure 6**) in differentiated LUHMES cells. Similarly, ASICs were shown to contribute to catecholamine secretion in SH-SY5Y cells (Xiong et al., 2012), a process dependent on intracellular Ca^{2+}. These findings therefore suggest that ASIC1a may modulate excitability, Ca^{2+} homeostasis and dopamine secretion in human dopaminergic neurons.

Midbrain dopaminergic neurons are spontaneously active pacemakers. Activity patterns and Ca^{2+} homeostasis are

important factors that contribute to their degeneration in Parkinson's disease (PD; Duda et al., 2016). Understanding the contribution of ASIC1a for the excitability and Ca^{2+} homeostasis in human dopaminergic neurons will therefore provide insight into the pathogenesis of PD and potentially provide targets for new treatment strategies. Neurodegeneration in PD likely , results not from a single insult, but from a network of events including in addition mitochondrial impairment, protein misfolding and inflammation (Lang and Espay, 2018). Sensing protons secreted by the inflammatory response might therefore constitute another role of ASIC1a in PD pathogenesis. Dopaminergic neurons of the SNc project to the striatum, where they modulate direct and indirect pathways through excitatory D_1 receptors and inhibitory D_2 receptors, respectively. This modulation is important for movement control; the loss of dopamine secretion in the striatum causes PD motor symptoms. In order to overcome current impediments of medical therapy in PD, non-dopaminergic pathways to modulate dopamine secretion and striatal physiology are increasingly investigated (Zhai et al., 2019). The contribution of ASIC1a could be studied in LUHMES cells and reveal new insights into movement control by midbrain dopaminergic neurons and potentially offer new treatment strategies for PD.

Dopaminergic neurons also project from the midbrain to the nucleus accumbens (NAc), which is homologous to the motor striatum and is involved in reward-based learning. ASIC1a is abundantly expressed in the NAc (Wemmie et al., 2003) and contributes to synaptic transmission and affects cocaine-conditioned learning (Kreple et al., 2014). ASIC1 is upregulated in the NAc upon either chronic systemic injection of cocaine (Zhang et al., 2009) or of amphetamines (Suman et al., 2010), suggesting that ASIC could be involved in drug addiction and reward-based learning. Although the NAc seems to have a key role for the modulation of drug-based learning by ASIC1a (Kreple et al., 2014), expression of ASIC1a in the SNc suggests that it might contribute to reward-based learning also *via* modulation of dopamine-release. This possibility warrants further investigation.

Our study revealed a striking transient surge in ASIC current density at d4–d6 of differentiation of LUHMES cells, when current densities were 3- to 4-fold higher than at d2 or d12 and reached 160 pA/pF (**Figure 2**). For comparison, the average ASIC current density was 30 pA/pF in a study using human cortical neurons (Li et al., 2010a) and 22 pA/pF in sensory neurons derived from human pluripotent stem cells (Young et al., 2014). ASIC current amplitude in human glioblastoma derived stem cell lines was variable but mostly <300 pA, corresponding to <15 pA/pF (with a mean cell capacitance of 20 pF; Tian et al., 2017). Thus, while the ASIC current density up to d2 and after d10 was comparable to other human neurons, at d5 it was substantially higher. This surge was not paralleled or preceded by a similar increase in ASIC1a mRNA of protein (**Figure 1**), suggesting that the increase in functional ASIC1a on the surface of LUHMES cells was due either to a more efficient forward trafficking of preformed channels that were for example residing in the ER or to a reduced endocytosis of functional channels. It has previously been shown that in CHO cells and mouse cortical neurons, most of the ASIC1a pool resides in intracellular compartments, mainly the ER, and that the ASIC current density in these cells can be rapidly (within 1 h) increased upon insulin depletion (Chai et al., 2010). The surge in ASIC current density during differentiation of LUHMES cells cannot be attributed to the depletion of insulin, however, because the N2 supplement in proliferation and in differentiation medium contains insulin. Moreover, the increase in ASIC current amplitude in our study occurred on the order of days while in the previous study after insulin depletion it occurred on the order of hours (Chai et al., 2010). Although the mechanism for the strong surge in ASIC current density during the first week of differentiation remains unknown, a more efficient forward trafficking is an attractive hypothesis.

The surge in ASIC current density parallels the appearance of excitability during differentiation of LUHMES cells (**Figure 5**). A previous study also found an almost linear increase in current density of voltage-gated Na^+ channels from d3 to d11 (Scholz et al., 2011). The high ASIC current density might ensure a robust depolarization by acidic stimuli when LUHMES cells are not terminally differentiated. As activation of ASIC1a at d5 also induced robust Ca^{2+} signals (**Figure 6**), ASICs might be essential for maturation of LUHMES cells. In support of this idea, the surge in ASIC expression coincides with a strong increase of synaptic markers in LUHMES cells, which occurs during the first day and peaks on d6 (Scholz et al., 2011). Moreover, a study characterizing ionic conductance's in rat neuronal precursor cells reported that amiloride-sensitive proton-activated Na^+ currents were of large amplitude and appeared in parallel to voltage-gated Na^+ and Ca^{2+} channels but preceded glutamate-gated ion channels by several days (Grantyn et al., 1989). The authors suggested that the proton-activated Na^+ currents are present during the earliest stages of neuronal development and may regulate a variety of Ca^{2+}-catalyzed processes during development of neurons (Grantyn et al., 1989). Our own results support this hypothesis. After d6, when LUHMES cells became more easily excitable and the resting membrane potential less negative with a decrease in rheobase current (**Figure 5**), ASIC1a current density decreased again (**Figure 2**).

It has previously been shown that transfection of ASIC1a into hippocampal slices increased the density of dendritic spines (Zha et al., 2006). Decreasing ASIC1a protein levels by siRNA had the opposite effect (Zha et al., 2006). In contrast, ASIC1a-deficient mice had no difference in hippocampal spine density compared with wildtype mice, suggesting compensatory mechanisms during development of ASIC1-knockout mice (Zha et al., 2006). The effects of ASIC1 on spine density required CaMKII, suggesting an important role for acid-induced Ca^{2+} increases (Zha et al., 2006). Our results show that in the presence of the ASIC pore blocker diminazene (Schmidt et al., 2017), the length of neurites was decreased (**Figure 7**), suggesting a role for ASIC1a for the maturation of LUHMES cells into neurons. Although preliminary, these results are similar to previous findings in mouse neuroblastoma-derived NS20Y cells (O'Bryant et al., 2016). Thus, one specific role for ASIC1a during neuronal maturation might be the Ca^{2+}-dependent maturation of neurites and dendrites.

In summary, our study establishes dopaminergic LUHMES cells as a valuable model to study the role of ASICs during neuronal development in a human cell line.

DATA AVAILABILITY STATEMENT

The original contributions presented in the study are included in the article, further inquiries can be directed to the corresponding author/s.

AUTHOR CONTRIBUTIONS

AN performed the qPCR, most voltage clamp experiments and determined neurite lengths. YT performed the Western blots, current clamp experiments and Ca^{2+} imaging. AR performed voltage clamp experiments with PcTx1. AN and YT analyzed the data and participated in the design of the study. SG and BF conceived the study, designed and coordinated the study, and participated in data analysis. AN, SG, and BF drafted the manuscript. All authors contributed to the article and approved the submitted version.

FUNDING

This work was supported by a grant from the Interdisciplinary Center for Clinical Research within the Faculty of Medicine at RWTH Aachen University to BF and SG.

ACKNOWLEDGMENTS

We thank A. Oslender-Bujotzek and S. Joussen for expert technical assistance. LUHMES cells were a kind gift from M. Leist, University of Konstanz, Germany.

REFERENCES

Arias, R. L., Sung, M. L. A., Vasylyev, D., Zhang, M. Y., Albinson, K., Kubek, K., et al. (2008). Amiloride is neuroprotective in an MPTP model of Parkinson's disease. *Neurobiol. Dis.* 31, 334–341. doi: 10.1016/j.nbd.2008.05.008

Askwith, C. C., Wemmie, J. A., Price, M. P., Rokhlina, T., and Welsh, M. J. (2004). Acid-sensing ion channel 2 (ASIC2) modulates ASIC1 H+-activated currents in hippocampal neurons. *J. Biol. Chem.* 279, 18296–18305. doi: 10.1074/jbc.M312145200

Babini, E., Paukert, M., Geisler, H. S., and Gründer, S. (2002). Alternative splicing and interaction with di- and polyvalent cations control the dynamic range of acid-sensing ion channel 1 (ASIC1). *J. Biol. Chem.* 277, 41597–41603. doi: 10.1074/jbc.M205877200

Baron, A., Voilley, N., Lazdunski, M., and Lingueglia, E. (2008). Acid sensing ion channels in dorsal spinal cord neurons. *J. Neurosci.* 28, 1498–1508. doi: 10.1523/JNEUROSCI.4975-07.2008

Baron, A., Waldmann, R., and Lazdunski, M. (2002). ASIC-like, proton-activated currents in rat hippocampal neurons. *J. Physiol.* 539, 485–494. doi: 10.1113/jphysiol.2001.014837

Bartoi, T., Augustinowski, K., Polleichtner, G., Gründer, S., and Ulbrich, M. H. (2014). Acid-sensing ion channel (ASIC) 1a/2a heteromers have a flexible 2:1/1:2 stoichiometry. *Proc. Natl. Acad. Sci. U S A* 111, 8281–8286. doi: 10.1073/pnas.1324060111

Bassilana, F., Champigny, G., Waldmann, R., De Weille, J. R., Heurteaux, C., and Lazdunski, M. (1997). The acid-sensitive ionic channel subunit ASIC and the mammalian degenerin MDEG form a heteromultimeric H+-gated Na+ channel with novel properties. *J. Biol. Chem.* 272, 28819–28822. doi: 10.1074/jbc.272.46.28819

Benson, C. J., Xie, J., Wemmie, J. A., Price, M. P., Henss, J. M., Welsh, M. J., et al. (2002). Heteromultimers of DEG/ENaC subunits form H+-gated channels in mouse sensory neurons. *Proc. Natl. Acad. Sci. U S A* 99, 2338–2343. doi: 10.1073/pnas.032678399

Chai, S., Li, M. H., Branigan, D., Xiong, Z. G., and Simon, R. P. (2010). Activation of acid-sensing ion channel 1a (ASIC1a) by surface trafficking. *J. Biol. Chemistry* 285, 13002–13011. doi: 10.1074/jbc.M109.086041

Chassagnon, I. R., Mccarthy, C. A., Chin, Y. K., Pineda, S. S., Keramidas, A., Mobli, M., et al. (2017). Potent neuroprotection after stroke afforded by a double-knot spider-venom peptide that inhibits acid-sensing ion channel 1a. *Proc. Natl. Acad. Sci. U S A* 114, 3750–3755. doi: 10.1073/pnas.1614728114

Chen, X., and Gründer, S. (2007). Permeating protons contribute to tachyphylaxis of the acid-sensing ion channel (ASIC) 1a. *J. Physiol.* 579, 657–670. doi: 10.1113/jphysiol.2006.120733

Chu, X. P., Wemmie, J. A., Wang, W. Z., Zhu, X. M., Saugstad, J. A., Price, M. P., et al. (2004). Subunit-dependent high-affinity zinc inhibition of acid-sensing ion channels. *J. Neurosci.* 24, 8678–8689. doi: 10.1523/JNEUROSCI.2844-04.2004

Dauer, W., and Przedborski, S. (2003). Parkinson's disease: mechanisms and models. *Neuron* 39, 889–909. doi: 10.1016/s0896-6273(03)00568-3

Delaunay, A., Gasull, X., Salinas, M., Noel, J., Friend, V., Lingueglia, E., et al. (2012). Human ASIC3 channel dynamically adapts its activity to sense the extracellular pH in both acidic and alkaline directions. *Proc. Natl. Acad. Sci. U S A* 109, 13124–13129. doi: 10.1073/pnas.1120350109

Doi, D., Samata, B., Katsukawa, M., Kikuchi, T., Morizane, A., Ono, Y., et al. (2014). Isolation of human induced pluripotent stem cell-derived dopaminergic progenitors by cell sorting for successful transplantation. *Stem Cell. Rep.* 2, 337–350. doi: 10.1016/j.stemcr.2014.01.013

Du, J., Reznikov, L. R., Price, M. P., Zha, X. M., Lu, Y., Moninger, T. O., et al. (2014). Protons are a neurotransmitter that regulates synaptic plasticity in the lateral amygdala. *Proc. Natl. Acad. Sci. U S A* 111, 8961–8966. doi: 10.1073/pnas.1407018111

Duda, J., Pötschke, C., and Liss, B. (2016). Converging roles of ion channels, calcium, metabolic stress and activity pattern of Substantia nigra dopaminergic neurons in health and Parkinson's disease. *J. Neurochem.* 139, 156–178. doi: 10.1111/jnc.13572

Escoubas, P., De Weille, J. R., Lecoq, A., Diochot, S., Waldmann, R., Champigny, G., et al. (2000). Isolation of a tarantula toxin specific for a class of proton-gated Na+ channels. *J. Biol. Chem.* 275, 25116–25121. doi: 10.1074/jbc.M003643200

Friese, M. A., Craner, M. J., Etzensperger, R., Vergo, S., Wemmie, J. A., Welsh, M. J., et al. (2007). Acid-sensing ion channel-1 contributes to axonal degeneration in autoimmune inflammation of the central nervous system. *Nat. Med.* 13, 1483–1489. doi: 10.1038/nm1668

García-Añoveros, J., Derfler, B., Neville-Golden, J., Hyman, B. T., and Corey, D. P. (1997). BNaC1 and BNaC2 constitute a new family of human neuronal sodium channels related to degenerins and epithelial sodium channels. *Proc. Natl. Acad. Sci. U S A* 94, 1459–1464. doi: 10.1073/pnas.94.4.1459

Gibb, W. R. G., and Lees, A. J. (1991). Anatomy, pigmentation, ventral and dorsal subpopulations of the substantia-nigra and differential cell-death in Parkinsons-disease. *J. Neurol. Neurosurg. Psychiatry* 54, 388–396. doi: 10.1136/jnnp.54.5.388

Gonzalez-Inchauspe, C., Urbano, F. J., Di Guilmi, M. N., and Uchitel, O. D. (2017). Acid-sensing ion channels activated by evoked released protons modulate synaptic transmission at the mouse calyx of held synapse. *J. Neurosci.* 37, 2589–2599. doi: 10.1523/JNEUROSCI.2566-16.2017

Grantyn, R., Perouansky, M., Rodriguez-Tebar, A., and Lux, H. D. (1989). Expression of depolarizing voltage- and transmitter-activated currents in neuronal precursor cells from the rat brain is preceded by a proton-activated sodium current. *Dev. Brain Res.* 49, 150–155. doi: 10.1016/0165-3806(89)90070-9

Gründer, S. (2020). "Acid-sensing ion channels," in *The Oxford Handbook of Neuronal Ion Channels*. ed A. Bhattacharjee (Oxford, UK: Oxford University Press), 1–56. doi: 10.1093/oxfordhb/9780190669164.013.12

Halliday, G. M., Leverenz, J. B., Schneider, J. S., and Adler, C. H. (2014). The neurobiological basis of cognitive impairment in Parkinson's disease. *Mov. Disord.* 29, 634–650. doi: 10.1002/mds.25857

Hattori, T., Chen, J., Harding, A. M., Price, M. P., Lu, Y., Abboud, F. M., et al. (2009). ASIC2a and ASIC3 heteromultimerize to form pH-sensitive channels in mouse cardiac dorsal root ganglia neurons. *Circ. Res.* 105, 279–286. doi: 10.1161/CIRCRESAHA.109.202036

Hoagland, E. N., Sherwood, T. W., Lee, K. G., Walker, C. J., and Askwith, C. C. (2010). Identification of a calcium permeable human acid-sensing ion channel 1 transcript variant. *J. Biol. Chem.* 285, 41852–41862. doi: 10.1074/jbc.M110.171330

Joeres, N., Augustinowski, K., Neuhof, A., Assmann, M., and Gründer, S. (2016). Functional and pharmacological characterization of two different ASIC1a/2a heteromers reveals their sensitivity to the spider toxin PcTx1. *Sci. Rep.* 6:27647. doi: 10.1038/srep27647

Kreple, C. J., Lu, Y., Taugher, R. J., Schwager-Gutman, A. L., Du, J., Stump, M., et al. (2014). Acid-sensing ion channels contribute to synaptic transmission and inhibit cocaine-evoked plasticity. *Nat. Neurosci.* 17, 1083–1091. doi: 10.1038/nn.3750

Lang, A. E., and Espay, A. J. (2018). Disease modification in Parkinson's disease: current approaches, challenges and future considerations. *Mov. Dis.* 33, 660–677. doi: 10.1002/mds.27360

Li, M., Inoue, K., Branigan, D., Kratzer, E., Hansen, J. C., Chen, J. W., et al. (2010a). Acid-sensing ion channels in acidosis-induced injury of human brain neurons. *J. Cereb. Blood Flow Metab.* 30, 1247–1260. doi: 10.1038/jcbfm.2010.30

Li, M., Kratzer, E., Inoue, K., Simon, R. P., and Xiong, Z. G. (2010b). Developmental change in the electrophysiological and pharmacological properties of acid-sensing ion channels in CNS neurons. *J. Physiol.* 588, 3883–3900. doi: 10.1113/jphysiol.2010.192922

Lingueglia, E., De Weille, J. R., Bassilana, F., Heurteaux, C., Sakai, H., Waldmann, R., et al. (1997). A modulatory subunit of acid sensing ion channels in brain and dorsal root ganglion cells. *J. Biol. Chem.* 272, 29778–29783. doi: 10.1074/jbc.272.47.29778

Lotharius, J., Barg, S., Wiekop, P., Lundberg, C., Raymon, H. K., Brundin, P., et al. (2002). Effect of mutant alpha-synuclein on dopamine homeostasis in a new human mesencephalic cell line. *J. Biol. Chem.* 277, 38884–38894. doi: 10.1074/jbc.M205518200

Lotharius, J., Falsig, J., Van Beek, J., Payne, S., Dringen, R., Brundin, P., et al. (2005). Progressive degeneration of human mesencephalic neuron-derived cells triggered by dopamine-dependent oxidative stress is dependent on the mixed-lineage kinase pathway. *J. Neurosci.* 25, 6329–6342. doi: 10.1523/JNEUROSCI.1746-05.2005

O'Bryant, Z., Leng, T. D., Liu, M. L., Inoue, K., Vann, K. T., Xiong, Z. G., et al. (2016). Acid Sensing Ion Channels (ASICs) in NS20Y cells - potential role in neuronal differentiation. *Mol. Brain* 9:68. doi: 10.1186/s13041-016-0249-8

Pidoplichko, V. I., and Dani, J. A. (2006). Acid-sensitive ionic channels in midbrain dopamine neurons are sensitive to ammonium, which may contribute to hyperammonemia damage. *Proc. Natl. Acad. Sci. U S A* 103, 11376–11380. doi: 10.1073/pnas.0600768103

Price, M. P., Snyder, P. M., and Welsh, M. J. (1996). Cloning and expression of a novel human brain Na+ channel. *J. Biol. Chem.* 271, 7879–7882. doi: 10.1074/jbc.271.14.7879

Schmidt, A., Rossetti, G., Joussen, S., and Gründer, S. (2017). Diminazene is a slow pore blocker of acid-sensing ion channel 1a (ASIC1a). *Mol. Pharmacol.* 92, 665–675.

Scholz, D., Poltl, D., Genewsky, A., Weng, M., Waldmann, T., Schildknecht, S., et al. (2011). Rapid, complete and large-scale generation of post-mitotic neurons from the human LUHMES cell line. *J. Neurochem.* 119, 957–971. doi: 10.1111/j.1471-4159.2011.07255.x

Sherwood, T. W., Lee, K. G., Gormley, M. G., and Askwith, C. C. (2011). Heteromeric acid-sensing ion channels (ASICs) composed of ASIC2b and ASIC1a display novel channel properties and contribute to acidosis-induced neuronal death. *J. Neurosci.* 31, 9723–9734. doi: 10.1523/JNEUROSCI.1665-11.2011

Suman, A., Mehta, B., Guo, M. L., Chu, X. P., Fibuch, E. E., Mao, L. M., et al. (2010). Alterations in subcellular expression of acid-sensing ion channels in the rat forebrain following chronic amphetamine administration. *Neurosci. Res.* 68, 1–8. doi: 10.1016/j.neures.2010.06.001

Tian, Y., Bresenitz, P., Reska, A., El Moussaoui, L., Beier, C.P., and Gründer, S. (2017). Glioblastoma cancer stem cell lines express functional acid sensing ion channels ASIC1a and ASIC3. *Sci. Rep.* 7:13674. doi: 10.1038/s41598-017-13666-9

Vaithia, A., Vullo, S., Peng, Z., Alijevic, O., and Kellenberger, S. (2019). Accelerated current decay kinetics of a rare human acid-sensing ion channel 1a variant that is used in many studies as wild type. *Front. Mol. Neurosci.* 12:133. doi: 10.3389/fnmol.2019.00133

Waldmann, R., Champigny, G., Bassilana, F., Heurteaux, C., and Lazdunski, M. (1997). A proton-gated cation channel involved in acid-sensing. *Nature* 386, 173–177. doi: 10.1038/386173a0

Wang, Y. Z., Wang, J. J., Huang, Y., Liu, F., Zeng, W. Z., Li, Y., et al. (2015). Tissue acidosis induces neuronal necroptosis *via* ASIC1a channel independent of its ionic conduction. *eLife* 4:e05682. doi: 10.7554/eLife.05682

Wemmie, J. A., Askwith, C. C., Lamani, E., Cassell, M. D., and Freeman, J. H. Jr. (2003). Acid-sensing ion channel 1 is localized in brain regions with high synaptic density and contributes to fear conditioning. *J. Neurosci.* 23, 5496–5502. doi: 10.1523/JNEUROSCI.23-13-05496.2003

Wu, L. J., Duan, B., Mei, Y. D., Gao, J., Chen, J. G., Zhuo, M., et al. (2004). Characterization of acid-sensing ion channels in dorsal horn neurons of rat spinal cord. *J. Biol. Chem.* 279, 43716–43724. doi: 10.1074/jbc.M403557200

Xi, J. J., Liu, Y., Liu, H. S., Chen, H., Emborg, M. E., Zhang, S. C., et al. (2012). Specification of midbrain dopamine neurons from primate pluripotent stem cells. *Stem Cells* 30, 1655–1663. doi: 10.1002/stem.1152

Xiong, Q. J., Hu, Z. L., Wu, P. F., Ni, L., Deng, Z. F., Wu, W. N., et al. (2012). Acid-sensing ion channels contribute to the increase in vesicular release from SH-SY5Y cells stimulated by extracellular protons. *Am. J. Physiol. Cell Physiol.* 303, C376–C384. doi: 10.1152/ajpcell.00067.2012

Xu, Y., Jiang, Y. Q., Li, C., He, M., Rusyniak, W. G., Annamdevula, N., et al. (2018). Human ASIC1a mediates stronger acid-induced responses as compared with mouse ASIC1a. *FASEB J.* 32, 3832–3843. doi: 10.1096/fj.201701367R

Young, G. T., Gutteridge, A., Fox, H., Wilbrey, A. L., Cao, L., Cho, L. T., et al. (2014). Characterizing human stem cell-derived sensory neurons at the single-cell level reveals their ion channel expression and utility in pain research. *Mol. Ther.* 22, 1530–1543. doi: 10.1038/mt.2014.86

Zha, X. M., Wemmie, J. A., Green, S. H., and Welsh, M. J. (2006). Acid-sensing ion channel 1a is a postsynaptic proton receptor that affects the density of dendritic spines. *Proc. Natl. Acad. Sci. U S A* 103, 16556–16561. doi: 10.1073/pnas.0608018103

Zhai, S. Y., Shen, W. X., Graves, S. M., and Surmeier, D. J. (2019). Dopaminergic modulation of striatal function and Parkinson's disease. *J. Neural Transm.* 126, 411–422. doi: 10.1007/s00702-019-01997-y

Zhang, G. C., Mao, L. M., Wang, J. Q., and Chu, X. P. (2009). Upregulation of acid-sensing ion channel 1 protein expression by chronic administration of cocaine in the mouse striatum *in vivo*. *Neurosci. Lett.* 459, 119–122. doi: 10.1016/j.neulet.2009.05.013

Conflict of Interest: The authors declare that the research was conducted in the absence of any commercial or financial relationships that could be construed as a potential conflict of interest.

frontiers in Physiology

OPINION
published: 07 September 2021
doi: 10.3389/fphys.2021.734418

Acid-Sensing Ion Channel 1 Contributes to Weak Acid-Induced Migration of Human Malignant Glioma Cells

Sareena Shah[1], *Yuyang Chu*[2], *Victoria Cegielski*[1] *and Xiang-Ping Chu*[1]*

[1] Department of Biomedical Sciences, School of Medicine, University of Missouri-Kansas City, Kansas City, MO, United States, [2] Feinberg School of Medicine, Northwestern University, Chicago, IL, United States

Keywords: acid-sensing ion channel 1, human malignant glioma cells, migration, acidosis, patch-clamp recording

OPEN ACCESS

Edited by:
Osvaldo D. Uchitel, University of Buenos Aires, Argentina

Reviewed by:
Mingli Liu, Morehouse School of Medicine, United States

***Correspondence:**
Xiang-Ping Chu
chux@umkc.edu

Specialty section:
This article was submitted to Membrane Physiology and Membrane Biophysics, a section of the journal Frontiers in Physiology

Received: *01 July 2021*
Accepted: *16 August 2021*
Published: *07 September 2021*

Citation:
Shah S, Chu Y, Cegielski V and Chu X-P (2021) Acid-Sensing Ion Channel 1 Contributes to Weak Acid-Induced Migration of Human Malignant Glioma Cells. Front. Physiol. 12:734418. doi: 10.3389/fphys.2021.734418

INTRODUCTION

Glioblastoma multiform (GBM), also referred to as glioblastoma, is the most common malignant tumor in the brain, known for its resistance to therapeutic agents and poor prognosis (Shergalis et al., 2018). Recent studies have seen success of some target compounds in combating GBMs in laboratory settings; however, these compounds failed in clinical trials (Mandel et al., 2018). Multiple factors may have contributed to this drug failure in GBM treatment, including difficulty penetrating the blood-brain barrier (BBB), an immunosuppressive microenvironment, and complex intratumoral heterogeneity (Khaddour et al., 2020; Ou et al., 2020). Difficulty in treating GBMs has led to a 5-year survival rate of <7.2% in humans. This is the lowest long-term rate of malignant brain tumors (Ostrom et al., 2020). Current treatment options for patients with GBM include surgical resection and a combination of chemotherapy, radiotherapy, and immunotherapy (Carlsson et al., 2014; Suter et al., 2020; Wen et al., 2020; Medikonda et al., 2021). Surgical resection is the most effective way to increase short-term survival rate, with research demonstrating a higher 1-year survival rate in patients with at least a 90% surgical resection compared to those without one (Medikonda et al., 2021). Yet, the long-term survival rate remains the same, suggesting that tumor recurrence is very likely (Yu et al., 2021).

GBMs, like many other tumors, have an acidic microenvironment due to the tumor's high rate of metabolism and limited blood supply (Tian et al., 2017). Acidosis may result from an accumulation of acid or an increase of partial pressure of carbon dioxide in tissues, which can cause lactic acid build-up in the brain (Chesler, 2003). Excessive lactic acid in the brain can damage metabolic functionality, hindering recirculation and reoxygenation throughout the body (Siesjö, 1982; Siesj et al., 1993; Rehncrona, 2005). Studies have demonstrated that acidosis can activate a family of ligand-gated ion channels: acid-sensing ion channels (ASICs), which are widely expressed in neurons (Waldmann et al., 1997; Xiong et al., 2004; Krishtal, 2015). ASICs are formed through different combinations of subunits, either homotrimeric or heterotrimeric, constituting different electrophysiological and pharmacological properties (Gründer and Pusch, 2015; Vullo and Kellenberger, 2020). The activation of ASICs induces neuronal depolarization and generates action potentials mostly due to the influx of Na^+ ions (Jiang et al., 2009; Boscardin et al., 2016). ASICs play critical roles in several physiological processes including synaptic plasticity, pain sensation, and fear conditioning (Wemmie et al., 2013; Huang et al., 2015; Uchitel et al., 2019; Storozhuka et al., 2021). They also contribute to several neurodegenerative disorders such as Parkinson's disease and multiple sclerosis (Chu and Xiong, 2012; Chu et al., 2014; Ortega-Ramírez et al., 2017). Additionally, ASICs are expressed in glial cells (Lin et al., 2010), particularly ASIC1, whose activation in glial cell lines has been linked to migration and proliferation of the GBMs

(Berdiev et al., 2003; Bubien et al., 2004; Kapoor et al., 2009, 2011; Rooj et al., 2012). Glioma tumors aggressively destroy surrounding tissues while growing in the brain, displaying acidosis and resulting in pathophysiological consequences (Honasoge and Sontheimer, 2013). ASIC expression in glioma cells generates a Na^+ current which contributes to its volume and migration (Rooj et al., 2012). Active conductance has been observed in gliomas due to the presence of ASICs and epithelial sodium channels, which can impact cell cycle progression (Kapoor et al., 2009). The impact of ASICs, particularly ASIC1, in glial cell lines is being further investigated in efforts to reduce glial cell migration, study the potential proliferation effects, and to understand how ASIC1 inhibitors can regulate apoptosis of glioma cells (Sun et al., 2013; Tian et al., 2017). ASIC1 gene expression in glioma cells can predict outcomes of carcinomas as they act as genomic biomarkers; therefore, finding more inhibitors to ASICs may provide potential therapeutic agents to inhibit glioma cell activity (Sun et al., 2013; Bychkov et al., 2020; Griffin et al., 2020).

ASIC1 CONTRIBUTES TO WEAK ACID-INDUCED MIGRATION OF HUMAN MALIGNANT CELLS

A recent study from Dr. Xiong's laboratory published in the *American Journal of Cancer Research* described a combination of wet-lab techniques, including whole-cell patch-clamp recording, Western blotting, cell viability assay, wound-healing assay and trans-well migration assay, that were used to determine if the activation of ASIC1 by a weak acid (e.g., pH 7.0) had a correlation with the migration and proliferation of glial cell lines U87MG and A172 (Sheng et al., 2021). The study determined the expression of ASIC1 in glioblastoma cell lines, along with the induction of transient inward currents when the pH was dropped from 7.4 to 6.0, suggesting the existence of acid-activated currents in glioblastoma cell lines. When PcTx1, a selective ASIC1 inhibitor, was introduced, there was a decrease in acid-activated currents, indicating that ASIC1 was involved. The study also examined cell viability of A172 and U87MG cells when treated under different pH conditions (e.g., pH 7.4 and pH 7.0) to determine if weak acidosis could affect proliferation of the cells; however, they found that neither acidosis nor the addition of PcTx1 had an influence on cell viability of the two glioma cells, suggesting that weak acidosis has no effect on proliferation of human glioma cells. Using a wound healing assay, they investigated whether weak acid could promote migration of A172 and U87MG cells and found that weak acid did increase the migration rate by 26% in A172 cells and 67% in U87MG cells, respectively. When PcTx1 was introduced, it inhibited both glioma cells from migrating. Further investigation of this migration was conducted using a trans-well migration assay and revealed similar results. They also found that there was a heavier expression of the ASIC1 protein in U87MG cells compared to the expression in A172 cells, indicating that different cell lines of GBMs have different levels of ASIC1 expression. The study also introduced ASIC1-siRNA to U87MG cells, which silences ASIC1 expression, to better understand the influence of this protein on migration induced by treatment of weak acidosis. When compared to the control group, application of ASIC1-siRNA decreased the expression of the ASIC1 protein and did not affect the proliferation of U87MG cells, but it reduced the migration of U87MG cells under weak acidic conditions. Collectively, the results demonstrate that activation of ASIC1 by weak acidosis in glioma cells A172 and U87MG promotes migration of the cells but not proliferation, while PcTx1 inhibits migration of glioma cells. These findings suggest that ASIC1 could serve as a potential therapeutic target for GBMs.

PERSPECTIVE

Although there are several studies of ASICs in the pathophysiology of glioma cells (Berdiev et al., 2003; Bubien et al., 2004; Kapoor et al., 2009, 2011; Rooj et al., 2012), this study uniquely dives deeper into the connection between weak acidosis activated ASIC1 and its effect on the migration of glioma cells (Sheng et al., 2021). A recent study from Dr. Grunder's group reported that glioblastoma stem cell (GSC) lines (R8 and R54) express functional ASIC1 and ASIC3, and their data suggest that expression of ASICs is associated with an improved survival in GSC lines (Tian et al., 2017). This result is inconsistent with other studies (Kapoor et al., 2009; Sheng et al., 2021). One possibility might be due to different glioblastoma cell lines used in different studies, suggesting the complexity of GBM. Therefore, additional studies might be necessary to further delineate the precise role of ASIC1 in high-grade glioblastoma. This study solely focuses on glial cells U87MG and A172, so it would be beneficial to utilize the same wet-lab techniques for cultured human glioma cells directly from the patients and see if parallel correlations are found. It would also be interesting to test PcTx1 on cultured human glioma cells to see whether it has any effects on glioma growth during a small pH drop (pH 7.0). In most whole-cell recordings, ASICs deactivate fast in response to brief pH stimulation (Gründer and Pusch, 2015). Even a small decrease in pH leads to profound steady state desensitization of ASICs. Therefore, it is intriguing how migration of high-grade gliomas could be promoted via ASIC continuously subjected to a slightly acidic pH, and the exact mechanism should be explored in the near future. Interestingly, a recent study demonstrates that the deactivation of ASIC1a is steeply dependent on the pH, spanning nearly three orders of magnitude from extremely fast (<1 ms) at pH 8.0 to very slow (more than 300 ms) at pH 7.0 (MacLean and Jayaraman, 2017). In addition, like most of ligand-gated ion channels, the desensitization of ASIC is also pH-dependent, with much slower desensitization occurs in response to a smaller pH drop (e.g., to 7.0) than a bigger pH drop (e.g., to 6.0). Although the current amplitude might be small with a small pH drop (Sheng et al., 2021), the current may last for a long period of time. Another possibility is that, in intact cells where cellular components are not washed out like in whole-cell recordings, the kinetics of ASIC1a current could be completely different. Additionally, the study from Dr. Xiong's group (Sheng et al., 2021) focuses on glial cells U87MG and A172 being

introduced to a weak acid, but it would be insightful to compare the migration of these glial cell lines when introduced to a larger pH drop (e.g., pH 6.0). Further investigation may determine the consequences of cell migration under permanent inhibition of ASIC1 in glioma cells. Several existing studies have used PcTx1 or Mambalgin-2 as an ASIC1 inhibitor (Kellenberger and Schild, 2015; Dibas et al., 2019). However, it is necessary to explore other therapeutic agents since PcTx1 and Mambalgin-2 cannot be used in clinical settings due to their inability to cross the BBB (Sun et al., 2013; Bychkov et al., 2020). Therefore, determining effective delivery pathways for ASIC1 inhibitors is needed for the clinical treatment of GBMs. From a more malignant standpoint, late-stage glioma cells express high levels of ASIC1a, which is not portrayed in normal astrocytes. Thus, learning more about how and why ASIC1 expression changes in higher-grade gliomas may be vital in determining optimal treatment plans for patients with gliomas (Sun et al., 2013; Wang et al., 2015).

AUTHOR CONTRIBUTIONS

All authors listed have made a substantial, direct and intellectual contribution to the work and approved it for publication.

FUNDING

The work was supported by grant from American Heart Association (19AIREA34470007) to X-PC.

ACKNOWLEDGMENTS

We thank Dr. Zhi-Gang Xiong from Morehouse School of Medicine for his critical reading of this manuscript.

REFERENCES

Berdiev, B. K., Xia, J., McLean, L. A., Markert, J. M., Gillespie, G. Y., Mapstone, T. B., et al. (2003). Acid-sensing ion channels in malignant gliomas. *J. Biol. Chem.* 278, 15023–15034. doi: 10.1074/jbc.M300991200

Boscardin, E., Alijevic, O., Hummler, E., Frateschi, S., and Kellenberger, S. (2016). The function and regulation of acid-sensing ion channels (ASICs) and the epithelial Na^+ channel (ENaC): IUPHAR Review 19. *Br. J. Pharmacol.* 173, 2671–2701. doi: 10.1111/bph.13533

Bubien, J. K., Ji, H. L., Gillespie, G. Y., Fuller, C. M., Markert, J. M., Mapstone, T. B., et al. (2004). Cation selectivity and inhibition of malignant glioma Na^+ channels by Psalmotoxin 1. *Am. J. Physiol,. Cell Physiol.* 287, C1282–1291. doi: 10.1152/ajpcell.00077.2004

Bychkov, M., Shulepko, M., Osmakov, D., Andreev, Y., Sudarikova, A., Vasileva, V., et al. (2020). Mambalgin-2 induces cell cycle arrest and apoptosis in glioma cells via interaction with ASIC1a. *Cancers* 12:1837. doi: 10.3390/cancers12071837

Carlsson, S. K., Brothers, S. P., and Wahlestedt, C. (2014). Emerging treatment strategies for glioblastoma multiforme. *EMBO Mol. Med.* 6, 1359–1370. doi: 10.15252/emmm.201302627

Chesler, M. (2003). Regulation and modulation of pH in the brain. *Physiol. Rev.* 83, 1183–1221. doi: 10.1152/physrev.00010.2003

Chu, X.-P., Grasing, K. A., and Wang, J. Q. (2014). Acid-sensing ion channels contribute to neurotoxicity. *Transl. Stroke Res.* 5, 69–78. doi: 10.1007/s12975-013-0305-y

Chu, X.-P., and Xiong, Z.-G. (2012). Physiological and pathological functions of acid-sensing ion channels in the central nervous system. *Curr. Drug Targets.* 13, 263–271. doi: 10.2174/138945012799201685

Dibas, J., Al-Saad, H., and Dibas, A. (2019). Basics on the use of acid-sensing ion channels' inhibitors as therapeutics. *Neural Regen. Res.* 14, 395–398. doi: 10.4103/1673-5374.245466

Griffin, M., Khan, R., Basu, S., and Smith, S. (2020). Ion channels as therapeutic targets in high grade gliomas. *Cancers* 12:3068. doi: 10.3390/cancers12103068

Gründer, S., and Pusch, M. (2015). Biophysical properties of acid-sensing ion channels (ASICs). *Neuropharmacology* 94, 9–18. doi: 10.1016/j.neuropharm.2014.12.016

Honasoge, A., and Sontheimer, H. (2013). Involvement of tumor acidification in brain cancer pathophysiology. *Front. Physiol.* 4:316. doi: 10.3389/fphys.2013.00316

Huang, Y., Jiang, N., Ji, Y., Xiong, Z., and Zha, X. (2015). Two aspects of ASIC function: synaptic plasticity and neuronal injury. *Neuropharmacology* 94, 42–48. doi: 10.1016/j.neuropharm.2014.12.010

Jiang, Q., Li, M. H., Papasian, C. J., Branigan, D., Xiong, Z. G., Wang, J. Q., et al. (2009). Characterization of acid-sensing ion channels in medium spiny neurons of mouse striatum. *Neuroscience* 162, 55–66. doi: 10.1016/j.neuroscience.2009.04.029

Kapoor, N., Bartoszewski, R., Qadri, Y. J., Bebok, Z., Bubien, J. K., Fuller, C. M., et al. (2009). Knockdown of ASIC1 and epithelial sodium channel subunits inhibits glioblastoma whole cell current and cell migration. *J. Biol. Chem.* 284, 24526–24541. doi: 10.1074/jbc.M109.037390

Kapoor, N., Lee, W., Clark, E., Bartoszewski, R., McNicholas, C. M., Latham, C. B., et al. (2011). Interaction of ASIC1 and ENaC subunits in human glioma cells and rat astrocytes. *Am. J. Physiol,. Cell Physiol.* 300, C1246–1259. doi: 10.1152/ajpcell.00199.2010

Kellenberger, S., and Schild, L. (2015). International union of basic and clinical pharmacology. XCI. structure, function, and pharmacology of acid-sensing ion channels and the epithelial Na+ channel. *Pharmacol. Rev.* 67, 1–35. doi: 10.1124/pr.114.009225

Khaddour, K., Johanns, T. M., and Ansstas, G. (2020). The landscape of novel therapeutics and challenges in glioblastoma multiforme: contemporary state and future directions. *Pharmaceuticals* 13:389. doi: 10.3390/ph13110389

Krishtal, O. (2015). Receptor for protons: First observations on acid sensing ion channels. *Neuropharmacology* 94, 4–8. doi: 10.1016/j.neuropharm.2014.12.014

Lin, Y. C., Liu, Y. C., Huang, Y. Y., and Lien, C. C. (2010). High-density expression of Ca^{2+}–permeable ASIC1a channels in NG2 glia of rat hippocampus. *PLoS ONE* 5:e12665. doi: 10.1371/journal.pone.0012665

MacLean, D. M., and Jayaraman, V. (2017). Deactivation kinetics of acid-sensing ion channel 1a are strongly pH-sensitive. *Proc. Natl. Acad. Sci. USA.* 114, E2504–E2513. doi: 10.1073/pnas.1620508114

Mandel, J. J., Youssef, M., Ludmir, E., Yust-Katz, S., Patel, A. J., and De Groot, J. F. (2018). Highlighting the need for reliable clinical trials in glioblastoma. *Expert Rev. Anticancer Ther.* 18, 1031–1040. doi: 10.1080/14737140.2018.1496824

Medikonda, R., Dunn, G., Rahman, M., Fecci, P., and Lim, M. (2021). A review of glioblastoma immunotherapy. *J. Neurooncol.* 151, 41–53. doi: 10.1007/s11060-020-03448-1

Ortega-Ramírez, A., Vega, R., and Soto, E. (2017). Acid-sensing ion channels as potential therapeutic targets in neurodegeneration and neuroinflammation. *Mediators Inflamm.* 2017:3728096. doi: 10.1155/2017/3728096

Ostrom, Q. T., Patil, N., Cioffi, G., Waite, K., Kruchko, C., and Barnholtz-Sloan, J. S. (2020). CBTRUS statistical report: primary brain and other central nervous system tumors diagnosed in the United States in 2013-2017. *Neuro Oncol.* 22, iv1–iv96. doi: 10.1093/neuonc/noaa200

Ou, A., Yung, W. K. A., and Majd, N. (2020). Molecular mechanisms of treatment resistance in glioblastoma. *Int. J. Mol. Sci.* 22:351. doi: 10.3390/ijms22010351

Rehncrona, S. (2005). Brain acidosis. *Ann. Emerg. Med.* 14, 770–776. doi: 10.1016/S0196-0644(85)80055-X

Rooj, A. K., McNicholas, C. M., Bartoszewski, R., Bebok, Z., Benos, D. J., and Fuller, C. M. (2012). Glioma-specific cation conductance regulates migration and cell cycle progression. *J. Biol. Chem.* 287, 4053–4065. doi: 10.1074/jbc.M111.311688

Sheng, Y., Wu, B., Leng, T., Zhu, L., and Xiong, Z. (2021). Acid-sensing ion channel 1 (ASIC1) mediates weak acid-induced migration of human malignant glioma cells. *Am. J. Cancer Res.* 11, 997–1008.

Shergalis, A., Bankhead, A. I. I. I., Luesakul, U., Muangsin, N., and Neamati, N. (2018). Current challenges and opportunities in treating glioblastoma. *Pharmacol. Rev.* 70, 412–445. doi: 10.1124/pr.117.014944

Siesj,ö, B. K., Katsura, K., Mellergård, P., Ekholm, A., Lundgren, J., and Smith, M. L. (1993). Acidosis-related brain damage. *Prog. Brain Res.* 96, 23–48. doi: 10.1016/S0079-6123(08)63257-4

Siesjö, B. K. (1982). Lactic acidosis in the brain: occurrence, triggering mechanisms and pathophysiological importance. *Ciba Found. Symp.*87, 77–100. doi: 10.1002/9780470720691.ch5

Storozhuka, M., Cherninskyia, A., Maximyuka, O., Isaeva, D., and Krishtala, O. (2021). Acid-sensing ion channels: focus on physiological and some pathological roles in the brain. *Curr. Neuropharmacol.* doi: 10.2174/1570159X19666210125151824. [Epub ahead of print].

Sun, X., Zhao, D., Li, Y., Sun, Y., Lei, X., Zhang, J., et al. (2013). Regulation of ASIC1 by Ca^{2+}/calmodulin-dependent protein kinase II in human glioblastoma multiforme. *Oncol. Rep.* 30, 2852–2858. doi: 10.3892/or.2013.2777

Suter, R. K., Rodriguez-Blanco, J., and Ayad, N. G. (2020). Epigenetic pathways and plasticity in brain tumors. *Neurobiol. Dis.*145:105060. doi: 10.1016/j.nbd.2020.105060

Tian, Y., Bresenitz, P., Reska, A., Moussaoui, L. E., Beier, C. P., and Gründer, S. (2017). Glioblastoma cancer stem cell lines express functional acid sensing ion channels ASIC1a and ASIC3. *Sci. Rep.* 7:13674. doi: 10.1038/s41598-017-13666-9

Uchitel, O. D., González Inchauspe, C., and Weissmann, C. (2019). Synaptic signals mediated by protons and acid-sensing ion channels. *Synapse* 73:e22120. doi: 10.1002/syn.22120

Vullo, S., and Kellenberger, S. (2020). A molecular view of the function and pharmacology of acid-sensing ion channels. *Pharmacol. Res.* 154:104166. doi: 10.1016/j.phrs.2019.02.005

Waldmann, R., Champigny, G., Bassilana, F., Heurteaux, C., and Lazdunski, M. (1997). A proton-gated cation channel involved in acid-sensing. *Nature* 386, 173–177. doi: 10.1038/386173a0

Wang, R., Gurguis, C., Gu, W., Ko, E. A., Lim, I., Bang, H., et al. (2015). Ion channel gene expression predicts survival in glioma patients. *Sci. Rep.* 5:11593. doi: 10.1038/srep11593

Wemmie, J. A., Taugher, R. J., and Kreple, C. J. (2013). Acid-sensing ion channels in pain and disease. *Nat. Rev. Neurosci.* 14, 461–471. doi: 10.1038/nrn3529

Wen, P. Y., Weller, M., Lee, E. Q., Alexander, B. M., Barnholtz-Sloan, J. S., Barthel, F. P., et al. (2020). Glioblastoma in adults: a Society for Neuro-Oncology (SNO) and European Society of Neuro-Oncology (EANO) consensus review on current management and future directions. *Neuro-oncology.* 22, 1073–1113. doi: 10.1093/neuonc/noaa106

Xiong, Z. G., Zhu, X. M., Chu, X. P., Minami, M., Hey, J., Wei, W. L., et al. (2004). Neuroprotection in ischemia: blocking calcium-permeable acid-sensing ion channels. *Cell* 118, 687–698. doi: 10.1016/j.cell.2004.08.026

Yu, L., Zhang, G., and Qi, S. (2021). Aggressive treatment in glioblastoma: what determines the survival of patients? *J. Neurol. Surg. A Cent. Eur. Neurosurg.* 82, 112–117. doi: 10.1055/s-0040-1713172

Conflict of Interest: The authors declare that the research was conducted in the absence of any commercial or financial relationships that could be construed as a potential conflict of interest.

Publisher's Note: All claims expressed in this article are solely those of the authors and do not necessarily represent those of their affiliated organizations, or those of the publisher, the editors and the reviewers. Any product that may be evaluated in this article, or claim that may be made by its manufacturer, is not guaranteed or endorsed by the publisher.

frontiers in Cellular Neuroscience

REVIEW
published: 17 September 2021
doi: 10.3389/fncel.2021.738043

Acid-Sensing Ion Channels: Expression and Function in Resident and Infiltrating Immune Cells in the Central Nervous System

Victoria S. Foster[1], Lachlan D. Rash[2], Glenn F. King[1,3] and Michelle M. Rank[4]*

[1] Institute for Molecular Bioscience, The University of Queensland, St Lucia, QLD, Australia, [2] School of Biomedical Sciences, The University of Queensland, St Lucia, QLD, Australia, [3] Australian Research Council Centre of Excellence for Innovations in Peptide and Protein Science, The University of Queensland, St Lucia, QLD, Australia, [4] Anatomy and Physiology, Medicine, Dentistry and Health Sciences, The University of Melbourne, Melbourne, VIC, Australia

Peripheral and central immune cells are critical for fighting disease, but they can also play a pivotal role in the onset and/or progression of a variety of neurological conditions that affect the central nervous system (CNS). Tissue acidosis is often present in CNS pathologies such as multiple sclerosis, epileptic seizures, and depression, and local pH is also reduced during periods of ischemia following stroke, traumatic brain injury, and spinal cord injury. These pathological increases in extracellular acidity can activate a class of proton-gated channels known as acid-sensing ion channels (ASICs). ASICs have been primarily studied due to their ubiquitous expression throughout the nervous system, but it is less well recognized that they are also found in various types of immune cells. In this review, we explore what is currently known about the expression of ASICs in both peripheral and CNS-resident immune cells, and how channel activation during pathological tissue acidosis may lead to altered immune cell function that in turn modulates inflammatory pathology in the CNS. We identify gaps in the literature where ASICs and immune cell function has not been characterized, such as neurotrauma. Knowledge of the contribution of ASICs to immune cell function in neuropathology will be critical for determining whether the therapeutic benefits of ASIC inhibition might be due in part to an effect on immune cells.

Keywords: acid-sensing ion channel (ASIC), central nervous system, immune cell, acidosis, neuropathology, neuroimmunology, ion channel

OPEN ACCESS

Edited by:
Enrique Soto, Meritorious Autonomous University of Puebla, Mexico

Reviewed by:
Zhigang Xiong, Morehouse School of Medicine, United States
Marcelo D. Carattino, University of Pittsburgh, United States

****Correspondence:***
Glenn F. King
glenn.king@imb.uq.edu.au

Specialty section:
This article was submitted to Cellular Neurophysiology, a section of the journal Frontiers in Cellular Neuroscience

Received: *08 July 2021*
Accepted: *30 August 2021*
Published: *17 September 2021*

Citation:
Foster VS, Rash LD, King GF and Rank MM (2021) Acid-Sensing Ion Channels: Expression and Function in Resident and Infiltrating Immune Cells in the Central Nervous System. Front. Cell. Neurosci. 15:738043. doi: 10.3389/fncel.2021.738043

Abbreviations: AD, Alzheimer's disease; ASIC, acid-sensing ion channel; BBB, blood–brain barrier; BCSFB, blood-cerebrospinal fluid barrier; BMM, bone marrow-derived macrophage; BSCB, blood-spinal cord barrier; CCL-2, C-C motif chemokine ligand 2; CNS, central nervous system; CRAC, calcium release-activated calcium channel; CXCL-8, interleukin-8; DAMP, damage-associated molecular pattern; DC, dendritic cell; Deg, degenerin; DRG, dorsal root ganglion; DS, lactate-based dialysis solution; EAE, experimental autoimmune encephalomyelitis; ENaC, epithelial sodium channel; HD, Huntington's disease; ICAM-1, intercellular adhesion molecule 1; i.c.v., intracerebroventricular; IFN−γ, interferon gamma; IL, interleukin; LPS, lipopolysaccharide; MCT, monocarboxylate transporter; MHC, major histocompatibility complex; MPO, myeloperoxidase; MS, multiple sclerosis; NHE-1, sodium-hydrogen antiporter 1; NK, natural killer; NO, nitric oxide; NOS, nitric oxide synthase; OLC, oligodendrocyte lineage cell; PECAM-1, platelet endothelial cell adhesion molecule 1; PAMP, pathogen associated molecular pattern; PD, Parkinson's disease; PNS, peripheral nervous system; PRR, pattern recognition receptor; RAW 264.7, mouse macrophage-like cell line; RIPK1, receptor-interacting serine/threonine-protein kinase 1; ROS, reactive oxygen species; SCI, spinal cord injury; SLE, systemic lupus erythematosus; SNP, single nucleotide polymorphism; TBI, traumatic brain injury; TCR, T cell receptor; TLE, temporal lobe epilepsy; TLR, Toll-like receptor; TNF, tumor necrosis factor; TRP, transient receptor potential.

ACID-SENSING ION CHANNELS

Acid-sensing ion channels (ASICs) are proton-gated ion channels that are permeable to Na^+ (Waldmann et al., 1997), and they constitute a subfamily of the epithelial sodium channel/degenerin (ENaC/Deg) superfamily (Kellenberger and Schild, 2015). ENaCs facilitate Na^+ reabsorption in the kidney, and they regulate the volume in the fluid/cilia interface in both the lung and colonic epithelial cells (Garty and Palmer, 1997; Enuka et al., 2012; Hanukoglu and Hanukoglu, 2016). ASICs have ∼30% sequence identity to ENaCs, and both groups are inhibited by the diuretic drug amiloride (Paukert et al., 2004). However, in contrast to ENaCs, ASICs appear to have evolved earlier, possibly first appearing in deuterostomes ∼600 million years ago (Lynagh et al., 2018). Humans possess four ASIC-coding genes (*ASIC1–ASIC4*), three of which (*ASIC1, ASIC2* and *ASIC3)* are alternatively spliced, to produce six main subunits with differing properties: ASIC1a, ASIC1b, ASIC2a, ASIC2b, ASIC3a, and ASIC4 (**Table 1**; Wemmie et al., 2013). ASIC3a is the major splice isoform of *ASIC3*, with little known about the function of ASIC3b and ASIC3c (Delaunay et al., 2012). ASICs form homotrimeric or heterotrimeric channels (Jasti et al., 2007) that have different pH thresholds for channel activation (see **Table 1**), different physiological and pathological roles, and different tissue distribution (**Figure 1**; Waldmann et al., 1997, 1999; Chen et al., 1998). ASIC1a homomers, ASIC1a/2b heteromers (but not ASIC1a/2a), and human ASIC1b mediate the influx of Ca^{2+} in addition to Na^+, although they are all more permeable to Na^+ (Waldmann et al., 1997; Olena et al., 2004; Hoagland et al., 2010; Sherwood et al., 2011).

ASICs are expressed in a range of tissues and have been associated with diverse pathologies, including diabetes, stroke, myocardial infarction, and epilepsy (see **Figure 1**; Xiong et al., 2004; Lv et al., 2011; Radu et al., 2014; Chassagnon et al., 2017; Redd et al., 2021). Most ASIC subtypes are present in the peripheral nervous system (PNS). However, ASIC1a is expressed at high levels and is the dominant subtype in both the human and rodent central nervous system (CNS) (Sluka et al., 2003; Wemmie et al., 2003; Baron et al., 2008), and it has been implicated in a variety of CNS disorders such as neurodegenerative diseases, depression, epilepsy, and ischemia-induced injury of the brain and spinal cord (Xiong et al., 2004; Friese et al., 2007; Wong et al., 2008; Ziemann et al., 2008; Coryell et al., 2009; Hu et al., 2011; Lv et al., 2011; Radu et al., 2014; Koehn et al., 2016; Chassagnon et al., 2017).

TABLE 1 | ASIC subtypes and their pH sensitivity.

Gene	Subtype	Alternative names	pH sensitivity (pH_{50})[1]
ASIC1	ASIC1a	ASIC, ASICα, BNaC2(α)	5.8–6.8
	ASIC1b	ASICβ, BNaC2(β)	6.1–6.2
ASIC2	ASIC2a	BNaC1(α), MDEG, BNC(1a)	4.5–4.9
	ASIC2b	BNaC1(β), MDEG2	Does not form pH-sensitive homomers; associates with other ASICs to form pH-sensitive channels
ASIC3	ASIC3	DRASIC, TNaC1, SLNAC1	6.4–6.6
ASIC4	ASIC4	BNAC4, ACCN4, SPASIC	Does not form pH-sensitive homomeric channels

[1] *The pH sensitivities of the homomeric ASIC channels are from Wemmie et al. (2013).*

INFLAMMATION

There is a growing body of literature suggesting that ASICs may contribute to immune cell function and neuroinflammation during CNS pathology. Inflammation is a complex biological response to an insult, which may be pathogenic or self-derived (i.e., induced by trauma, ischemia, or autoimmune processes). It is driven by the innate immune system, dependent on immune cell infiltration, and results in the release of plethora of inflammatory mediators including histamines, bradykinins, arachidonic acid, leukotrienes, prostaglandins, cytokines and chemokines. Plasma leakage from capillary beds causes swelling, alongside extravasation of granulocytes into the tissue which is facilitated by P-selectin and platelet endothelial cell adhesion molecule 1 (PECAM-1) (Woodfin et al., 2007). Chronic inflammation causes long term alterations to cell populations, such as an increase in the number of white blood cells such as lymphocytes. This infiltration and persistent involvement of immune cells results in both healing alongside further damage. Neuroinflammation is an inflammatory response within the CNS, leading to immune cell infiltration (of CNS or peripheral origin) and increased levels of cytokines, chemokines, and reactive oxygen species (ROS). It is worth noting that inflammation can be "sterile," occurring without a pathogenic external source [e.g., pathogen associated molecular patterns (PAMPs)] and instead resulting from damage-associated molecular patterns (DAMPs) triggered by trauma, ischemia or other environmental factors (e.g., ultraviolet radiation) (Rock et al., 2010; Feldman et al., 2015).

Neuroinflammation has been implicated in degenerative and traumatic conditions and even mental health disorders such as depression and anxiety. Despite robust intrinsic CNS barriers, resident peripheral immune cells frequently cross into the CNS parenchyma when the blood-brain barrier (BBB), blood-spinal cord barrier (BSCB), or blood-cerebrospinal fluid barrier (BCSFB) become porous. The BBB, BSCB, and BCSFB are often disrupted and left partially open for weeks after a physical injury such as spinal cord injury (SCI) and traumatic brain injury (TBI), or after ischemic insults such as stroke (Sinescu et al., 2010; Chodobski et al., 2011; Suzuki et al., 2016). Degenerative disorders such as Alzheimer's disease (AD), Parkinson's disease (PD), and multiple sclerosis (MS) also cause pervasive disruption to CNS barriers that results in CNS invasion by peripheral immune cells (Ffrench-Constant, 1994; Town et al., 2005; Polman et al., 2006). Breakdown of the BBB is also thought to contribute to the etiology of epilepsy (Marchi et al., 2012).

Neutrophils, macrophages, T cells, and dendritic cells (DCs) have each been shown to occupy the CNS after an insult. Neutrophil chemoattractants such as PGF2α, complement component C5a, and interleukin-8 (CXCL-8) are produced by

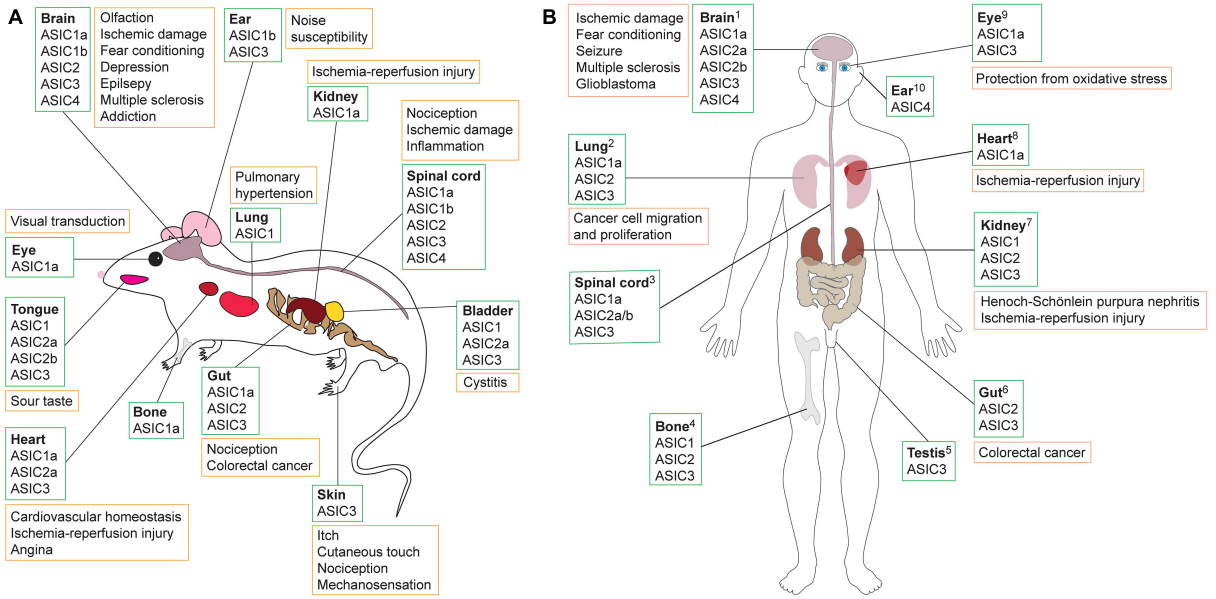

FIGURE 1 | Schematic showing tissues in which ASICs are expressed (green boxes) and their putative role in various pathologies (orange boxes) in **(A)** rodents and **(B)** humans. Data summarized here are drawn from **Supplementary Table 1**, with expression sites and pathology based on studies that used antibody staining, transcriptomic data, proteomics and/or functional methods. Additional information is available in the Human Protein Atlas (www.proteinatlas.org). References supporting the putative roles of ASICs in human pathologies are as follows: [1]**Brain:** ASIC1a detected using RT-PCR and Western blot; acidosis-mediated damage to cultured human brain neurons rescued by ASIC1a inhibition with PcTx1 (Li et al., 2010). Significant association between ASIC1a SNPs, amygdala volume, and panic disorder in humans (Smoller et al., 2014). Elevated levels of ASIC1a (Yang et al., 2016) and ASIC3 (Cao et al., 2016) in brains of patients with temporal lobe epilepsy shown using immunostaining and Western blot. ASIC expression in CNS; treatment with amiloride alleviated patient symptoms of MS (Arun et al., 2013). ASIC1 and ASIC3 found in glioblastoma stem cell lines using RT-PCR and Western blot; microarray data revealed that ASIC expression is associated with improved survival in glioma patients (Tian et al., 2017). [2]**Lung:** ASICs expressed in human lung cancer cell line A549 determined using RT-PCR, immunofluorescence, and Western blot. Proliferation and migration promoted by overexpression of ASIC1a and inhibited by PcTx1 (Wu et al., 2017). [3]**Spinal cord:** ASICs in human spinal cord, stained with ASIC1 antibody (Arun et al., 2013). [4]**Bone:** ASIC expression in human skeleton shown using RT-PCR and antibody staining performed on human chondrocytes (Jahr et al., 2005). [5]**Testis:** ASIC3 in human testis based on Northern blot (Ishibashi and Marumo, 1998). [6]**Gut:** ASIC2 measured using RT-PCR and immunostaining in human colorectal cancer cells, with ASIC2 promoting cell invasion and proliferation in xenografts (worsened via overexpression and impeded with ASIC2 knockout) (Zhou et al., 2017). [7]**Kidney:** ASICs found in human proximal tubular cell line using RT-PCR and Western blotting; apoptosis of cells due to ischemia-reperfusion injury reduced by ASIC1a inhibition using PcTx1 (Song et al., 2019). ASIC1, ASIC2 and ASIC3 protein expression in patients with Henoch-Schönlein purpura nephritis; ASIC blockade with amiloride reduced expression of damage marker proteins (Yuan et al., 2010). [8]**Heart:** Transcriptomics revealed presence of ASIC1a in human induced pluripotent stem cell-derived cardiomyocytes (hiPSC-CMs); ASIC1a inhibition with Hi1a or PcTx1 improved viability of hiPSC-CMs under conditions of hypoxia and acidosis, whereas viability was further reduced in the presence of the ASIC1a activator MitTx (Redd et al., 2021). [9]**Eye:** ASIC1a detected in retinal pigment epithelial cells using RT-PCR and Western blotting; PcTx1 protects cells from oxidative stress (Tan et al., 2013). ASIC3 mRNA detected using RT-PCR on human retina samples (Maubaret et al., 2002). [10]**Ear:** Presence of ASIC4 shown using RT-PCR and Northern blot (Gründer et al., 2000).

ischemic tissues, suggesting that these leukocytes do not just passively filter through the disrupted BBB/BSCB but are actively recruited to the CNS following the insult (Kilgore et al., 1994; Arnould et al., 2001; De Bondt et al., 2020). Consistent with this, neutrophil migration is altered by acidity, which is discussed further below (Rotstein et al., 1988). There is conflicting evidence as to whether neutrophils are beneficial or detrimental once they have infiltrated the CNS, which may be due to the heterogenous nature of neutrophil activation states (e.g., differential expression of proteins), but they are accepted to contribute to SCI severity (Taoka et al., 1998; Neirinckx et al., 2014; Deniset and Kubes, 2018). Infiltrating macrophages/monocytes and possibly neutrophils initiate demyelination of CNS neurons through phagocytic and inflammatory processes (Ajami et al., 2011; Yamasaki et al., 2014; Stranahan et al., 2016; De Bondt et al., 2020). T cells that cross a porous BBB contribute significantly to MS pathology by causing central demyelination through attack and degradation of the myelin sheath (Bielekova et al., 2004). During experimental autoimmune encephalomyelitis (EAE), an animal model of MS, DCs also breach the CNS and subsequently prime T cells to exacerbate the autoimmune inflammation (Karman et al., 2006; Sagar et al., 2012). In summary, recruitment of peripheral immune cells into the CNS during inflammation contributes to the wave of secondary damage that emanates from the initial site of injury.

TISSUE ACIDIFICATION

Vascular damage after SCI, hemorrhagic stroke, or occlusion of cerebral arteries during an ischemic stroke, causes a marked reduction in blood flow to the injured region. Neurons and supporting glial cells in the center of the ischemic territory (i.e., where blood flow is lowest) are rapidly, and perhaps irreparably,

damaged. At the periphery of this ischemic core (the penumbra), an expanding wave of secondary damage (i.e., progression of injury beyond the initial insult, as outlined in **Figure 2**) develops more slowly because supplementary blood flow from adjacent regions maintains perfusion above the threshold for immediate cell death (Moskowitz et al., 2010). However, in the absence of adequate blood flow, oxygen deprivation (hypoxia) in areas surrounding the primary ischemic insult forces neurons to resort to anaerobic glycolysis for their energy needs, which causes lactic acidosis and acidification of the tissue (Rehncrona, 1985). The resultant acidosis contributes to secondary damage through activation of ASICs (e.g., ASIC1a), which is discussed further below. Patients admitted with trauma often exhibit a decrease in blood pH as part of the "triad of death"—systemic hypothermia, acidosis, and coagulopathy—which contributes to mortality and is also a reminder that in trauma, acidification is not limited to the CNS or just the site of damage (Mikhail, 1999; Mitra et al., 2012).

Acidification is not solely linked to traumatic and ischemic insults. Extracellular acidosis has been reported in spinal cord tissue of EAE mice, and increased levels of tissue lactate have also been reported in human MS brain tissue, sufficient to activate ASIC1a (Bitsch et al., 1999; Friese et al., 2007). In both animal models of Huntington's disease (HD) and in patients with HD, a significant build-up of lactic acid has been observed in the brain (Tsang et al., 2006; Josefsen et al., 2010).

Tissue acidosis and inflammation influence one another and, as shown by research within an intensive care unit, alterations in the acid/base status of patients contribute to differences in their interleukin (IL) and cytokine profile (Zampieri et al., 2014). We have highlighted thus far that both inflammation and acidity contribute to tissue damage in pathological CNS conditions, with the former moderated by immune cells and the latter by receptors such as ASICs. Immune cells themselves are also modulated by acidity, and in the following sections we present an overview of immune cells, their response to acidic conditions, and the potential role of immune-cell ASICs in neuroinflammation.

OVERVIEW OF IMMUNE CELLS

White blood cell lineages (peripheral immune cells) arise from hemopoietic stem cells in the bone marrow (**Figure 3**), in particular the common myeloid progenitor and the common lymphoid progenitor cells. Common myeloid progenitors give rise to granulocytes (mast cells, eosinophils, basophils and neutrophils) and monocytes (which can differentiate into macrophages and DCs), while the common lymphoid progenitor produces various classes of lymphocytes: natural killer (NK) cells, T cells and B cells (Kondo et al., 2003; **Figure 3**). T cells are produced in the bone marrow and mature in the thymus, and they can be further subdivided into memory, cytotoxic, regulatory, and helper T cells. T cells express T cell receptors (TCRs) on their surface to recognize antigens.

Peripheral immune cells are separated from CNS immune cells by two distinct barriers that divide the central and peripheral vascular systems: the BBB/BSCB and the BCSFB. The BBB/BSCB and BCSFB allow the CNS to maintain its own regulatory environment with a distinct set of immune cells comprising the neuroglia (microglia, astrocytes, oligodendrocytes) and ependymal cells (**Figure 4**).

Immune Cell Response to Tissue Acidification

Although often referred as neuronal ion channels, ASICs are expressed in numerous types of immune cells (Huang et al., 2010; Tong et al., 2011; Kong et al., 2013; Yu et al., 2015) and they are potentiated by molecules associated with neuroinflammation such as arachidonic acid, histamine, lactate, and nitric oxide (Immke and McCleskey, 2001; Cadiou et al., 2007; Smith et al., 2007; Rash, 2017; Shteinikov et al., 2017). Acidity can provoke different responses in immune cells depending on the source of the acidosis, as exemplified in **Table 2** for macrophages. Therefore, whether or how inflammation is triggered by acidity depends on the source of the lowered pH. As proton-coupled monocarboxylate transporters (MCTs) shuttle lactate in a 1:1 ratio with H^+ (Hertz and Dienel, 2005), altering lactate levels will have secondary effects on the H^+ concentration.

Neutrophils exposed to acidic pH undergo various functional changes, including significantly impaired migration, defective chemotaxis, reduced speed of apoptosis, increased CD18 expression, and increased phagocytosis but with decreased bactericide action (Rotstein et al., 1988; Trevani et al., 1999;

TABLE 2 | The effects of pH on inflammatory mediators in macrophages (Kellum et al., 2004).

Acid	pH_o[1]	Cells	LPS[2]	Effect	References
HCl	6.5	Alveolar macrophages	+	↑TNF[3] mRNA	Heming et al., 2001a
HCl	5.5	Alveolar macrophages	+	↑TNF mRNA ↓TNF secretion	Heming et al., 2001a
HCl	5.5	RAW 264.7 cell line[4]	+	No ΔTNF mRNA ↓TNF secretion	Heming et al., 2001b
HCl	7.0	Alveolar macrophages	+	↓TNF secretion	Bidani et al., 1998
HCl	7.0	Peritoneal macrophages	–	↑NO[5], ↑TNF[6], ↑NF-κB[7]	Bellocq et al., 1998
HCl	7.2	RAW 264.7 cell line	+	↑NO	Huang et al., 2002
Lactate	6.7	Peritoneal macrophages	+	↑TNF mRNA ↑TNF secretion	Jensen et al., 1990
DS[8]	6.0	Peritoneal macrophages	+	↓TNF mRNA ↓TNF secretion	Jörres et al., 1995
DS[8]	6.5	Human blood-borne macrophages	+	↓TNF mRNA ↓NF-κB	Douvdevani et al., 1995

[1] *pH_o, extracellular pH.*
[2] *LPS, lipopolysaccharide.*
[3] *TNF, tumor necrosis factor.*
[4] *RAW 264.7, mouse macrophage-like cell line.*
[5] *NO, nitric oxide.*
[6] *TNF not measured directly.*
[7] *NF-κB, nuclear factor-κB.*
[8] *DS, lactate-based dialysis solution.*

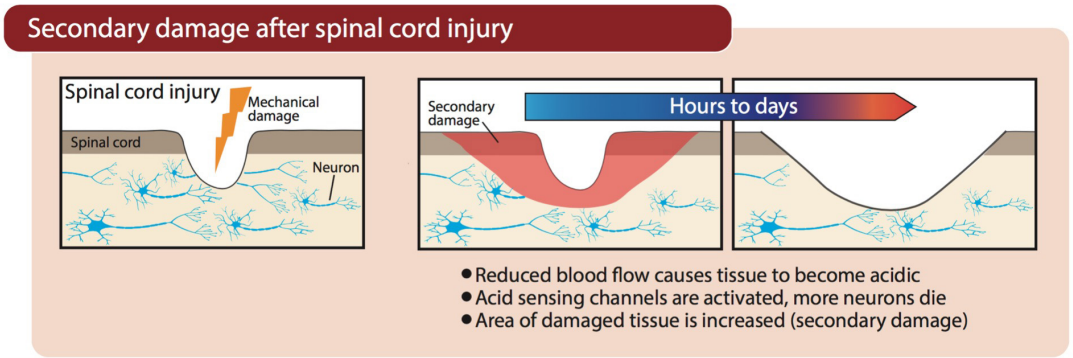

FIGURE 2 | Progression of secondary damage after physical damage is inflicted on the spinal cord. Blood flow is restricted as a result of damaged blood vessels, causing tissue acidification and subsequent activation of ASICs.

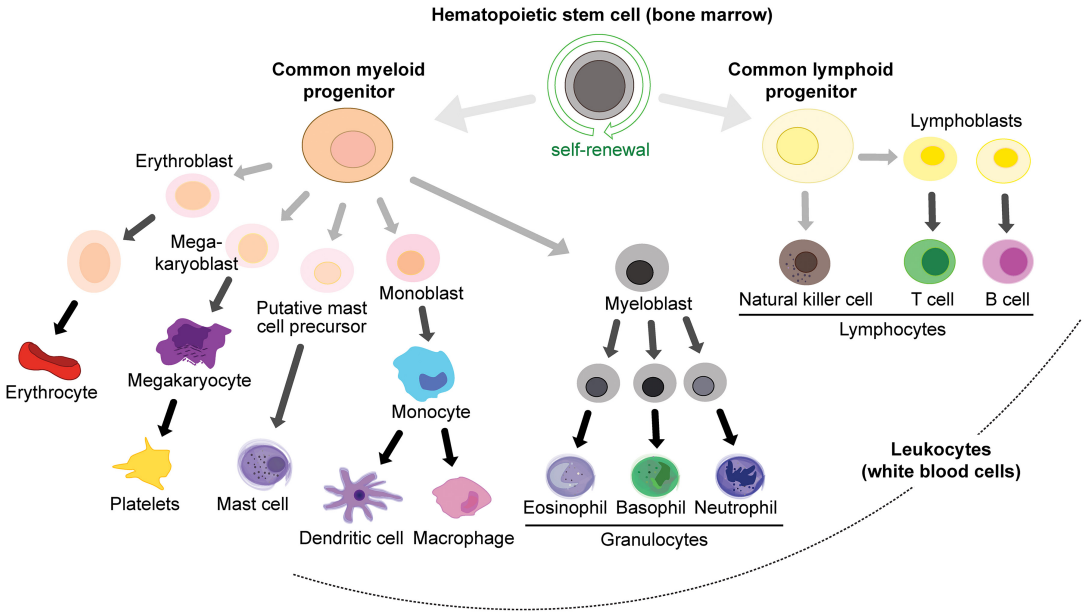

FIGURE 3 | Immune cell lineages in the periphery.

Cao et al., 2015). The combination of acidosis-induced decreases in migration, chemotaxis and apoptosis together with increased phagocytic activity might suggest that once neutrophils enter a region of low pH, they become trapped there with enhanced lifespan and inflammatory activity. CD18 is a cell-surface molecule expressed by neutrophils that promotes cell adhesion, a process that allows neutrophils to aid tissue repair in the periphery. Altered expression of CD18 is believed to facilitate neutrophil breach into the CNS (Serrano et al., 1996; Neri et al., 2018). The acidic blood pH after trauma (as low as 6.6) likely induces altered CD18 expression on peripheral neutrophils which then undergo facilitated extravasation into the CNS, where they accumulate in acidic regions (Mitra et al., 2012). Furthermore, in patients with SCI, neutrophils exhibit a higher "respiratory burst" in the blood (Kanyilmaz et al., 2013). The myeloperoxidase (MPO) produced by neutrophils enhances conversion of H_2O_2 to HOCl, and thus contributes to the secondary damage after SCI (Kubota et al., 2012). Neutrophils in the blood of SCI patients in rehabilitation have decreased ability to phagocytose *Escherichia coli* and *Staphylococcus aureus* (Campagnolo et al., 1997; Kanyilmaz et al., 2013). These data suggest that, at least for neutrophils, typical immune responses are altered in the presence of acidity and this may explain why neutrophils can have a detrimental impact in the CNS after neurotrauma.

Vermeulen et al. (2004) and Martínez et al. (2007) found that murine and human DCs mature upon exposure to acidity. Acidosis modifies the inflammatory profile of monocytes and macrophages, and is proposed to induce an inflammatory state in the latter (Riemann et al., 2016). Microglial motility decreases after exposure to acidic pH (Faff and Nolte, 2000).

Rat macrophages exposed to acidic environments (pH below 7.4) upregulate nitric oxide synthase (NOS), and thus increase production of NO (Bellocq et al., 1998). Excess amounts of NO are detrimental in neurodegenerative pathologies such as HD and after striatal lesions, causing DNA damage and oxidative stress to cells (Schulz et al., 1996; Browne and Beal, 2006; Calabrese et al., 2007). These responses are discussed further below when considering the role of ASICs.

Decreased extracellular pH, therefore, can modify the function of immune cells by altering motility, impacting phagocytosis, aiding CNS invasion, and increasing the production of potentially neurodamaging agents such as NO. Although the function of neutrophils is modified by acidity, there are, to date, no studies on whether they express ASICs. Thus, the role of ASICs in acidosis-induced responses of neutrophils is currently unknown.

Receptors and Ion Channels on Immune Cells

The key immune cell receptors involved in the innate immune response are complement and cytokine/chemokine receptors and pattern recognition receptors (PRRs) such as Toll-like receptors (TLRs). The PRRs recognize both PAMPs and also DAMPs which are produced by dying or damaged cells and trigger sterile inflammatory processes. As part of the adaptive immune response, the TCRs and antibody-binding receptors are involved in cascades that facilitate the immune cell response. Immune cells also possess ion channels that are important for their function, including the voltage-gated potassium channel Kv1.3, the calcium-activated potassium channel KCa3.1, calcium release-activated calcium channels (CRAC), and transient receptor potential (TRP) channel M7 (Cadiou et al., 2007; Chandy and Norton, 2017; Chiang et al., 2017; Nadolni and Zierler, 2018; Clemens and Lowell, 2019). The function of these ion channels in immune cells and their contribution to pathology have been reviewed (Feske et al., 2015; Vaeth and Feske, 2018) but neither of these reviews discuss the presence or role of ASICs in immune cells.

ACID-SENSING ION CHANNEL EXPRESSION IN CELLS THAT CONTRIBUTE TO NEUROPATHOLOGY

Acid-Sensing Ion Channels in Microglia

Microglia are the main immune cell type in the CNS. Although considered CNS-resident macrophages, microglia branch off earlier in development from yolk sac precursors (Ginhoux et al., 2010; Schulz et al., 2012; Kierdorf et al., 2013). In non-pathological conditions, microglia are involved in clearing tissue debris and surveying the environment (Nimmerjahn et al., 2005). During neuropathology, microglia can enter an activated state and release enzymes such as NADPH oxidase, which causes neuronal damage. Microglia can additionally modify myelination, affecting developmental myelination as well as beneficial re-myelination processes (Popovich et al., 2002; Butovsky et al., 2006). The divergent context-specific roles of microglia in CNS pathologies is an emergent field and has been recently reviewed (Norris and Kipnis, 2019; Butler et al., 2021).

It has been known for some time that the severity of disease progression in MS patients is linked to microglial activation (Heppner et al., 2005; Jack et al., 2005; Geladaris et al., 2021), and it seems that microglial phagocytosis of stressed neurons contributes to neurodegeneration in AD, PD, ischemic stroke, CNS viral infections, and aging (Butler et al., 2021). Rat microglia have been shown to express ASIC1, ASIC2a and ASIC3. In cultured primary rat microglia stimulated with lipopolysaccharide (LPS), a known immune activator, ASIC1 and ASIC2a expression increased both at the surface and intracellularly (Yu et al., 2015) and ASIC-specific inward currents could be recorded using whole-cell patch-clamp electrophysiology. Both PcTx1 and amiloride reduced the amplitude of these currents and reduced the expression of inflammatory cytokines (Yu et al., 2015). Treatment of cultured primary microglia with amiloride also decreased the extent of phagocytosis under acidic conditions (Vergo et al., 2011). A decrease in phagocytosis was also seen in microglia cultured from ASIC1$^{-/-}$ mice, with no change upon the addition of amiloride, indicating that the effect of amiloride is ASIC1-mediated.

These data collectively show that ASICs, and ASIC1a specifically, are present in microglia and contribute to their function in acidic microenvironments. In turn, this indicates that microglial ASIC1a contributes to microglia function, affecting release of inflammatory cytokines and phagocytosis, potentially impacting the immune response in the CNS during MS and many other CNS pathologies.

Acid-Sensing Ion Channels in Astrocytes

Astrocytes fulfill a variety of roles in the CNS, such as regulating the formation and maintenance of the BBB (Abbott et al., 2006). After brain injury and disease, astrocytes can become reactive, participating in repair cascades and gene upregulation, and forming an astroglial scar (Zamanian et al., 2012; Anderson et al., 2016). Reactive astrocytes are key players in CNS disease, an area reviewed recently by Dossi et al. (2018). Stimulation of astrocytes by cytokines such as interferon gamma (IFN−γ) leads to expression of the antigen-presenting major histocompatibility complex II (MHC II) on the cell surface alongside other costimulatory molecules such as intercellular adhesion molecule 1 (ICAM-1) (Wong et al., 1984; Lee et al., 2000). MHC II expression occurs in MS plaques and may contribute to the inflammatory cascade through antigen presentation to T cells (Zeinstra et al., 2000). Ponath et al. (2018) recently reviewed the differing roles of astrocytes in MS.

ASIC1, ASIC2a, ASIC3 are expressed in the nucleus of rat astrocytes, and astrocytes express an ASIC-like current that is blocked by amiloride (Huang et al., 2010; Yu et al., 2015). Yang et al. (2016) noted increased ASIC1a expression in the membrane and cytoplasm of reactive astrocytes from the hippocampi of deceased TLE patients, findings which were replicated in a mouse model of chronic epileptogenesis. To explore normal astrocytic function, the group used primary cultures from wild-type mice. At 24 h after stimulation with LPS, astrocytes upregulated ASIC1a

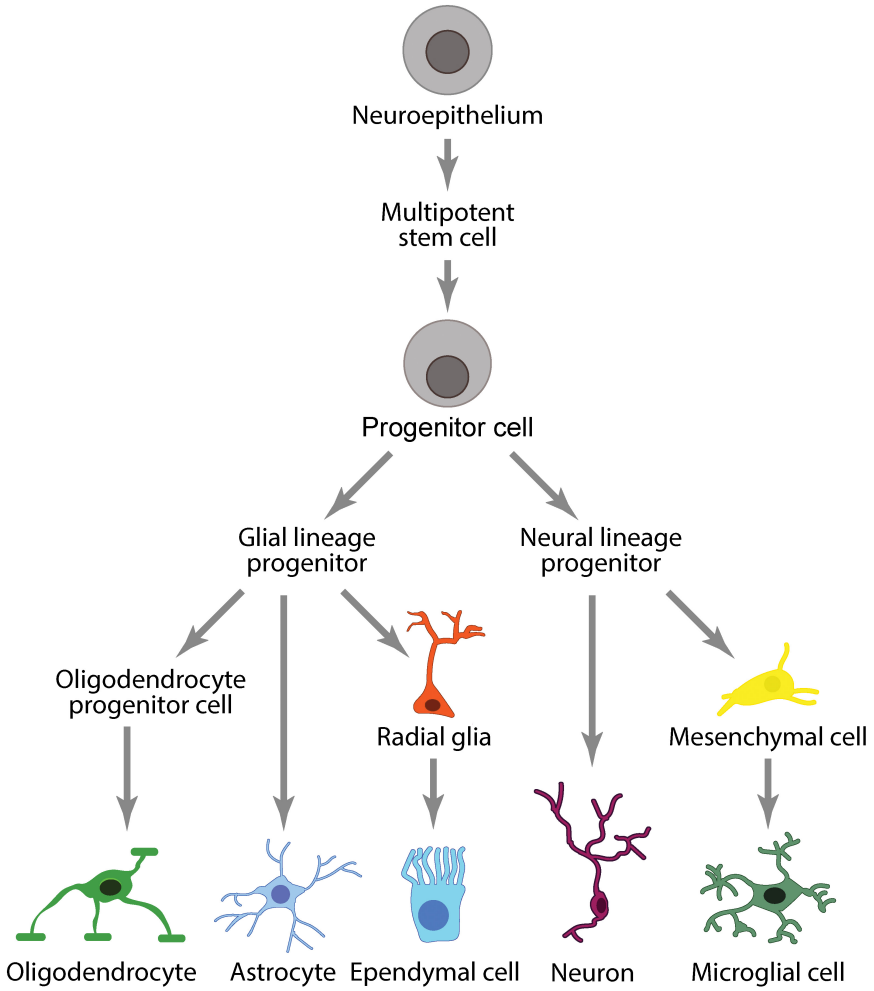

FIGURE 4 | Immune cell lineages in the CNS.

and exhibited increased Ca^{2+} influx upon exposure to pH 6.0, which was significantly reduced by PcTx1.

Yang et al. (2016) showed that seizure frequency in TLE mice is reduced by knockdown of astrocytic ASIC1a, with restoration of the *ASIC1* gene increasing the frequency of spontaneous seizures. Thus, in contrast to what is believed regarding epilepsy and the beneficial function of ASIC1a (likely via neuronal expression), these data suggest that activation of astrocytic ASIC1a causes pathological Ca^{2+} influx and contributes to the pathogenesis of TLE.

Acid-Sensing Ion Channels in Oligodendrocytes

Oligodendrocytes deliver critical trophic support to neurons, producing the proteins and lipids that comprise the myelin sheath that wrap around and insulate axons, and they engage in significant cross-talk with microglia during the process of myelination (Peferoen et al., 2014). Oligodendrocytes secrete cytokines such as C-C motif chemokine ligand 2 (CCL-2) and IL-8 in response to neuroborreliosis, the neurological manifestation of Lyme's disease (Ramesh et al., 2012). IL-8 and CCL-2 are chemotaxic for a number of peripheral immune cells, such as neutrophils and T cells respectively (Turner et al., 2014).

Oligodendrocytes are especially sensitive to ischemic insults (Bradl and Lassmann, 2010), and resident ASICs may contribute to ischemia-induced injury of these cells. ASIC1 is upregulated in oligodendrocytes in chronic brain lesions of patients with MS, and use of amiloride in patients provided neuroprotection at primary stages of the disease (Arun et al., 2013). ASIC1a, ASIC2a/b (non-selective primers were used, and thus ASIC2a and ASIC2b could not be distinguished), and ASIC4 mRNA were found in oligodendrocytes, and ASIC-specific inward currents recorded from oligodendrocyte lineage cells (OLCs) were inhibited by PcTx1 (Feldman et al., 2008). Cultured mouse oligodendrocytes express ASIC1 (ASIC1a and ASIC1b were not separable) and they were protected from acidosis-induced damage by PcTx1, as were oligodendrocytes derived from *ASIC1* KO mice (Vergo et al., 2011). Thus, the combined data suggest

that ASIC1 activation contributes to oligodendrocyte injury during and after periods of tissue acidosis.

Acid-Sensing Ion Channels in Macrophages

Macrophages are key players in inflammation and autoimmune disease. They produce NO under acidic conditions and promote demyelination in the CNS (Bellocq et al., 1998; Yamasaki et al., 2014; Li and Barres, 2018). RT-PCR and Western blots were used to demonstrate expression of ASIC1 and ASIC3 in the cytoplasm of macrophages (Kong et al., 2013). When exposed to acidic conditions (pH 6.5), bone marrow-derived macrophages (BMMs) increase their rate of phagocytosis (Kong et al., 2013). Extracellular acidosis also causes an upregulation of key cell surface markers related to BMM maturation (e.g., CD80, CD86 and MHC II). These effects were blocked by application of amiloride before exposure to tissue acidosis. Interestingly, expression of IL-10—thought to be a beneficial anti-inflammatory cytokine—was increased in macrophages after acid exposure.

Thus, the limited available data suggest that ASICs can modulate the macrophage response to acidic microenvironments. CNS macrophages/monocytes are believed to be a primary contributor to MS demyelination, and ASICs may contribute to their response in this pathology (Yamasaki et al., 2014).

Acid-Sensing Ion Channels in T Cells

T cells play a major role in coordinating and executing multiple functions of the adaptive immune response. Autoreactive T cells that have lost their ability to differentiate self (i.e., host cells and antigens) from non-self (i.e., foreign/pathogenic cells and antigens) are major players in autoimmune diseases such as MS. In the first study that identified a role for ASIC1a in the neuropathology of MS, ASIC1b, ASIC3 and ASIC4 were identified at the mRNA level in mouse T cells, with the presence of ASIC1 protein confirmed in these immune cells via Western blot (Friese et al., 2007). In this study, no obvious function for ASIC1 in T cells was observed based on responses of wild-type and ASIC1 knockout T cells in terms of proliferation and cytokine secretion. Thus, the role of ASICs in T cells remains to be determined, but they do not seem to play a role in these cells in the context of MS, at least not in the mouse EAE model.

Acid-Sensing Ion Channels in Dendritic Cells

Mature DCs are professional antigen presenting cells that constitute a key part of the inflammatory cascade, forming a major link between the innate and adaptive immune systems. The expression of MHC II and co-stimulatory molecules such as CD86 on their cell surface allows them to present antigens to T cells leading to T cell activation and proliferation (Reis e Sousa, 2006; Dudek et al., 2013).

When mature DCs are exposed to acidic conditions (pH 6.5) for a moderate time period (∼4 h), the expression of their specific cell-surface markers is increased (Vermeulen et al., 2004). Human DCs exposed to acidosis increase production of proinflammatory IL-12 and the authors suggest that this triggers a bias toward a proinflammatory Th1 response (Martínez et al., 2007). The acidosis-induced increase in cell-surface marker expression was replicated using cultured DCs derived from mouse bone marrow, a response that was blocked by amiloride (Tong et al., 2011). Using non-specific antibodies for ASIC subtypes (i.e., not distinguishing between splice isoforms), Tong et al. (2011) found that mouse DCs express ASIC protein in the cytoplasm (ASIC1 and ASIC2), on the plasma membrane (ASIC2), in the endoplasmic reticulum and perinuclear regions (ASIC1), and in the mitochondria (ASIC3). Functional surface expression of ASICs was confirmed using patch-clamp electrophysiology experiments and the observation of amiloride-sensitive, acidosis-induced inward currents with a pH_{50} of ∼6.0. Acidosis (pH 6.5) increased the antigen-presenting ability of DCs as assessed by increased ability to stimulate T cell proliferation, and this effect was blocked by amiloride (Tong et al., 2011).

These results strongly suggest that ASIC activation on DCs enhances expression of cell-surface proteins involved in antigen presentation and subsequent T cell activation and proliferation. As T cells can be highly destructive to healthy tissue in chronic inflammatory conditions, acidosis-enhanced communication between these two CNS-invading peripheral immune cells may exacerbate CNS damage in disease (Korn and Kallies, 2017).

Acid-Sensing Ion Channels in Natural Killer Cells

Data from the human binary protein interactome (Luck et al., 2020) indicate an interaction between ASIC1a and the killer cell immunoglobulin-like receptor 3DL3, a key regulator of NK cell function. Reduced levels of NK cells have also been implicated in depression (in which immune responses tend to be impaired). Brain acidity is altered in several mental health conditions (Coryell et al., 2009; Suzuki et al., 2017), but it is not yet clear whether this impacts on NK levels or function or whether ASICs have any role in these changes.

NEUROPATHOLOGIES IN WHICH ACID-SENSING ION CHANNELS ARE IMPLICATED

ASIC1a is expressed in the cell body, dendritic arbor and postsynaptic dendritic spines of brain neurons (Wemmie et al., 2002; Alvarez de La Rosa et al., 2003; Vukicevic and Kellenberger, 2004; Zha et al., 2006). The brain can suffer significant pH reductions during CNS pathologies, falling to as low as 6.0 during severe cerebral ischemia (Rehncrona, 1985). Given that the pH_{50} for activation of ASIC1a in human cortical neurons is 6.6 (Li et al., 2010), such drops in brain pH are sufficient to robustly activate ASIC1a. ASIC1a expression is upregulated in both dorsal root ganglia (DRG) and spinal dorsal horn neurons in response to inflammation, and in DRGs this upregulation is suppressed by ASIC inhibitors (Voilley et al., 2001; Duan et al., 2007). Prevention of ASIC1a endocytosis caused elevated death of

cortical neurons exposed to acidosis in wild-type, but not ASIC1a knockout, mice (Zeng et al., 2013).

Multiple Sclerosis and Other Neurodegenerative Diseases

Axonal degeneration plays a major role in MS, with associated inflammation causing dysfunctional activity of mitochondria (Waxman, 2006). Using the EAE model of MS, it was found that mice in which the *ASIC1* gene was genetically inactivated or the channel was inhibited with amiloride exhibited marked axonal preservation (Friese et al., 2007). Consistent with the hypothesis that ASIC1a is activated during MS, increased levels of lactate are found in brain lesions of MS patients (Bitsch et al., 1999). ASICs are also expressed in microglia, astrocytes and oligodendrocytes, major players in MS that engage in crosstalk (Domingues et al., 2016). While microglia are the primary phagocytotic cells in the CNS, astrocytes also possess the ability to phagocytose neuronal debris, axonal mitochondria, and pathological protein aggregates (Lee and Chung, 2021). In aging mice, microglia appear to accumulate myelin debris at the same time as myelin degeneration (Hill et al., 2018). Indeed, Popovich et al. (2002) demonstrated that direct activation of "CNS macrophages" (covering both invading peripheral macrophages and CNS resident microglia) results in axonal damage and demyelination. This conclusion has gained strong support over the past 20 years and activated microglia in particular seem to represent promising targets in MS (Geladaris et al., 2021). As described above, ASICs are functionally expressed in both macrophages and microglia, and contribute to their activation during periods of acidosis. Thus, the protection afforded by ASIC1a inhibition in the EAE mouse model of MS is possibly due to decreased macrophage/microglial activation as well as direct neuroprotection.

In a PD model, knockout of ASIC1a made no difference to the number of dopaminergic neurons, the key subset of neurons that are lost in this pathology and lead to motor impairment (Komnig et al., 2016). A significant build-up of lactate has been observed across all brain regions in animal models of HD, and in the frontal cortex of HD patients (Harms et al., 1997; Dautry et al., 1999; Tsang et al., 2006). Administration of an amiloride derivative in a HD model caused a reduction in polyQ aggregation, one potential effector in this pathology, both *in vivo* and *in vitro* (Wong et al., 2008). Although the authors state that this indicates a role for ASIC1a in HD, their use of a non-specific ASIC inhibitor means that one cannot rule out the potential involvement of other channels/transporters in this neurodegenerative disease.

Seizures

Epileptic seizures are associated with increased acidity in the brain, and upon CO_2 administration the resultant hypercapnia allows for seizure termination through lowering of brain pH (Lennox, 1928; Wang and Sonnenschein, 1955; Miller, 2011). Overexpression of ASIC1a in mice appears to limit the duration and progression of chemoconvulsant-induced seizures, but not the number, and knockout of the gene has the converse effect (Ziemann et al., 2008). Furthermore, the beneficial effect of CO_2 inhalation requires ASIC1a to interrupt induced seizures. This may be due to activation of ASICs causing generation of action potentials in inhibitory interneurons, although ASICs are also expressed in excitatory pyramidal neurons (Cho and Askwith, 2008; Ziemann et al., 2008; Weng et al., 2010). Another study found that amiloride suppressed pilocarpine-induced seizures, but the use of this pan-ASIC inhibitor makes it difficult to relate this outcome to specific involvement of ASIC1a (Liang et al., 2015). Consistent with ASIC1a playing a role in seizure termination, hippocampal levels of ASIC1a are elevated in patients with temporal lobe epilepsy (TLE) and in epileptic mice (Yang et al., 2016). It has been suggested that in a neurotypical system, seizures should be self-limiting due to the ASIC1a response to increased acidity at seizure onset; in support of this hypothesis, a single nucleotide polymorphism (SNP) in the *ASIC1* gene is associated with TLE (Lv et al., 2011; Wemmie et al., 2013).

Mental Health

Patients with schizophrenia exhibit lower pH and increased lactate in the cerebellum (Halim et al., 2008), whereas patients with bipolar disorder show decreased pH in the dorsolateral prefrontal cortex and increased lactate in gray matter regions of the brain (Dager et al., 2004; Sun et al., 2006). The frontal cortex and brain homogenate of rodent models replicated these findings with both increased lactate and reduced pH observed (Halim et al., 2008; Hagihara et al., 2017). ASIC1a is abundantly expressed in the amygdala, a brain region that has been described as a chemosensor that promotes fear behavior after detection of CO_2 and/or acidosis (Wemmie et al., 2003; Coryell et al., 2007; Ziemann et al., 2009). Activation or inhibition/disruption of ASIC1a and altered expression of the *ASIC1* gene all modify fear-related behaviors. Coryell et al. (2007) found that loss of the *ASIC1* gene affected neuronal activity in the amygdala after exposure to fear-inducing odors. Not only do *ASIC1* KO mice exhibit reduced fear, overexpression of the channel increases fear responses (Wemmie et al., 2002, 2004). In humans, two SNPs in the *ASIC1* gene are associated with anxiety, linking with amygdala structure and function and also risk of panic disorder (Smoller et al., 2014). Lastly, Coryell and colleagues used a mouse model to examine the link between ASIC1a and depression. They found that pharmacological inhibition and or genetic ablation of ASIC1a reduced depression like-symptoms, while restoring the gene to the amygdala returned responses back to baseline (Coryell et al., 2009).

Central Nervous System Trauma and Ischemia

As described earlier, vascular disruption due to trauma can result in acidification of the brain, and the resultant drop in pH is often sufficient to activate neuronal ASIC1a (Xiong et al., 2004; Li et al., 2010; Chassagnon et al., 2017). It was originally envisaged that neuronal ASIC1a might exacerbate ischemia-induced brain injury by contributing to excitotoxicity by virtue of its ability to mediate flux of Ca^{2+} into neurons in addition to Na^{+} (Xiong et al., 2004; Yermolaieva et al., 2004). However, recent studies suggests that, at least in the brain, activation of ASIC1a

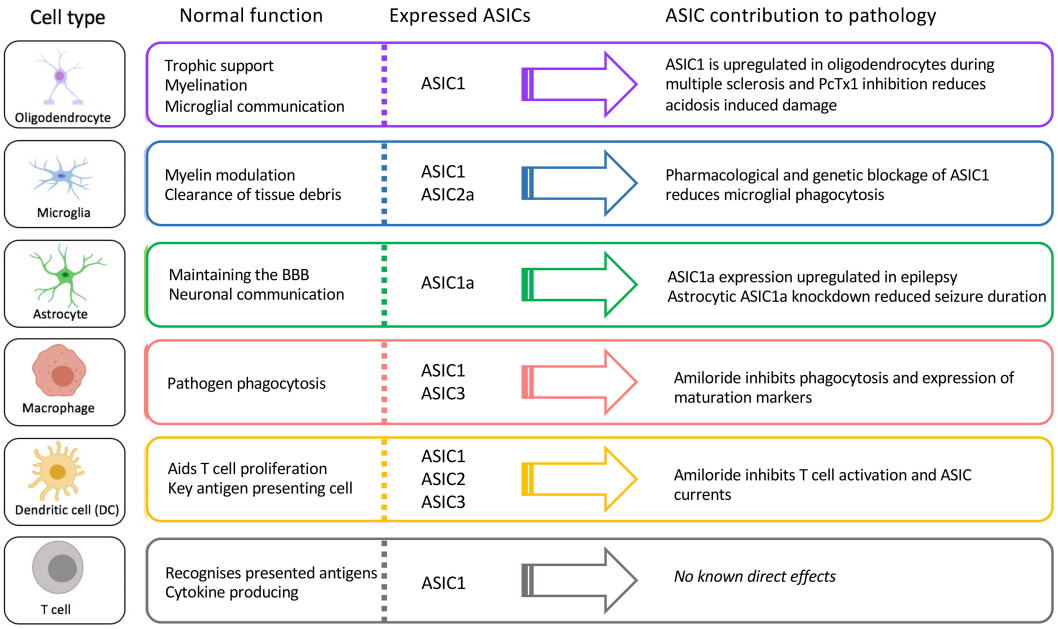

FIGURE 5 | Function, ASIC profile, and putative role of ASICs in CNS immune cells.

also leads to recruitment and activation of receptor-interacting serine/threonine-protein kinase 1 (RIPK1), a key mediator of necroptosis (Wang et al., 2015, 2020). Remarkably, this activation of RIPK1 occurs independently of ion flow through the channel (Wang et al., 2015).

How does ASIC1a contribute to ischemic injury when it is subject to rapid steady-state desensitisation (SSD) when exposed to sustained acidic pH *in vitro* (Gründer and Chen, 2010), and is distinguished from other ASICs by a reduced responsiveness to successive acid stimulations, a phenomenon known as tachyphylaxis (Chen and Grunder, 2007)? One might assume that these properties would limit the persistence of ASIC1a currents during sustained periods of tissue acidosis *in vivo*. However, a variety of ensuing biochemical events act to persistently activate ASIC1a during a sustained drop in tissue pH. First, ASIC1a currents are potentiated by several ischemia-related factors, including: (i) extracellular lactate which increases from a basal level of 1–2 mM to 12–20 mM during ischemia (Allen and Attwell, 2002; Gonzalez-Inchauspe et al., 2020); (ii) membrane stretch resulting from the rise in extracellular $[K^+]$ (Allen and Attwell, 2002); and (iii) CaMKII phosphorylation of ASIC1a (Gao et al., 2005). Second, during ischemic stroke, the increase in extracellular spermine prolongs ASIC1a currents and enhances recovery from SSD (Duan et al., 2011). Third, the increase in intracellular Ca^{2+} inhibits tachyphylaxis. Fourth, arachidonic acid, which is elevated during stroke due to activation of phospholipase A_2 (PLA_2), potentiates ASIC1a currents and enhances the sustained component of the current (Allen and Attwell, 2002). Finally, and perhaps most importantly, the train of cell-death signaling set off by the initial activation of ASIC1a continues regardless of the subsequent state of the channel. This includes activation of necroptosis (Wang et al., 2015; Redd et al., 2021), apoptosis (Song et al., 2019), and the stimulation of cell executioners such as calcium-activated proteases, endonucleases, and PLA_2 due to the increased levels of intracellular Ca^{2+} (Yermolaieva et al., 2004; Xiong et al., 2007).

Thus, despite its susceptibility to desensitization (which has largely been studied under control conditions in *in vitro* assays), activation of ASIC1a during sustained tissue acidosis is a major contributor to ischemic injury, as evidenced by the fact that genetic ablation or specific pharmacological inhibition of ASIC1a greatly reduces the tissue damage caused by ischemic stroke (Xiong et al., 2004; McCarthy et al., 2015; Chassagnon et al., 2017). Genetic knockout or knockdown of ASIC1a, as well as pharmacological inhibition of the channel, also provide neuroprotective effects post-SCI (Hu et al., 2011; Koehn et al., 2016). However, it should be noted that these studies have focused exclusively on the role of ASIC1a in CNS neurons. Despite the critical role of immune cells in damage progression after CNS trauma, very few studies have explored whether the resident population of ASIC1a, or other ASICs, in immune cells contributes to ischemic jury of the CNS.

CONCLUSION

Here we have described what is currently known about the expression and role of ASICs in immune cells known to contribute to a wide range of neuropathologies. We highlight the fact that ASICs are expressed in many key CNS-resident and infiltrating immune cells involved in these pathologies and are not only expressed in neurons (**Figure 5**). Thus, it is important to consider whether the therapeutic benefit provided by ASIC

inhibitors in some of these pathologies is exerted not only via effects on neurons, but also on immune cells.

A common theme across immune cells is alterations to phagocytosis after exposure to acidity. Ineffective phagocytosis contributes to autoimmune diseases such as systemic lupus erythematosus (SLE) and polyarthritis (Nagata et al., 2010). Whether ASICs are the primary mediators of acidity-induced alterations in phagocytosis remains to be determined. Their role may depend on the type and severity of the pathology, in turn leading to beneficial or negative outcomes, as seen for other receptors such as P2X7 (Savio et al., 2018). The CNS is heterogenous in its way of dealing with acidity (Chesler, 2003) and immune cells also respond differently to the "type" of acidity (Kellum et al., 2004). The resultant complexity of pH-induced effects results in a multitude of unique outcomes dependent on CNS region and immune cell type, as well as the ways in which acidity is induced. To unravel the role of immune-cell ASICs in neuropathology will likely require standardization of models, including the method of acidosis induction.

Another caveat of current research on the role of ASICs in immune-cell function is the widespread use of amiloride as a broad-spectrum ASIC inhibitor. Unfortunately, amiloride has targets outside of the ASIC family, including sodium-hydrogen antiporter 1 (NHE-1), which is involved in acid-sensing and pH regulation by immune cells. Amiloride can also inhibit TRPP3 channels (Dai et al., 2007), which are thought to be involved in acid sensing in mouse spinal cord and alkaline sensing in lamprey (Huang et al., 2006; Dai et al., 2007; Jalalvand et al., 2016). This raises the question of whether the beneficial effects of amiloride in human MS patients is solely due to inhibition of ASICs (Arun et al., 2013). Much more potent and specific ASIC inhibitors are available, such as Hi1a (Chassagnon et al., 2017) and PcTx1 (Escoubas et al., 2000) for ASIC1a, mambalgins for rodent ASIC1a and ASIC1b (Diochot et al., 2012) (although they potentiate human ASIC1b under the levels of acidosis likely encountered *in vivo;* Cristofori-Armstrong et al., 2021) and the sea-anemone peptide APETx2 for ASIC3 (Diochot et al., 2004), and they should be used in preference to amiloride wherever possible. Unfortunately, there are no specific inhibitors available for ASIC1b and ASIC2a. A final concern with investigations of ASIC protein expression is ongoing challenges with the specificity of available ASIC antibodies. As highlighted by Lin et al. (2015), examples of lack of specificity include "positive" ASIC1a staining in a pan-ASIC1a knockout mouse (Vig et al., 2014). Thus, due to the limitations of currently available commercial antibodies, antibody staining data should always be combined with proteomics and/or functional data using subtype-specific inhibitors to provide confirmation of ASIC localization.

There are some studies where subtype-specific inhibitors or specific genetic ablation has been used to definitively demonstrate a role for ASICs in CNS pathologies, such as ischemic stroke (Pignataro et al., 2007; McCarthy et al., 2015; Chassagnon et al., 2017). However, even in these instances, the relative contribution of neuronal and immune-cell ASICs was not considered. Our understanding of how immune-cell ASICs contribute to neuropathology would be significantly enhanced by utilizing technologies that allow direct study of these channels in specific immune cells. This was achieved in an eloquent study by Yang et al. (2016) through knockdown and then restoration of ASIC1a solely on astrocytes in a mouse model of TLE. Such techniques, particularly in combination with selective pharmacological tools, will allow determination of whether pan-inhibition of specific ASIC subtypes or their inhibition only in specific cell types is likely to be therapeutically useful.

In conclusion, the role of ASIC in immune cells is an exciting frontier in neurological research. Merging CNS immune function studies with cutting-edge molecular techniques will provide greater insight into whether immune-cell ASICs are likely to be useful drug targets for CNS disorders.

AUTHOR CONTRIBUTIONS

VF conceived the study and wrote the first draft of the manuscript. LR, MR, and GK revised and streamlined the manuscript. MR and GK contributed funding and mentored VF. All authors contributed to the article and approved the submitted version.

FUNDING

We acknowledge funding from the Australian Research Council (Centre of Excellence Grant CE200100012 to GK), Australian National Health and Medical Research Council (Principal Research Fellowship APP1136889 to GK and Project Grant APP1154622 to LR), and The University of Queensland (International Ph.D. Scholarship to VF).

SUPPLEMENTARY MATERIAL

The Supplementary Material for this article can be found online at: https://www.frontiersin.org/articles/10.3389/fncel.2021.738043/full#supplementary-material

REFERENCES

Abbott, N., Rönnbäck, L., and Hansson, E. (2006). Astrocyte-endothelial interactions at the blood-brain barrier. *Nat. Rev. Neurosci.* 7, 41–53.

Ajami, B., Bennett, J., Krieger, C., McNagny, K., and Rossi, F. M. (2011). Infiltrating monocytes trigger EAE progression, but do not contribute to the resident microglia pool. *Nat. Neurosci.* 14, 1142–1149. doi: 10.1038/nn.2887

Allen, N. J., and Attwell, D. (2002). Modulation of ASIC channels in rat cerebellar Purkinje neurons by ischaemia-related signals. *J. Physiol.* 543, 521–529. doi: 10.1113/jphysiol.2002.020297

Alvarez de La Rosa, D., Krueger, S. R., Kolar, A., Shao, D., Fitzsimonds, R. M., and Canessa, C. M. (2003). Distribution, subcellular localization and ontogeny of ASIC1 in the mammalian central nervous system. *J. Physiol.* 546, 77–87.

Anderson, M., Burda, J., Ren, Y., Ao, Y., O'Shea, T., Kawaguchi, R., et al. (2016). Astrocyte scar formation aids central nervous system axon regeneration. *Nature* 532, 195–200. doi: 10.1038/nature17623

Arnould, T., Thibaut-Vercruyssen, R., Bouaziz, N., Dieu, M., Remacle, J., and Michiels, C. (2001). PGF2α, a prostanoid released by endothelial cells activated by hypoxia, is a chemoattractant candidate for neutrophil recruitment. *Am. J. Pathol.* 159, 345–357. doi: 10.1016/S0002-9440(10)61701-4

Arun, T., Tomassini, V., Sbardella, E., de Ruiter, M., Matthews, L., Leite, M., et al. (2013). Targeting ASIC1 in primary progressive multiple sclerosis: evidence of neuroprotection with amiloride. *Brain* 136, 106–115. doi: 10.1093/brain/aws325

Baron, A., Voilley, N., Lazdunski, M., and Lingueglia, E. (2008). Acid sensing ion channels in dorsal spinal cord neurons. *J. Neurosci.* 28, 1498–1508. doi: 10.1523/jneurosci.4975-07.2008

Bellocq, A., Suberville, S., Philippe, C., Bertrand, F., Perez, J., Fouqueray, B., et al. (1998). Low environmental pH is responsible for the induction of nitric-oxide synthase in macrophages. Evidence for involvement of nuclear factor-kappaB activation. *J. Biol. Chem.* 273, 5086–5092.

Bidani, A., Wang, C. Z., Saggi, S. J., and Heming, T. A. (1998). Evidence for pH sensitivity of tumor necrosis factor-alpha release by alveolar macrophages. *Lung* 176, 111–121. doi: 10.1007/pl00007593

Bielekova, B., Sung, M.-H., Kadom, N., Simon, R., McFarland, H., and Martin, R. (2004). Expansion and functional relevance of high-avidity myelin-specific $CD4^+$ T cells in multiple sclerosis. *J. Immunol.* 172, 3893–3904.

Bitsch, A., Bruhn, H., Vougioukas, V., Stringaris, A., Lassmann, H., Frahm, J., et al. (1999). Inflammatory CNS demyelination: histopathologic correlation with in vivo quantitative proton MR spectroscopy. *Am. J. Neuroradiol.* 20, 1619–1627.

Bradl, M., and Lassmann, H. (2010). Oligodendrocytes: biology and pathology. *Acta Neuropathol.* 119, 37–53. doi: 10.1007/s00401-009-0601-5

Browne, S. E., and Beal, M. F. (2006). Oxidative damage in Huntington's disease pathogenesis. *Antioxid. Redox Signal.* 8, 2061–2073.

Butler, C. A., Popescu, A. S., Kitchener, E. J. A., Allendorf, D. H., Puigdellivol, M., and Brown, G. C. (2021). Microglial phagocytosis of neurons in neurodegeneration, and its regulation. *J. Neurochem.* 158, 621–639. doi: 10.1111/jnc.15327

Butovsky, O., Ziv, Y., Schwartz, A., Landa, G., Talpalar, A., Pluchino, S., et al. (2006). Microglia activated by IL-4 or IFN-gamma differentially induce neurogenesis and oligodendrogenesis from adult stem/progenitor cells. *Mol. Cell. Neurosci.* 31, 149–160. doi: 10.1016/j.mcn.2005.10.006

Cadiou, H., Studer, M., Jones, N. G., Smith, E. S. J., Ballard, A., McMahon, S. B., et al. (2007). Modulation of acid-sensing ion channel activity by nitric oxide. *J. Neurosci.* 27, 13251–13260. doi: 10.1523/JNEUROSCI.2135-07.2007

Calabrese, V., Mancuso, C., Calvani, M., Rizzarelli, E., Butterfield, D., and Giuffrida Stella, A. (2007). Nitric oxide in the central nervous system: neuroprotection versus neurotoxicity. *Nat. Rev. Neurosci.* 8, 766–775. doi: 10.1038/nrn2214

Campagnolo, D. I., Bartlett, J. A., Keller, S. E., Sanchez, W., and Oza, R. (1997). Impaired phagocytosis of *Staphylococcus aureus* in complete tetraplegics. *Am. J. Phys. Med. Rehabil.* 76, 276–280. doi: 10.1097/00002060-199707000-00005

Cao, Q., Wang, W., Gu, J., Jiang, G., Wang, K., Xu, Z., et al. (2016). Elevated expression of acid-sensing ion channel 3 inhibits epilepsy via activation of interneurons. *Mol. Neurobiol.* 53, 485–498. doi: 10.1007/s12035-014-9014-0

Cao, S., Liu, P., Zhu, H., Gong, H., Yao, J., Sun, Y., et al. (2015). Extracellular acidification acts as a key modulator of neutrophil apoptosis and functions. *PLoS One* 10:e0137221. doi: 10.1371/journal.pone.0139500

Chandy, K. G., and Norton, R. S. (2017). Peptide blockers of Kv1.3 channels in T cells as therapeutics for autoimmune disease. *Curr. Opin. Chem. Biol.* 38, 97–107. doi: 10.1016/j.cbpa.2017.02.015

Chassagnon, I. R., McCarthy, C. A., Chin, Y. K., Pineda, S. S., Keramidas, A., Mobli, M., et al. (2017). Potent neuroprotection after stroke afforded by a double-knot spider-venom peptide that inhibits acid-sensing ion channel 1a. *Proc. Natl. Acad. Sci. USA* 114, 3750–3755. doi: 10.1073/pnas.1614728114

Chen, C. C., England, S., Akopian, A. N., and Wood, J. N. (1998). A sensory neuron-specific, proton-gated ion channel. *Proc. Natl. Acad. Sci. USA* 95, 10240–10245. doi: 10.1073/pnas.95.17.10240

Chen, X. M., and Grunder, S. (2007). Permeating protons contribute to tachyphylaxis of the acid-sensing ion channel (ASIC) 1a. *J. Physiol.* 579, 657–670. doi: 10.1113/jphysiol.2006.120733

Chesler, M. (2003). Regulation and modulation of pH in the brain. *Physiol. Rev.* 83, 1183–1221. doi: 10.1152/physrev.00010.2003

Chiang, E. Y., Li, T., Jeet, S., Peng, I., Zhang, J., Lee, W. P., et al. (2017). Potassium channels Kv1.3 and KCa3.1 cooperatively and compensatorily regulate antigen-specific memory T cell functions. *Nat. Commun.* 8:14644. doi: 10.1038/ncomms14644

Cho, J.-H., and Askwith, C. (2008). Presynaptic release probability is increased in hippocampal neurons from ASIC1 knockout mice. *J. Neurophysiol.* 99, 426–441.

Chodobski, A., Zink, B. J., and Szmydynger-Chodobska, J. (2011). Blood–brain barrier pathophysiology in traumatic brain injury. *Transl. Stroke Res.* 2, 492–516. doi: 10.1007/s12975-011-0125-x

Clemens, R. A., and Lowell, C. A. (2019). CRAC channel regulation of innate immune cells in health and disease. *Cell Calcium* 78, 56–65. doi: 10.1016/j.ceca.2019.01.003

Coryell, M. W., Wunsch, A. M., Haenfler, J. M., Allen, J. E., Schnizler, M., Ziemann, A. E., et al. (2009). Acid-sensing ion channel-1a in the amygdala, a novel therapeutic target in depression-related behavior. *J. Neurosci.* 29, 5381–5388. doi: 10.1523/jneurosci.0360-09.2009

Coryell, M. W., Ziemann, A. E., Westmoreland, P. J., Haenfler, J. M., Kurjakovic, Z., Zha, X.-M., et al. (2007). Targeting ASIC1a reduces innate fear and alters neuronal activity in the fear circuit. *Biol. Psychiatry* 62, 1140–1148. doi: 10.1016/j.biopsych.2007.05.008

Cristofori-Armstrong, B., Budusan, E., and Rash, L. D. (2021). Mambalgin-3 potentiates human acid-sensing ion channel 1b under mild to moderate acidosis: implications as an analgesic lead. *Proc. Natl. Acad. Sci. USA* 118:e2021581118. doi: 10.1073/pnas.2021581118

Dager, S. R., Friedman, S. D., Parow, A., Demopulos, C., Stoll, A. L., Lyoo, I. K., et al. (2004). Brain metabolic alterations in medication-free patients with bipolar disorder. *Arch. Gen. Psychiatry* 61, 450–458. doi: 10.1001/archpsyc.61.5.450

Dai, X. Q., Ramji, A., Liu, Y., Li, Q., Karpinski, E., and Chen, X. Z. (2007). Inhibition of TRPP3 channel by amiloride and analogs. *Mol. Pharmacol.* 72, 1576–1585. doi: 10.1124/mol.107.037150

Dautry, C., Condé, F., Brouillet, E., Mittoux, V., Beal, M. F., Bloch, G., et al. (1999). Serial 1H-NMR spectroscopy study of metabolic impairment in primates chronically treated with the succinate dehydrogenase inhibitor 3-nitropropionic acid. *Neurobiol. Dis.* 6, 259–268. doi: 10.1006/nbdi.1999.0244

De Bondt, M., Hellings, N., Opdenakker, G., and Struyf, S. (2020). Neutrophils: underestimated players in the pathogenesis of Multiple Sclerosis (MS). *Int. J. Mol. Sci.* 21:4558. doi: 10.3390/ijms21124558

Delaunay, A., Gasull, X., Salinas, M., Noël, J., Friend, V., Lingueglia, E., et al. (2012). Human ASIC3 channel dynamically adapts its activity to sense the extracellular pH in both acidic and alkaline directions. *Proc. Natl. Acad. Sci. USA* 109, 13124–13129. doi: 10.1073/pnas.1120350109

Deniset, J. F., and Kubes, P. (2018). Neutrophil heterogeneity: Bona fide subsets or polarization states? *J. Leukocyte Biol.* 103, 829–838. doi: 10.1002/JLB.3RI0917-361R

Diochot, S., Baron, A., Rash, L. D., Deval, E., Escoubas, P., Scarzello, S., et al. (2004). A new sea anemone peptide, APETx2, inhibits ASIC3, a major acid-sensitive channel in sensory neurons. *EMBO J.* 23, 1516–1525. doi: 10.1038/sj.emboj.7600177

Diochot, S., Baron, A., Salinas, M., Douguet, D., Scarzello, S., Dabert-Gay, A. S., et al. (2012). Black mamba venom peptides target acid-sensing ion channels to abolish pain. *Nature* 490, 552–555. doi: 10.1038/nature11494

Domingues, H. S., Portugal, C. C., Socodato, R., and Relvas, J. B. (2016). Oligodendrocyte, astrocyte, and microglia crosstalk in myelin development, damage, and repair. *Front. Cell Dev. Biol.* 4:71. doi: 10.3389/fcell.2016.00071

Dossi, E., Vasile, F., and Rouach, N. (2018). Human astrocytes in the diseased brain. *Brain Res. Bull.* 136, 139–156. doi: 10.1016/j.brainresbull.2017.02.001

Douvdevani, A., Abramson, O., Tamir, A., Konforty, A., Isakov, N., and Chaimovitz, C. (1995). Commercial dialysate inhibits TNFα mRNA expression and NF-κB DNA-binding activity in LPS-stimulated macrophages. *Kidney Int.* 47, 1537–1545. doi: 10.1038/ki.1995.217

Duan, B., Wang, Y.-Z., Yang, T., Chu, X.-P., Yu, Y., Huang, Y., et al. (2011). Extracellular spermine exacerbates ischemic neuronal injury through sensitization of ASIC1a channels to extracellular acidosis. *J. Neurosci.* 31, 2101–2112. doi: 10.1523/JNEUROSCI.4351-10.2011

Duan, B., Wu, L. J., Yu, Y. Q., Ding, Y., Jing, L., Xu, L., et al. (2007). Upregulation of acid-sensing ion channel ASIC1a in spinal dorsal horn neurons contributes to inflammatory pain hypersensitivity. *J. Neurosci.* 27, 11139–11148. doi: 10.1523/JNEUROSCI.3364-07.2007

Dudek, A. M., Martin, S., Garg, A. D., and Agostinis, P. (2013). Immature, semi-mature, and fully mature dendritic cells: toward a DC-cancer cells interface that augments anticancer immunity. *Front. Immunol.* 4:438. doi: 10.3389/fimmu.2013.00438

Enuka, Y., Hanukoglu, I., Edelheit, O., Vaknine, H., and Hanukoglu, A. (2012). Epithelial sodium channels (ENaC) are uniformly distributed on motile cilia in the oviduct and the respiratory airways. *Histochem. Cell Biol.* 137, 339–353. doi: 10.1007/s00418-011-0904-1

Escoubas, P., De Weille, J. R., Lecoq, A., Diochot, S., Waldmann, R., Champigny, G., et al. (2000). Isolation of a tarantula toxin specific for a class of proton-gated Na^+ channels. *J. Biol. Chem.* 275, 25116–25121. doi: 10.1074/jbc.M003643200

Faff, L., and Nolte, C. (2000). Extracellular acidification decreases the basal motility of cultured mouse microglia via the rearrangement of the actin cytoskeleton. *Brain Res. Bull.* 853, 22–31. doi: 10.1016/S0006-8993(99)02221-0

Feldman, D., Horiuchi, M., Keachie, K., McCauley, E., Bannerman, P., Itoh, A., et al. (2008). Characterization of acid-sensing ion channel expression in oligodendrocyte-lineage cells. *Glia* 56, 1238–1249. doi: 10.1002/glia.20693

Feldman, N., Rotter-Maskowitz, A., and Okun, E. (2015). DAMPs as mediators of sterile inflammation in aging-related pathologies. *Ageing Res. Rev.* 24, 29–39. doi: 10.1016/j.arr.2015.01.003

Feske, S., Wulff, H., and Skolnik, E. Y. (2015). Ion channels in innate and adaptive immunity. *Annu. Rev. Immunol.* 33, 291–353. doi: 10.1146/annurev-immunol-032414-112212

Ffrench-Constant, C. (1994). Pathogenesis of multiple sclerosis. *Lancet* 343, 271–275.

Friese, M. A., Craner, M. J., Etzensperger, R., Vergo, S., Wemmie, J. A., Welsh, M. J., et al. (2007). Acid-sensing ion channel-1 contributes to axonal degeneration in autoimmune inflammation of the central nervous system. *Nat. Med.* 13, 1483–1489. doi: 10.1038/nm1668

Gao, J., Duan, B., Wang, D. G., Deng, X. H., Zhang, G. Y., Xu, L., et al. (2005). Coupling between NMDA receptor and acid-sensing ion channel contributes to ischemic neuronal death. *Neuron* 48, 635–646. doi: 10.1016/j.neuron.2005.10.011

Garty, H., and Palmer, L. (1997). Epithelial sodium channels: Function, structure, and regulation. *Physiol. Rev.* 77, 359–396. doi: 10.1152/physrev.1997.77.2.359

Geladaris, A., Hausler, D., and Weber, M. S. (2021). Microglia: the missing link to decipher and therapeutically control MS progression? *Int. J. Mol. Sci.* 22:3461. doi: 10.3390/ijms22073461

Ginhoux, F., Greter, M., Leboeuf, M., Nandi, S., See, P., Gokhan, S., et al. (2010). Fate mapping analysis reveals that adult microglia derive from primitive macrophages. *Science* 330, 841–845. doi: 10.1126/science.1194637

Gonzalez-Inchauspe, C., Gobetto, M. N., and Uchitel, O. D. (2020). Modulation of acid sensing ion channel dependent protonergic neurotransmission at the mouse calyx of Held. *Neuroscience* 439, 195–210. doi: 10.1016/j.neuroscience.2019.04.023

Gründer, S., and Chen, X. (2010). Structure, function, and pharmacology of acid-sensing ion channels (ASICs): focus on ASIC1a. *Int. J. Physiol. Pathophysiol. Pharmacol.* 2, 73–94.

Gründer, S., Geisler, H., Bässler, L., and Ruppersberg, J. P. (2000). Cloning of ASIC 4, a new member of acid-sensing ion channels from pituitary gland. *Eur. J. Neurosci.* 12:22.

Hagihara, H., Catts, V. S., Katayama, Y., Shoji, H., Takagi, T., Huang, F. L., et al. (2017). Decreased brain pH as a shared endophenotype of psychiatric disorders. *Neuropsychopharmacology* 43, 459–468. doi: 10.1038/npp.2017.167

Halim, N. D., Lipska, B. K., Hyde, T. M., Deep-Soboslay, A., Saylor, E. M., Herman, M. M., et al. (2008). Increased lactate levels and reduced pH in postmortem brains of schizophrenics: medication confounds. *J. Neurosci. Methods* 169, 208–213. doi: 10.1016/j.jneumeth.2007.11.017

Hanukoglu, I., and Hanukoglu, A. (2016). Epithelial sodium channel (ENaC) family: Phylogeny, structure–function, tissue distribution, and associated inherited diseases. *Gene* 579, 95–132. doi: 10.1016/j.gene.2015.12.061

Harms, L., Meierkord, H., Timm, G., Pfeiffer, L., and Ludolph, A. C. (1997). Decreased N-acetyl-aspartate/choline ratio and increased lactate in the frontal lobe of patients with Huntington's disease: a proton magnetic resonance spectroscopy study. *J. Neurol. Neurosurg. Psych.* 62, 27–30. doi: 10.1136/jnnp.62.1.27

Heming, T. A., Davé, S. K., Tuazon, D. M., Chopra, A. K., Peterson, J. W., and Bidani, A. (2001a). Effects of extracellular pH on tumour necrosis factor-alpha production by resident alveolar macrophages. *Clin. Sci.* 101, 267–274.

Heming, T. A., Tuazon, D. M., Davé, S. K., Chopra, A. K., Peterson, J. W., and Bidani, A. (2001b). Post-transcriptional effects of extracellular pH on tumour necrosis factor-alpha production in RAW 246.7 and J774 A.1 cells. *Clin. Sci.* 100, 259–266.

Heppner, F. L., Greter, M., Marino, D., Falsig, J., Raivich, G., Hovelmeyer, N., et al. (2005). Experimental autoimmune encephalomyelitis repressed by microglial paralysis. *Nat. Med.* 11:146.

Hertz, L., and Dienel, G. A. (2005). Lactate transport and transporters: general principles and functional roles in brain cells. *J. Neurosci. Res.* 79, 11–18. doi: 10.1002/jnr.20294

Hill, R. A., Li, A. M., and Grutzendler, J. (2018). Lifelong cortical myelin plasticity and age-related degeneration in the live mammalian brain. *Nat. Neurosci.* 21, 683–695. doi: 10.1038/s41593-018-0120-6

Hoagland, E. N., Sherwood, T. W., Lee, K. G., Walker, C. J., and Askwith, C. C. (2010). Identification of a calcium permeable human acid-sensing ion channel 1 transcript variant. *J. Biol. Chem.* 285, 41852–41862. doi: 10.1074/jbc.M110.171330

Hu, R., Duan, B., Wang, D. S., Yu, Y., Li, W. G., Luo, H. S., et al. (2011). Role of acid-sensing ion channel 1a in the secondary damage of traumatic spinal cord injury. *Ann. Surg.* 254, 353–362. doi: 10.1097/SLA.0b013e31822645b4

Huang, A. L., Chen, X., Hoon, M. A., Chandrashekar, J., Guo, W., Tränkner, D., et al. (2006). The cells and logic for mammalian sour taste detection. *Nature* 442, 934–938. doi: 10.1038/nature05084

Huang, C. J., Haque, I. U., Slovin, P. N., Nielsen, R. B., Fang, X., and Skimming, J. W. (2002). Environmental pH regulates LPS-induced nitric oxide formation in murine macrophages. *Nitric Oxide* 6, 73–78. doi: 10.1006/niox.2001.0391

Huang, C., Hu, Z.-L., Wu, W.-N., Yu, D.-F., Xiong, Q.-J., Song, J.-R., et al. (2010). Existence and distinction of acid-evoked currents in rat astrocytes. *Glia* 58, 1415–1424. doi: 10.1002/glia.21017

Immke, D., and McCleskey, E. (2001). Lactate enhances the acid-sensing Na^+ channel on ischemia-sensing neurons. *Nat. Neurosci.* 4, 869–870. doi: 10.1038/nn0901-869

Ishibashi, K., and Marumo, F. (1998). Molecular cloning of a DEG/ENaC sodium channel cDNA from human testis. *Biochem. Biophys. Res. Commun.* 245, 589–593. doi: 10.1006/bbrc.1998.8483

Jack, C., Ruffini, F., Bar-Or, A., and Antel, J. P. (2005). Microglia and multiple sclerosis. *J. Neurosci. Res.* 81, 363–373. doi: 10.1002/jnr.20482

Jahr, H., van Driel, M., van Osch, G. J. V. M., Weinans, H., and van Leeuwen, J. P. T. M. (2005). Identification of acid-sensing ion channels in bone. *Biochem. Biophys. Res. Commun.* 337, 349–354.

Jalalvand, E., Robertson, B., Tostivint, H., Wallén, P., and Grillner, S. (2016). The spinal cord has an intrinsic system for the control of pH. *Curr. Biol.* 26, 1346–1351. doi: 10.1016/j.cub.2016.03.048

Jasti, J., Furukawa, H., Gonzales, E. B., and Gouaux, E. (2007). Structure of acid-sensing ion channel 1 at 1.9 Å resolution and low pH. *Nature* 449:316. doi: 10.1038/nature06163

Jensen, J. C., Buresh, C., and Norton, J. A. (1990). Lactic acidosis increases tumor necrosis factor secretion and transcription in vitro. *J. Surg. Res.* 49, 350–353. doi: 10.1016/0022-4804(90)90036-2

Jörres, A., Gahl, G. M., and Frei, U. (1995). In vitro studies on the effect of dialysis solutions on peritoneal leukocytes. *Peritoneal Dialysis Int.* 15, S41–S45.

Josefsen, K., Nielsen, S., Campos, A., Seifert, T., Hasholt, L., Nielsen, J., et al. (2010). Reduced gluconeogenesis and lactate clearance in Huntington's disease. *Neurobiol. Dis.* 40, 656–662. doi: 10.1016/j.nbd.2010.08.009

Kanyilmaz, S., Hepguler, S., Atamaz, F., Gokmen, N., Ardeniz, O., and Sin, A. (2013). Phagocytic and oxidative burst activity of neutrophils in patients with spinal cord injury. *Arch. Phys. Med. Rehabil.* 94, 369–374.

Karman, J., Chu, H., Co, D., Seroogy, C. M., Sandor, M., and Fabry, Z. (2006). Dendritic cells amplify T cell-mediated immune responses in the central nervous system. *J. Immunol.* 177, 7750–7760.

Kellenberger, S., and Schild, L. (2015). International union of basic and clinical pharmacology. XCI. structure, function, and pharmacology of acid-sensing

ion channels and the epithelial Na^+ channel. *Pharmacol. Rev.* 67, 1–35. doi: 10.1124/pr.114.009225

Kellum, J. A., Song, M., and Li, J. (2004). Science review: extracellular acidosis and the immune response: clinical and physiologic implications. *Crit. Care* 8, 331–336. doi: 10.1186/cc2900

Kierdorf, K., Erny, D., Goldmann, T., Sander, V., Schulz, C., Perdiguero, E., et al. (2013). Microglia emerge from erythromyeloid precursors via Pu.1- and Irf8-dependent pathways. *Nat. Neurosci.* 16, 273–280. doi: 10.1038/nn.3318

Kilgore, K. S., Friedrichs, G. S., Homeister, J. W., and Lucchesi, B. R. (1994). The complement system in myocardial ischaemia/reperfusion injury. *Cardiovasc. Res.* 28, 437–444. doi: 10.1093/cvr/28.4.437

Koehn, L. M., Noor, N. M., Dong, Q., Er, S.-Y., Rash, L. D., King, G. F., et al. (2016). Selective inhibition of ASIC1a confers functional and morphological neuroprotection following traumatic spinal cord injury. *F1000Research* 5:1822. doi: 10.12688/f1000research.9094.2

Komnig, D., Imgrund, S., Reich, A., Grunder, S., and Falkenburger, B. H. (2016). ASIC1a deficient mice show unaltered neurodegeneration in the subacute MPTP model of Parkinson disease. *PLoS One* 11:e0165235. doi: 10.1371/journal.pone.0165235

Kondo, M., Wagers, A. J., Manz, M. G., Prohaska, S. S., Scherer, D. C., Beilhack, G. F., et al. (2003). Biology of hematopoietic stem cells and progenitors: implications for clinical application. *Annu. Rev. Immunol.* 21, 759–806. doi: 10.1146/annurev.immunol.21.120601.141007

Kong, X., Tang, X., Du, W., Tong, J., Yan, Y., Zheng, F., et al. (2013). Extracellular acidosis modulates the endocytosis and maturation of macrophages. *Cell. Immunol.* 281, 44–50. doi: 10.1016/j.cellimm.2012.12.009

Korn, T., and Kallies, A. (2017). T cell responses in the central nervous system. *Nat. Rev. Immunol.* 17:179. doi: 10.1038/nri.2016.144

Kubota, K., Saiwai, H., Kumamaru, H., Maeda, T., Ohkawa, Y., Aratani, Y., et al. (2012). Myeloperoxidase exacerbates secondary injury by generating highly reactive oxygen species and mediating neutrophil recruitment in experimental spinal cord injury. *Spine* 37, 1363–1369. doi: 10.1097/BRS.0b013e31824b9e77

Lee, S. J., Drabik, K., Van Wagoner, N. J., Lee, S., Choi, C., Dong, Y., et al. (2000). ICAM-1-induced expression of proinflammatory cytokines in astrocytes: involvement of extracellular signal-regulated kinase and p38 mitogen-activated protein kinase pathways. *J. Immunol.* 165, 4658–4666.

Lee, S. Y., and Chung, W. S. (2021). The roles of astrocytic phagocytosis in maintaining homeostasis of brains. *J. Pharmacol. Sci.* 145, 223–227. doi: 10.1016/j.jphs.2020.12.007

Lennox, W. G. (1928). The effect on epileptic seizures of varying the composition of the respired air. *J. Clin. Invest.* 6, 23–24.

Li, M., Inoue, K., Branigan, D., Kratzer, E., Hansen, J. C., Chen, J. W., et al. (2010). Acid-sensing ion channels in acidosis-induced injury of human brain neurons. *J. Cerebral Blood Flow Metab.* 30, 1247–1260. doi: 10.1038/jcbfm.2010.30

Li, Q., and Barres, B. (2018). Microglia and macrophages in brain homeostasis and disease. *Nat. Rev. Immunol.* 18, 225–242. doi: 10.1038/nri.2017.125

Liang, J.-J., Huang, L.-F., Chen, X.-M., Pan, S.-Q., Lu, Z.-N., and Xiao, Z.-M. (2015). Amiloride suppresses pilocarpine-induced seizures via ASICs other than NHE in rats. *Int. J. Clin. Exp. Path.* 8, 14507–14513.

Lin, S. H., Sun, W. H., and Chen, C. C. (2015). Genetic exploration of the role of acid-sensing ion channels. *Neuropharmacology* 94, 99–118. doi: 10.1016/j.neuropharm.2014.12.011

Luck, K., Kim, D. K., Lambourne, L., Spirohn, K., Begg, B. E., Bian, W., et al. (2020). A reference map of the human binary protein interactome. *Nature* 580, 402–408. doi: 10.1038/s41586-020-2188-x

Lv, R. J., He, J. S., Fu, Y. H., Zhang, Y. Q., Shao, X. Q., Wu, L. W., et al. (2011). ASIC1a polymorphism is associated with temporal lobe epilepsy. *Epilepsy Res.* 96, 74–80. doi: 10.1016/j.eplepsyres.2011.05.002

Lynagh, T., Mikhaleva, Y., Colding, J. M., Glover, J. C., and Pless, S. A. (2018). Acid-sensing ion channels emerged over 600 Mya and are conserved throughout the deuterostomes. *Proc. Natl. Acad. Sci. USA* 115, 8430–8435. doi: 10.1073/pnas.1806614115

Marchi, N., Granata, T., Ghosh, C., and Janigro, D. (2012). Blood-brain barrier dysfunction and epilepsy: pathophysiologic role and therapeutic approaches. *Epilepsia* 53, 1877–1886. doi: 10.1111/j.1528-1167.2012.03637.x

Martínez, D., Vermeulen, M., von Euw, E., Sabatté, J., Maggíni, J., Ceballos, A., et al. (2007). Extracellular acidosis triggers the maturation of human dendritic cells and the production of IL-12. *J. Immunol.* 179, 1950–1959. doi: 10.4049/jimmunol.179.3.1950

Maubaret, C., Delettre, C., Sola, S., and Hamel, C. P. (2002). Identification of preferentially expressed mRNAs in retina and cochlea. *DNA Cell Biol.* 21, 781–791. doi: 10.1089/104454902320908432

McCarthy, C. A., Rash, L. D., Chassagnon, I. R., King, G. F., and Widdop, R. E. (2015). PcTx1 affords neuroprotection in a conscious model of stroke in hypertensive rats via selective inhibition of ASIC1a. *Neuropharmacology* 99, 650–657. doi: 10.1016/j.neuropharm.2015.08.040

Mikhail, J. (1999). The trauma triad of death: hypothermia, acidosis, and coagulopathy. *AACN Clin. Issues* 10, 85–94.

Miller, J. W. (2011). Stopping seizures with carbon dioxide. *Epilepsy Curr.* 11, 114–115. doi: 10.5698/1535-7511-11.4.114

Mitra, B., Tullio, F., Cameron, P. A., and Fitzgerald, M. (2012). Trauma patients with the 'triad of death'. *Emerg. Med. J.* 29, 622–625. doi: 10.1136/emj.2011.113167

Moskowitz, M., Lo, E., and Iadecola, C. (2010). The science of stroke: mechanisms in search of treatments. *Neuron* 67, 181–198. doi: 10.1016/j.neuron.2010.07.002

Nadolni, W., and Zierler, S. (2018). The channel-kinase TRPM7 as novel regulator of immune system homeostasis. *Cells* 7:109. doi: 10.3390/cells7080109

Nagata, S., Hanayama, R., and Kawane, K. (2010). Autoimmunity and the clearance of dead cells. *Cell* 140, 619–630. doi: 10.1016/j.cell.2010.02.014

Neirinckx, V., Coste, C., Franzen, R., Gothot, A., Rogister, B., and Wislet, S. (2014). Neutrophil contribution to spinal cord injury and repair. *J. Neuroinflamm.* 11:150. doi: 10.1186/s12974-014-0150-2

Neri, T., Scalise, V., Passalacqua, I., Giusti, I., Lombardi, S., Balia, C., et al. (2018). CD18-mediated adhesion is required for the induction of a proinflammatory phenotype in lung epithelial cells by mononuclear cell-derived extracellular vesicles. *Exp. Cell Res.* 365, 78–84. doi: 10.1016/j.yexcr.2018.02.023

Nimmerjahn, A., Kirchhoff, F., and Helmchen, F. (2005). Resting microglial cells are highly dynamic surveillants of brain parenchyma in vivo. *Science* 308, 1314–1318. doi: 10.1126/science.1110647

Norris, G. T., and Kipnis, J. (2019). Immune cells and CNS physiology: Microglia and beyond. *J. Exp. Med.* 216, 60–70. doi: 10.1084/jem.20180199

Olena, Y., Leonard, A. S., Mikael, K. S., Francois, M. A., and Michael, J. W. (2004). Extracellular acidosis increases neuronal cell calcium by activating acid-sensing ion channel 1a. *Proc. Natl. Acad. Sci. USA* 101, 6752–6757. doi: 10.1073/pnas.0308636100

Paukert, M., Babini, E., Pusch, M., and Grunder, S. (2004). Identification of the Ca^{2+} blocking site of acid-sensing ion channel (ASIC)1: implications for channel gating. *J. Gen. Physiol.* 124, 383–394. doi: 10.1085/jgp.200308973

Peferoen, L., Kipp, M., Valk, P., Noort, J. M., and Amor, S. (2014). Oligodendrocyte-microglia cross-talk in the central nervous system. *Immunology* 141, 302–313. doi: 10.1111/imm.12163

Pignataro, G., Simon, R. P., and Xiong, Z.-G. (2007). Prolonged activation of ASIC1a and the time window for neuroprotection in cerebral ischaemia. *Brain* 130, 151–158. doi: 10.1093/brain/awl325

Polman, C. H., O'Connor, P. W., Havrdova, E., Hutchinson, M., Kappos, L., Miller, D. H., et al. (2006). A randomized, placebo-controlled trial of natalizumab for relapsing multiple sclerosis. *New Engl. J. Med.* 354, 899–910. doi: 10.1056/NEJMoa044397

Ponath, G., Park, C., and Pitt, D. (2018). The role of astrocytes in multiple sclerosis. *Front. Immunol.* 9:217. doi: 10.3389/fimmu.2018.00217

Popovich, G. P., Guan, F. Z., McGaughy, M. V., Fisher, M. L., Hickey, M. W., and Basso, M. D. (2002). The neuropathological and behavioral consequences of intraspinal microglial/macrophage activation. *J. Neuropathol. Exp. Neurol.* 61, 623–633. doi: 10.1093/jnen/61.7.623

Radu, B. M., Dumitrescu, D. I., Marin, A., Banciu, D. D., Iancu, A. D., Selescu, T., et al. (2014). Advanced type 1 diabetes is associated with ASIC alterations in mouse lower thoracic dorsal root ganglia neurons. *Cell Biochem. Biophys.* 68, 9–23. doi: 10.1007/s12013-013-9678-5

Ramesh, G., Benge, S., Pahar, B., and Philipp, M. T. (2012). A possible role for inflammation in mediating apoptosis of oligodendrocytes as induced by the Lyme disease spirochete *Borrelia burgdorferi*. *J. Neuroinflamm.* 9, 72. doi: 10.1186/1742-2094-9-72

Rash, L. D. (2017). Acid-sensing ion channel pharmacology, past, present, and future. *Adv. Pharmacol.* 79, 35–66. doi: 10.1016/bs.apha.2017.02.001

Redd, M. A., Scheuer, S. E., Saez, N. J., Yoshikawa, Y., Chiu, H. S., Gao, L., et al. (2021). Therapeutic inhibition of acid sensing ion channel 1a recovers heart function after ischemia-reperfusion injury. *Circulation* doi: 10.1161/CIRCULATIONAHA.121.054360

Rehncrona, S. (1985). Brain acidosis. *Ann. Emerg. Med.* 14, 770–776. doi: 10.1016/S0196-0644(85)80055-X

Reis e Sousa, C. (2006). Dendritic cells in a mature age. *Nat. Rev. Immunol.* 6, 476–483. doi: 10.1038/nri1845

Riemann, A., Wußling, H., Loppnow, H., Fu, H., Reime, S., and Thews, O. (2016). Acidosis differently modulates the inflammatory program in monocytes and macrophages. *Biochim. Biophys. Acta* 1862, 72–81. doi: 10.1016/j.bbadis.2015.10.017

Rock, K. L., Latz, E., Ontiveros, F., and Kono, H. (2010). The sterile inflammatory response. *Ann. Rev. Immunol.* 28, 321–342. doi: 10.1146/annurev-immunol-030409-101311

Rotstein, O. D., Fiegel, V. D., Simmons, R. L., and Knighton, D. R. (1988). The deleterious effect of reduced pH and hypoxia on neutrophil migration in vitro. *J. Surg. Res.* 45, 298–303. doi: 10.1016/0022-4804(88)90079-0

Sagar, D., Lamontagne, A., Foss, C. A., Khan, Z. K., Pomper, M. G., and Jain, P. (2012). Dendritic cell CNS recruitment correlates with disease severity in EAE via CCL2 chemotaxis at the blood–brain barrier through paracellular transmigration and ERK activation. *J. Neuroinflamm.* 9:245. doi: 10.1186/1742-2094-9-245

Savio, L. E. B., de Andrade Mello, P., da Silva, C. G., and Coutinho-Silva, R. (2018). The P2X7 receptor in inflammatory diseases: angel or demon? *Front. Pharmacol.* 6:52. doi: 10.3389/fphar.2018.00052

Schulz, C., Chorro, L., Szabo-Rogers, H., Cagnard, N., Kierdorf, K., Prinz, M., et al. (2012). A lineage of myeloid cells independent of myb and hematopoietic stem cells. *Science* 336, 86–90. doi: 10.1126/science.1219179

Schulz, J. B., Huang, P. L., Matthews, R. T., Passov, D., Fishman, M. C., and Beal, M. F. (1996). Striatal malonate lesions are attenuated in neuronal nitric oxide synthase knockout mice. *J. Neurochem.* 67, 430–433.

Serrano, C., Fraticelli, A., Paniccia, R., Teti, A., Noble, B., Corda, S., et al. (1996). pH dependence of neutrophil-endothelial cell adhesion and adhesion molecule expression. *Am. J. Physiol. Cell Physiol.* 271, C962–C970.

Sherwood, T. W., Lee, K. G., Gormley, M. G., and Askwith, C. C. (2011). Heteromeric acid-sensing ion channels (ASICs) composed of ASIC2b and ASIC1a display novel channel properties and contribute to acidosis-induced neuronal death. *J. Neurosci.* 31, 9723–9734. doi: 10.1523/JNEUROSCI.1665-11.2011

Shteinikov, V. Y., Korosteleva, A. S., Tikhonova, T. B., Potapieva, N. N., and Tikhonov, D. B. (2017). Ligands of histamine receptors modulate acid-sensing ion channels. *Biochem. Biophys. Res. Commun.* 490, 1314–1318. doi: 10.1016/j.bbrc.2017.07.019

Sinescu, C., Popa, F., Grigorean, V. T., Onose, G., Sandu, A., Popescu, M., et al. (2010). Molecular basis of vascular events following spinal cord injury. *J. Med. Life* 3, 254–261.

Sluka, K., Price, M. P., Breese, N., Stucky, C., Wemmie, J., and Welsh, M. (2003). Chronic hyperalgesia induced by repeated acid injections in muscle is abolished by the loss of ASIC3, but not ASIC1. *Pain* 106, 229–239. doi: 10.1016/S0304-3959(03)00269-0

Smith, E. S., Cadiou, H., and McNaughton, P. A. (2007). Arachidonic acid potentiates acid-sensing ion channels in rat sensory neurons by a direct action. *Neuroscience* 145, 686–698. doi: 10.1016/j.neuroscience.2006.12.024

Smoller, J. W., Gallagher, P. J., Duncan, L. E., McGrath, L. M., Haddad, S. A., Holmes, A. J., et al. (2014). The human ortholog of acid-sensing ion channel gene ASIC1a is associated with panic disorder and amygdala structure and function. *Biol. Psychiat.* 76, 902–910. doi: 10.1016/j.biopsych.2013.12.018

Song, N., Lu, Z., Zhang, J., Shi, Y., Ning, Y., Chen, J., et al. (2019). Acid-sensing ion channel 1a is involved in ischaemia/reperfusion induced kidney injury by increasing renal epithelia cell apoptosis. *J. Cell. Mol. Med.* 23, 3429–3440. doi: 10.1111/jcmm.14238

Stranahan, A. M., Hao, S., Dey, A., Yu, X., and Baban, B. (2016). Blood-brain barrier breakdown promotes macrophage infiltration and cognitive impairment in leptin receptor-deficient mice. *J. Cerebral. Blood Flow Metab.* 36, 2108–2121. doi: 10.1177/0271678X16642233

Sun, X., Wang, J.-F., Tseng, M., and Young, L. T. (2006). Downregulation in components of the mitochondrial electron transport chain in the postmortem frontal cortex of subjects with bipolar disorder. *J. Psychiatry Neurosci.* 31, 189–196.

Suzuki, H., Savitz, J., Kent Teague, T., Gandhapudi, S. K., Tan, C., Misaki, M., et al. (2017). Altered populations of natural killer cells, cytotoxic T lymphocytes, and regulatory T cells in major depressive disorder: Association with sleep disturbance. *Brain Behav. Immun.* 66, 193–200. doi: 10.1016/j.bbi.2017.06.011

Suzuki, Y., Nagai, N., and Umemura, K. (2016). A review of the mechanisms of blood-brain barrier permeability by tissue-type plasminogen activator treatment for cerebral ischemia. *Front. Cell. Neurosci.* 10:2. doi: 10.3389/fncel.2016.00002

Tan, J., Xu, Y. P., Liu, G. P., and Ye, X. H. (2013). Involvement of acid-sensing ion channel 1a in functions of cultured human retinal pigment epithelial cells. *J. Huazhong Univ. Sci. Technol. Med. Sci.* 33, 137–141. doi: 10.1007/s11596-013-1086-y

Taoka, Y., Okajima, K., Murakami, K., Johno, M., and Naruo, M. (1998). Role of neutrophil elastase in compression-induced spinal cord injury in rats. *Brain Res. Bull.* 799, 264–269. doi: 10.1016/S0006-8993(98)00459-4

Tian, Y., Bresenitz, P., Reska, A., El Moussaoui, L., Beier, C. P., and Gründer, S. (2017). Glioblastoma cancer stem cell lines express functional acid sensing ion channels ASIC1a and ASIC3. *Sci. Rep.* 7:13674. doi: 10.1038/s41598-017-13666-9

Tong, J., Wu, W.-N., Kong, X., Wu, P.-F., Tian, L., Du, W., et al. (2011). Acid-sensing ion channels contribute to the effect of acidosis on the function of dendritic cells. *J. Immunol.* 186, 3686–3692.

Town, T., Tan, J., Flavell, R. A., and Mullan, M. (2005). T-cells in Alzheimer's disease. *Neuro Mol. Med.* 7, 255–264. doi: 10.1385/NMM:7:3:255

Trevani, A. S., Andonegui, G., Giordano, M., López, D. H., Gamberale, R., Minucci, F., et al. (1999). Extracellular acidification induces human neutrophil activation. *J. Immunol.* 162, 4849–4857.

Tsang, T. M., Woodman, B., McLoughlin, G. A., Griffin, J. L., Tabrizi, S. J., Bates, G. P., et al. (2006). Metabolic characterization of the R6/2 transgenic mouse model of Huntington's disease by high-resolution MAS ^{1}H NMR spectroscopy. *J. Proteome Res.* 5, 483–492.

Turner, M. D., Nedjai, B., Hurst, T., and Pennington, D. J. (2014). Cytokines and chemokines: at the crossroads of cell signalling and inflammatory disease. *Biochim. Biophys. Acta* 1843, 2563–2582.

Vaeth, M., and Feske, S. (2018). Ion channelopathies of the immune system. *Curr. Opin. Immunol.* 52, 39–50. doi: 10.1016/j.coi.2018.03.021

Vergo, S., Craner, M., Etzensperger, R., Attfield, K., Friese, M., Newcombe, J., et al. (2011). Acid-sensing ion channel 1 is involved in both axonal injury and demyelination in multiple sclerosis and its animal model. *Brain* 134, 571–584. doi: 10.1093/brain/awq337

Vermeulen, M. E., Gamberale, R., Trevani, A. S., Martinez, D., Ceballos, A., Sabatte, J., et al. (2004). The impact of extracellular acidosis on dendritic cell function. *Crit. Rev. Immunol.* 24, 363–384. doi: 10.1615/CritRevImmunol.v24.i5.40

Vig, P. J. S., Hearst, S. M., Shao, Q. M., and Lopez, M. E. (2014). Knockdown of Acid-Sensing Ion Channel 1a (ASIC1a) suppresses disease phenotype in SCA1 mouse model. *Cerebellum* 13, 479–490. doi: 10.1007/s12311-014-0563-6

Voilley, N., de Weille, J., Mamet, J., and Lazdunski, M. (2001). Nonsteroid anti-inflammatory drugs inhibit both the activity and the inflammation-induced expression of acid-sensing ion channels in nociceptors. *J. Neurosci.* 21, 8026–8033. doi: 10.1523/JNEUROSCI.21-20-08026.2001

Vukicevic, M., and Kellenberger, S. (2004). Modulatory effects of acid-sensing ion channels on action potential generation in hippocampal neurons. *Am. J. Physiol. Cell Physiol.* 287, C682–C690.

Waldmann, R., Champigny, G., Bassilana, F., Heurteaux, C., and Lazdunski, M. (1997). A proton-gated cation channel involved in acid-sensing. *Nature* 386, 173. doi: 10.1038/386173a0

Waldmann, R., Champigny, G., Lingueglia, E., De Weille, J. R., Heurteaux, C., and Lazdunski, M. (1999). H^+-gated cation channels. *Ann. N.Y. Acad. Sci.* 868, 67–76.

Wang, J.-J., Liu, F., Yang, F., Wang, Y.-Z., Qi, X., Li, Y., et al. (2020). Disruption of auto-inhibition underlies conformational signaling of ASIC1a to induce neuronal necroptosis. *Nat. Commun.* 11:475. doi: 10.1038/s41467-019-13873-0

Wang, R. I., and Sonnenschein, R. R. (1955). pH of cerebral cortex during induced convulsions. *J. Neurophysiol.* 18, 130–137. doi: 10.1152/jn.1955.18.2.130

Wang, Y.-Z., Wang, J.-J., Huang, Y., Liu, F., Zeng, W.-Z., Li, Y., et al. (2015). Tissue acidosis induces neuronal necroptosis via ASIC1a channel independent of its ionic conduction. *eLife* 4:e05682. doi: 10.7554/eLife.05682

Waxman, S. G. (2006). Axonal conduction and injury in multiple sclerosis: the role of sodium channels. *Nat. Rev. Neurosci.* 7, 932–941. doi: 10.1038/nrn2023

Wemmie, J. A., Chen, J., Askwith, C. C., Hruska-Hageman, A. M., Price, M. P., Nolan, B. C., et al. (2002). The acid-activated ion channel ASIC contributes to synaptic plasticity, learning, and memory. *Neuron* 34, 463–477. doi: 10.1016/s0896-6273(02)00661-x

Wemmie, J. A., Coryell, M. W., Askwith, C. C., Lamani, E., Leonard, A. S., Sigmund, C. D., et al. (2004). Overexpression of acid-sensing ion channel 1a in transgenic mice increases acquired fear-related behavior. *Proc. Natl. Acad. Sci. USA* 101, 3621–3626. doi: 10.1073/pnas.0308753101

Wemmie, J., Askwith, C., Lamani, E., Cassell, M. D., Freeman, J., and Welsh, M. (2003). Acid-sensing ion channel 1 is localized in brain regions with high synaptic density and contributes to fear conditioning. *J. Neurosci.* 23, 5496–5502.

Wemmie, J., Taugher, R., and Kreple, C. (2013). Acid-sensing ion channels in pain and disease. *Nat. Rev. Neurosci.* 14, 461–471. doi: 10.1038/nrn3529

Weng, J. Y., Lin, Y. C., and Lien, C. C. (2010). Cell type-specific expression of acid-sensing ion channels in hippocampal interneurons. *J. Neurosci.* 30, 6548–6558. doi: 10.1523/jneurosci.0582-10.2010

Wong, G. H. W., Bartlett, P. F., Clark-Lewis, I., McKimm-Breschkin, J. L., and Schrader, J. W. (1984). Interferon-γ induces the expression of H-2 and Ia antigens on brain cells. *J. Neuroimmunol.* 7, 255–278. doi: 10.1016/S0165-5728(84)80026-0

Wong, H. K., Bauer, P. O., Kurosawa, M., Goswami, A., Washizu, C., Machida, Y., et al. (2008). Blocking acid-sensing ion channel 1 alleviates Huntington's disease pathology via an ubiquitin-proteasome system-dependent mechanism. *Hum. Mol. Genet.* 17, 3223–3235. doi: 10.1093/hmg/ddn218

Woodfin, A., Voisin, M.-B., and Nourshargh, S. (2007). PECAM-1: a multi-functional molecule in inflammation and vascular biology. *Arterioscler. Thromb. Vasc. Biol.* 27, 2514–2523. doi: 10.1161/ATVBAHA.107.151456

Wu, Y., Gao, B., Xiong, Q. J., Wang, Y. C., Huang, D. K., and Wu, W. N. (2017). Acid-sensing ion channels contribute to the effect of extracellular acidosis on proliferation and migration of A549 cells. *Tumour Biol.* 39:1010428317705750. doi: 10.1177/1010428317705750

Xiong, Z. G., Chu, X. P., and Simon, R. P. (2007). Acid sensing ion channels—novel therapeutic targets for ischemic brain injury. *Front. Biosci.* 12, 1376–1386. doi: 10.2741/2154

Xiong, Z.-G., Zhu, X.-M., Chu, X.-P., Minami, M., Hey, J., Wei, W.-L., et al. (2004). Neuroprotection in ischemia: blocking calcium-permeable acid-sensing ion channels. *Cell* 118, 687–698.

Yamasaki, R., Lu, H., Butovsky, O., Ohno, N., Rietsch, A. M., Cialic, R., et al. (2014). Differential roles of microglia and monocytes in the inflamed central nervous system. *J. Exp. Med.* 211, 1533–1549. doi: 10.1084/jem.20132477

Yang, F., Sun, X., Ding, Y., Ma, H., Yang, T. O., Ma, Y., et al. (2016). Astrocytic acid-sensing ion channel 1a contributes to the development of chronic epileptogenesis. *Sci. Rep.* 6:31581. doi: 10.1038/srep31581

Yermolaieva, O., Leonard, A. S., Schnizler, M. K., Abboud, F. M., and Welsh, M. J. (2004). Extracellular acidosis increases neuronal cell calcium by activating acid-sensing ion channel 1a. *Proc. Natl. Acad. Sci. USA* 101, 6752–6757.

Yu, X.-W., Hu, Z.-L., Ni, M., Fang, P., Zhang, P.-W., Shu, Q., et al. (2015). Acid-sensing ion channels promote the inflammation and migration of cultured rat microglia. *Glia* 63, 483–496. doi: 10.1002/glia.22766

Yuan, F. L., Chen, F. H., Lu, W. G., Li, X., Li, J. P., Li, C. W., et al. (2010). Inhibition of acid-sensing ion channels in articular chondrocytes by amiloride attenuates articular cartilage destruction in rats with adjuvant arthritis. *Inflamm. Res.* 59, 939–947. doi: 10.1007/s00011-010-0206-4

Zamanian, J., Xu, L., Foo, L. C., Nouri, N., Zhou, L., Giffard, R. G., et al. (2012). Genomic analysis of reactive astrogliosis. *J. Neurosci.* 32, 6391–6410. doi: 10.1523/JNEUROSCI.6221-11.2012

Zampieri, F. G., Kellum, J. A., Park, M., Ranzani, O. T., Barbeiro, H. V., de Souza, H. P., et al. (2014). Relationship between acid-base status and inflammation in the critically ill. *Crit. Care* 18:R154. doi: 10.1186/cc13993

Zeinstra, E., Wilczak, N., Streefland, C., and De Keyser, J. (2000). Astrocytes in chronic active multiple sclerosis plaques express MHC class II molecules. *NeuroReport* 11, 89–91. doi: 10.1097/00001756-200001170-00018

Zeng, W., Liu, D., Duan, B., Song, X. L., Wang, X., Wei, D., et al. (2013). Molecular mechanism of constitutive endocytosis of acid-sensing ion channel 1a and its protective function in acidosis-induced neuronal death. *J. Neurosci.* 33, 7066–7078. doi: 10.1523/JNEUROSCI.5206-12.2013

Zha, X. M., Wemmie, J. A., Green, S. H., and Welsh, M. J. (2006). Acid-sensing ion channel 1a is a postsynaptic proton receptor that affects the density of dendritic spines. *Proc. Natl. Acad. Sci. USA* 103, 16556–16561. doi: 10.1073/pnas.0608018103

Zhou, Z.-H., Song, J.-W., Li, W., Liu, X., Cao, L., Wan, L.-M., et al. (2017). The acid-sensing ion channel, ASIC2, promotes invasion and metastasis of colorectal cancer under acidosis by activating the calcineurin/NFAT1 axis. *J. Exp. Clin. Cancer Res.* 36:130. doi: 10.1186/s13046-017-0599-9

Ziemann, A. E., Allen, J. E., Dahdaleh, N. S., Drebot, I. I., Coryell, M. W., Wunsch, A. M., et al. (2009). The amygdala is a chemosensor that detects carbon dioxide and acidosis to elicit fear behavior. *Cell* 139, 1012–1021. doi: 10.1016/j.cell.2009.10.029

Ziemann, A. E., Schnizler, M. K., Albert, G. W., Severson, M. A., Howard, M. A., Welsh, M. J., et al. (2008). Seizure termination by acidosis depends on ASIC1a. *Nat. Neurosci.* 11, 816–822. doi: 10.1038/nn.2132

Conflict of Interest: The authors declare that the research was conducted in the absence of any commercial or financial relationships that could be construed as a potential conflict of interest.

Publisher's Note: All claims expressed in this article are solely those of the authors and do not necessarily represent those of their affiliated organizations, or those of the publisher, the editors and the reviewers. Any product that may be evaluated in this article, or claim that may be made by its manufacturer, is not guaranteed or endorsed by the publisher.

frontiers in Cellular Neuroscience

ORIGINAL RESEARCH
published: 05 October 2021
doi: 10.3389/fncel.2021.735414

Signaling Pathways in Proton and Non-proton ASIC1a Activation

*Libia Catalina Salinas Castellanos, Osvaldo Daniel Uchitel and Carina Weissmann**

Instituto de Fisiología, Biología Molecular y Neurociencias (IFIBYNE—UBA CONICET), Facultad de Ciencias, Exactas y Naturales de la Universidad de Buenos Aires, Buenos Aires, Argentina

Acid-sensing ion channels (ASICs) regulate synaptic activities and play important roles in neurodegenerative diseases as well as pain conditions. Classically, ASICs are described as transiently activated by a reduced pH, followed by desensitization; the activation allows sodium influx, and in the case of ASIC1a-composed channels, also calcium to some degree. Several factors are emerging and extensively analyzed as modulators, activating, inhibiting, and potentiating specific channel subunits. However, the signaling pathways triggered by channel activation are only starting to be revealed. The channel has been recently shown to be activated through a mechanism other than proton-mediated. Indeed, the large extracellular loop of these channels opens the possibility that other non-proton ligands might exist. One such molecule discovered was a toxin present in the Texas coral snake venom. The finding was associated with the activation of the channel at neutral pH *via* the toxin and causing intense and unremitting pain. By using different pharmacological tools, we analyzed the downstream signaling pathway triggered either by the proton and non-proton activation for human, mouse, and rat ASIC1a-composed channels in *in vitro* models. We show that for all species analyzed, the non-protonic mode of activation determines the activation of the ERK signaling cascade at a higher level and duration compared to the proton mode. This study adds to the growing evidence of the important role ASIC1a channels play in different physiological and pathological conditions and also hints at a possible pathological mechanism for a sustained effect.

Keywords: ASIC1a, proton activation, non-proton activation, ERK, MitTx, pain

OPEN ACCESS

Edited by:
Josef Bischofberger, University of Basel, Switzerland

Reviewed by:
Eric Gonzales, TCU & UNTHSC School of Medicine, United States
Lachlan Rash, The University of Queensland, Australia

****Correspondence:***
Carina Weissmann
carina.weissmann@gmail.com

Specialty section:
This article was submitted to Cellular Neurophysiology, a section of the journal Frontiers in Cellular Neuroscience

Received: *02 July 2021*
Accepted: *09 September 2021*
Published: *05 October 2021*

Citation:
Salinas Castellanos LC, Uchitel OD and Weissmann C (2021) Signaling Pathways in Proton and Non-proton ASIC1a Activation. Front. Cell. Neurosci. 15:735414. doi: 10.3389/fncel.2021.735414

INTRODUCTION

ASICs, also called proton-gated channels belong to the degenerin/epithelial Na^+ channel gene family (Boscardin et al., 2016). Five genes encode at least seven ASIC subtypes in rodents and humans, and three subunits constitute a functional unit in either homotrimeric or heterotrimeric structures (Boscardin et al., 2016). These channels are primarily expressed in the nervous system (Zha, 2013) and linked to several physiological (Uchitel et al., 2019) and pathological conditions (Chu and Xiong, 2013), thus different pharmacological tools have been developed as potential therapeutic treatments.

Abbreviations: ASIC, Acid Sensing Ion Chanel; eASIC, eGFP-ASIC1a; eASICx1 or eASICx3, eGFP-ASIC1a expressed at a single or triple-level; ERK, extracellular signal-regulated kinase; CaMKII, Calcium/Calmodulin kinase II.

ASICs are Na^+-selective ion channels, and ASIC1a,—a key subunit in the central nervous system (Wang et al., 2016)—, show, in addition to its Na^+ permeability, a small permeability to Ca^{2+} (Gründer and Chen, 2010). ASIC1a has been linked to neurodegenerative diseases (Friese et al., 2007; Wong et al., 2008; Sluka et al., 2009; Sun et al., 2011), ischemia (Xiong and Xu, 2012), and pain (Duan et al., 2007; Wemmie et al., 2013; Fan et al., 2018). The unique permeability to calcium compared with other subunits makes ASIC1a a candidate to play a prominent role in neuronal death (Hoagland et al., 2010).

Under experimental conditions, ASICs are activated only by rapid pH drops, and, particularly homomeric ASIC1a channels desensitize rapidly in the continuous presence of acidic pH (Chu and Xiong, 2013). This fact remains puzzling, as to whether a significant amount of ASIC1a current can be activated in pathological conditions, and as to whether the effect of its activation could be long-lasting (Chu and Xiong, 2013; Tikhonov et al., 2019; Alijevic et al., 2020); thus the functional significance of these channels remains to be determined. As pointed out by Zha (2013), although the canonical ligands for ASICs are protons, the massive extracellular domain of ASICs has led to the speculation that these receptors may also respond to other ligands (Zha, 2013) like MitTx purified from the venom of the Texas coral (Kweon and Suh, 2013). The toxin has been instrumental to document ASIC1a channels in an open state (Baconguis et al., 2014). MitTx elicits robust pain-related behavior in mice *via* activation of ASIC1 channels on capsaicin-sensitive nerve fibers (Bohlen et al., 2012).

Gautschi et al. (2017) on the unresolved question of the unphysiological pH values used to activate the channels and the transient nature of the proton evoked ASIC current, described another type of activation other than acid, as a "non-proton" mechanism (exemplified by MitTx), that activated a large sustained and non-desensitizing current at neutral pH and exceeding in magnitude the maximal current evoked by the proton mode (Gautschi et al., 2017).

Many studies have focused on the mechanism regulating the trafficking of the channel (Zeng et al., 2014; Boscardin et al., 2016; Wu et al., 2016), leading to changes in the amount of channel at the plasma membrane. The downstream signaling of ASIC channels, however, is only starting to be documented.

As an example, the activation of ERK *via* ASIC1a (downstream ASIC1a activation) has been analyzed in different pathological conditions (Chen et al., 2016; Sun et al., 2018; Zhu et al., 2020, 2021). In addition, this pathway has also been linked to inflammation (Yu et al., 2015). Conversely, the effect of MAP kinases on ASIC1a (upstream of ASIC1a activation) has also been analyzed in different scenarios (Duan et al., 2012; Aissouni et al., 2017; Peng and Kellenberger, 2021; Wei et al., 2021) especially in association to its effect on the insertion of channels, and thus increase of channels in the plasma membrane.

Work by Yu et al in striatal neurons established a critical link between ASIC1a activity and CaMKII-ERK signaling in the regulation of striatal synaptic remodeling (Yu et al., 2018). In addition, they showed up-regulation of the ERK pathway in HEK cells *via* acid activation of ASIC1a endogenous channels.

The ERK kinase belongs to the family of mitogen-activated protein kinases (MAPK) that operate within signaling cascades (Maik-Rachline et al., 2019). The activation of this pathway and the duration of the activation (Marshall, 1995; Kriegsheim et al., 2009) can lead to different biological responses that can determine the fate of a cell. In addition, the activation of the pathway has been implicated in pain research. Activation of the kinase *via* phosphorylation in the dorsal root ganglia has been linked to different models of pain in animals (Cruz and Cruz, 2007; Maruta et al., 2019). Different levels of activation of ERK were distinguished in response to acute noxious stimulation or chronic noxious stimulation by Cruz and Cruz (2007), with more intense levels of ERK phosphorylation and longer duration in animals with chronic inflammation of the hind paw or joint. In the study, spinal ERK activation was upregulated and became persistent (Cruz and Cruz, 2007).

In this study, we aim to address aspects of the downstream effects triggered by non-proton activation of ASIC1a channels.

MATERIALS AND METHODS

Cellular and Molecular Biology

Human embryonic kidney 293 (HEK) cells [passage 18–26, American Type Culture Collection (ATCC) number CRL-1573] were maintained by serial passages. Primary striatal cultures were prepared from mice of the C57BL/6 genetic background as control and ASIC1a−/− mice (generated using mice of the C57BL/6 genetic background) were provided by the laboratory of Dr. John A. Wemmie (University of Iowa, Iowa City, IA) as used before (González-Inchauspe et al., 2017) and prepared according to the protocol used in Sodero et al. (2011). All experiments involving mice were performed following national guidelines for the humane treatment of laboratory animals from the University of Buenos Aires (CICUAL Protocol #112), which are comparable to those of the USA National Institutes of Health. For biochemical analysis, six or 12-plates were coated with 0.1 mg/mL of poly-L-lysine (PLL, Sigma, P2636), and dissociated neuronal and HEK cells were plated at a density of 2.2×10^5 or 1.4×10^5 cells respectively. HEK cells were grown in Dulbecco's Modified Eagle's Medium containing 4 mM L-glutamine, 4.5 g/L glucose, and 110 ml/L sodium pyruvate and supplemented with 10% Fetal Calf Serum (NatoCor). Transfection of the cells was performed with the calcium phosphate method as described previously (Weissmann et al., 2013). The eGFP-ASIC1a encoding plasmid used was a gift of Dr. Stefan Gründer. Transfected cells were used 2 days after transfection. Neurons were grown in Neurobasal medium™ (Thermo Fisher) with B27 supplement (Thermo Fisher) and used after 7–8 days *in vitro*. HEK and neurons were both kept at 37°C and under 5% CO_2. For microscopy experiments, cells were plated on glass coverslips (12 mm rounded Carolina® Assistant-Brand Cover), coated with 1 mg/ml of PLL (Sigma, P2636). All materials were purchased from Sigma unless stated otherwise.

Drugs and Treatments

Incubation of cells: ASIC inhibitors were used at the following concentrations before incubation with other reagents: Pctx-1

(Alomone, STP-200), 20 nM, 30 min before; as previously used in Salinas et al. (2020). MitTx (Alomone, M-100) was used at a concentration of 20 nM for 2, 10 min according to Alomone Labs and (Bohlen et al., 2012). Solutions used for the different incubations were prepared as follows: for incubation of cells with the different reagents and controls were: solution at pH 7.3, containing the following (in mM): NaCl 128, KCl 2.5, $CaCl_2$ 2, $MgCl_2$ 1, glucose 15, sucrose 15, HEPES 5, MES 5 adjusted to pH 7.4; and for treatments to activate through the proton mechanism solution were adjusted to pH 6 with HCl ("pH6").

Western Blotting (WB)

Western blots were performed according to standard procedures. In brief, cells were resuspended in a 1% SDS HEPES pH 7.4 lysis buffer containing a protease inhibitor cocktail (Roche, cOmplete^{TM}); in the case of lysates used for detection of phosphorylated ERK, the buffer included 50 mM sodium fluoride, 2 mM sodium orthovanadate. Proteins were resolved by 4–10% polyacrylamide gels and transferred onto Immobilon®-FL PVDF membranes. Non-specific binding was blocked by 1% non-fat powdered milk in TBS containing 0.2% Tween-20 for 60 min at RT. Membranes were incubated overnight at 4°C with primary antibodies in 1% BSA in TBS, followed by the addition of secondary antibodies in 1% non-fat powdered milk in TBS.

The following primary antibodies were used: rabbit polyclonal anti ASIC1 (Alomone ASC-014, 1:1,000); mouse monoclonal anti-tubulin (DM1a; Cell signaling #3873, 1:5,000); rabbit polyclonal anti total ERK (Santa Cruz, C9, 1:500); rabbit polyclonal anti phosphoERK (Cell Signaling, SC-7383, 1:500); pCaMKII (Phosphosolutions, p1005-286). Initially, each antibody was detected in full membranes to verify that only the expected MW bands were present and the optimal dilution was decided upon. Accordingly, membranes were cut using MW standards as a guide to detect different proteins in the same membrane. No membrane stripping protocols were performed, thus bands of the same MW were obtained from the same samples run on different membranes. Reactive bands were detected by the LI-COR Odyssey system, using secondary antibodies: 926-68073 IRDye 680RD Donkey anti-Rabbit IgG or 926-32212 IRDye 800CW Donkey anti-Mouse.

Images were taken using the LI-COR Odyssey system and quantified with ImageJ software (NIH, USA).

Detection of Proteins by Immunofluorescence (IF)

Cells grown on PLL-coated glass coverslips were fixated with 4% p- formaldehyde in PBS, permeabilized with 0.1% Triton x-100 (10 min), and treated with blocking solution (1% BSA, 0.01% Triton x-100 in PBS) for an hour at RT. Coverslips were incubated then with the primary antibody for overnight in blocking buffer, washed in PBS, and incubated with the secondary antibody for 60 min in blocking buffer. After a final wash in PBS, coverslips, were placed onto a slide and covered with a mounting medium. The antibodies used were rabbit polyclonal antibody against mouse monoclonal anti-tubulin (DM1a; Cell Signaling, #3873, 1:2,000); rabbit polyclonal anti-phospho ERK (Phosphosolutions, p160–202, 1:100). Images were taken using an Olympus FV300/BX61 microscope with a 60× (1.4 NA) oil-immersion objective. Alexa-647 and Alexa-488-conjugated secondary antibodies (ThermoFisher) were used.

RESULTS

Activation of pERK Through ASIC1a *via* Non-proton Mechanisms

The effect of MitTx on the activation of ERK on mouse striatum cells was studied since the toxin can activate ASIC1a channels at neutral pH and for a longer duration (Bohlen et al., 2012). The effect was studied at the mouse striatum neurons as these cells are enriched in ASIC1 channels composed predominantly of ASIC1a subunits constituting homomeric channels (Jiang et al., 2009). Furthermore, Yu et al. (2018) showed at the striatum that a decrease in pH triggered the activation of the CaMKII signaling pathway leading to the activation of ERK kinases.

We decided to analyze whether the downstream effects of MitTx activation would lead to the same signaling pathways as those triggered by proton activation.

For this purpose, mouse striatal cultures were treated with MitTx and compared to cultures treated with acidic solutions. As shown in **Figures 1A–D**, MitTx-treated cultures evidence an increase in phospho ERK levels following the same pattern as phospho CaMKII activation which is much stronger than that shown for pH6-treated cultures at 2 min (as documented by Yu et al., 2018) or 30 min. The signal ratio of pERK/tERK for pH6 2' treated cells is four times greater than control cells (*pH6 2'* 3.77 ± 0.07), and *MitTx for 2'* leads to more than a 5-fold increase (*MitTx 2'* 5.39 ± 0.08). This effect is not present in striatal cultures obtained from ASIC1a knock-out cultures and treated either with pH6 solutions or MitTx (**Figure 1B**).

Proton and Non-proton Activation of ASIC1a Human Subunits

The effect of the non-proton activation of ASIC1a channels was analyzed further with MitTx on HEK cells that endogenously express ASIC1a subunits (Gunthorpe et al., 2001). Human, rat, and mice ASIC1a channels show differences, as shown for instance by a different degree of glycosylation that leads to different surface channel levels (Kadurin et al., 2008) and levels of activation (Xu et al., 2018). Therefore, we also tested the mechanism on this subunit. The activation of the pERK pathway has also been shown through the treatment of HEK cultures with pH6 solutions (Yu et al., 2018). **Figure 2** shows the effects of either pH6 or MitTx treatments of cultures for different durations and also after incubation of cultures with Psalmotoxin (Pctx-1) a toxin that stabilizes the desensitized state of the channel constituted by ASIC1a subunits (Chen et al., 2005).

The degree of ERK phosphorylation is not only greater through the non-proton mechanism [compare *pH6 2'* 6.10 ± 0.13 (6-fold increase) vs. *MitTx 2'* 7.98 ± 0.10, 8-fold increase] but also, these levels increase in time compared to the transient activation of ERK *via* the proton mechanism (*MitTx 10'* 10.90 ± 0.17, 10-fold increase to control levels). In both cases,

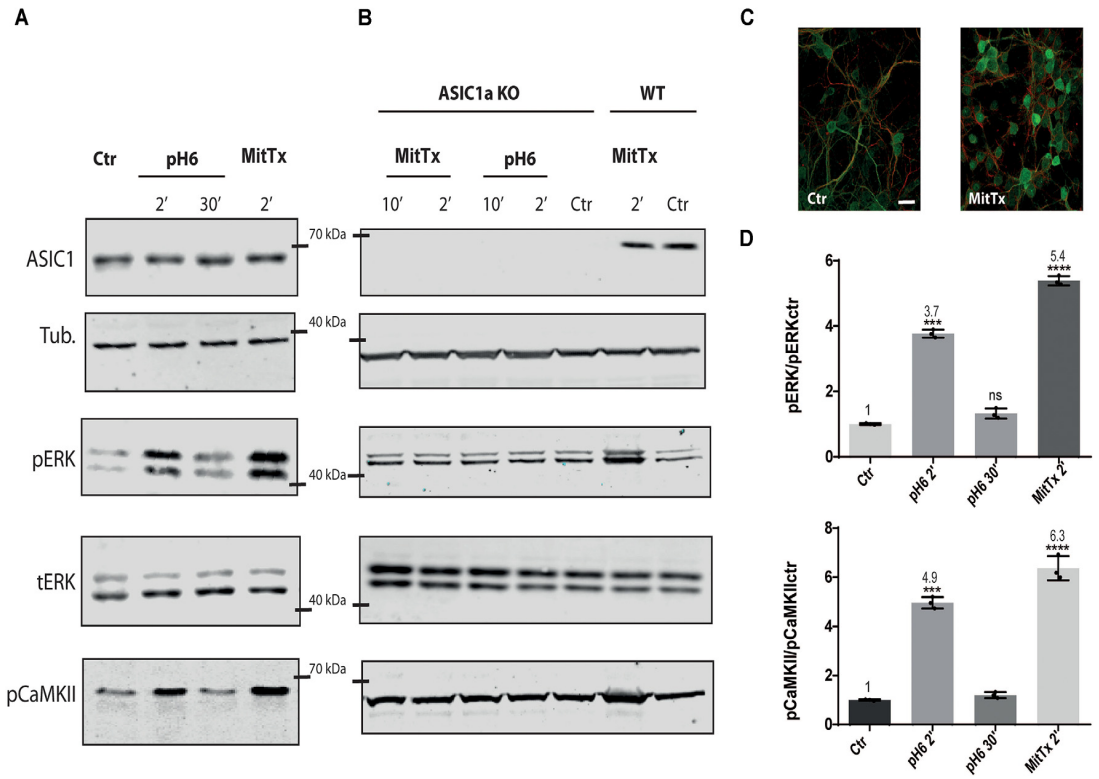

FIGURE 1 | Non-proton activation of ASIC1a in striatal neurons. Representative membranes of lysates from 7 DIV wild type **(A)**, and ASIC1a knockout **(B)** C57 mice striatal neuronal cultures were incubated with MitTx and compared to treatment with pH6 solutions for the time indicated (2, 10, or 30 min). The detection was performed with anti ASIC1, tubulin (Tub), phospho ERK (pERK), total ERK (tERK), or phospho CaMKII (pCaMKII) antibodies, and Licor secondary antibodies. **(C)** Examples of images of striatal cultures used and treated with MitTx and stained with tubulin (red) and phosphoERK (green) antibodies and secondary Alexa fluor antibodies, 60× objective used. Scale bar 10 μm. **(D)** Result of the bands detected in **(A)** for pERK/ERKt levels relative to control samples showing an increase in both, pH6 or MitTx treatments and the same pattern of increase for pCaMKII. Notice the lack of effect in ASIC1a knock-out derived cultures. **(A)** Notice that plots are the result of the signal intensity of the bands detected for each antibody, and tERK and tubulin are used as loading controls between loaded samples. Data are presented as the mean ± SEM ANOVA and Dunnet *post hoc* test for treatments against the control were performed, mean values above bars; $n = 3$ membranes, $^{****}p < 0.0001$; $^{***}p$ 0.0001–0.001; ns: no significant differences. Mean values expressed relative to control (**Ctr**) levels ± SEM are as follows: for pERK/tERK: **pH6 2'** 3.77 ± 0.07; **pH6 30'** 1.32 ± 0.09; **MitTx 2'** 5.39 ± 0.08. For pCaMKII/Tub: **pH6 2'** 4.97 ± 0.14; **pH6 30'** 1.20 ± 0.07; **MitTx 2'** 6.37 ± 0.28.

Pctx-1 can inhibit the activation of ERK to control levels. Phosphorylated ERK was detected even after 30 min incubation with MitTx (not shown).

Effect of Proton and Non-proton Activation and Different Levels of ASIC Channels

Different pathological conditions show an increase in ASIC1a levels (Duan et al., 2007). To model this situation and analyze the signaling pathway triggered by the non-proton activation of the channel, we used HEK cells transfected with different levels of ASIC1a channels using a plasmid encoding for the rat ASIC1a subunit fused to eGFP (eASIC), thus distinctively detected in WB *via* the different molecular weights (due to the eGFP tag added), as used before (Salinas et al., 2020).

As depicted in **Figure 3**, rat ASIC1a is also activated to a greater level when incubated with MitTx instead of pH6 (*MitTx* 3.42 ± 0.15 vs. *pH6* 1.85 ± 0.08). When HEK cells overexpress the channel (**Figures 3B,C**), the activation of the ERK pathway is increased at basal levels (compare **Ctr and eASICx1** bands, **Figure 3A**; and **eASICx3** 3.16 ± 0.06, normalized to eASICx1 levels), and is activated further *via* the proton or non-proton signaling mechanism. But as the increase becomes greater (compare transfection of plasmids to different levels, either "1x" or "3x"), the non-proton mechanism is still able to activate the channel to greater levels (**eASICx3 MitTx** 9.96 ± 0.12), whereas the proton activation is no longer able to reflect this change (**Figures 3A,B**). Interestingly, the pERK/tERK ratio of eASICx1-MitTx/eASICx1 and eASICx3-MitTx/eASICx3 remains about the same (3-fold increase).

DISCUSSION

In this study, we analyzed the signaling pathway triggered by the activation of ASIC1a channels through a non-proton mechanism.

We show that this mechanism determines the activation of the CaMKII-ERK pathway for a longer period than that resulting

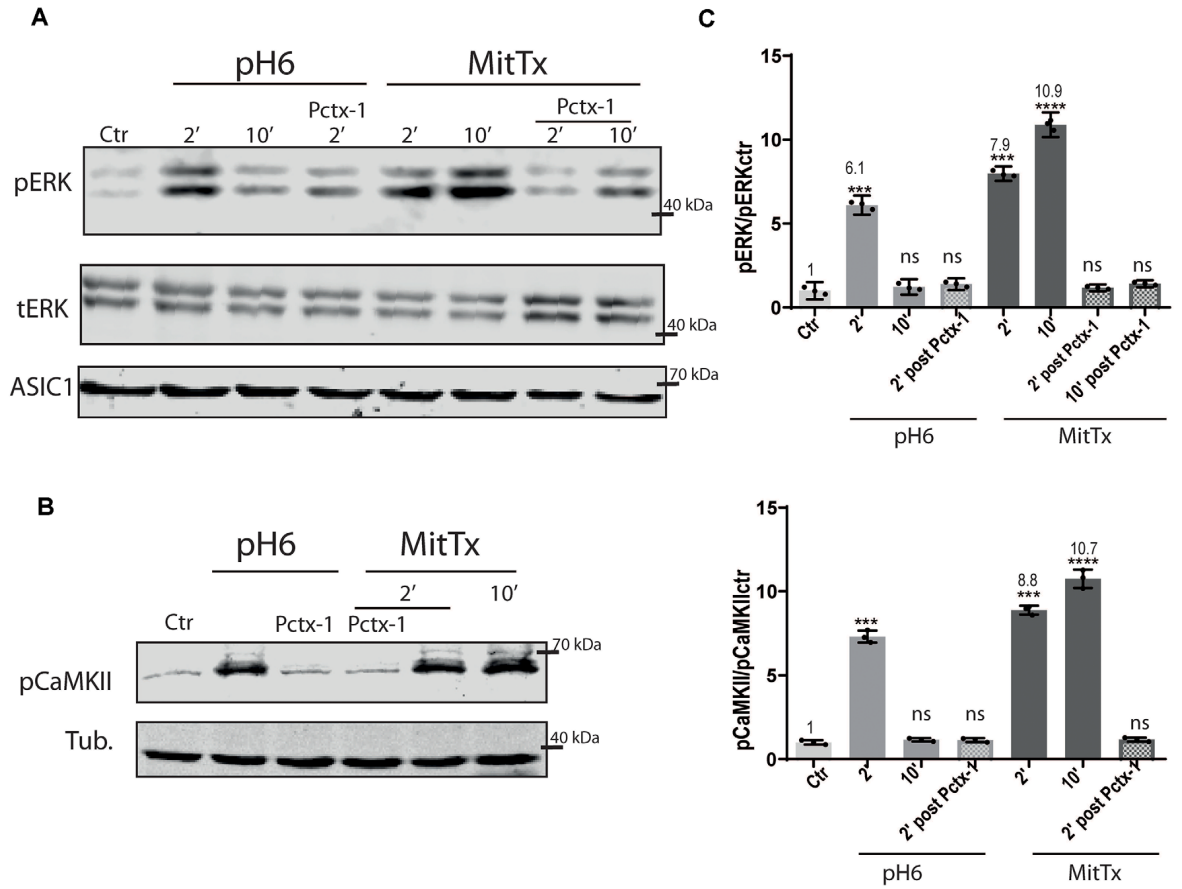

FIGURE 2 | Proton and non-proton activation of ASIC1a in HEK cells. **(A)** Representative membranes of lysates of HEK cells treated with pH6 or MitTx for 2 or 10 min or preincubated with Pctx-1 compared to untreated cells (control, Ctr) and detected with phosphoERK (pERK), total ERK (tERK), and ASIC1 antibodies. **(B)** Representative membrane of the same lysates to detect pCaMKII levels. **(C)** Plots showing detected levels of pERK (top panel) or pCaMKII (lower panel). Notice that the increase in kinase levels goes further at a later time point (2 vs. 10 min) in MitTx treated cultures compared to pH6 treated ones that show an increase at 2 min followed by a reversal to control levels consistent with the proton-activated desensitizing mechanism. **(A)** Notice that plots are the result of the signal intensity of the bands—with tERK and tubulin used as loading controls between loaded samples—and expressed relative to control samples. Data are presented as the mean ± SEM ANOVA and Dunnet *post hoc* test for treatments against the control were performed, mean values above bars; $n = 3$ membranes, ****$p < 0.0001$; ***p 0.0001–0.001; ns: no significant differences. Mean values expressed relative to control (**Ctr**) levels ± SEM are as follows: for pERK/tERK: **pH6 2'** 6.10 ± 0.13; **pH6 10'** 1.23 ± 0.11; **pH6 2' Pctx** 1.39 ± 0.08; **MitTx 2'** 7.98 ± 0.10; **Mittx10**' 10.90 ± 0.17; **MitTx 2' Pctx** 1.18 ± 0.05**; MitTx 10' Pctx** 1.42 ± 0.05. For pCaMKII/Tub: **pH6 2'** 7.31 ± 0.21; **pH6 10'** 1.16 ± 0.06; **pH6 2' Pctx**1.14±0.07; **Mittx 2'** 8.88 ± 0.15; **Mittx 10'** 10.76 ± 0.32; **Mittx 2' Pctx** 1.17 ± 0.07.

from proton activation. This mechanism was conserved for the different ASIC1a subunits analyzed (mouse, in **Figure 1**, human in **Figure 2**, and rat in **Figure 3**) in the different *in vitro* models. Furthermore, the mechanism could even reach higher levels if ASIC1a subunits were expressed at higher levels (**Figure 3**). The fact that mouse striatal KO cultures showed no evidence for this mechanism reinforces the argument that these mechanisms analyzed act *via* ASIC1a and no other pH-sensitive receptor.

The pathway (downstream ASIC1a activation) has been shown as signaling for different events relevant in physiological as well as pathological conditions (Kriegsheim et al., 2009). The mechanism, which is dependent on a stimulus that leads to the three-tier activation cascade with sequential kinase activation, has also been shown to crosstalk with the CaMKII pathway in many cells (Illario et al., 2003; Salzano et al., 2012). Accordingly, for some stimuli and cell models, CaMKII is necessary for ERK activation, and the activation of both has been shown for striatal cells through the proton-mediated activation of ASIC1a channels (Yu et al., 2018). Nevertheless, whether the mechanism requires the conducting channel is a matter of debate. We showed that the presence of Pctx-1 prevents this mechanism and that CaMKII is activated, but whether the mechanism could rely on a conduction-independent pathway cannot be ruled out. As an example, ASIC1a phosphorylation by RIP1 leading to necroptosis pathways does not rely on conducting channels (Wang et al., 2015, 2020). Future experiments will reveal more details on the mechanism.

A comparative analysis of both mechanisms analyzed in this work shows that the proton mechanism leads to transient activation of ERK which can no longer be detected after 5 min. Increases or a decrease in pERK levels were detected in previous work *via* ASIC1a. Amiloride significantly decreased

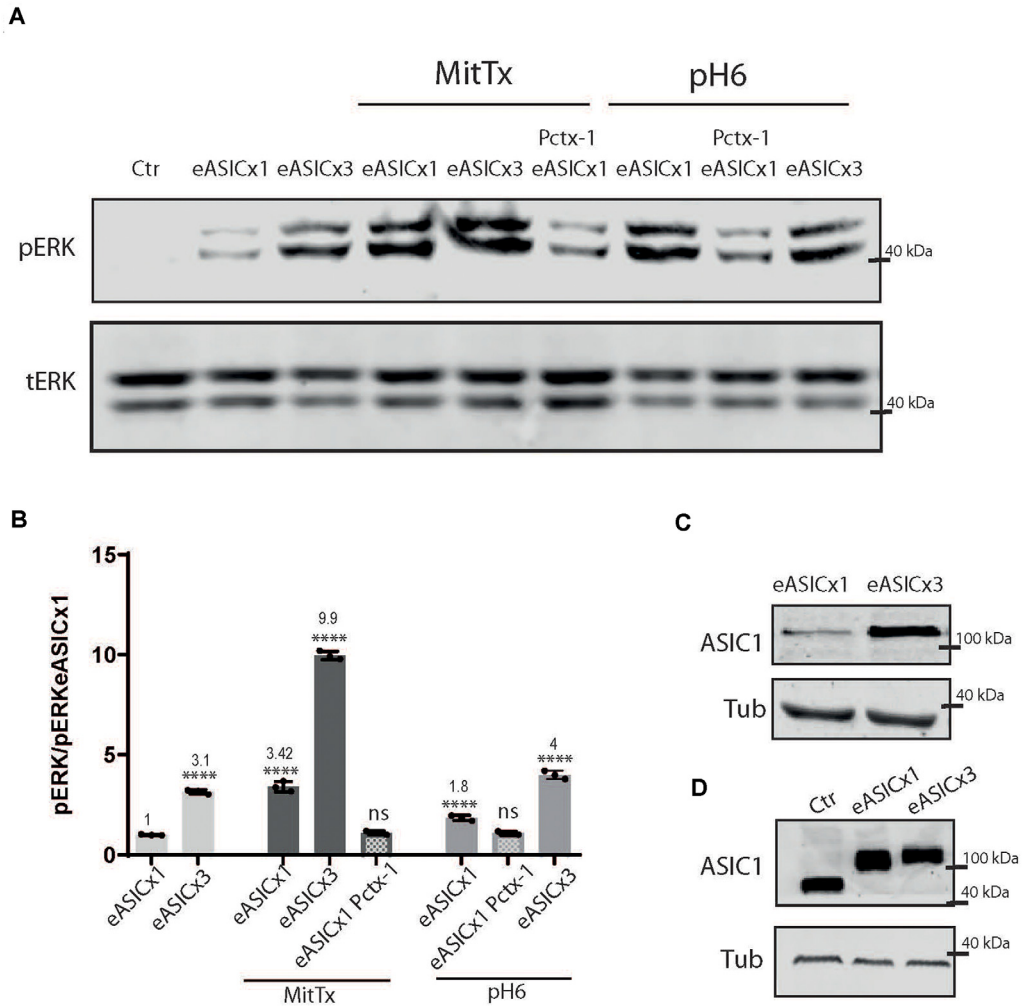

FIGURE 3 | Proton and non-proton activation of overexpressed ASIC1a channels. **(A)** Representative membranes of lysates of cells control (ctr) or transfected with eGFP-ASIC1a (eASIC) at two levels (1x or x3) to obtained different levels of expression of the protein ("eASICx1 or eASICx3"), and treated with pH6 or MitTx with or without pre-incubation of Pctx-1 or untreated. **(B)** Plots showing the increase in pERK and pCaMKII levels calculated from membranes as that shown in **(A)**, consistent with the increase in eASIC expressed. Notice the level of increase achievable *via* MitTx incubation at the highest overexpressed level of eASIC, higher than that obtained *via* pH6. **(C)** Representative membrane showing the different levels of eASIC in cells overexpressing the channel (1x or 3x), detected with an ASIC1 antibody. **(D)** Comparison between the different ASIC1 proteins expressed (the endogenous human ASIC1a; of approx. 67 kDa) and the overexpressed eASIC (approx. 110 kDa, and expressed at different levels; x1 or x3). **(A)** Notice that plots are the result of the signal intensity of the band detected, —tERK and tubulin are used as loading controls between loaded samples—and expressed relative to eASICx1 levels. Data are presented as the mean ± SEM ANOVA and Dunnet *post hoc* test for treatments and conditions were performed, mean values above bars; $n = 3$ membranes, $^{****}p < 0.0001$; ns: no significant differences. Mean values expressed relative to **eASICx1** levels ± SEM are as follows: **eASICx3** 3.16 ± 0.06; **eASIC MitTx** 3.42 ± 0.15; **eASICx3 MitTx** 9.96 ± 0.12; **eASIC MitTx Pctx** 1.10 ± 0.05; **eASIC pH6 2'** 1.85 ± 0.08; **eASIC pH6 2' Pctx** 1.08 ± 0.05; **eASICx3 pH6 2'** 4.00 ± 0.12.

(an approximately half-fold) the levels of CaMKKß and ERK phosphorylation in a cell line of hepatic fibroblasts stimulated by high glucose and PDGF (Wang et al., 2019). Zhu et al. (2020) showed a contribution of ASIC1a to increased ERK phosphorylation in the mechanism of liver fibrosis, as Pctx-1 treatment decreased the approximate 2-fold increase (without treatment) to a 1.5-fold increase. The same can be observed in ERK phosphorylated levels as the bands show a greater intensity for ERK-mediated NF-κB activation through ASIC1 in response to acidosis (although not quantified; Chen et al., 2016). In striatal and HEK cells, Yu et al. (2018) showed an increase in phosphorylation levels through pH 6 incubation reaching approximately 230% for ERK1 and 250% for ERK2 higher levels than control cells. In this work, we detected an increase in total phosphorylated ERK levels *via* the proton mechanism. In contrast, the non-proton activation of ASIC1a channels leads to the phosphorylation of ERK to a greater extent and for a longer period, as no desensitization is present (still active at 30 min). Thus, the activation of the channel in a non-proton mechanism (as in a Texas coral snake bite) would trigger sustained phosphorylation of ERK that could lead to further signaling. Additionally, we noted that the

increased phosphorylation of ERK (measured as the signal detected in pERK to tERK levels) reached the same level whether channels were expressed at higher levels as if the signaling could be the result of a fraction of occupied receptor mechanism (Andrews et al., 2016) that should be analyzed in the future.

The kinetics of ERK phosphorylation has been the subject of various studies (Kriegsheim et al., 2009; Ahmed et al., 2014; Shindo et al., 2016; Maik-Rachline et al., 2019). These studies revealed different aspects of the complexity in the regulation of ERK signaling, providing mathematical models accounting for different levels of regulation. Among these, negative feedback on ERK activation through upregulation of phosphatases that dephosphorylate ERK, as well as depletion of the stimulus (either through internalization or removal from the extracellular medium; Cirit et al., 2010) were shown to play a role in the transient shape of the signal. Additionally, ERK translocation to the nucleus and binding to cytosolic and nuclear substrates and dephosphorylation was also shown to play a main role in the kinetics of ERK signaling (Ahmed et al., 2014). Indeed, the translocation of ERK was later interpreted as a key to transforming a graded response (stimulus activating ERK) into a switch (ERK translocated to the nucleus) that can determine the fate of a cell (Shindo et al., 2016). Thus, ERK phosphorylated transiently (up to 5 min) or in a sustained manner determines a different biological response.

Nuclear ERK can determine the stabilization of immediate early gene products that can trigger further effects as observed by c-fos-mediated signaling when ERK is activated in a sustained manner (Murphy et al., 2002).

Our studies show that the proton-mediated activation of ASIC1a channels acts transiently activating ERK, the channel is desensitized and can no longer trigger the activation mechanism. This could be comparable to depletion of the stimulus.

The ERK pathway has been described as a network functioning as a potential switch, oscillator, or memory (Shindo et al., 2016). All these mechanisms concerning pain could lead to acute or persistent effects. Whether endogenous ligands for ASIC1a exist, however, remains to be determined. Nevertheless, the possibility that this pathway might explain aspects of pain warrants further analysis for potential therapies.

DATA AVAILABILITY STATEMENT

The original contributions presented in the study are included in the article, further inquiries can be directed to the corresponding author.

ETHICS STATEMENT

The animal study was reviewed and approved by CICUAL, University of Buenos Aires, Argentina.

AUTHOR CONTRIBUTIONS

ODU and CW contributed to the conception and design of the study. LCSC performed experiments and the statistical analysis. ODU and CW wrote the manuscript. All authors contributed to the article and approved the submitted version.

FUNDING

This work was supported by Grant 01/Q666 [20020130100666BA; Universidad de Buenos Aires Ciencia y Tecnología (UBACYT)] from University of Buenos Aires (to ODU), PICT 2016 # 3642 (to ODU), and Investigator-Initiated Research grant (no. IIR-AR-002659) funded by Takeda Pharmaceuticals International AG Singapore Branch (to ODU).

ACKNOWLEDGMENTS

We thank Dr. Stefan Gründer (RWTH-Aachen) for kindly providing us with the eGFP-ASIC1a plasmid, Valeria Buggiano for her help with cell lines, and Zaira Naguila and Fernanda Toledo for their help in the breeding of mice.

REFERENCES

Ahmed, S., Grant, K. G., Edwards, L. E., Rahman, A., Cirit, M., Goshe, M. B., et al. (2014). Data-driven modeling reconciles kinetics of ERK phosphorylation, localization and activity states. *Mol. Syst. Biol.* 10:718. doi: 10.1002/msb.134708

Aissouni, Y., El Guerrab, A., Mahdy Hamieh, A., Ferrier, J., Chalus, M., Lemaire, D., et al. (2017). Acid-sensing ion channel 1a in the amygdala is involved in pain and anxiety-related behaviours associated with arthritis. *Sci. Rep.* 7:43617. doi: 10.1038/srep43617

Alijevic, O., Bignucolo, O., Hichri, E., Peng, Z., Kucera, J. P., and Kellenberger, S. (2020). Slowing of the time course of acidification decreases the acid-sensing ion channel 1a current amplitude and modulates action potential firing in neurons. *Front. Cell. Neurosci.* 14:41. doi: 10.3389/fncel.2020.00041

Andrews, S. S., Peria, W. J., Yu, R. C., Colman-Lerner, A., and Brent, R. (2016). Push-pull and feedback mechanisms can align signaling system outputs with inputs. *Cell Syst.* 3, 444–455. doi: 10.1016/j.cels.2016.10.002

Baconguis, I., Bohlen, C. J., Goehring, A., Julius, D., and Gouaux, E. (2014). X-ray structure of acid-sensing ion channel 1-snake toxin complex reveals open state of a Na+-selective channel. *Cell* 156, 717–729. doi: 10.1016/j.cell.2014.01.011

Bohlen, C. J., Chesler, A. T., Sharif-Naeini, R., Medzihradszky, K. F., Zhou, S., King, D., et al. (2012). A heteromeric texas coral snake toxin targets acid-sensing ion channels to produce pain HHS public access. *Nature* 479, 410–414. doi: 10.1038/nature10607

Boscardin, E., Alijevic, O., Hummler, E., Frateschi, S., and Kellenberger, S. (2016). The Function and regulation of acid-sensing ion channels (ASICs) and the epithelial Na+channel (ENaC): IUPHAR review 19. *Br. J. Pharmacol.* 173, 2671–2701. doi: 10.1111/bph.13533

Chen, X., Kalbacher, H., and Gründer, S. (2005). The tarantula toxin psalmotoxin 1 inhibits acid-sensing ion channel (ASIC) 1a by increasing its apparent H+ affinity. *J. Gen. Physiol.* 126, 71–79. doi: 10.1085/jgp.200509303

Chen, B., Liu, J., Ho, T. T., Ding, X., and Mo, Y. Y. (2016). ERK-mediated NF-κB activation through ASIC1 in response to acidosis. *Oncogenesis* 5:e279. doi: 10.1038/oncsis.2016.81

Chu, X. P., and Xiong, Z. G. (2013). Acid-sensing ion channels in pathological conditions. *Adv. Exp. Med. Biol.* 961, 419–431. doi: 10.1007/978-1-4614-4756-6_36

Cirit, M., Wang, C. C., and Haugh, J. M. (2010). Systematic quantification of negative feedback mechanisms in the extracellular signal-regulated kinase (ERK) signaling network. *J. Biol. Chem.* 285, 36736–36744. doi: 10.1074/jbc.M110.148759

Cruz, C. D. C., and Cruz, F. (2007). The ERK 1 and 2 pathway in the nervous system: from basic aspects to possible clinical applications in pain and visceral dysfunction. *Curr. Neuropharmacol.* 5, 244–252. doi: 10.2174/157015907782793630

Duan, B., Liu, D.-S., Huang, Y., Zeng, W.-Z., Wang, X., Yu, H., et al. (2012). PI3-Kinase/Akt pathway-regulated membrane insertion of acid-sensing ion channel 1a underlies BDNF-induced pain hypersensitivity. *J. Neurosci.* 32, 6351–6363. doi: 10.1523/JNEUROSCI.4479-11.2012

Duan, B., Wu, L.-J., Yu, Y.-Q., Ding, Y., Jing, L., Xu, L., et al. (2007). Upregulation of acid-sensing ion channel ASIC1a in spinal dorsal horn neurons contributes to inflammatory pain hypersensitivity. *J. Neurosci.* 27, 11139–11148. doi: 10.1523/JNEUROSCI.3364-07.2007

Fan, S., Hao, Z.-Y., Zhang, L., Zhou, J., Zhang, Y.-F., Tai, S., et al. (2018). ASIC1a contributes to the symptom of pain in a rat model of chronic prostatitis. *Asian J. Androl.* 20, 300–305. doi: 10.4103/aja.aja_55_17

Friese, M. A., Craner, M. J., Etzensperger, R., Vergo, S., Wemmie, J. A., Welsh, M. J., et al. (2007). Acid-sensing ion channel-1 contributes to axonal degeneration in autoimmune inflammation of the central nervous system. *Nat. Med.* 13, 1483–1489. doi: 10.1038/nm1668

Gautschi, I., Van Bemmelen, M. X., and Schild, L. (2017). Proton and non-proton activation of ASIC channels. *PLoS One* 12:e0175293. doi: 10.1371/journal.pone.0175293

González-Inchauspe, C., Urbano, F. J., Di Guilmi, M. N., Uchitel, O. D., Carlota Gonzalez-Inchauspe, F. J., Di Guilmi, U. M. N., et al. (2017). Acid-sensing ion channels activated by evoked released protons modulate synaptic transmission at the mouse calyx of held synapse. *J. Neurosci.* 37, 2589–2599. doi: 10.1523/JNEUROSCI.2566-16.2017

Gründer, S., and Chen, X. (2010). Structure, function and pharmacology of acid-sensing ion channels (ASICs): focus on ASIC1a. *Int. J. Physiol. Pathophysiol. Pharmacol.* 2, 73–94.

Gunthorpe, M. J., Smith, G. D., Davis, J. B., and Randall, A. D. (2001). Characterisation of a human acid-sensing ion channel (HASIC1a) endogenously expressed in HEK293 cells. *Pflugers Arch.* 442, 668–674. doi: 10.1007/s004240100584

Hoagland, E. N., Sherwood, T. W., Lee, K. G., Walker, C. J., and Askwith, C. C. (2010). Identification of a calcium permeable human acid-sensing ion channel 1 transcript variant. *J. Biol. Chem.* 285, 41852–41862. doi: 10.1074/jbc.M110.171330

Illario, M., Cavallo, A. L., Ulrich Bayer, K., Di Matola, T., Fenzi, G., Rossi, G., et al. (2003). Calcium/calmodulin-dependent protein kinase II binds to Raf-1 and modulates integrin-stimulated ERK activation. *J. Biol. Chem.* 278, 45101–45108. doi: 10.1074/jbc.M305355200

Jiang, Q., Li, M.-H., Papasian, C. J., Branigan, D., Xiong, Z.-G., Wang, J. Q., et al. (2009). Characterization of acid-sensing ion channels in medium spiny neurons of mouse striatum. *Neuroscience* 162, 55–66. doi: 10.1016/j.neuroscience.2009.04.029

Kadurin, I., Golubovic, A., Leisle, L., Schindelin, H., and Gründer, S. (2008). Differential effects of N-glycans on surface expression suggest structural differences between the acid-sensing ion channel (ASIC) 1a and ASIC1b. *Biochem. J.* 412, 469–475. doi: 10.1042/BJ20071614

Kriegsheim, A. V., Baiocchi, D., Birtwistle, M., Sumpton, D., Bienvenut, W., Morrice, N., et al. (2009). Cell fate decisions are specified by the dynamic ERK interactome. *Nat. Cell Biol.* 11, 1458–1464. doi: 10.1038/ncb1994

Kweon, H.-J., and Suh, B.-C. (2013). Acid-sensing ion channels (ASICs): therapeutic targets for neurological diseases and their regulation. *BMB Rep.* 46, 295–304. doi: 10.5483/bmbrep.2013.46.6.121

Maik-Rachline, G., Hacohen-Lev-Ran, A., and Seger, R. (2019). Nuclear Erk: mechanism of translocation, substrates and role in cancer. *Int. J. Mol. Sci.* 20:1194. doi: 10.3390/ijms20051194

Marshall, C. J. (1995). Specificity of receptor tyrosine kinase signaling: transient versus sustained extracellular signal-regulated kinase activation. *Cell* 80, 179–185. doi: 10.1016/0092-8674(95)90401-8

Maruta, T., Nemoto, T., Hidaka, K., Koshida, T., Shirasaka, T., Yanagita, T., et al. (2019). Upregulation of ERK phosphorylation in rat dorsal root ganglion neurons contributes to oxaliplatin-induced chronic neuropathic pain. *PLoS One* 14:e0225586. doi: 10.1371/journal.pone.0225586

Murphy, L. O., Smith, S., Huei Chen, R., Fingar, D. C., and Blenis, J. (2002). Molecular, interpretation of ERK signal duration by immediate early gene products. *Nat. Cell Biol.* 4, 556–564. doi: 10.1038/ncb822

Peng, Z., and Kellenberger, S. (2021). Hydrogen sulfide upregulates acid-sensing ion channels *via* the MAPK-Erk1/2 signaling pathway. *Function* 2:zqab007. doi: 10.1093/function/zqab007

Salinas, L. C. C., Rozenfeld, P., Gabriel Gatto, R., Claudio Reisin, R., Daniel Uchitel, O., Weissmann, C., et al. (2020). Upregulation of ASIC1a channels in an *in vitro* model of fabry disease. *Neurochem. Int.* 140:104824. doi: 10.1016/j.neuint.2020.104824

Salzano, M., Rosaria Rusciano, M., Russo, E., Bifulco, M., Postiglione, L., and Vitale, M. (2012). Calcium/calmodulin-dependent protein kinase II (CaMKII) phosphorylates Raf-1 at serine 338 and mediates ras-stimulated Raf-1 activation. *Cell Cycle* 11, 2100–2106. doi: 10.4161/cc.20543

Shindo, Y., Iwamoto, K., Mouri, K., Hibino, K., Tomita, M., Kosako, H., et al. (2016). Conversion of graded phosphorylation into switch-like nuclear translocation *via* autoregulatory mechanisms in ERK signalling. *Nat. Commun.* 7:10485. doi: 10.1038/ncomms10485

Sluka, K. A., Winter, O. C., and Wemmie, J. A. (2009). Acid-sensing ion channels: a new target for pain and CNS diseases. *Curr. Opin. Drug Discov. Devel.* 12, 693–704.

Sodero, A. O., Weissmann, C., Ledesma, M. D., and Dotti, C. G. (2011). Cellular stress from excitatory neurotransmission contributes to cholesterol loss in hippocampal neurons aging *in vitro*. *Neurobiol. Aging* 32, 1043–1053. doi: 10.1016/j.neurobiolaging.2010.06.001

Sun, X., Cao, Y.-B., Hu, L.-F., Yang, Y.-P., and Li, J. (2011). ASICs mediate the modulatory effect by paeoniflorin on alpha-synuclein autophagic degradation. *Brain Res.* 1396, 77–87. doi: 10.1016/j.brainres.2011.04.011

Sun, C., Wang, S., and Hu, W. (2018). Acid-sensing ion channel 1a mediates acid-induced inhibition of matrix metabolism of rat articular chondrocytes *via* the MAPK signaling pathway. *Mol. Cell. Biochem.* 443, 81–91. doi: 10.1007/s11010-017-3212-9

Tikhonov, D. B., Magazanik, L. G., and Nagaeva, E. I. (2019). Ligands of acid-sensing ion channel 1a: mechanisms of action and binding sites. *Acta Naturae* 11, 4–13. doi: 10.32607/20758251-2019-11-1-4-13

Uchitel, O. D., González Inchauspe, C., and Weissmann, C. (2019). Synaptic signals mediated by protons and acid-sensing ion channels. *Synapse* 73:e22120. doi: 10.1002/syn.22120

Wang, J. J., Liu, F., Yang, F., Wang, Y. Z., Qi, X., Li, Y., et al. (2020). Disruption of auto-inhibition underlies conformational signaling of ASIC1a to induce neuronal necroptosis. *Nat. Commun.* 11:475. doi: 10.1038/s41467-019-13873-0

Wang, Y., O'Bryant, Z., Wang, H., and Huang, Y. (2016). Regulating factors in acid-sensing ion channel 1a function. *Neurochem. Res.* 41, 631–645. doi: 10.1007/s11064-015-1768-x

Wang, Y., Sun, Y., Zuo, L., Wang, Y., and Huang, Y. (2019). ASIC1a promotes high glucose and PDGF-induced hepatic stellate cell activation by inducing autophagy through CaMKKβ/ERK signaling pathway. *Toxicol. Lett.* 300, 1–9. doi: 10.1016/j.toxlet.2018.10.003

Wang, Y. Z., Wang, J. J., Huang, Y., Liu, F., Zeng, W. Z., Li, Y., et al. (2015). Tissue acidosis induces neuronal necroptosis *via* ASIC1a channel independent of its ionic conduction. *eLife* 4:e05682. doi: 10.7554/eLife.05682

Wei, S., Qiu, C. Y., Jin, Y., Liu, T. T., and Hu, W. P. (2021). TNF-α acutely enhances acid-sensing ion channel currents in rat dorsal root ganglion neurons *via* a P38 MAPK pathway. *J. Neuroinflammation* 18:92. doi: 10.1186/s12974-021-02151-w

Weissmann, C., Di Guilmi, M. N., Urbano, F. J., and Uchitel, O. D. (2013). Acute effects of pregabalin on the function and cellular distribution of Ca(V)2.1 in HEK293t cells. *Brain Res. Bull.* 90, 107–113. doi: 10.1016/j.brainresbull.2012.10.001

Wemmie, J. A., Taugher, R. J., and Kreple, C. J. (2013). Acid-sensing ion channels in pain and disease. *Nat. Rev. Neurosci.* 14, 461–471. doi: 10.1038/nrn3529

Wong, H. K., Bauer, P. O., Kurosawa, M., Goswami, A., Washizu, C., Machida, Y., et al. (2008). Blocking acid-sensing ion channel 1 alleviates Huntington's disease pathology *via* an ubiquitin-proteasome system-dependent mechanism. *Hum. Mol. Genet.* 17, 3223–3235. doi: 10.1093/hmg/ddn218

Wu, J., Xu, Y., Jiang, Y.-Q., Xu, J., Hu, Y., and Zha, X.-M. (2016). ASIC subunit ratio and differential surface trafficking in the brain. *Mol. Brain* 9:4. doi: 10.1186/s13041-016-0185-7

Xiong, Z. G., and Xu, T. L. (2012). The role of ASICs in cerebral ischemia. *Wiley Interdiscip. Rev. Membr. Transport Signal.* 1, 655–662. doi: 10.1002/wmts.57

Xu, Y., Jiang, Y.-Q., Li, C., He, M., George Rusyniak, W., Annamdevula, N., et al. (2018). Human ASIC1a mediates stronger acid-induced responses as compared with mouse ASIC1a. *FASEB J.* 32, 3832–3843. doi: 10.1096/fj.201701367R

Yu, X.-W., Hu, Z.-L., Ni, M., Fang, P., Zhang, P.-W., Shu, Q., et al. (2015). Acid-sensing ion channels promote the inflammation and migration of cultured rat microglia. *Glia* 63, 483–496. doi: 10.1002/glia.22766

Yu, Z., Jiao Wu, Y.-J., Zhi Wang, Y.-Z., Shi Liu, D.-S., Lei Song, X.-L., Jiang, Q., et al. (2018). The acid-sensing ion channel ASIC1a mediates striatal synapse remodeling and procedural motor learning. *Sci. Signal.* 11:eaar4481. doi: 10.1126/scisignal.aar4481

Zeng, W. Z., Liu, D. S., and Xu, T. L. (2014). Acid-sensing ion channels: trafficking and pathophysiology. *Channels (Austin)* 8, 481–487. doi: 10.4161/19336950.2014.958382

Zha, X.-M. (2013). Acid-sensing ion channels: trafficking and synaptic function. *Mol. Brain* 6:1. doi: 10.1186/1756-6606-6-1

Zhu, Y., Pan, X., Du, N., Li, K., Hu, Y., Wang, L., et al. (2020). ASIC1a regulates miR-350/SPRY2 by N 6 -methyladenosine to promote liver fibrosis. *FASEB J.* 34, 14371–14388. doi: 10.1096/fj.202001337R

Zhu, L., Yin, J., Zheng, F., Ji, L., Yu, Y., and Liu, H. (2021). ASIC1 inhibition impairs the proliferation and migration of pancreatic stellate cells induced by pancreatic cancer cells. *Neoplasma* 68, 174–179. doi: 10.4149/neo_2020_200803N811

Conflict of Interest: ODU, coauthor to this manuscript is also editor of this special topic.

The remaining authors declare that the research was conducted in the absence of any commercial or financial relationships that could be construed as a potential conflict of interest.

Publisher's Note: All claims expressed in this article are solely those of the authors and do not necessarily represent those of their affiliated organizations, or those of the publisher, the editors and the reviewers. Any product that may be evaluated in this article, or claim that may be made by its manufacturer, is not guaranteed or endorsed by the publisher.

frontiers in Cellular Neuroscience

MINI REVIEW
published: 08 October 2021
doi: 10.3389/fncel.2021.730641

Neurodegenerative Disease: What Potential Therapeutic Role of Acid-Sensing Ion Channels?

Dalila Mango[1,2]* *and Robert Nisticò*[1,2]

[1] *Laboratory of Pharmacology of Synaptic Plasticity, European Brain Research Institute, Rome, Italy,* [2] *School of Pharmacy, University of Rome "Tor Vergata", Rome, Italy*

Acidic pH shift occurs in many physiological neuronal activities such as synaptic transmission and synaptic plasticity but also represents a characteristic feature of many pathological conditions including inflammation and ischemia. Neuroinflammation is a complex process that occurs in various neurodegenerative diseases such as Alzheimer's disease, Parkinson's disease, multiple sclerosis, and Huntington's disease. Acid-sensing ion channels (ASICs) represent a widely expressed pH sensor in the brain that play a key role in neuroinflammation. On this basis, acid-sensing ion channel blockers are able to exert neuroprotective effects in different neurodegenerative diseases. In this review, we discuss the multifaceted roles of ASICs in brain physiology and pathology and highlight ASIC1a as a potential pharmacological target in neurodegenerative diseases.

Keywords: ASIC1a, neurodegenerative disease, neuroinflammation, pH shift, acidosis

OPEN ACCESS

Edited by:
Osvaldo D. Uchitel, University of Buenos Aires, Argentina

Reviewed by:
David MacLean, Medical Center, University of Rochester, United States
Hee Jung Chung, University of Illinois at Urbana-Champaign, United States

***Correspondence:**
Dalila Mango
d.mango@ebri.it

Specialty section:
This article was submitted to Cellular Neurophysiology, a section of the journal Frontiers in Cellular Neuroscience

Received: *25 June 2021*
Accepted: *15 September 2021*
Published: *08 October 2021*

Citation:
Mango D and Nisticò R (2021) Neurodegenerative Disease: What Potential Therapeutic Role of Acid-Sensing Ion Channels? Front. Cell. Neurosci. 15:730641. doi: 10.3389/fncel.2021.730641

INTRODUCTION

The maintenance of cytosolic pH in its physiological range is required for normal neuronal activity, and even minor alterations can have serious consequences. Under normal physiological conditions, intra- and extracellular pH is maintained between 7.0 and 7.3; however, normal neuronal activity causes local pH changes (Chen and Chesler, 1992; Chesler and Kaila, 1992; Makani and Chesler, 2007; Magnotta et al., 2012). In the mammalian central nervous system (CNS), increased neuronal activity and the intense synchronous synaptic activity occurring in the synaptic plasticity process alter pH, producing alkalinization followed by acidification (DeVries, 2001; Du et al., 2014).

Under pathological conditions, including ischemic strokes, seizures, and inflammation associated with several neurodegenerative diseases, the pH shifts toward a persistent acidification that is correlated with neuronal hyperexcitability (Chiacchiaretta et al., 2017).

Neuroinflammation within the brain or spinal cord is mediated by the release of cytokines, chemokines, reactive oxygen species produced from resident microglia and astrocytes, endothelial cells, and peripherally derived immune cells (DiSabato et al., 2016). In the last decades, correlation between neuroinflammation and neurodegeneration has become increasingly solid in the light of accumulating evidence gathered on Alzheimer's disease (AD), Parkinson's disease (PD), and multiple sclerosis (MS) (Salter and Stevens, 2017).

Several studies in animal models and in humans have demonstrated that neurodegenerative diseases, characterized by a persistent inflammatory state, are associated with a significant reduction in the brain pH (Amor et al., 2010; Tyrtyshnaia et al., 2016; Decker et al., 2021), suggesting that neuroinflammation *per se* affects brain pH level. All this evidence has prompted the investigation of the role of acid-sensing ion channels (ASICs) in neurodegenerative diseases. The present work provides an overview of the possible roles of ASIC1a in neurodegenerative conditions and highlights this protein as a new potential therapeutic target.

ACID-SENSING ION CHANNEL CHANNELS: pH SENTINELS IN THE BRAIN

ASICs belong to a class of voltage-insensitive cation channels, which are widely expressed in the central and peripheral nervous systems (Sherwood et al., 2012; Vullo and Kellenberger, 2020; Rook et al., 2021). Today, it is well accepted that protons (H^+) can act as neurotransmitters through the specific activation of proton-sensing channels, and these channels were cloned and named for the first time as ASICs in 1997 (Waldmann et al., 1997). Thereafter, many studies have investigated their structure, expression, and localization, and many experimental ligands, to explore and understand the role and function of ASIC in physiological and pathological processes, were developed (**Figure 1**; Chesler, 2003; Mango and Nisticò, 2020; Rook et al., 2021). Among six different mammalian protein subunits that have been cloned (ASIC1a, ASIC1b, ASIC2a, ASIC2b, ASIC3, and ASIC4), ASIC1 and ASIC2 are predominant subunits in the CNS (Waldmann et al., 1997; Chen et al., 1998; Bässler et al., 2001). Each ASIC subunit has two transmembrane domains and a large extracellular domain enriched with acidic residues. ASICs can be assembled as either homotrimers or heterotrimers to form functional channels (Bassilana et al., 1997; Babinski et al., 1999; Jasti et al., 2007; Gonzales et al., 2009; Magnotta et al., 2012; Rook et al., 2021).

The most important characteristic of ASICs is the high pH sensitivity (Wemmie et al., 2013) making them the best candidates for pH sentinels in the brain that can detect and respond to small pH variations (Papalampropoulou-Tsiridou et al., 2020; Rook et al., 2021). A recent study has provided insights into the role of ASIC currents in the generation of action potential (AP) firing in neurons in relation to the speed of pH change. The authors demonstrate that moderate acidification (4–10 s) mediates AP increase, while slow acidification (>10 s) is not able to induce AP changes, suggesting a new important parameter that influences ASIC modulation of neuronal depolarization (Alijevic et al., 2020).

Most studies are focused on the most abundant form of an ASIC channel expressed in the CNS, which is represented by ASIC1a. Activation of ASIC1a plays a key role in pathological processes by promoting neuronal death *via* calcium (Ca^{2+})-mediated toxicity (Yermolaieva et al., 2004). The abundant expression of ASIC1a in discrete regions of the brain, such as the hippocampus, cortex, striatum, and amygdala (Alvarez de la Rosa et al., 2003; Wemmie et al., 2003; Coryell et al., 2009) and the characteristic to be Ca^{2+} permeable has suggested a role for this channel in calcium-related processes such as synaptic plasticity, learning and memory, as well as neuronal death (Wemmie et al., 2002; Gao et al., 2015; Wang et al., 2015). Accordingly, blocking ASIC1a affects multiple forms of synaptic plasticity in many brain regions including the amygdala and hippocampus (Wemmie et al., 2002, 2003; Du et al., 2014; Mango et al., 2017; Mango and Nisticò, 2020). Inhibition of ASIC1a produces a reduction in magnitude of both forms of synaptic plasticity long-term potentiation (LTP) and long-term depression (LTD) and ASIC1a KO mice show impairment of learning and memory evaluated with the Morris water maze and elevated-plus maze behavioral tests.

Moreover, the interplay between ASIC1a and NMDA, AMPA, and GABA receptors represents a potential target for acidotoxicity and exitotoxicity that occur in pathological conditions, such as ischemia (Gao et al., 2005, 2016; Chen et al., 2011; González-Inchauspe et al., 2017). Intriguingly, protons are able to modulate different synaptic receptors including AMPA and NMDA glutamate receptors (Tang et al., 1990; Traynelis and Cull-Candy, 1990; Lei et al., 2001), as well as GABAA receptors (Kaila, 1994; Dietrich and Morad, 2010), indicating that pH changes affect neuronal excitability, neurotransmission, and post-synaptic responses (Chen and Chesler, 1992; Makani and Chesler, 2007; Dietrich and Morad, 2010).

NEUROINFLAMMATION PROCESS AND pH SHIFT IN NEURODEGENERATIVE DISORDERS

Growing evidence supports the relationship between neuroinflammation and synaptic degeneration as a common feature in neurodegenerative diseases including AD, PD, and MS (Nisticò et al., 2017; Guzman-Martinez et al., 2019). Acidosis and accumulation of protons in the extracellular space represent hallmarks of the inflammatory process (see Diaz et al., 2018). The shift to the acidic pH was observed in normal aging and in patients affected by a variety of neurodegenerative disorders and was also confirmed in experimental models of neuroinflammation (Roberts and Sick, 1996; Roberts and Chih, 1997; Friese et al., 2007; Vergo et al., 2011; Mandal et al., 2012; Tyrtyshnaia et al., 2016).

To date, there is limited experimental evidence linking ASICs to neuroinflammation. For example, NSAIDs were reported to act against ASICs by both preventing inflammation-induced increase in expression and directly inhibiting the channels (Voilley et al., 2001). Our group has published that CHF5074 (also called CSP-1103), a flurbiprofen derivative, induces inhibition of ASIC1a-mediated currents elicited by application of pH 5.5 bath medium (IC50 ∼50 nM) (Mango et al., 2014). A previous work has also demonstrated an increased expression of ASIC3 on nerve afferents supplying joints in response to inflammatory stimulus and an anti-inflammatory action exerted by ASIC3 inhibitors in animal models of rheumatoid arthritis. Notably, $ASIC^{-/-}$ animals manifest higher joint inflammation and destruction compared with $ASIC^{+/+}$ controls (Sluka et al., 2013).

Therefore, ASICs represent the receptors on which the protons act as neurotransmitter and prolonged changes in pH shift likely contribute to the chronic inflammatory states underlying the neurodegenerative process.

Alzheimer's Disease

AD is a major cause of dementia in the world population. AD is characterized by chronic neurodegeneration with progressive memory impairment (Chapman et al., 1999), and currently, there is limited effective treatment or cure.

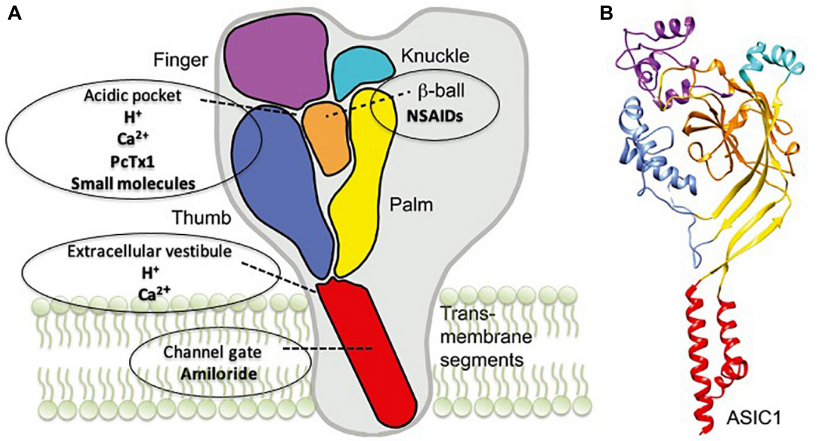

FIGURE 1 | Acid-sensing ion channel 1a (ASIC1a) structure and the binding sites of its modulators. **(A)** A schematic view of the ASIC1 subunit highlighting the different domains: finger (purple), knuckle (turquoise), β-ball (orange), palm (yellow), and thumb (blue) and transmembrane domains (red). The binding sites for the different drugs are also indicated. **(B)** Crystal structure of an ASIC1 subunit obtained from chicken ASIC1 binding Mit-Tx (Baconguis et al., 2014). The domains are colored as in panel **A**. Readapted from Boscardin et al. (2016).

Several studies highlighted a shift to acidic pH in the AD brain caused by reduced cerebral perfusion (Siesjo, 1988). Changes in pH have also been observed in cerebrospinal fluid and post-mortem brain tissue of AD patients (Liu et al., 1999; Preece and Cairns, 2003).

ASIC1a plays a key role in synaptic plasticity processes including neurotransmission, dendritic structural remodeling, learning and memory, and fear response. This has been widely demonstrated in non-clinical studies using electrophysiological and behavioral approaches in mice (Wemmie et al., 2002, 2003; Chu and Xiong, 2012; Huang et al., 2015; Mango and Nisticò, 2019).

However, the role of ASIC1a in the synaptic alterations underlying AD remains still elusive. Indeed, our group has previously demonstrated an involvement of ASIC1a in hippocampal LTD ion in two experimental models of AD (Mango and Nisticò, 2018). Specifically, blocking ASIC1a with the selective blocker psalmotoxin-1 inhibited the enhancement of mGlu receptor-dependent LTD seen in the hippocampal slices, which were either treated with Aβ oligomers or obtained from Tg2576 mouse model of AD (Mango and Nisticò, 2018). The significance of these results remains to be established, and further studies need to be conducted in order to clarify the ASIC1a involvement in AD pathophysiology.

Parkinson's Disease

PD is a neurodegenerative disorder characterized by progressive and selective degeneration of dopaminergic neurons localized in the substantia nigra pars compacta (SNpc) area of the brain and cytoplasmic inclusions of alpha-synuclein aggregates, called Lewy bodies (Gelders et al., 2018). The neurodegeneration is responsible for motor and non-motor symptomatology including tremor, rigidity, bradykinesia, olfactory dysfunction, sleep disturbance, and cognitive impairment (Gelders et al., 2018).

Several studies described an elevated concentration of neuroinflammatory markers in PD patients suggesting the hypothesis that inflammation plays a role in neurodegeneration (Gelders et al., 2018). Also, PD is associated with lactic acidosis, and a study performed using an animal model of PD, the MPTP-treated mouse, described an involvement of ASIC1a in neurodegeneration of dopaminergic neurons. Indeed, blocking ASIC1a with amiloride or psalmotoxin-1 preserved dopaminergic neurons of SNpc from degeneration (Arias et al., 2008). Mutations in *Parkin* gene associated with autosomal recessive juvenile onset of PD (Kitada et al., 1998) or lack of the Parkin gene facilitate ASIC1a currents in hippocampal neurons evoked by application of acidic extracellular solution, and increase vulnerability of dopaminergic neurons, suggesting a significant role of ASIC1a in PD pathophysiology (Joch et al., 2007).

Nevertheless, not many studies have been performed to verify the role of ASIC1a as a therapeutic target for PD.

Multiple Sclerosis

MS is a chronic autoimmune inflammatory disease characterized by demyelination and axonal degeneration processes (Goldenberg, 2012).

Many studies investigated the involvement of ASIC1a in MS using a well-accepted animal model of MS that is the experimental autoimmune encephalomyelitis (EAE) model (Friese et al., 2007; Bjelobaba et al., 2018). Previous studies found ASIC1a upregulation in axons and oligodendrocytes in the EAE model and in MS patients (Vergo et al., 2011). In MS patients, a relationship between elevated ASIC1a expression and axon injury markers was demonstrated, and this was also confirmed in EAE mice (Vergo et al., 2011; Arun et al., 2013). Also, administration of ASIC blocker amiloride attenuated demyelination and neuronal damage in EAE animal model as well as in a cohort of MS patients (Arun et al., 2013), indicating that

ASIC1a inhibition is neuroprotective and represents a promising therapeutic strategy for MS.

Huntington's Disease

HD is a rare hereditary neurodegenerative disease characterized by movement and cognitive disorders and polyglutamine repeat as pathologic hallmarks (Agostinho et al., 2013). Not much evidence is present in literature linking ASIC1a to HD. The acidosis that occurs in the brain of HD patients and in mouse models of HD suggests an involvement of these channels in the pathophysiology of HD (Tsang et al., 2006; Josefsen et al., 2010). Notably, blocking ASIC1a with an amiloride derivative benzamil was able to alleviate pathology through reduction of Huntingtin–polyglutamine aggregation, the HD hallmark in the striatum of R6/2 mice model of HD (Wong et al., 2008).

ACID-SENSING ION CHANNEL MODULATORS AND THEIR POTENTIAL THERAPEUTIC USE

Experimental evidence suggests that ASIC1a could represent a new therapeutic target for neurodegenerative diseases. Below, we present the main ligands targeting ASIC1a, and the binding sites of ASIC1a are illustrated in **Figure 1**.

Amiloride

Amiloride a potassium-sparing diuretic agent and acts as a non-specific ASIC1a inhibitor in the range of 1–100 μM, which act by binding to the ion pore (Schild et al., 1997; Leng et al., 2016). Clinical studies have detected a neuroprotective and myeloprotective effect in patients with primary progressive MS (Arun et al., 2013). Nevertheless, amiloride was not effective in reducing the brain atrophy in patients with secondary progressive multiple sclerosis (De Angelis et al., 2020). In the light of these data, it could be important to test other amiloride analogs, such as benzamil with increased potency and selectivity for ASIC1a (Leng et al., 2016).

Non-steroidal Anti-inflammatory Drugs

Non-steroidal anti-inflammatory drugs (NSAIDs) are a class of drugs widely used for the treatment of inflammation, pain, and many other disorders (Voilley, 2004). Previous studies have demonstrated that flurbiprofen, ibuprofen, and derivates mediate a direct inhibition of ASIC currents acting on the β-ball domain, with a significant reduction in evoked currents by the application of acidic medium (Voilley et al., 2001; Mango et al., 2014).

Small Molecules

Different small molecules targeting ASICs were developed and represent new pharmacological tools used to study the ASICs function. Some of these molecules are clinically tested for therapeutic use, as PPC-5650 for the irritable bowel syndrome (Dubé et al., 2009; Olesen et al., 2015).

In this class can be cited NS-383 small potent inhibitor of ASIC1a (Munro et al., 2016) and two potent allosteric antagonists of ASIC1a JNJ-799760 and JNJ-67869386, which act by binding to the acidic pocket (Liu et al., 2021). Other new potent antagonists are represented by A-317567 and 5b (Dubé et al., 2005; Buta et al., 2015).

Psalmotoxin-1

Psalmotoxin-1 (PcTx-1) was the first toxin identified as a selective ASIC1a inhibitor, which acts by binding to an acidic pocket (Escoubas et al., 2000). Although, the structure of PcTx-1 does not allow passage through the blood–brain barrier, previous studies demonstrated its neuroprotective effect in different experimental models of neurodegenerative diseases *via* intrathecal or intracerebroventricular administration (Diochot et al., 2012; Baron et al., 2013; Chassagnon et al., 2017).

ASC06-IgG1

ASC06-IgG1 is a novel selective ASIC1a-blocking monoclonal antibody, which showed potent, sustained, and highly selective inhibition of ASIC1a (Qiang et al., 2018). This specific antibody shows a neuroprotective effect against ischemia (Qiang et al., 2018). Further studies are needed to investigate the neuroprotective effect of ASC06-IgG in experimental models of neurodegenerative diseases. Today, numerous monoclonal antibodies have been approved or are under development for neurological diseases (Sirbu et al., 2021), but many limitations, including the route of administration, as well as class-specific and target-associated risks, have limited their use (Loureiro et al., 2014, 2017; Teleanu et al., 2019).

CONCLUSION

Neurodegenerative diseases are characterized by different and multifactorial processes sharing accumulation of misfolding proteins, damage of specific neuronal populations, and chronic inflammation state neuroinflammation. Another common feature is the shift to the acidic pH in the brain, which might contribute to apoptosis, protein misfolding, excitotoxicity, and neurodegeneration (Parton et al., 1991; Bender et al., 1997; Ding et al., 2000; Liu et al., 2012; Wang et al., 2012).

Emerging evidence supports the role of ASIC activation in several physiological processes such as synaptic plasticity and memory. On the other hand, ASICs are implicated in the pathophysiology of inflammatory and neurodegenerative diseases including PD, MS, AD, and HD.

The complex molecular pathways leading to neurodegeneration makes the search for novel effective agents difficult. In this frame, the development of potent and specific blockers for individual ASIC subunits, as well as the targeting of endogenous signaling molecules modulating the function of ASICs, might represent a new approach for the treatment of neurodegenerative conditions.

AUTHOR CONTRIBUTIONS

DM conceived the idea and prepared the manuscript. RN reviewed the drafts. Both authors contributed to the writing and approved final version of the manuscript.

REFERENCES

Agostinho, L. A., Dos Santos, S. R., Alvarega, R. M., and Paiva, C. L. (2013). A systematic review of the intergenerational aspects and the diverse genetic profiles of Huntington's disease. *Genet. Mol. Res.* 12, 1974–1981.

Alijevic, O., Bignucolo, O., Hichri, E., Peng, Z., Kucera, J. P., and Kellenberger, S. (2020). Slowing of the time course of acidification decreases the acid-sensing ion channel 1a current amplitude and modulates action potential firing in neurons. *Front. Cell. Neurosci.* 28:41. doi: 10.3389/fncel.2020.00041

Alvarez de la Rosa, D., Krueger, S. R., Kolar, A., Shao, D., Fitzsimonds, R. M., and Canessa, C. M. (2003). Distribution, subcellular localization and ontogeny of ASIC1 in the mammalian central nervous system. *J. Physiol.* 546, 77–87. doi: 10.1113/jphysiol.2002.030692

Amor, S., Puentes, F., Baker, D., and van der Valk, P. (2010). Inflammation in neurodegenerative diseases. *Immunology* 129, 154–169.

Arias, R. L., Sung, M. L. I., Vasylyev, D., Zhang, M. Y., Albinson, K., Kubek, K., et al. (2008). Amiloride is neuroprotective in an MPTP model of Parkinson's disease. *Neurobiol. Dis.* 31, 334–341. doi: 10.1016/j.nbd.2008.05.008

Arun, T., Tomassini, V., Sbardella, E., de Ruiter, M. B., Matthews, L., Leite, M. I., et al. (2013). Targeting ASIC1 in primary progressive multiple sclerosis: evidence of neuroprotection with amiloride. *Brain* 136, 106–115. doi: 10.1093/brain/aws325

Babinski, K., Le, K. T., and Seguela, P. (1999). Molecular cloning and regional distribution of a human proton receptor subunit with biphasic functional properties. *J. Neurochem.* 72, 51–57. doi: 10.1046/j.1471-4159.1999.0720051.x

Baconguis, I., Bohlen, C. J., Goehring, A., Julius, D., and Gouaux, E. (2014). X-ray structure of acid-sensing ion channel 1-snake toxin complex reveals open state of a Na(+)-selective channel. *Cell* 156, 717–729. doi: 10.1016/j.cell.2014.01.011

Baron, A., Diochot, S., Salinas, M., Deval, E., Noel, J., and Lingueglia, E. (2013). Venom toxin in the exploration of molecular, physiological and pathophysiological functions of acid-sensing ion channels. *Toxicon* 75, 187–204. doi: 10.1016/j.toxicon.2013.04.008

Bassilana, F., Champigny, G., Waldmann, R., de Weille, J. R., Heurteaux, C., and Lazdunski, M. (1997). The acid-sensitive ionic channel subunit ASIC and the mammalian degenerin MDEG form a heteromultimeric H+-gated Na+ channel with novel properties. *J. Biol. Chem.* 272, 28819–28822. doi: 10.1074/jbc.272.46.28819

Bässler, E. L., Ngo-Anh, T. J., Geisler, H. S., Ruppersberg, J. P., and Gründer, S. (2001). Molecular and functional characterization of acid-sensing ion channel (ASIC) 1b. *J. Biol. Chem.* 276, 33782–33787. doi: 10.1074/jbc.m104030200

Bender, A. S., Young, L. P., and Norenberg, M. D. (1997). Effect of lactic acid on L-glutamate uptake in cultured astrocytes: Mediators of Inflammation mechanistic considerations. *Brain Res.* 1, 59–66. doi: 10.1016/s0006-8993(96)01331-5

Bjelobaba, I., Bergovic-Kupresanin, V., Pekovic, S., and Lavnja, I. (2018). Animal models of multiple sclerosis: Focus on experimental autoimmuneencephalomyelitis. *J. Neurosci. Res.* 96, 1021–1042. doi: 10.1002/jnr.24224

Boscardin, E., Alijevic, O., Hummler, E., Frateschi, S., and Kellenberger, S. (2016). The function and regulation of acid-sensing ion channels (ASICs) and the epithelian Na+ channel (ENaC): IUPHAR Review 19. *Br. J. Pharmacol.* 173, 2671–2701. doi: 10.1111/bph.13533

Buta, A., Maximyuk, O., Kovalskyy, D., Sukach, V., Vovk, M., Ievglevskyi, O., et al. (2015). Novel potent orthosteric antagonist of ASIC1a prevents NMDAR-dependent LTP induction. *J. Med. Chem.* 58, 4449–4461. doi: 10.1021/jm5017329

Chapman, P. F., White, G. L., Jones, M. W., Cooper-Blacketer, D., Marshall, V. J., Irizarry, M., et al. (1999). Impaired synaptic plasticity and learning in aged amyloid precursor protein transgenic mice. *Nat. Neurosci.* 2, 271–276. doi: 10.1038/6374

Chassagnon, I. R., McCarthy, C. A., Chin, Y. K., Pineda, S. S., Keramidasd, A., Moblie, M., et al. (2017). Potent neuroprotection after stroke afforded by a double-knot spider-venom peptide that inhibits acid-sensing ion channel 1a. *Proc. Natl. Acad. Sci. U.S.A.* 114, 3750–3755. doi: 10.1073/pnas.1614728114

Chen, C. C., England, S., Akopian, A. N., and Wood, J. N. (1998). A sensory neuron-specific, proton-gated ion channel. *Proc. Natl. Acad. Sci. U.S.A.* 95, 10240–10245. doi: 10.1073/pnas.95.17.10240

Chen, J. C., and Chesler, M. (1992). pH transients evoked by excitatory synaptic transmission are increased by inhibition of extracellular carbonic anhydrase. *Proc. Natl. Acad. Sci. U.S.A* 89, 7786–7790. doi: 10.1073/pnas.89.16.7786

Chen, X., Whissell, P., Orser, B. A., and MacDonald, J. F. (2011). Functional modifications of acid-sensing ion channels by ligand-gated chloride channels. *PLoS One* 6:e21970. doi: 10.1371/journal.pone.0021970

Chesler, M. (2003). Regulation and modulation of pH in the brain. *Physiol. Rev.* 83, 1183–1221. doi: 10.1152/physrev.00010.2003

Chesler, M., and Kaila, K. (1992). Modulation of pH by neuronal activity. *Trends Neurosci.* 15, 396–402. doi: 10.1016/0166-2236(92)90191-a

Chiacchiaretta, M., Latifi, S., Bramini, M., Fadda, M., Fassio, A., Benfenati, F., et al. (2017). Neuronal hyperactivity causes Na +/H + exchanger-induced extracellular acidification at active synapses. *J. Cell Sci.* 130, 1435–1449. doi: 10.1242/jcs.198564

Chu, X. P., and Xiong, Z. G. (2012). Physiological and pathological functions of Acid-sensing ion channels in the central nervous system. *Curr. Drug Targets* 13, 263–271. doi: 10.2174/138945012799201685

Coryell, M. W., Wunsch, A. M., Haenfler, J. M., Allen, J. E., Schnizler, M., Ziemann, A. E., et al. (2009). Acid-sensing ion channel-1a in the amygdala, a novel therapeutic target in depression-related behavior. *J. Neurosci.* 29, 5381–5388. doi: 10.1523/JNEUROSCI.0360-09.2009

De Angelis, F., Connick, P., Parker, R. A., Plantone, D., Doshi, A., John, N., et al. (2020). Amiloride, fluoxetine or riluzole to reduce brain volume loss in secondary progressive multiple sclerosis: the MS-SMART four-arm RCT. *Effic. Mech. Eval.* 7:32453521. doi: 10.3310/eme07030

Decker, Y., Németh, E., Schomburg, R., Chemla, A., Fülöp, L., Menger, M. D., et al. (2021). Decreased pH in the aging brain and Alzheimer's disease. *Neurobiol. Aging* 101, 40–49. doi: 10.1016/j.neurobiolaging.2020.12.007

DeVries, S. H. (2001). Exocytosen protons feedback to suppress the Ca^{2+} current in mammalian cone photoreceptors. *Neuron* 32, 1107–1117. doi: 10.1016/s0896-6273(01)00535-9

Diaz, F. E., Dantas, E., and Geffner, J. (2018). Unrevelling the interplay between extracellular acidosis and immune cells. *Mediators of Inflamm.* 2018:1218297. doi: 10.1155/2018/1218297

Dietrich, C. J., and Morad, M. (2010). Synaptic acidification enhances GABAA signaling. *J. Neurosci.* 30, 16044–16052. doi: 10.1523/JNEUROSCI.6364-09.2010

Ding, D., Moskowitz, S. I, Li, R., Lee, S. B., Esteban, M., Tomaselli, K., et al. (2000). Acidosis induces necrosis and apoptosis of cultured hippocampal neurons. *Exp. Neurol.* 162, 1–12. doi: 10.1006/exnr.2000.7226

Diochot, S., Baron, A., Salinas, M., Douguet, D., Scarzello, S., Dabert-Gay, A. S., et al. (2012). Black mamba venom peptides target acid-sensing ion channels to abolish pain. *Nature* 490, 552–555. doi: 10.1038/nature11494

DiSabato, D. J., Quan, N., and Godbout, J. P. (2016). Neuroinflammation: the devil is in the details. *J. Neurochem.* 139(Suppl. 2), 136–153. doi: 10.1111/jnc.13607

Du, J., Reznikov, L. R., Price, M. P., Zha, X. M., Lu, Y., Moninger, T. O., et al. (2014). Protons are a neurotransmitter that regulates synaptic plasticity in the lateral amygdala. *Proc. Natl. Acad. Sci. U.S.A.* 111, 8961–8966. doi: 10.1073/pnas.1407018111

Dubé, G. R., Elagoz, A., and Mangat, H. (2009). Acid sensing ion channels and acid nociception. *Curr. Pharm. Des.* 15, 1750–1766. doi: 10.2174/138161209788186263

Dubé, G. R., Lehto, S. G., Breese, N. M., Baker, S. J., Wang, X., Matulenko, M. A., et al. (2005). Electrophysiological and in vivo characterization of A-317567, a novel blocker of acid sensing ion channels. *Pain* 117, 88–96. doi: 10.1016/j.pain.2005.05.021

Escoubas, P., de Weille, J. R., Lecoq, A., Diochot, S., Waldmann, R., Champigny, G., et al. (2000). Isolation of a tarantula toxin specific for a class of proton-gated Na+ channels. *J. Biol. Chem.* 33, 25116–25121. doi: 10.1074/jbc.M003643200

Friese, M. A., Craner, M. J., Etzensperger, R., Vergo, S., Wemmie, J. A., Welsh, M. J., et al. (2007). Acid-sensing ion channel-1 contributes to axonal degeneration in autoimmune inflammation of the central nervous system. *Nat. Med.* 13, 1483–1489. doi: 10.1038/nm1668

Gao, J., Duan, B., Wang, D. G., Deng, X. H., Zhang, G. Y., Xu, L., et al. (2005). Coupling between NMDA receptor and acid-sensing ion channel contributes to ischemic neuronal death. *Neuron* 48, 635–646. doi: 10.1016/j.neuron.2005.10.011

Gao, S., Yu, Y., Ma, Z., Sun, H., Zhang, Y. L., Wang, X. T., et al. (2015). NMDA-Mediated hippocampal neuronal death is exacerbated by activities of ASIC1a. *Neurotox Res.* 28, 122-137. doi: 10.1007/s12640-015-9530-3

Gao, S., Yu, Y., Ma, Z. Y., Sun, H., Zhang, Y. L., Wang, X. T., et al. (2016). NMDAR-mediated hippocampal neuronal death is exacerbated by activities of ASIC1a. *Neurotox. Res.* 28, 122–137. doi: 10.1007/s12640-015-9530-3

Gelders, G., Baekelandt, V., and Van der Perren, A. (2018). Linking neuroinflammation and neurodegeneration in Parkinson's disease. *J. Immunol. Res.* 2018:4784268. doi: 10.1155/2018/4784268

Goldenberg, M. M. (2012). Multiple sclerosis review. *Pharm. Therap.* 37, 175–184.

Gonzales, E. B., Kawate, T., and Gouaux, E. (2009). Pore architecture and ion sites in acid- sensing ion channels and P2X receptors. *Nature* 460, 599–604. doi: 10.1038/nature08218

González-Inchauspe, C., Urbano, F. J., Di Guilmi, M. N., and Uchitel, O. D. (2017). Acid-Sensing ion channels activated by evoked released protons modulate synaptic transmission at the mouse calyx of held synapse. *J. Neurosci.* 37, 2589–2599. doi: 10.1523/JNEUROSCI.2566-16.2017

Guzman-Martinez, L., Maccioni, R. B., Andrade, V., Navarrete, L. P., Pastor, M. G., and Ramos-Escobar, N. (2019). Neuroinflammation as a common feature of neurodegenerative disorders. *Front. Pharmacol.* 10:1008. doi: 10.3389/fphar.2019.01008

Huang, Y., Jiang, N., Li, J., Ji, Y. H., Xiong, Z. J., and Zha, X. M. (2015). Two aspects of ASIC function: synaptic plasticity and neuronal injury. *Neuropharmacology* 94, 42–48. doi: 10.1016/j.neuropharm.2014.12.010

Jasti, J., Furukawa, H., Gonzales, E. B., and Gouaux, E. (2007). Structure of acid-sensing ion channel 1 at 1.9 A resolution and low pH. *Nature* 449, 316–323. doi: 10.1038/nature06163

Joch, M., Ase, A. R., Chen, C. X., MacDonald, P. A., Kontogiannea, M., Corera, A. T., et al. (2007). Parkin-mediated monoubiquitination of the PDZ protein PICK1 regulates the activity of acid-sensing ion channels. *Mol. Biol. Cell* 18, 3105–3118. doi: 10.1091/mbc.e05-11-1027

Josefsen, K., Nielsen, S. M., Campos, A., Seifert, T., Hasholt, L., Nielsen, J. E., et al. (2010). Reduced gluconeogenesis and lactate clearance in Huntington's disease. *Neurobiol. Dis.* 40, 656–662. doi: 10.1016/j.nbd.2010.08.009

Kaila, K. (1994). Ionic basis of GABAA receptor channel function in the nervous system. *Prog. Neurobiol.* 42, 489–537. doi: 10.1016/0301-0082(94)90049-3

Kitada, T., Asakawa, S., Hattori, N., Matsumine, H., Yamamura, Y., Minoshima, S., et al. (1998). Mutations in the parkin gene cause autosomal recessive juvenile Parkinsonism. *Nature* 392, 605–608. doi: 10.1038/33416

Lei, S., Orser, B. A., Thatcher, G. R., Reynolds, J. N., and MacDonald, J. F. (2001). Positive allosteric modulators of AMPA receptors reduce proton-induced receptor desensitization in rat hippocampal neurons. *J. Neurophysiol.* 85, 2030–2038.

Leng, T. D., Si, H. F., Li, J., Yang, T., Zhu, M., Wang, B., et al. (2016). Amiloride Analogs as ASIC1a Inhibitors. *CNS Neurosci. Ther.* 22, 468–476.

Liu, C. H., Zhang, F., Krisrian, T., Polster, B., Fiskum, G. M., and Hu, B. (2012). "Protein aggregation and multiple organelle damage after brain ischemia," in *Translational Stroke Research* eds P. Lapchak, and J. Zhang (Berlin: Springer), 101–116

Liu, R. Y., Zhou, J. N., van Heerikhuize, J., Hofman, M. A., and Swaab, D. F. (1999). Decreased melatonin levels in postmortem cerebrospinal fluid in relation to aging, Alzheimer's disease, and apolipoprotein E-epsilon4/4 genotype. *J. Clin. Endocrinol. Metab.* 84, 323–327. doi: 10.1210/jcem.84.1.5394

Liu, Y., Ma, J., DesJarlais, R. L., Hagan, R., Rech, J., Lin, D., et al. (2021). Molecular mechanism and structural basis of small-molecule modulation of the gating of acid-sensing ion channel 1. *Commun. Biol.* 4:174. doi: 10.1038/s42003-021-01678-1

Loureiro, J. A., Andrade, S., Duarte, A., Neves, A. R., Queiroz, J. F., Nunes, C., et al. (2017). Resveratrol and Grape Extract-loaded solid lipid nanoparticles for the treatment of Alzheimenr's disease. *Molecules* 13, 222–277.

Loureiro, J. A., Gomes, B., Coelho, M. A., Carmo Pereira, M., and Rocha, S. (2014). Targeting nanoparticles across the blood-brain barrier with monoclonal antobodies. *Nanomedicine* 9, 709–722. doi: 10.2217/nnm.14.27

Magnotta, V. A., Heo, H. Y., Dlouhy, B. J., Dahdaleh, N. S., Follmer, R. L., Thedens, D. R., et al. (2012). Detecting activity- evoked pH changes in human brain. *Proc. Natl. Acad. Sci. U.S.A.* 109, 8270–8273. doi: 10.1073/pnas.1205902109

Makani, S., and Chesler, M. (2007). Endogenous alkaline transients boost postsynaptic NMDA receptor responses in hippocampal CA1 pyramidal neurons. *J. Neurosci.* 27, 7438–7446.

Mandal, P. K., Akolkar, H., and Tripathi, M. (2012). Mapping of hippocampal pH and neurochemicals from in vivo multi-voxel 31P study in healthy normal young male/female, mild cognitive impairment, and Alzheimer's disease. *J. Alzheimers Dis.* 3, S75–S86.

Mango, D., and Nisticò, R. (2018). Role of ASIC1a in Aβ-induced synaptic alterations in the hippocampus. *Pharmacol. Res.* 131, 61–65. doi: 10.1016/j.phrs.2018.03.016

Mango, D., and Nisticò, R. (2019). Acid-Sensing ion channel 1a is involved in N-Methyl D-aspartate receptor-dependent long-term depression in the hippocampus. *Front. Pharmacol.* 10:555. doi: 10.3389/fphar.2019.00555

Mango, D., and Nisticò, R. (2020). Role of ASIC1a in normal and pathological synaptic plasticity. *Rev. Physiol. Biochem. Pharmacol.* 177, 83–100. doi: 10.1007/112_2020_45

Mango, D., Barbato, G., Piccirilli, S., Panico, M. B., Feligioni, M., Schepisi, C., et al. (2014). Electrophysiological and metabolic effects of CHF5074 in the hippocampus: protection against in vitro ischemia. *Pharmacol. Res.* 81, 83–90. doi: 10.1016/j.phrs.2014.02.010

Mango, D., Braksator, E., Battaglia, G., Marcelli, S., Mercuri, N. B., Feligioni, M., et al. (2017). Acid-sensing ion channel 1a is required for mGlu receptor dependent long-term depression in the hippocampus. *Pharmacol. Res.* 119, 12–19. doi: 10.1016/j.phrs.2017.01.028

Munro, G., Christensen, J. K., Erichsen, H. K., Dyhring, T., Demnitz, J., Dam, E., et al. (2016). NS383 selectively inhibits acid-sensing ion channels containing 1a and 3 subunits to reverse inflammatory and neuropathic hyperalgesia in rats. *CNS Neurosci. Ther.* 22, 135–145. doi: 10.1111/cns.12487

Nisticò, R., Salter, E., Nicolas, C., Feligioni, M., Mango, D., Bortolotto, Z. A., et al. (2017). Synaptoimmunology - roles in health and disease. *Mol. Brain* 10:26. doi: 10.1186/s13041-017-0308-9

Olesen, A. E., Nielsen, L. M., Larsen, I. M., and Drewes, A. M. (2015). Randomized clinical trial: efficacy and safety of PPC-5650 on experimental esophageal pain and hyperalgesia in healthy volunteer. *Scand. J. Gastroenterol.* 50, 138–144. doi: 10.3109/00365521.2014.966319

Papalampropoulou-Tsiridou, M., Labrecque, S., Godin, A. G., De Koninck, Y., and Wang, F. (2020). Differential expression of acid – sensing ion channels in mouse primary afferents in naïve and injured conditions. *Front Cell Neurosci.* 14:103. doi: 10.3389/fncel.2020.00103

Parton, R. G., Dotti, C. G., Bacallao, R., Kurtz, I., Simons, K., and Prydz, K. (1991). pH-induced microtubule-dependent redistribution of late endosomes in neuronal and epithelial cells. *J. Cell Biol.* 113, 261–274. doi: 10.1083/jcb.113.2.261

Preece, P., and Cairns, N. J. (2003). Quantifying mRNA in postmortem human brain: influence of gender, age at death, postmortem interval, brain pH, agonal state and inter-lobe mRNA variance. *Brain Res. Mol. Brain Res.* 118, 60–71. doi: 10.1016/S0169-328X(03)00337-1

Qiang, M., Dong, X., Zha, Z., Zuo, X.K., Song, X.L., Zhao, L., et al. (2018). Selectiom of an ASIC1a-blocking combinatorial antibody that protects cells from ischemic death. *PNAS U.S.A.* 115, E7469–E7477. doi: 10.1073/pnas.1807233115

Roberts, E. L., and Chih, C. P. (1997). The influence of age of pH regulation in hippocampal slices before, during, and after anoxia. *J. Cereb. Blood Flow Metab.* 17, 560–566. doi: 10.1097/00004647-199705000-00010

Roberts, E. L., and Sick, T. J. (1996). Aging impairs regulation of intracellular pH in rat hippocampal slices. *Brain Res.* 735, 339–342.

Rook, M. L., Musgaard, M., and MacLean, D. M. (2021). Coupling structure with function in acid-sensing ion channels: challenges in pursuit of proton sensors. *J. Physiol.* 599, 417–430. doi: 10.1113/JP278707

Salter, M. W., and Stevens, B. (2017). Microglia emerge as central players in brain disease. *Nat. Med.* 23, 1018–1027. doi: 10.1038/nm.4397

Schild, L., Schneeberger, E., Gautschi, I., and Firsov, D. (1997). Identification of amino acid residues in the alpha, beta, and gamma subunits of the epithelial sodium channel (ENaC) involved in amiloride block and ion permeation. *J. Gen. Physiol.* 1, 15–26.

Sherwood, T. W., Frey, E. N., and Askwith, C. C. (2012). Structure and activity of the acid-sensing ion channels. *Am. J. Physiol. Cell Physiol.* 303, C699–C710. doi: 10.1152/ajpcell.00188.2012

Siesjo, B. K. (1988). Acidosis and ischemic brain damage. *Neurochem. Pathol.* 9, 31–88.

Sirbu, C. A., Ghinescu, M. C., Axelerad, A. D., Sirbu, A. M., and Ionita-Radu, F. (2021). A new era for monoclonal antibodies with applications in neurology. *Exp. Ther. Med.* 21:86. doi: 10.3892/etm.2020.9519

Sluka, K. A., Rasmussen, L. A., Edgar, M. M., O'Donnell, J. M., Walder, R. Y., Kolker, S. J., et al. (2013). Acid-sensing ion channel 3 deficiency increases inflammation but decreases pain behavior in murine arthritis. *Arthritis Rheum.* 65, 1194–1202. doi: 10.1002/art.37862

Tang, C. M., Dichter, M., and Morad, M. (1990). Modulation of the N-methyl-D- aspartate channel by extracellular H+. *Proc. Natl. Acad. Sci. U.S.A.* 87, 6445–6449. doi: 10.1073/pnas.87.16.6445

Teleanu, D. M., Negut, I., Grumezescu, V., Grumezescu, A. M., and Teleanu, R. I. (2019). Nanomaterials for drug delivery to the central nervous system. *Nanomaterials* 9:E371. doi: 10.3390/nano9030371

Traynelis, S. F., and Cull-Candy, S. G. (1990). Proton inhibition of N-methyl-D-aspartate receptors in cerebellar neurons. *Nature* 345, 347–350.

Tsang, T. M., Woodman, B., Mcloughlin, G. A., Griffin, J. L., Tabrizi, S. J., Bates, G. P., et al. (2006). Metabolic characterization of the R6/2 transgenic mouse model of Huntington's disease by high-resolution MAS1H NMR spectroscopy. *J. Proteome Res.* 5, 483–492. doi: 10.1021/pr050244o

Tyrtyshnaia, A. A., Lysenko, L. V., Madamba, F., Manzhulo, I. V., Khotimchenko, M. Y., and Kleschevnikov, A. M. (2016). Acute neuroinflammation provokes intracellular acidification in mouse hippocampus. *J. Neuroinflamm.* 13:283. doi: 10.1186/s12974-016-0747-8

Vergo, S., Craner, M. J., Etzensperger, R., Attfield, K., Friese, M. A., Newcombe, J., et al. (2011). Acid-sensing ion channel 1 is involved in both axonal injury and demyelination in multiple sclerosis and its animal model. *Brain* 134, 571–584. doi: 10.1093/brain/awq337

Voilley, N. (2004). Acid-sensing ion channels (ASICs): new targets for the analgesic effects of non-steroid anti-inflammatory drugs (NSAIDs). *Curr. Drug Targets Inflamm. Allergy* 3, 71–79. doi: 10.2174/1568010043483980

Voilley, N., de Weille, J., Mamet, J., and Lazdunski, M. (2001). Nonsteroid anti-inflammatory drugs inhibit both the activity and the inflammation-induced expression of acid-sensing ion channels in nociceptors. *J. Neurosci.* 21, 8026–8033. doi: 10.1523/JNEUROSCI.21-20-08026.2001

Vullo, S., and Kellenberger, S. (2020). A molecular view of the function and pharmacology of acid-sensing ion channels. *Pharmacol. Res.* 154:104166. doi: 10.1016/j.phrs.2019.02.005

Waldmann, R., Champigny, G., Bassilana, F., Heurteaux, C., and Lazdunski, M. (1997). A proton-gated cation channel involved in acid-sensing. *Nature* 386, 173–177. doi: 10.1038/386173a0

Wang, J. Z., Xi, L., Zhu, G. F., Han, Y. G., Luo, Y., Wang, M., et al. (2012). The acidic pH-induced structural changes in Pin1 as revealed by spectral methodologies. *Spectrochim. Acta Part A Mol. Biomol. Spectrosc.* 98, 199–206. doi: 10.1016/j.saa.2012.07.105

Wang, Y. Z., Wang, J. J., Huang, Y., Liu, F., Zeng, W. Z., Li, Y., et al. (2015). Tissue acidosis induces neuronal necroptosis via ASIC1a channel independent of its ionic conduction. *ELife* 4:e05682. doi: 10.7554/eLife.05682.021

Wemmie, J. A., Askwith, C. C., Lamani, E., Cassell, M. D., Freeman, J. H. Jr., and Welsh, M. J. (2003). Acid-sensing ion channel 1 is localized in brain regions with high synaptic density and contributes to fear conditioning. *J. Neurosci.* 23, 5496–5502. doi: 10.1523/JNEUROSCI.23-13-05496.2003

Wemmie, J. A., Chen, J., Askwith, C. C., Hruska-Hageman, A. M., Price, M. P., Nolan, B. C., et al. (2002). The acid-activated ion channel ASIC contributes to synaptic plasticity, learning, and memory. *Neuron* 34, 463–477. doi: 10.1016/S0896-6273(02)00661-X

Wemmie, J. A., Taugher, R. J., and Kreple, C. J. (2013). Acid-sensing ion channels in pain and disease. *Nat. Rev. Neurosci.* 14, 461–471. doi: 10.1038/nrn3529

Wong, H. K., Bauer, P. O., Kurosawa, M., Goswami, A., Washizu, C., Machida, Y., et al. (2008). Blocking acid-sensing ion channel 1 alleviates Huntington's disease pathology via an ubiquitin-proteasome system-dependent mechanism. *Hum. Mol. Genet.* 17, 3223–3235. doi: 10.1093/hmg/ddn218

Yermolaieva, O., Leonard, A. S., Schnizler, M. K., Abboud, F. M., and Welsh, M. J. (2004). Extracellular acidosis increases neuronal cell calcium by activating acid-sensing ion channel 1a. *Proc. Natl. Acad. Sci. U.S.A.* 101, 6752–6757. doi: 10.1073/pnas.0308636100

Conflict of Interest: The authors declare that the research was conducted in the absence of any commercial or financial relationships that could be construed as a potential conflict of interest.

Publisher's Note: All claims expressed in this article are solely those of the authors and do not necessarily represent those of their affiliated organizations, or those of the publisher, the editors and the reviewers. Any product that may be evaluated in this article, or claim that may be made by its manufacturer, is not guaranteed or endorsed by the publisher.

frontiers in Cellular Neuroscience

ORIGINAL RESEARCH
published: 15 October 2021
doi: 10.3389/fncel.2021.732869

Changes in H^+, K^+, and Ca^{2+} Concentrations, as Observed in Seizures, Induce Action Potential Signaling in Cortical Neurons by a Mechanism That Depends Partially on Acid-Sensing Ion Channels

*Omar Alijevic†, Zhong Peng† and Stephan Kellenberger**

Department of Biomedical Sciences, University of Lausanne, Lausanne, Switzerland

OPEN ACCESS

Edited by:
David MacLean,
University of Rochester, United States

Reviewed by:
Lachlan Rash,
The University of Queensland, Australia
Matthew Van Hook,
University of Nebraska Medical Center, United States

***Correspondence:**
Stephan Kellenberger
stephan.kellenberger@unil.ch

† These authors have contributed equally to this work and share first authorship

Specialty section:
This article was submitted to Cellular Neurophysiology, a section of the journal Frontiers in Cellular Neuroscience

Received: *29 June 2021*
Accepted: *27 September 2021*
Published: *15 October 2021*

Citation:
Alijevic O, Peng Z and Kellenberger S (2021) Changes in H^+, K^+, and Ca^{2+} Concentrations, as Observed in Seizures, Induce Action Potential Signaling in Cortical Neurons by a Mechanism That Depends Partially on Acid-Sensing Ion Channels. Front. Cell. Neurosci. 15:732869. doi: 10.3389/fncel.2021.732869

Acid-sensing ion channels (ASICs) are activated by extracellular acidification. Because ASIC currents are transient, these channels appear to be ideal sensors for detecting the onset of rapid pH changes. ASICs are involved in neuronal death after ischemic stroke, and in the sensation of inflammatory pain. Ischemia and inflammation are associated with a slowly developing, long-lasting acidification. Recent studies indicate however that ASICs are unable to induce an electrical signaling activity under standard experimental conditions if pH changes are slow. In situations associated with slow and sustained pH drops such as high neuronal signaling activity and ischemia, the extracellular K^+ concentration increases, and the Ca^{2+} concentration decreases. We hypothesized that the concomitant changes in H^+, K^+, and Ca^{2+} concentrations may allow a long-lasting ASIC-dependent induction of action potential (AP) signaling. We show that for acidification from pH7.4 to pH7.0 or 6.8 on cultured cortical neurons, the number of action potentials and the firing time increased strongly if the acidification was accompanied by a change to higher K^+ and lower Ca^{2+} concentrations. Under these conditions, APs were also induced in neurons from ASIC1a$^{-/-}$ mice, in which a pH of $\leq$ 5.0 would be required to activate ASICs, indicating that ASIC activation was not required for the AP induction. Comparison between neurons of different ASIC genotypes indicated that the ASICs modulate the AP induction under such changed ionic conditions. Voltage-clamp measurements of the Na^+ and K^+ currents in cultured cortical neurons showed that the lowering of the pH inhibited Na^+ and K^+ currents. In contrast, the lowering of the Ca^{2+} together with the increase in the K^+ concentration led to a hyperpolarizing shift of the activation voltage dependence of voltage-gated Na^+ channels. We conclude that the ionic changes observed during high neuronal activity mediate a sustained AP induction caused by the potentiation of Na^+ currents,

a membrane depolarization due to the changed K^+ reversal potential, the activation of ASICs, and possibly effects on other ion channels. Our study describes therefore conditions under which slow pH changes induce neuronal signaling by a mechanism involving ASICs.

Keywords: ASIC, acidification, action potential, neuronal signaling, modification of gating by ions, calcium

INTRODUCTION

The pH of body fluids is tightly controlled. The extracellular pH is normally close to 7.4. Rapid local pH fluctuations occur for example in synapses during neuronal activity (Chesler, 2003; Boscardin et al., 2016; Soto et al., 2018). Slower tissue acidification accompanies inflammation and ischemia (Cobbe and Poole-Wilson, 1980). Extracellular acidification induces action potentials (APs) in neurons. The transient receptor potential cation channel subfamily V member 1 (TRPV1) is an important pH sensor in the peripheral nervous system (PNS). It is activated by pH $\leq$ 6.5, with a pH of half-maximal activation, pH_{50}, of ∼5.3 (Caterina et al., 1997; Tominaga et al., 1998). Acid-sensing ion channels (ASICs) are low pH-activated channels that are widely expressed in the peripheral and central nervous system (CNS) (Wemmie et al., 2013; Kellenberger and Schild, 2015). Several studies have shown that TRPV1 and ASICs are the pH sensors for acid-induced AP generation in the PNS (Deval et al., 2003; Blanchard and Kellenberger, 2011), while acid-induced AP generation in the CNS depends essentially on ASICs (Baron et al., 2002; Vukicevic and Kellenberger, 2004). In contrast to its effect on TRPV1 and ASICs, extracellular acidification inhibits many excitatory ion channels, such as glutamate receptors and voltage-gated Ca^{2+} and Na^+ channels (reviewed in Boscardin et al., 2016).

The main ASIC subunits are ASIC1a, −1b, −2a, −2b, −3, and −4 (Wemmie et al., 2013; Kellenberger and Schild, 2015). In rodents, ASIC1a, −2a, −2b, and −4 are expressed in the CNS, while all ASIC subunits except ASIC4 are found in the PNS. The hetero- or homotrimeric assembly of ASIC subunits forms Na^+-selective ion channels (Yang and Palmer, 2014; Lynagh et al., 2017) that differ in their H^+ sensitivity [pH_{50} values between 6.6 (ASIC3) and 4.3 (ASIC2a)] and kinetics (Wemmie et al., 2013; Kellenberger and Schild, 2015; Schuhmacher et al., 2015; Rook et al., 2020, 2021). ASIC4 has so far not been shown to form functional channels and may regulate the expression of other ASICs (Akopian et al., 2000; Gründer et al., 2000; Lin et al., 2015). ASIC currents are transient because these channels enter a non-conducting, desensitized state after opening (Kellenberger and Schild, 2015; Rook et al., 2021). ASIC3 and some heterotrimeric ASICs produce in addition to the transient also a smaller sustained current. Animal studies identified roles of ASICs in synaptic plasticity and learning, fear-related behaviors, pain sensation, neuronal death after ischemic stroke and in neurodegenerative diseases (Wemmie et al., 2003; Xiong et al., 2004; Coryell et al., 2007; Friese et al., 2007; Pignataro et al., 2007; Deval et al., 2008, 2011; Kreple et al., 2014; Chiang et al., 2015; Sluka and Gregory, 2015; Lee and Chen, 2018; Chang et al., 2019). ASICs are potential drug targets of high interest. However, none of the available ASIC inhibitors is currently used in clinic (Baron and Lingueglia, 2015; Rash, 2017).

Traditionally, rapid solution changes are used to activate ASICs in studies in which ASIC currents are measured. However, some of the physiological and pathological processes in which ASICs are involved, are associated with slow and sustained pH changes, as e.g., inflammatory pain sensation or neurodegeneration after ischemic stroke. In a recent study we have investigated the activation of recombinant ASIC1a and of endogenous ASICs of cultured cortical neurons by pH ramps of defined speed (Alijevic et al., 2020). This analysis showed a strong decrease of the acid-induced current amplitude when the pH change was slowed, because a fraction of the channels desensitized without opening. If the pH ramp from 7.4 to 6.6 or 6.0 lasted 4–10 s, it induced longer bursts of action potentials (APs) in cultured cortical neurons than did faster pH ramps. However, with pH changes that took > 10 s to complete, APs were only very rarely induced. It seemed therefore that additional, currently unknown modulatory mechanisms are needed to allow an ASIC activation with such slow pH changes.

ASIC function is modulated by many compounds. Short peptides containing an Arg-Phe motif add a small sustained current to the transient ASIC1a current and shift its pH dependence of steady-state desensitization (the transition from the closed to the desensitized state) to more acidic values (Askwith et al., 2000; Sherwood and Askwith, 2009; Vick and Askwith, 2015; Bargeton et al., 2019; Borg et al., 2020) and have similar effects on ASIC3-containing channels. Molecules related to 2-guanidine-4-methylquinazoline induce a sustained activity in ASIC3 (Li et al., 2011). Reducing agents were shown to increase, while oxidizing reagents inhibit ASIC currents (Andrey et al., 2005; Chu et al., 2006; Cadiou et al., 2007; Cho and Askwith, 2007). ASIC function is also modulated by divalent cations (Babini et al., 2002; Chu et al., 2004). It is known that under some conditions that induce acidification, the concentrations of other ions are also changed. During high neuronal activity, seizures and ischemia, the extracellular concentrations of H^+ and K^+ increase in the CNS, while the Ca^{2+} concentration decreases (Heinemann and Louvel, 1983; Krishtal et al., 1987; Chesler, 2003; Brocard et al., 2013; Sibille et al., 2015; Larsen et al., 2016).

Abbreviations: AP, action potential; ASIC, acid-sensing ion channel; FCS, fetal calf serum; FT, firing time; G-V curve, conductance-voltage curve; I-V curve, current-voltage curve; Na_V, voltage-gated Na^+ channel; NMDG, N-Methyl-D-Glucamine; NT, neurotransmission; pH_{50}, pH of half-maximal activation; SL, seizure-like; TRPV1, transient receptor potential cation channel subfamily V member 1; Tyr, tyrode; $V_{1/2}$, voltage of half-maximal activation; WT, wild-type.

These changes in ion concentration occur within seconds to minutes. During high neuronal activity, the extracellular K^+ concentration reaches 6–10 mM, while the extracellular Ca^{2+} concentration, on the other hand, decreases to values as low as 0.8 mM (Heinemann et al., 1977; Brocard et al., 2013; Raimondo et al., 2015; Sibille et al., 2015; Larsen et al., 2016). In the present study we have investigated whether the above-described changes of K^+ and Ca^{2+} concentrations may affect acid-induced AP generation. We show that such changes in K^+ and Ca^{2+} concentration accompanied by a pH change to pH7.0 or 6.8 induced APs in cultured cortical neurons, even if the solution change was slow. The expressed ASIC subtype shaped the response; however, ASIC activity was not required for AP induction under these circumstances. Analysis of the modulation of channel function suggests that changed properties of voltage-gated Na^+ channels, together with a depolarization induced by the increase in extracellular K^+ concentration, as well as the activation of ASICs contribute to the AP induction under these ionic conditions.

MATERIALS AND METHODS

Embryonic Mouse Cerebral Cortex Neuron Culture

All animal handling procedures were carried out according to the Swiss federal law on animal welfare, and were approved by the committee on animal experimentation of the Canton de Vaud (License VD1750). ASIC1a$^{-/-}$ and ASIC2$^{-/-}$ mice were provided by Dr. John Wemmie (University of Iowa). The cortex neuronal culture was done as previously described (Alijevic et al., 2020). Cerebral cortices of fetuses of day E14–15 from C57BL/6 genetic background of WT, ASIC1a$^{-/-}$ or ASIC2$^{-/-}$ pregnant mice were dissected. They were placed in ice-cold HBSS medium (Thermo Fisher Scientific) complemented with 5 mM HEPES, chopped into small pieces (∼1 mm) and incubated at 37°C for 15 min in HBSS medium containing 0.05% Trypsin-EDTA (Thermo Fisher Scientific). The cortical tissues were then washed three times in Neurobasal medium (Thermo Fisher Scientific) containing 10% fetal calf serum (FCS) and dissociated to single cells by gentle trituration using 1 mL blue tips (cut to 0.4 cm diameter) in the Neurobasal/FCS medium containing additionally 1 mg/mL DNase (Sigma-Aldrich: DN25), before centrifugation at 1,000 rpm for 5 min. The neurons were re-suspended in Neurobasal/FCS medium and seeded at 40,000 – 200,000 cells/dish on 35-mm petri dishes containing three 15-mm diameter glass coverslips previously coated with poly-L-lysine. After 3 h the medium was replaced by Neurobasal Medium, Electro (Thermo Fisher Scientific:) containing B27 serum-free supplement, Electro (Thermo Fisher Scientific), GlutaMAX supplement (Thermo Fisher Scientific) and gentamicin (10 mg/ml final concentration; Thermo Fisher Scientific). Neuronal cultures were maintained in an incubator (37°C, 5% CO_2 in humidified air) and every 2–3 days half of the medium was replaced with fresh plating medium. Patch-clamp experiments of cortical neurons were performed in a Warner Instruments RC-42LP measuring chamber after at least 14 days post-seeding, to account for sufficient expression of both ASIC1 and ASIC2 channels (Li et al., 2010).

Electrophysiological Measurements

Electrophysiological measurements were carried out at room temperature (20–25°C) using the whole-cell configuration of the patch-clamp technique in voltage- and current-clamp mode with an EPC10 patch-clamp amplifier (HEKA Elektronik-Harvard Bioscience). Data were acquired with Patchmaster software and analysis of the currents and potentials was carried out with Fitmaster (HEKA Elektronik-Harvard Bioscience). The sampling interval and the low-pass filtering were set in voltage-clamp experiments to 0.02 ms and to 5 kHz, respectively, and in current-clamp experiments to 1 ms and 3 kHz (part of data of **Figures 1**–**3**) and 0.05 ms and 5 kHz (data for **Figure 4** and most of the data of **Figures 1**–**3**). Recording pipettes were made of borosilicate glass (thin-wall capillaries, World Precision Instruments, United States) with a Narishige PC-10 puller and had resistances between 2 and 4 MΩ when filled with the pipette solution. In voltage-clamp experiments we set the series resistance compensation to 70–90% and the holding potential to −60 mV or as indicated.

Extracellular Tyrode solution contained (in mM): 140 NaCl, 4 KCl, 2 $CaCl_2$, 1 $MgCl_2$, 10 HEPES, 10 MES, 10 glucose; pH was adjusted to the desired value using NaOH/HCl. The two following solutions were designed to represent concentration changes of K^+ and Ca^{2+} that are observed during high neuronal activity and during seizures (see main text). Extracellular "neurotransmission solution" (NT) contained (in mM): 137 NaCl, 6 KCl, 1 $CaCl_2$, 1 $MgCl_2$, 10 HEPES, 10 MES, 1 glucose. Extracellular "seizure-like" (SL) solution contained (in mM): 135 NaCl, 8 KCl, 0.8 $CaCl_2$, 1 $MgCl_2$, 10 MES, 10 HEPES, 10 glucose; Low Na^+ extracellular solution contained (in mM): 30 NaCl, 114 TEA-Cl, 0.1 $CdCl_2$, 2 $BaCl_2$, 1 $MgCl_2$, 10 MES, 10 HEPES, 10 glucose, 20 sucrose; Extracellular solution for K^+ channel recording contained (in mM): 140 N-Methyl-D-Glucamine (NMDG), 4 KCl, 2 $CaCl_2$, 1 $MgCl_2$, 10 MES, 10 HEPES, 10 glucose, 30 sucrose. The pipette solution used for voltage-clamp experiments contained (in mM): 90 K gluconate, 10 NaCl, 10 KCl, 1 $MgCl_2$, 60 HEPES, 10 EGTA; pH was adjusted to pH7.3 with KOH. The pipette solution for current-clamp experiments and for the experiments with voltage-gated currents contained (in mM): 90 K gluconate, 10 NaCl, 10 KCl, 3 $MgCl_2$, 2 ATP-Na_2, 0.3 GTP-Li^+, 60 HEPES, 10 EGTA; pH was adjusted to pH7.3 with KOH. The intracellular solution used with low Na^+ extracellular solution contained (in mM): 100 CsCl, 10 NaCl, 3 $MgCl_2$, 10 EGTA, 2 ATP-Na_2, 0.3 GTP-Li^+, 60 HEPES; pH was adjusted to pH7.3 with CsOH. The pH of the solutions was controlled on the day of the experiment and adjusted if necessary. Rapid solution exchange was achieved using computer-controlled electrovalves (cF-8VS) and the MPRE8 perfusion head (Cell MicroControls, Norfolk, VA). pH ramps were generated using a pair of programmable pumps with 60 ml syringes (Aladdin syringe pump, World Precision Instruments, United States), whose output came together in a perfusion head. The hyperterminal program (Windows Operating System) was used for commanding the two syringe pumps. The total output

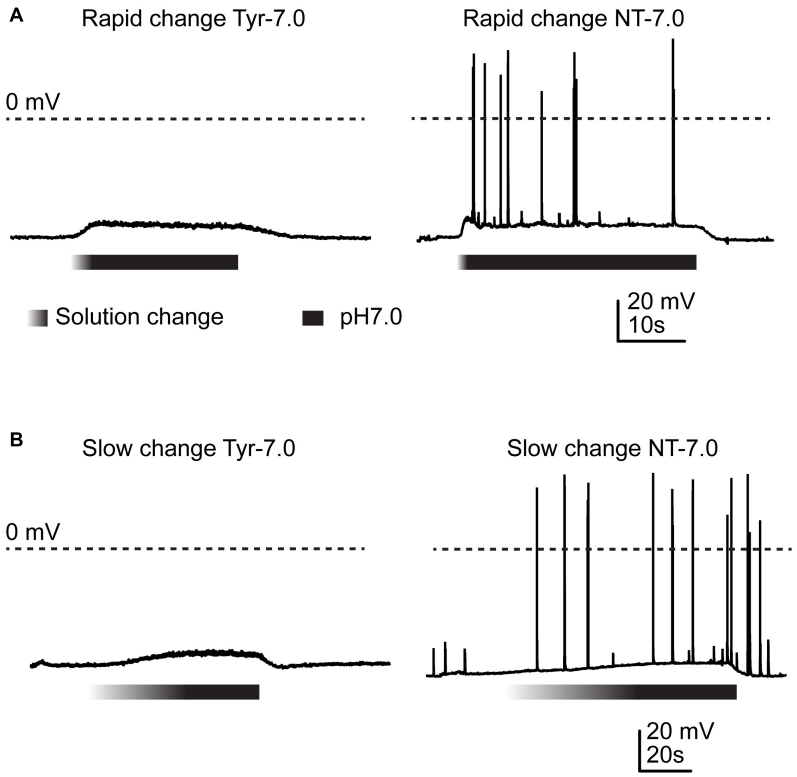

FIGURE 1 | Action potential induction by changes in Ca^{2+} and K^{+} concentration. Current-clamp experiments with cortical neurons. Baseline current was injected to obtain a resting membrane potential close to –60 mV in the pH7.4 Tyrode (Tyr) solution. Solution change from Tyr solution at pH7.4 to either Tyr solution at pH7.0 or "neurotransmission" (NT) solution at pH7.0. The Ca^{2+} and K^{+} concentrations of the Tyr solution were 2 and 4 mM, respectively, and those of the NT solution 1 and 6 mM. The gradient part of the bar indicates the pH ramp, the black part the perfusion with pH7.0. **(A)** Rapid changes, **(B)** slow changes.

rate of the two syringe pumps together was maintained constant at 100 ml/h. In current-clamp experiments, baseline current was injected to obtain a membrane potential close to −60 mV in presence of the pH7.4 Tyrode solution. This adjustment was made to start with similar resting membrane potential in all experiments. For the measurement of voltage-gated currents, the holding voltage was −90 mV, and currents were elicited by 100 ms steps of increasing amplitude to −90 to + 50 mV at 5 or 10 mV increments. The sweep interval was 4s. Leak current subtraction was done with the P/4 method.

Extracellular pH Imaging

The speed of the solution change was determined for experiments in which pH ramps were applied. pH imaging experiments were performed using an inverted fluorescence microscope (Zeiss Axio Observer, AX10) with a 63x objective (Plan-Apochromat) and a CoolSnap HQ2 camera (Photometrics, United States). The time resolution of the imaging part was ∼ 440 ms. Images were recorded using the Metafluor software (v.7.3.3, Molecular Devices, Sunnyvale, United States). Briefly, cells were grown in Fluorodish cell culture dishes (World Precision Instruments, United States) or on 15-mm diameter glass coverslips (VWR, Germany) and incubated prior to the experiment in Tyrode solution containing 10 μM of 5(6)-FAM SE (5-(and-6)-Carboxyfluorescein, succinimidyl ester mixed isomers (BIOTIUM, United States), a ratiometric dye able to sense extracellular pH changes (excitation 460/488 nm, emission 520 nm) for 15 min in an incubator (37°C, 5% CO_2). The amine-reactive succinimidyl ester form of the dye binds exclusively amine groups on cell surface proteins. The baseline of the 5(6)-FAM SE ratio measured during the perfusion of the tyrode solution showed a certain degree of photobleaching. We corrected for the photobleaching using Origin PRO software (OriginLab Corp., Northampton, United States). After baseline correction, the 90–10% fall time of the fluorescence signal was determined to classify the time course of the pH changes.

Analysis and Statistics

The conductance-voltage curves of Na_Vs were fitted to a Boltzmann function: $G(V) = G_{max}/(1 + \exp[(V-V_{1/2})/k]$, where G is the conductance, G_{max} the maximal conductance, V the voltage, $V_{1/2}$ the voltage of half-maximal activation and k the slope factor. The conductance was calculated at each test voltage as $G(V) = I/(V-V_{rev})$, where I is the current and V_{rev} the reversal potential obtained for each current-voltage (I–V) curve by linear interpolation or as indicated. The number of action potentials in current-clamp experiments was determined with FitMaster, measured over the same duration in pH ramps

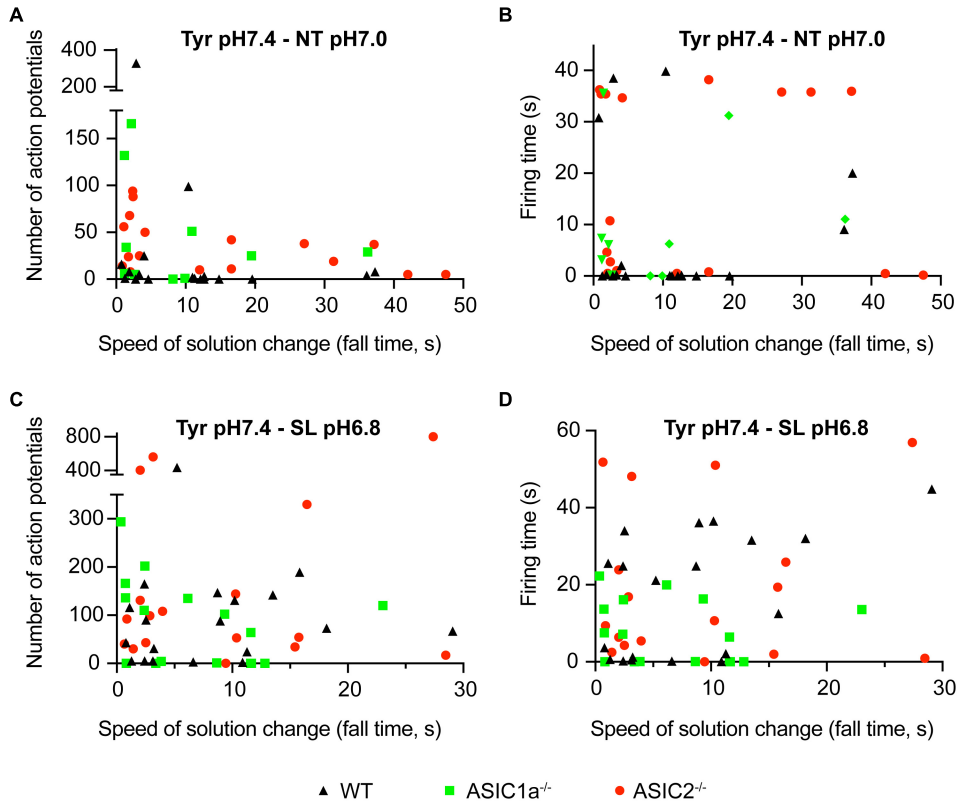

FIGURE 2 | Dependence of AP number and firing time on the kinetics of solution change. Current-clamp experiments with cortical neurons. Baseline current was injected to obtain a resting membrane potential close to –60 mV in the pH7.4 Tyr solution. In these experiments the solution was changed from Tyrode solution at pH7.4 to either NT solution at pH7.0 or SL solution at pH6.8. In the Tyr solution, Ca^{2+} and K^+ concentrations are 2 and 4 mM, respectively, while they are 1 and 6 mM in the NT and 0.8 and 8 mM in the SL solution. Number of APs **(A,C)** and the firing time (FT; **B,D**) are plotted as a function of ramp fall time of the solution change, as indicated; n = 12–21 per genotype and condition. The FT was determined as the time between the start of the first and the end of the last AP.

of different duration. The normality of the data distribution was determined by using the Shapiro-Wilk normally test. For normally distribution data we used student *t*-test for comparison between two groups or for paired comparisons and ANOVA followed by appropriate *post hoc* tests when more than two groups were involved. For not normally distribution data we used the Mann-Whitney test (for comparison between two groups) and the Kruskal-Wallis followed by Tukey *post hoc* test (or other appropriate tests, as indicated, for comparison between more than two groups). *P*-values of < 0.05 were considered significant. Data are presented as mean ± S.E.M.

RESULTS

Changes to Solutions That Mimic the Composition Observed With High Neuronal Activity Induce Action Potentials

Several studies have shown that extracellular acidification induces a neuronal depolarization in neurons via the activation of ASICs, which leads to the generation of APs (Baron et al., 2002; Deval et al., 2003; Vukicevic and Kellenberger, 2004). We have recently shown that slowing of the pH change reduces the ASIC current amplitude and affects the ASIC-mediated AP induction in neurons (Alijevic et al., 2020). In this previous study we showed that acidification to pH6.6 or 6.0 in the presence of physiological ion concentrations induced APs in cultured mouse cortical neurons if the duration of the completion of the pH change was not longer than ∼10 s. As mentioned in the introduction, situations of high neuronal activity induce concentration changes of several ions, among them an increase in extracellular K^+ and a decrease in extracellular Ca^{2+} concentration (Heinemann and Louvel, 1983; Frohlich et al., 2008; Brocard et al., 2013; Raimondo et al., 2015; Larsen et al., 2016). The difference in K^+ concentration changes the equilibrium potential of K^+ currents; a lowering of the extracellular Ca^{2+} concentration increases the pH sensitivity of ASICs (Babini et al., 2002), and strong reductions in Ca^{2+} concentrations were shown to induce a hyperpolarizing shift of the voltage dependence of activation of voltage-gated Na^+ channels (Na_Vs) (Hille, 2001). Acidification has been shown to inhibit Na_V function (Hille, 2001). We reasoned that an acidification, if accompanied by changes in K^+ and Ca^{2+} concentration, may induce even with slower pH ramps a long-lasting ASIC-mediated neuronal activity. To test

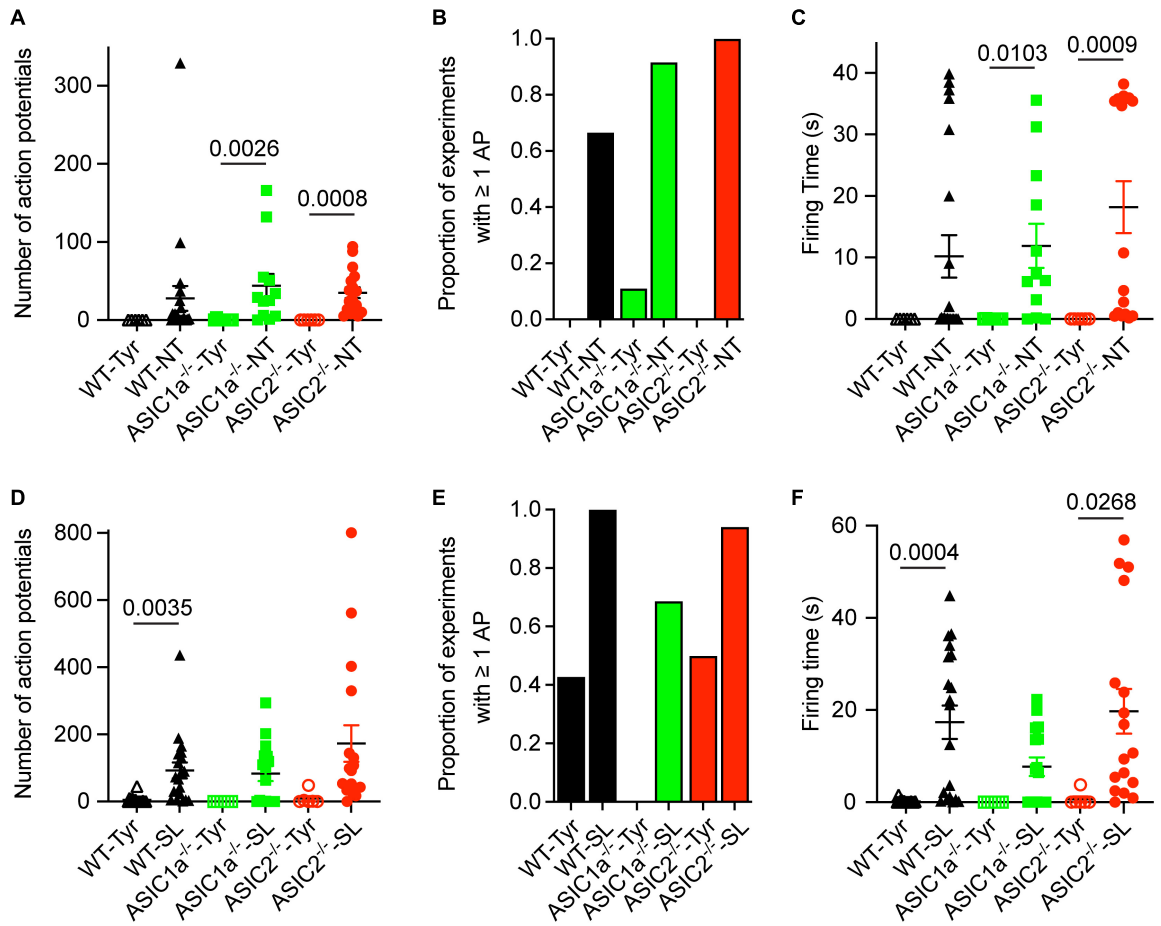

FIGURE 3 | Analysis of AP number and firing time as a function of genotype and ion composition. The data were obtained from current-clamp experiments with cortical neurons as described in the legend to **Figure 2**. **(A,D)** Number of APs induced by solution changes from Tyr-pH7.4 to the solutions indicated, at pH7.0 **(A)** or pH6.8 **(D)**, in WT, ASIC1a$^{-/-}$ and ASIC2$^{-/-}$ cortical neurons (n = 6–21). **(B,E)** The proportion of experiments in which at least 1 AP was induced is indicated for the different conditions and genotypes, Tyr and NT solution at pH7.0 in **(B)** and Tyr and SL solution at pH6.8 in **(E)**, n = 6–21. **(C,F)** FT, determined as described in the legend to **Figure 2**, for the indicated experimental conditions [**(C)** pH7.0, **(F)** pH6.8], n = 6–21. For this analysis, the data solution changes with different kinetics were pooled, since the pH ramp kinetics did not influence the AP induction (**Figure 2**). The statistical significance of the differences between mean values was tested with the Kruskal-Wallis test, followed by Dunn's multiple comparisons test.

this hypothesis, the Ca^{2+}, H^+ and K^+ concentrations were simultaneously changed. When, in current-clamp experiments with physiological ion concentrations ("Tyrode" (Tyr) solution), the pH was rapidly changed from 7.4 to 7.0, generally no APs were induced (**Figure 1A**, left panel). Rodent cortical neurons express homotrimeric ASIC1a channels, heterotrimers composed of ASIC1a together with ASIC2a and/or ASIC2b, and ASIC2a homotrimers (Askwith et al., 2004; Wemmie et al., 2013; Kellenberger and Schild, 2015). The pH_{50} of these channels depends on the ASIC subunit combination. Homotrimeric ASIC1a has a pH_{50} of ∼6.4, while the pH_{50} of ASIC2a is ∼4.5; pH_{50} values of heteromeric ASIC1a/2 channels are in-between. We have previously measured a pH_{50} value of 6.3 in wild type (WT) mouse cortical neurons (Alijevic et al., 2020). This analysis showed that a pH change from 7.4 to 7.0 induced only very small ASIC currents that would probably not depolarize the membrane potential sufficiently to activate voltage-gated Na^+ channels and induce action potentials, consistent with our observation in **Figure 1A**. If, however, the Tyrode solution at pH7.4 was changed to one at pH7.0 that mimics a situation of high neuronal activity, with 6 instead of 4 mM K^+, and 1 instead of 2 mM Ca^{2+} ("neurotransmission" (NT) solution), action potentials were induced (**Figure 1A**, right panel). When the experiments described in **Figure 1A** were repeated with a slow pH change, the result was very similar (**Figure 1B**). In these experiments, the extracellular pH was gradually changed from 7.4 to 7.0 using two syringes for the perfusion, one at pH7.4 and one at 7.0 (Materials and methods). The solution at pH7.0 contained physiological K^+ and Ca^{2+} concentrations for the experiment shown in the left panel, and 6 mM K^+ and 1 mM Ca^{2+} for the experiment shown on the right.

Next it was determined whether the AP induction depended on the kinetics of the solution change from the Tyrode solution pH7.4 to the NT solution at pH7.0. To this end, experiments of

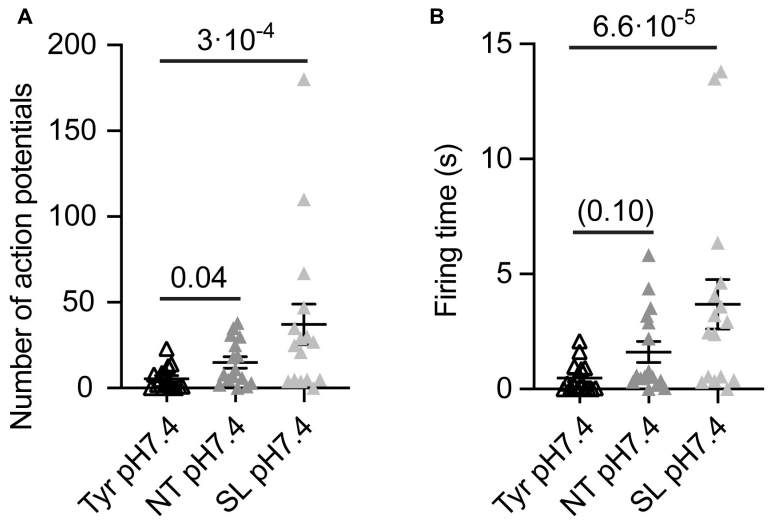

FIGURE 4 | Analysis of AP number and firing time as a function of ion composition at pH7.4 from WT cortical neurons. The data were obtained from current-clamp experiments with cortical neurons as described in the legend to **Figure 2**. Note that in these experiments there was a signaling activity even at Tyr-pH7.4, probably due to a higher neuron density than in the experiments of **Figures 1–3**. The solutions were changed with a rapid solution change system from Tyr-pH7.4 to Tyr-pH7.4, NT-pH7.4 or SL-pH7.4 in each of the neurons tested to obtain a direct comparison between the three conditions of the number of APs **(A)** and the FT (**B**, $n = 16$). The statistical significance of the differences between mean values was tested with the Friedman test, followed by Dunn's multiple comparisons test.

the kind described in **Figure 1** were carried out at different speeds of solution change. **Figure 2A** plots the number of induced APs as a function of the fall time (time to pass from 10 to 90%) of the solution change. This showed that for WT neurons (black triangles), there was no clear correlation between the kinetics of the solution change and the number of induced APs. As expected, the AP burst duration ("firing time," FT, **Figure 2B**) did not show a dependence on the kinetics of the solution change either. Similarly to WT neurons, the number of induced APs and the FT did not depend on the kinetics of the solution change in ASIC1a$^{-/-}$ and ASIC2$^{-/-}$ neurons. In most measured neurons, the number of APs, and with it the FT, were relatively low. We had previously shown that acidification to 6.0 or 6.6 under physiological K^+ and Ca^{2+} concentrations led to APs in WT and ASIC2$^{-/-}$, but not in ASIC1a$^{-/-}$ neurons (Alijevic et al., 2020). The absence of APs in ASIC1a$^{-/-}$ neurons is due to the much lower pH sensitivity of ASICs formed by ASIC2 subunits. Changing to the NT solution at pH7.0 induced APs as expected in WT and ASIC2$^{-/-}$ neurons. Surprisingly, the AP induction was also observed in ASIC1a$^{-/-}$ neurons, suggesting that the ASIC activation is not required for NT solution-induced APs. As discussed above, the NT solution represents ionic conditions observed in high neuronal activity. During seizures, there occur even stronger changes in K^+, Ca^{2+} and H^+ concentrations (Raimondo et al., 2015; Boscardin et al., 2016). AP induction was in an additional set of experiments investigated for such a "seizure-like" (SL) condition (8 instead of 4 mM K^+, 0.8 instead of 2 mM Ca^{2+} at pH6.8; **Figures 2C,D**). These experiments showed qualitatively similar results as observed with the NT solution, with a tendency of higher numbers of APs, however. **Supplementary Figure 1A** plots the depolarization, thus the difference between the basal membrane potential and the maximal membrane potential reached during the exposure to the test solution, as measured between the APs. A three-way ANOVA analysis confirmed as sources of variation the pH ($p < 0.0001$), the genotype ($p = 0.0005$) and the solution type (Tyr as compared to NT or SL; $p = 0.0207$). The figure illustrates the smaller depolarization induced by pH7.0 as compared to pH6.8 solutions. With changes to pH7.0, the depolarization appears higher with the NT as compared to the Tyr solution. The observation that acidification to pH6.8 in the Tyr solution induced a depolarization of 16 ± 2 mV ($n = 6$; **Supplementary Figure 1A**), suggests that these neurons may express other pH sensors than ASICs, or that the acidification may inhibit K^+ channels (Boscardin et al., 2016). There was no clear correlation between the depolarization amplitude and the number of induced APs or the firing time (**Supplementary Figures 1B,C**). The overall conclusions of these experiments are that AP induction by NT and SL solutions 1) does not depend on the kinetics of the solution change and 2) does not require the activation of ASICs.

Analysis of Action Potential Number and Firing Time of Pooled Data

Since the AP properties did not depend on the kinetics of solution change, data with different kinetics of solution change were pooled for the analysis and grouped according to the genotype and type of solution change. The FT values and numbers of APs were highly variable, as illustrated for the NT and SL conditions in **Figure 2**. Similarly to WT neurons, pH changes to the NT, but not the Tyrode solution of pH7.0, induced APs in ASIC1a$^{-/-}$ and ASIC2$^{-/-}$ neurons (**Figure 3A**). The increase in AP numbers in the NT compared to the Tyr solution was statistically significant in ASIC1a$^{-/-}$ and ASIC2$^{-/-}$ neurons.

The plot of the proportion of experiments showing at least 1 AP (**Figure 3B**) further illustrates the effect of the changes in K^+ and Ca^{2+} concentration. For changes to the Tyr solution at pH7.0, there were no APs in WT and ASIC2$^{-/-}$ neurons; in one experiment with ASIC1a$^{-/-}$ neurons, APs were induced. With the NT solution at pH7.0, at least one AP was observed in ∼65–90% of the experiments with WT and ASIC1a$^{-/-}$ neurons, and in all experiments with ASIC2$^{-/-}$ neurons. Due to the almost complete absence of APs with pH changes to pH7.0 in the Tyrode solution, the FT in this condition was 0s, while average FTs for experiments with APs in the NT condition were 10.2, 11.9 and 18.2 s for WT, ASIC1a$^{-/-}$ and ASIC2$^{-/-}$ neurons, respectively (**Figure 3C**). These values were significantly higher in the NT than the Tyr condition in ASIC1a$^{-/-}$ and ASIC2$^{-/-}$ neurons. Analogous experiments with the SL solution at pH6.8 showed higher numbers of APs compared to the Tyr solution at pH6.8 in WT neurons, and tendencies of higher numbers in ASIC1a$^{-/-}$ and ASIC2$^{-/-}$ neurons (p = 0.059 for ASIC1a$^{-/-}$ and p = 0.0518 for ASIC2$^{-/-}$ neurons; **Figure 3D**). In contrast to the experiments with acidification to pH7.0, the pH change to pH6.8 induced also with the Tyr solution ≥ 1 AP in ∼40% of the experiments with WT and ASIC2$^{-/-}$ neurons. In ASIC1a$^{-/-}$ neurons, no APs were induced in these conditions (**Figure 3E**). The change to the SL condition at pH6.8 induced APs in almost all WT and ASIC2$^{-/-}$ neurons, and in 70% of ASIC1a$^{-/-}$ neurons. The FT was < 1 s for the Tyr solution at pH6.8 in WT and ASIC2$^{-/-}$ neurons, and 17.4, 7.7, and 19.7 s for WT, ASIC1a$^{-/-}$ and ASIC2$^{-/-}$ neurons, respectively, with the SL condition (**Figure 3F**); this increase was statistically significant for WT and ASIC2$^{-/-}$ neurons. The AP numbers and FTs were not significantly different between the SL and the NT condition for a given genotype.

To evaluate the impact of the Ca^{2+} and K^+ changes alone on the neuronal excitability, we measured the number of APs and FT induced by solution changes from Tyr-pH7.4 to Tyr-pH7.4, NT-pH7.4, or SL-pH7.4 solutions in WT cortical neurons. In this set of experiments, we observed a basal signaling activity even in the Tyr-pH7.4 solution, most likely due to higher neuronal density and consequently an increased number of interneuronal connections than in the previous cultures. In the absence of any pH changes, a higher number of APs, and a tendency to longer FTs was observed in NT as compared to the Tyr solution (**Figures 4A,B**). In SL solution at pH7.4, the number of APs and FT increased with regard to the Tyr solution (**Figures 4A,B**). This indicates that the increased signaling activity in NT and SL solutions did not require the acidification. Switching from the Tyr-pH7.4 to the NT-pH7.4 or the SL-pH7.4 solution induced in these experiments a sustained depolarization of 6.2 ± 0.4 and 12.7 ± 0.4 mV, respectively (n = 16).

Our experiments show that concomitant changes of H^+, Ca^{2+}, and K^+ ion concentrations, as they occur during high neuronal activity or epileptic seizures, can induce long bursts of action potentials in cultured mouse cortical neurons, independently of the speed of solution change. In the two particular conditions that were studied here (corresponding to high neutrotransmission and seizure-like situations), the acidification was less important for the AP induction than was the change in Ca^{2+} and K^+ ion concentrations. In the following we investigated which changes in ion channel function led to the observed increased excitability in NT and SL conditions.

Lowering of the pH Induces Small Changes of Voltage Dependence and Current Amplitude of Na_Vs

We analyzed first how the pH changes used to activate ASICs and induce APs affect the voltage-gated Na^+ and K^+ channels. **Figures 5A–C** shows Na_V I–V curves obtained from WT neurons in a solution with physiological K^+ and Ca^{2+} concentrations at pH7.4 and 6.6. The pH6.6, which is 0.2 units below the value of the more extreme condition investigated in current-clamp experiments, was chosen to make sure not to miss any effect of the pH. For these experiments, the Na^+ concentration had been lowered to 30 mM (section "Materials and Methods") to allow a better voltage-clamp of the currents. Changing the extracellular pH from pH7.4 to 6.6 showed in direct comparison a tendency of a depolarizing shift with acidification in WT neurons (**Figures 5C,D**; $V_{1/2}$, pH7.4: −33.5 ± 1.2 mV and pH6.6, −31.3 ± 0.7 mV, n = 10, p = 0.066). A similar, statistically significant shift was observed in cortical neurons of ASIC1a$^{-/-}$ and ASIC2$^{-/-}$ mice (**Figures 5E–G**). The peak amplitude of Na_V currents, measured at −25 mV, was decreased by acidification to pH6.6 in WT, ASIC1a$^{-/-}$ and ASIC2$^{-/-}$ cortical neurons (**Figure 5H**). This inhibition amounted to 24 ± 4% in WT (n = 10), 37 ± 4% in ASIC1a$^{-/-}$ (n = 7) and 24 ± 3% in ASIC2$^{-/-}$ neurons (n = 9).

Small Effects of pH on K^+ Currents

Acidification from pH7.4 to 6.6 led to an apparent decrease in K^+ current amplitudes as illustrated in representative current traces and the I-V curves (**Figures 6A–E**). Since the reversal potential could not be measured reliably due to the small inward currents, conductance-voltage (G-V) curves were constructed based on a reversal potential of −83 mV, calculated from the nominal K^+ concentrations in the measuring solutions (**Supplementary Figure 2**). The G-V curves obtained at pH7.4 and 6.6 from the same neurons indicated that the acidification does not affect the voltage dependence. Comparison of the current amplitudes at + 30 mV showed decreased values at pH6.6 (**Figure 6F**). This difference was significant in ASIC1a$^{-/-}$ and ASIC2$^{-/-}$, but not WT neurons. Inspection of the I-V curves at pH7.4 and 6.6 shows that the ratio of the current amplitude between the two conditions is the same over the voltage range of −20 to + 50 mV, and thus the difference between the amplitudes measured at the two conditions increases with positive voltage.

Changes of Ca^{2+} and K^+ Concentrations Affect Na_V Currents

To determine the effect of changes in Ca^{2+} and K^+ concentrations on Na_V currents, a first series of experiments was carried out at pH7.4, either in physiological extracellular Tyrode solution, or in a solution with 0.8 mM Ca^{2+} and 8 mM K^+, mimicking thus in this regard a seizure-like condition (SL solution). These experiments were carried out with WT

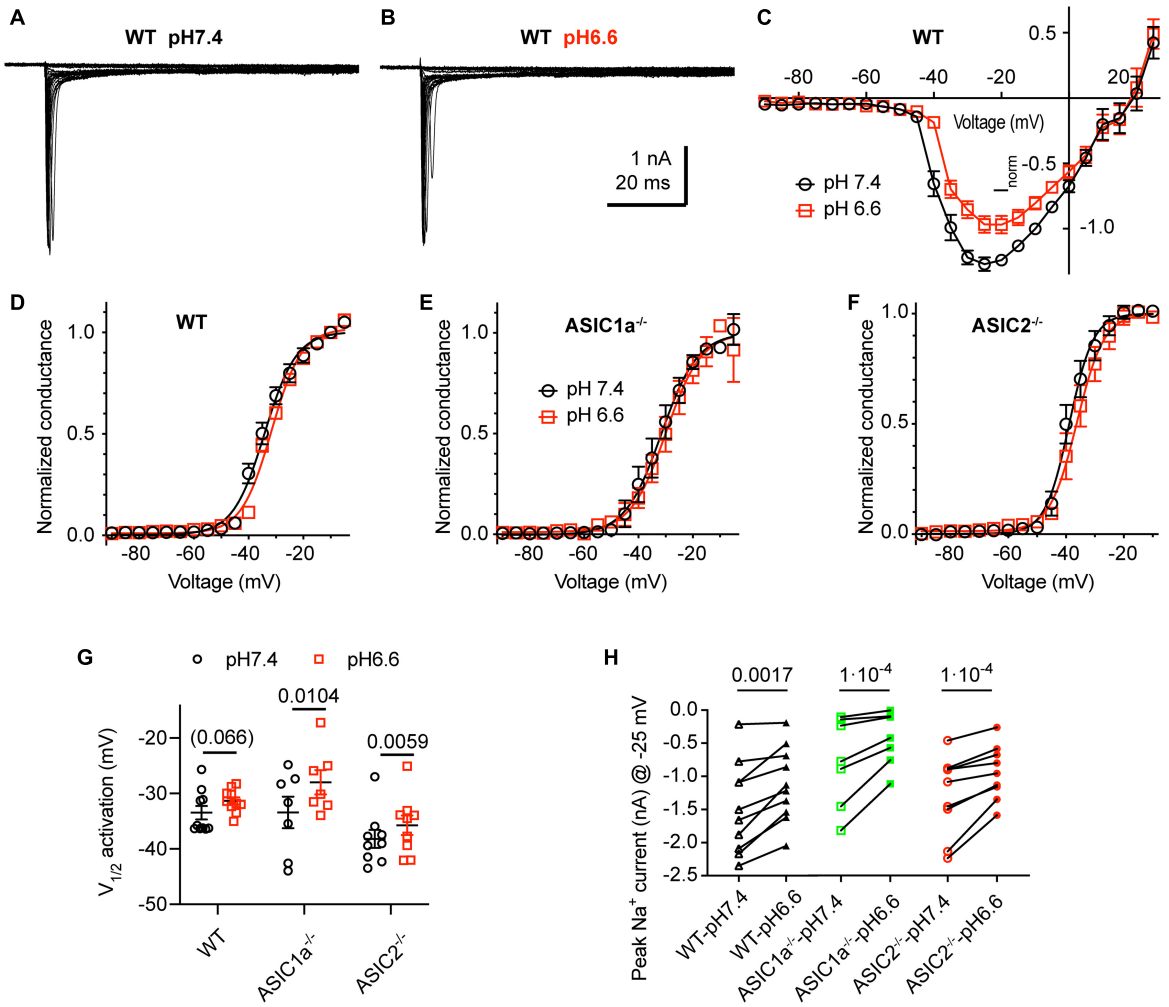

FIGURE 5 | Acidification to pH6.6 induces a small inhibition of voltage-gated Na^+ channels. Experiments were done in whole-cell voltage-clamp on cortical neurons. The voltage protocols are described under *Materials and methods*. The response to two different solutions was directly compared in the same cell. Only the pH was changed between the two conditions. **(A,B)** Representative current traces obtained at pH7.4 **(A)** and pH6.6 **(B)** from the same WT neuron **(C)** Na_V I-V curve at pH 7.4 and 6.6. Current amplitudes were normalized in each cell to the amplitude measured at pH7.4 at –10 mV, $n = 10$. **(D–F)** Na_V conductance-voltage curve at pH 7.4 and 6.6. The conductance was normalized to the conductance at –10 mV. **(D)** Neurons from WT mice. The $V_{1/2}$, determined from a Boltzmann fit, was –33.5 ± 1.2 mV (pH7.4) and –31.3 ± 0.7 mV (pH6.6, $p = 0.066$, $n = 10$). **(E)** Neurons from ASIC1a$^{-/-}$ mice. The $V_{1/2}$ values were –33.4 ± 2.8 mV (pH7.4) and –28.0 ± 2.2 mV (pH6.6, $p = 0.0104$, $n = 7$). **(F)** Neurons from ASIC2$^{-/-}$ mice. The $V_{1/2}$ values were –38.2 ± 1.6 mV (pH7.4), –35.7 ± 1.8 mV (pH6.6, $p = 0.0059$, $n = 9$). **(G)** Plot of the $V_{1/2}$ values obtained in experiments described in **(D–F)**. **(H)** Na_V current amplitude at –25 mV, measured from WT, ASIC1a$^{-/-}$ and ASIC2$^{-/-}$ cortical neurons, $n = 7$–10. Data of **Figure 5** were obtained in an extracellular solution with decreased Na^+ concentration to improve the clamp control (Materials and methods). *P*-values derived from paired *t*-tests are indicated in **(G,H)**.

neurons. The change to the SL solution led to a hyperpolarizing shift of the voltage dependence of activation (**Figures 7A,B**; $V_{1/2}$, Tyr-pH7.4, −39.0 ± 1.6 mV; SL-pH7.4, −42.3 ± 2.1 mV, $p = 0.041$, $n = 10$). The SL solution did not significantly change the Na_V peak current amplitude measured at −25 mV (**Figure 7C**). To test the consequences of the combined effect of Ca^{2+} and K^+ concentration changes and a lowering of the pH, Na_V currents were measured in a second set of paired experiments in Tyr-pH7.4 and SL-pH6.8 solutions (**Figures 7D–F**). The voltage dependence of activation was shifted negatively in the SL-pH6.8 solution (**Figure 7E**, $V_{1/2}$, Tyr-pH7.4, −34.2 ± 2.1 mV; SL-pH6.8, −41.0 ± 2.9 mV, $p = 0.0083$, $n = 10$). Although the I-V curves suggests slightly smaller current amplitudes in the SL-pH6.8 condition, the Na_V current amplitudes at −25 mV were not significantly different between the two conditions (**Figure 7F**). The hyperpolarizing shift of the activation voltage dependence in the SL-pH6.8 condition is expected to contribute to an increased excitability of the cortical neurons. Thus, the lowering of the Ca^{2+} together with the increasing of the K^+ concentration has an opposite effect on the Na_V function compared to the acidification alone. Our analysis shows that the hyperpolarizing shift of the voltage dependence predominates when these changes in Ca^{2+} and K^+ concentrations are combined with an acidification to pH6.8.

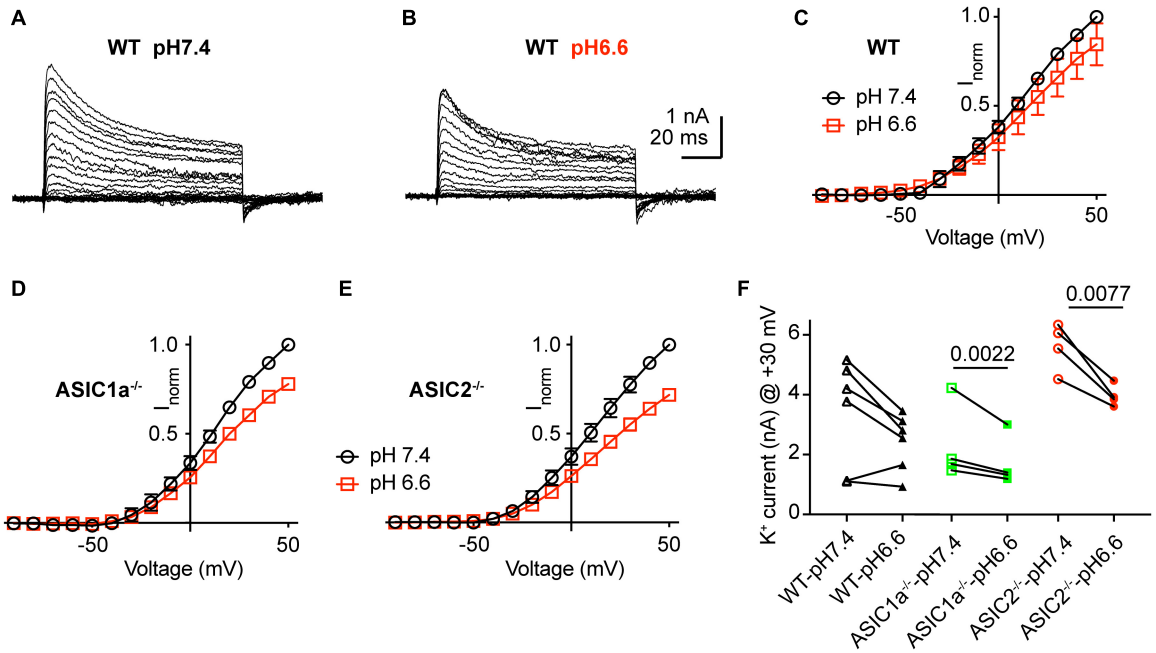

FIGURE 6 | Inhibition of K^+ currents by acidification to pH6.6. Experiments were done in whole-cell voltage-clamp on cortical neurons. The response to two different solutions was directly compared in the same cell. Only the pH was changed between the two conditions. **(A,B)** Representative current traces obtained at pH7.4 **(A)** and pH6.6 **(B)** from the same neuron. **(C–E)** I–V curve of K^+ currents, measured at pH7.4 and pH6.6. Current amplitudes were normalized in each cell to the amplitude measured at pH7.4 at + 50 mV. **(C)** Neurons from WT mice, $n = 6$, **(D)** ASIC1a$^{-/-}$ mice, $n = 4$ and **(E)** ASIC2$^{-/-}$ mice, $n = 4$. **(F)** Peak K^+ current amplitudes measured at + 30 mV, at pH7.4 and 6.6, from WT, ASIC1a$^{-/-}$ and ASIC2$^{-/-}$ cortical neurons, $n = 4$–6. *P*-values obtained with paired *t*-tests are indicated in **(F)** if they were < 0.05.

For the K^+ currents, changing at pH7.4 from normal Tyrode to SL solution did not affect the voltage dependence, nor the current amplitudes (**Figures 7G,H**). If this change was accompanied by an acidification to pH6.8, apparently smaller current amplitudes were observed in the SL-pH6.8 condition (**Figure 7I**) that were however not significantly different from the current amplitudes measured in the Tyr-pH7.4 solution in paired experiments (**Figure 7J**).

DISCUSSION

Extracellular acidification induces neuronal activity via the activation of pH-sensing ion channels. ASICs are important pH sensors of the nervous system. It was documented in several studies that they contribute to the sensation of inflammatory pain and to neurodegeneration after ischemic stroke, two processes associated with slowly developing pH changes. In a recent study we showed that pH changes from pH7.4 to 6.6 or 6.0 that take more than 10 s to complete are unlikely to induce APs in neurons of the CNS (Alijevic et al., 2020). Since conditions of high neuronal activity and ischemia are associated with concentration changes of other ions besides protons, we tested here whether concentration changes of Ca^{2+} and K^+ ions modulated acid-induced AP generation. We observed that small acidifications combined with lowering of the Ca^{2+} and increasing of the K^+ concentration induced APs efficiently, independently of the speed of solution change. This AP induction did not require ASICs, was however modulated by ASICs. Investigation of the effects of these concentration changes on voltage-gated Na^+ and K^+ currents showed an inhibition of Na^+ and K^+ channels by the lowering of the pH, and a hyperpolarization of the activation voltage dependence of Na_Vs if the acidification was combined with a lowering of the Ca^{2+} and an increase of the K^+ concentration.

Effects of the Acid-Sensing Ion Channel Genotype

The experiments in which the speed of the change to the NT or SL solution was varied, indicated that the number of induced APs and the FT did not depend on the kinetics of the changes in ion concentrations, in opposition to the limitation observed in experiments with solutions of physiological ion concentrations (Alijevic et al., 2020), in which the AP induction required ASIC activation.

The ASIC subunits that can contribute to functional ASICs in CNS neurons are ASIC1a, ASIC2a, and ASIC2b. ASIC2b cannot form pH-activated homotrimeric channels but participates in the formation of heteromers (Lingueglia et al., 1997). Homotrimeric ASIC1a has a higher H^+ sensitivity than ASIC2a, as discussed above. In CNS neurons of ASIC1a$^{-/-}$ mice, lower pH values than pH5.0 are required to induce ASIC currents (Askwith et al., 2004). CNS neurons of ASIC2$^{-/-}$ mice have ASICs that are more sensitive to pH than is found in WT neurons, because functional

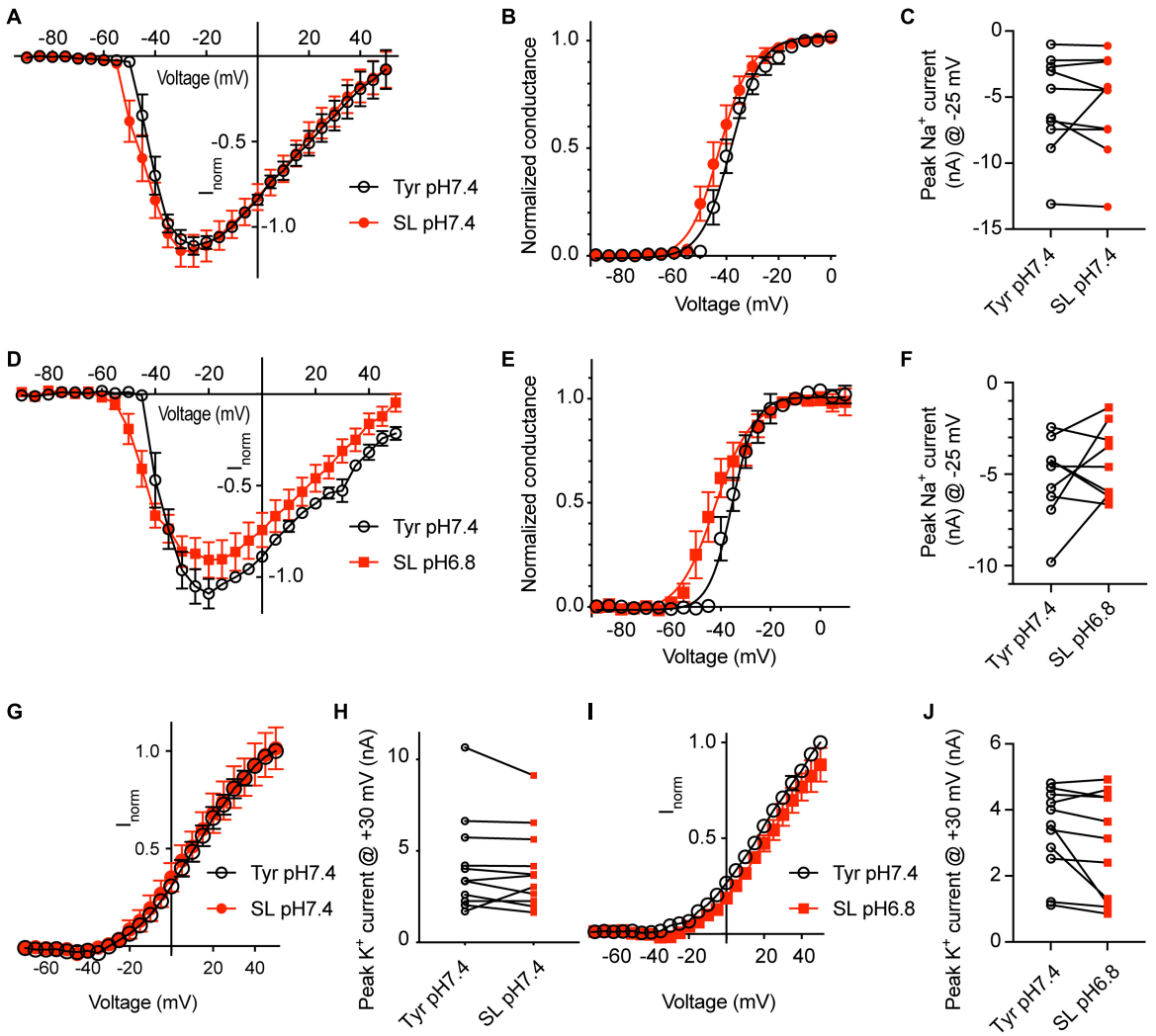

FIGURE 7 | Solutions mimicking seizure-like conditions change the voltage dependence of voltage-gated Na^+ channels. Experiments were done in whole-cell voltage-clamp on cortical neurons from WT mice. The response to two different solutions was directly compared in the same cell. **(A–C)** Between the two conditions, only the Ca^{2+} and K^+ concentration, but not the pH was changed. **(A)** Na_V I-V curve in Tyr-pH7.4 or SL-pH7.4 solution. Current amplitudes were normalized in each cell to the amplitude measured in the Tyr solution at –10 mV, $n = 10$. **(B)** Na_V conductance-voltage curve in Tyr-pH7.4 or SL-pH7.4 solution. The conductance was normalized for each condition to the conductance determined at –10 mV. The $V_{1/2}$ values were –39.0 ± 1.6 mV (Tyr) and –42.3 ± 2.1 mV (SL, $p = 0.041$, $n = 10$, paired t-test). **(C)** Na_V peak current amplitudes at –25 mV, measured in Tyr and SL solution at pH7.4 ($n = 10$). **(D–F)** Comparison of Na_V properties between Tyr-pH7.4 and SL-pH6.8 conditions in paired experiments. **(D)** Na_V I-V curve in Tyr-pH7.4 or SL-pH6.8 solution from paired experiments. Current amplitudes were normalized in each cell to the amplitude measured in the Tyr solution at –10 mV, $n = 10$. **(E)** Na_V conductance-voltage curve in Tyr-pH7.4 or SL-pH6.8 solution. The conductance was normalized for each condition to the conductance determined at –10 mV. The $V_{1/2}$ values were –34.2 ± 2.1 mV (Tyr-pH7.4) and –41.0 ± 3.0 mV (SL-pH6.8). **(F)** Na_V peak current amplitudes at –25 mV, measured in Tyr-pH7.4 and SL-pH6.8 solution ($n = 10$). **(G)** I–V curve of K^+ currents, measured in Tyr-pH7.4 and SL-pH7.4 solution, $n = 11$. **(H)** K^+ peak amplitude, measured at + 30 mV, in Tyr-pH7.4 and SL-pH7.4 solution, $n = 11$. **(I)** I–V curve of K^+ currents, measured in Tyr-pH7.4 and SL-pH6.8 solution, $n = 11$. **(J)** K^+ peak amplitude at + 30 mV, measured in Tyr-pH7.4 and SL-pH6.8 solution, $n = 11$. The current amplitudes compared in **(C,F,H,J)** were not different between the two conditions tested. **(G,I)** In each cell, the current amplitudes measured were normalized to the amplitude measured in the Tyr-pH7.4 condition at +50 mV.

ASICs in this background are essentially ASIC1a homotrimers. The pH_{50} of ASIC activation in cortical neurons of WT mice was ∼6.3, while this value was ∼6.7 in ASIC2$^{-/-}$, and < 4.3 in ASIC1a$^{-/-}$ neurons (Alijevic et al., 2020). These pH_{50} values in the ASIC knockout neurons are close to the reported pH_{50} values of recombinant ASIC1a and ASIC2a, respectively, strongly suggesting that there is no compensatory upregulation of other ASIC subunits in the knockout animals. Changes to the Tyr solution induced APs in ≤ 10% of the experiments, if the final pH was 7.0. In contrast, a change to the Tyr solution at pH6.8 induced APs in ∼40% of the experiments in WT and ASIC2$^{-/-}$ neurons, consistent with previous observations that acidification to pH6.8 induces small ASIC currents. In ASIC1a$^{-/-}$ neurons, APs were not induced with the pH6.8 Tyr

solution, because of the reduced pH sensitivity of the ASIC1a-less channels.

The NT and SL solutions at pH7.0 and 6.8, respectively, induced APs also in neurons from ASIC1a$^{-/-}$ mice, suggesting that the activation of ASICs was not required for AP induction. The ASIC genotype of the neurons influenced the AP induction in the Tyr-pH6.8 condition. We did, however, not observe any significant differences between the ASIC genotypes regarding the AP induction with the NT and SL solutions. The AP generation in neurons depends on many factors, resulting in a high neuron-to-neuron variability, which may have precluded the detection of a contribution of ASICs to AP induction in the other test conditions. It is expected that with smaller concentration changes of Ca^{2+} and K^+ than tested here, the activation of ASICs by the acidification would contribute more significantly to the AP generation.

In a separate set of experiments in WT neurons, we have directly compared AP induction by the Ca^{2+} and K^+ changes alone, without concomitant acidification. The comparison of the three solutions in the same neurons indicates that the lowering of the Ca^{2+} together with the increase of the K^+ concentration increased the signaling activity independently of an acidification.

Changes in Ion Concentrations Observed During High Neuronal Activity and Seizures

Variations in interstitial ion concentrations in the brain occur under many physiological conditions (Ding et al., 2016). Higher concentration changes were observed under pathological conditions. The basal extracellular K^+ concentration in brain was measured as 3–4 mM. During high neuronal activity, such as seizures, this concentration increased up to 10, maximally 12 mM (Heinemann and Louvel, 1983; Frohlich et al., 2008; Brocard et al., 2013; Raimondo et al., 2015; Larsen et al., 2016). Basal Ca^{2+} concentrations in the brain were between 1 and 2 mM, in many studies close to 1.2 mM. During high neuronal activity, this concentration decreased to ∼0.8 mM (Heinemann and Louvel, 1983; Brocard et al., 2013) or even lower concentrations (Raimondo et al., 2015). Following an ischemic stroke, even more dramatic changes in Ca^{2+} and K^+ concentrations were observed (Kristian and Siesjo, 1998; Mori et al., 2002). An increase of the extracellular K^+ concentration depolarizes the neuronal membrane potential, decreases input resistance, and can activate bursting in some neuron types (reviewed in Frohlich et al., 2008). On the level of the neuronal circuitry, increases in K^+ concentration reduce synaptic inhibition, because the K^+-Cl^--cotransporter KCC2 will operate with a reduced electrochemical driving force, and extrude less Cl^- (Frohlich et al., 2008). Consequently, the GABAergic transmission might show excitatory effects as long as the increased extracellular K^+ concentration is able to maintain a reduced KCC2 activity. The resting pH value of the interstitial fluid of the brain is generally 0.1–0.2 pH units more acidic than the pH of the blood (Mutch and Hansen, 1984; Syková and Svoboda, 1990). Repetitive electrical stimulation induced in several studies first a short alkalinization of 0.01–0.2 pH units, which was followed by a slower developing, long-lasting acidic shift of 0.1–0.25 pH units (Chesler, 1990, 2003; Makani and Chesler, 2010). The acidification occurring in synapses was estimated to 0.2–0.6 pH units (DeVries, 2001; Vessey et al., 2005). A study with rats showed a brain tissue acidification induced by seizures of ∼0.36 pH units in normoxic, and of 0.51 pH units in moderately hypoxic animals (Siesjö et al., 1985).

One of the consequences of the extracellular acidification is dampening the excitatory neurotransmission, while the concomitant reduction of external calcium and rise of potassium ions appear to have a counterbalancing effect for restoring the excitatory tone. The changes in Na_V function that we observed with the SL solution are consistent with earlier studies that investigated the dependence of Na_V function on the Ca^{2+} concentration. Reducing the extracellular Ca^{2+} concentration shifts the conductance-voltage relationship of Na_Vs and other voltage-gated channels to more hyperpolarized values (Campbell and Hille, 1976; Hille, 2001). In frog skeletal muscle, lowering the extracellular Ca^{2+} concentration from 2 to 0.5 mM shifted the conductance-voltage curve by −8 mV (Campbell and Hille, 1976). This effect may be due to reduced surface charge screening (Hille, 2001). The extracellular Ca^{2+} concentration co-defines also the pH dependence of ASICs. There appears to be a competition between Ca^{2+} and H^+. Therefore, lowering of the Ca^{2+} concentration induces an alkaline shift of the pH dependence of activation and steady-state desensitization (Babini et al., 2002). Ca^{2+} concentration changes between 2 and 0.5 mM appear to induce rather small shifts in ASIC1a pH dependence (Babini et al., 2002). Millimolar Ca^{2+} concentrations are known to lead to a weak pore block of several ion channels, as Na_Vs and ASICs among others. For ASIC1a, the IC_{50} for inhibition is ∼5 mM (Paukert et al., 2004).

Extracellular protons have been shown to induce a pore block of Na_V currents. A midpoint of inhibition between pH4.6 and 5.4 has been reported for amphibian Na_Vs (reviewed in Hille, 2001). Extracellular pH is known to affect also the voltage dependence of Na_Vs. In amphibian nerve fibers, lowering the extracellular pH to values < 5.5 induced a depolarizing shift of the voltage dependence of activation (Hille, 1968). Acidification to pH6.0 induced a ∼30% reduction of the current amplitude and did not affect the voltage dependence of recombinantly expressed rat $Na_V1.2$ (Vilin et al., 2012). An earlier study using rat CA1 neurons showed that a change from pH7.4 to 6.4 induced a small depolarizing shift in the voltage dependence of activation and did not affect steady-state inactivation and current kinetics (Tombaugh and Somjen, 1996). Our observations are consistent with these earlier findings obtained in different organisms and cell systems at more acidic pH ranges.

Another prominent ion channel type whose activity depends on the extracellular Ca^{2+} concentration is the calcium homeostasis modulator 1 (CALHM1), which is permeable to monovalent cations and to Ca^{2+}, and is expressed in mouse cortical neurons. Its activity depends on the membrane voltage and the extracellular Ca^{2+} concentration (Ma et al., 2012, 2016). The IC_{50} for Ca^{2+} inhibition of CALHM1 was estimated as ∼0.2 mM at −60 mV (Ma et al., 2012), suggesting that CALHM1 would only be partially potentiated by the Ca^{2+} concentration changes investigated in our study.

Changing to Neurotransmission or Seizure-Like Solutions Increases Neuronal Excitability

The increased AP induction with NT and SL solutions is due to the effects of the H^+, K^+, and Ca^{2+} concentrations on different targets. Our voltage-clamp analysis of Na^+ and K^+ channels provided the following information. Lowering of the pH to 6.6 induced in our experimental conditions a decrease of the Na_V current amplitude, in accordance with previous studies, as well as a small depolarizing shift of the activation voltage dependence. It decreased in addition the amplitude of K^+ currents. If the pH was kept at 7.4, but the K^+ and Ca^{2+} concentrations were changed to the SL conditions, thus from 4 to 8 mM for K^+, and from 2 to 0.8 mM for Ca^{2+}, the Na_V current amplitude was not affected, and the activation voltage dependence was shifted to more hyperpolarized values. If these changes in K^+ and Ca^{2+} concentrations were combined with an acidification to pH6.8, which corresponds to the SL-pH6.8 condition tested in the current-clamp experiments of **Figures 2**, **3**, the effect of the K^+ and Ca^{2+} concentration changes was predominant over the effect of the acidification, resulting thus in a hyperpolarizing shift, which is expected to increase the neuronal excitability, consistent with the observed effects on AP induction. The K^+ current amplitudes were not affected by the change to the SL conditions, although this solution change induced a theoretical shift of + 18 mV of the reversal potential, and with this a reduced driving force.

In situations in which the H^+, K^+, and Ca^{2+} concentrations change, the effect of acidification on ASICs can induce APs if acidification is fast, or prevent ASIC-mediated APs, if the acidification is slow, because of desensitization of ASICs (Alijevic et al., 2020), while the effects of K^+ and Ca^{2+} concentration changes on neuronal excitability do not depend on the speed of the solution change. Such changes in K^+ and Ca^{2+} concentration will allow a contribution of ASICs to neuronal signaling under pH conditions in which ASICs are normally not or not sufficiently activated. The different dependence of H^+-induced ASIC activity and of K^+ and Ca^{2+} concentration-dependent changes in neuronal signaling on the kinetics of the concentration changes add an additional level of complexity to the regulation of AP signaling.

In conclusion, the efficient induction of APs by the NT and SL solutions in our experiments is therefore due in part to changed properties of Na_Vs, for which the positive modulation by the decrease of the Ca^{2+} concentration is stronger than the negative modulation by the increase in H^+ concentration. The increased K^+ concentration led to a depolarization of the membrane potential. On ASICs, the lowering of the Ca^{2+} concentration shifted the pH-response curve to more alkaline values, while the acidification led to a partial activation, at least in the SL condition. It is highly probable that these ion concentration changes also affect other channels or transporters that may further contribute to the changed excitability. Our study describes conditions under which an acidification, independently of the speed of the solution change, induces APs. Although the ASICs were not required for the AP induction, they contributed to it in some of the tested conditions.

DATA AVAILABILITY STATEMENT

The original contributions presented in the study are included in the article/**Supplementary Material**, further inquiries can be directed to the corresponding author/s.

ETHICS STATEMENT

The animal study was reviewed and approved by the committee on animal experimentation of the Canton de Vaud, Service vétérinaire.

AUTHOR CONTRIBUTIONS

OA and SK designed the project and wrote the manuscript. ZP and OA carried out the experiments. All authors approved the final manuscript.

FUNDING

This research was supported by the Swiss National Science Foundation grant 31003A_172968 to SK.

ACKNOWLEDGMENTS

We thank Jan P. Kucera and Ophélie Molton for discussions and for comments on the manuscript.

SUPPLEMENTARY MATERIAL

The Supplementary Material for this article can be found online at: https://www.frontiersin.org/articles/10.3389/fncel.2021.732869/full#supplementary-material

REFERENCES

Akopian, A. N., Chen, C. C., Ding, Y. N., Cesare, P., and Wood, J. N. (2000). A new member of the acid-sensing ion channel family. *Neuroreport* 11, 2217–2222.

Alijevic, O., Bignucolo, O., Hichri, E., Peng, Z., Kucera, J. P., and Kellenberger, S. (2020). Slowing of the time course of acidification decreases the acid-sensing ion channel 1a current amplitude and modulates action potential firing in neurons. *Front. Cell. Neurosci.* 14:41. doi: 10.3389/fncel.2020.00041

Andrey, F., Tsintsadze, T., Volkova, T., Lozovaya, N., and Krishtal, O. (2005). Acid sensing ionic channels: modulation by redox reagents. *Biochim. Biophys. Acta* 1745, 1–6. doi: 10.1016/j.bbamcr.2005.01.008

Askwith, C. C., Cheng, C., Ikuma, M., Benson, C., Price, M. P., and Welsh, M. J. (2000). Neuropeptide FF and FMRFamide potentiate acid-evoked currents

from sensory neurons and proton-gated DEG/ENaC channels. *Neuron* 26, 133–141.

Askwith, C. C., Wemmie, J. A., Price, M. P., Rokhlina, T., and Welsh, M. J. (2004). ASIC2 modulates ASIC1 H^+-activated currents in hippocampal neurons. *J. Biol. Chem.* 279, 18296–18305.

Babini, E., Paukert, M., Geisler, H. S., and Grunder, S. (2002). Alternative splicing and interaction with di- and polyvalent cations control the dynamic range of acid-sensing ion channel 1 (ASIC1). *J. Biol. Chem.* 277, 41597–41603. doi: 10.1074/jbc.M205877200

Bargeton, B., Iwaszkiewicz, J., Bonifacio, G., Roy, S., Zoete, V., and Kellenberger, S. (2019). Mutations in the palm domain disrupt modulation of acid-sensing ion channel 1a currents by neuropeptides. *Sci. Rep.* 9:2599. doi: 10.1038/s41598-018-37426-5

Baron, A., and Lingueglia, E. (2015). Pharmacology of acid-sensing ion channels - Physiological and therapeutical perspectives. *Neuropharmacology* 94, 19–35. doi: 10.1016/j.neuropharm.2015.01.005

Baron, A., Waldmann, R., and Lazdunski, M. (2002). ASIC-like, proton-activated currents in rat hippocampal neurons. *J. Physiol.* 539, 485–494.

Blanchard, M. G., and Kellenberger, S. (2011). Effect of a temperature increase in the non-noxious range on proton-evoked ASIC and TRPV1 activity. *Pflugers Arch.* 461, 123–139. doi: 10.1007/s00424-010-0884-3

Borg, C. B., Braun, N., Heusser, S. A., Bay, Y., Weis, D., Galleano, I., et al. (2020). Mechanism and site of action of big dynorphin on ASIC1a. *Proc. Natl. Acad. Sci. U S A* 117, 7447–7454. doi: 10.1073/pnas.1919323117

Boscardin, E., Alijevic, O., Hummler, E., Frateschi, S., and Kellenberger, S. (2016). The function and regulation of acid-sensing ion channels (ASICs) and the epithelial Na^+ channel (ENaC): IUPHAR Review 19. *Br. J. Pharmacol.* 173, 2671–2701. doi: 10.1111/bph.13533

Brocard, F., Shevtsova, N. A., Bouhadfane, M., Tazerart, S., Heinemann, U., Rybak, I. A., et al. (2013). Activity-dependent changes in extracellular Ca^{2+} and K^+ reveal pacemakers in the spinal locomotor-related network. *Neuron* 77, 1047–1054. doi: 10.1016/j.neuron.2013.01.026

Cadiou, H., Studer, M., Jones, N. G., Smith, E. S., Ballard, A., McMahon, S. B., et al. (2007). Modulation of acid-sensing ion channel activity by nitric oxide. *J. Neurosci.* 27, 13251–13260. doi: 10.1523/JNEUROSCI.2135-07.2007

Campbell, D. T., and Hille, B. (1976). Kinetic and pharmacological properties of the sodium channel of frog skeletal muscle. *J. Gen. Physiol.* 67, 309–323. doi: 10.1085/jgp.67.3.309

Caterina, M. J., Schumacher, M. A., Tominaga, M., Rosen, T. A., Levine, J. D., and Julius, D. (1997). The capsaicin receptor: a heat-activated ion channel in the pain pathway. *Nature* 389, 816–824. doi: 10.1038/39807

Chang, C. T., Fong, S. W., Lee, C. H., Chuang, Y. C., Lin, S. H., and Chen, C. C. (2019). Involvement of acid-sensing ion channel 1b in the development of acid-induced chronic muscle pain. *Front. Neurosci.* 13:1247. doi: 10.3389/fnins.2019.01247

Chesler, M. (1990). The regulation and modulation of pH in the nervous system. *Progr. Neurobiol.* 34, 401–427.

Chesler, M. (2003). Regulation and modulation of pH in the brain. *Physiol. Rev.* 83, 1183–1221. doi: 10.1152/physrev.00010.2003

Chiang, P. H., Chien, T. C., Chen, C. C., Yanagawa, Y., and Lien, C. C. (2015). ASIC-dependent LTP at multiple glutamatergic synapses in amygdala network is required for fear memory. *Sci. Rep.* 5:10143. doi: 10.1038/srep10143

Cho, J. H., and Askwith, C. C. (2007). Potentiation of acid-sensing ion channels by sulfhydryl compounds. *Am. J. Physiol. Cell. Physiol.* 292, C2161–C2174. doi: 10.1152/ajpcell.00598.2006

Chu, X. P., Close, N., Saugstad, J. A., and Xiong, Z. G. (2006). ASIC1a-specific modulation of acid-sensing ion channels in mouse cortical neurons by redox reagents. *J. Neurosci.* 26, 5329–5339.

Chu, X. P., Wemmie, J. A., Wang, W. Z., Zhu, X. M., Saugstad, J. A., Price, M. P., et al. (2004). Subunit-dependent high-affinity zinc inhibition of acid-sensing ion channels. *J. Neurosci.* 24, 8678–8689.

Cobbe, S. M., and Poole-Wilson, P. A. (1980). Tissue acidosis in myocardial hypoxia. *J. Mol. Cell. Cardiol.* 12, 761–770. doi: 10.1016/0022-2828(80)90078-4

Coryell, M. W., Ziemann, A. E., Westmoreland, P. J., Haenfler, J. M., Kurjakovic, Z., Zha, X. M., et al. (2007). Targeting ASIC1a reduces innate fear and alters neuronal activity in the fear circuit. *Biol. Psychiatry* 62, 1140–1148. doi: 10.1016/j.biopsych.2007.05.008

Deval, E., Baron, A., Lingueglia, E., Mazarguil, H., Zajac, J. M., and Lazdunski, M. (2003). Effects of neuropeptide SF and related peptides on acid sensing ion channel 3 and sensory neuron excitability. *Neuropharmacology* 44, 662–671.

Deval, E., Noel, J., Gasull, X., Delaunay, A., Alloui, A., Friend, V., et al. (2011). Acid-sensing ion channels in postoperative pain. *J. Neurosci.* 31, 6059–6066. doi: 10.1523/JNEUROSCI.5266-10.2011

Deval, E., Noel, J., Lay, N., Alloui, A., Diochot, S., Friend, V., et al. (2008). ASIC3, a sensor of acidic and primary inflammatory pain. *EMBO J.* 27, 3047–3055.

DeVries, S. H. (2001). Exocytosed protons feedback to suppress the Ca^{2+} current in mammalian cone photoreceptors. *Neuron* 32, 1107–1117.

Ding, F., O'Donnell, J., Xu, Q., Kang, N., Goldman, N., and Nedergaard, M. (2016). Changes in the composition of brain interstitial ions control the sleep-wake cycle. *Science* 352, 550–555. doi: 10.1126/science.aad4821

Friese, M. A., Craner, M. J., Etzensperger, R., Vergo, S., Wemmie, J. A., Welsh, M. J., et al. (2007). Acid-sensing ion channel-1 contributes to axonal degeneration in autoimmune inflammation of the central nervous system. *Nat. Med.* 13, 1483–1489. doi: 10.1038/nm1668

Frohlich, F., Bazhenov, M., Iragui-Madoz, V., and Sejnowski, T. J. (2008). Potassium dynamics in the epileptic cortex: new insights on an old topic. *Neuroscientist* 14, 422–433. doi: 10.1177/1073858408317955

Gründer, S., Geissler, H.-S., Bässler, E.-L., and Ruppersberg, J. P. (2000). A new member of acid-sensing ion channels from pituitary gland. *Neuroreport* 11, 1607–1611.

Heinemann, U., and Louvel, J. (1983). Changes in $[Ca^{2+}]_o$ and $[K^+]_o$ during repetitive electrical stimulation and during pentetrazol induced seizure activity in the sensorimotor cortex of cats. *Pflugers Arch.* 398, 310–317. doi: 10.1007/BF00657240

Heinemann, U., Lux, H. D., and Gutnick, M. J. (1977). Extracellular free calcium and potassium during paroxsmal activity in the cerebral cortex of the cat. *Exp. Brain Res.* 27, 237–243.

Hille, B. (1968). Charges and potentials at the nerve surface : divalent ions and pH. *J. Gen. Physiol.* 51, 221–236.

Hille, B. (2001). *Ion channels of excitable membranes*. Sunderland: Sinauer Associates.

Kellenberger, S., and Schild, L. (2015). International union of basic and clinical pharmacology. XCI. Structure, function, and pharmacology of acid-sensing ion channels and the epithelial Na^+ Channel. *Pharmacol. Rev.* 67, 1–35. doi: 10.1124/pr.114.009225

Kreple, C. J., Lu, Y., Taugher, R. J., Schwager-Gutman, A. L., Du, J., Stump, M., et al. (2014). Acid-sensing ion channels contribute to synaptic transmission and inhibit cocaine-evoked plasticity. *Nat. Neurosci.* 17, 1083–1091. doi: 10.1038/nn.3750

Krishtal, O. A., Osipchuk, Y. V., Shelest, T. N., and Smirnoff, S. V. (1987). Rapid extracellular pH transients related to synaptic transmission in rat hippocampal slices. *Brain Res.* 436, 352–356.

Kristian, T., and Siesjo, B. K. (1998). Calcium in ischemic cell death. *Stroke* 29, 705–718. doi: 10.1161/01.str.29.3.705

Larsen, B. R., Stoica, A., and MacAulay, N. (2016). Managing brain extracellular K^+ during neuronal activity: The physiological role of the Na^+/K^+-ATPase subunit isoforms. *Front. Physiol.* 7:141. doi: 10.3389/fphys.2016.00141

Lee, C. H., and Chen, C. C. (2018). Roles of ASICs in nociception and proprioception. *Adv. Exp. Med. Biol.* 1099, 37–47. doi: 10.1007/978-981-13-1756-9_4

Li, M., Kratzer, E., Inoue, K., Simon, R. P., and Xiong, Z. G. (2010). Developmental change in the electrophysiological and pharmacological properties of acid-sensing ion channels in CNS neurons. *J. Physiol.* 588, 3883–3900. doi: 10.1113/jphysiol.2010.192922

Li, W. G., Yu, Y., Zhang, Z. D., Cao, H., and Xu, T. L. (2011). ASIC3 channels integrate agmatine and multiple inflammatory signals through the nonproton ligand sensing domain. *Mol. Pain* 6:88. doi: 10.1186/1744-8069-6-88

Lin, S.-H., Chien, Y.-C., Chiang, W.-W., Liu, Y.-Z., Lien, C.-C., and Chen, C.-C. (2015). Genetic mapping of ASIC4 and contrasting phenotype to ASIC1a in modulating innate fear and anxiety. *Eur. J. Neurosci.* 41, 1553–1568. doi: 10.1111/ejn.12905

Lingueglia, E., de Weille, J. R., Bassilana, F., Heurteaux, C., Sakai, H., Waldmann, R., et al. (1997). A modulatory subunit of acid sensing ion channels in brain and dorsal root ganglion cells. *J. Biol. Chem.* 272, 29778–29783.

Lynagh, T., Flood, E., Boiteux, C., Wulf, M., Komnatnyy, V. V., Colding, J. M., et al. (2017). A selectivity filter at the intracellular end of the acid-sensing ion channel pore. *Elife* 6:e24630. doi: 10.7554/eLife.24630

Ma, Z., Siebert, A. P., Cheung, K. H., Lee, R. J., Johnson, B., Cohen, A. S., et al. (2012). Calcium homeostasis modulator 1 (CALHM1) is the pore-forming subunit of an ion channel that mediates extracellular Ca^{2+} regulation of neuronal excitability. *Proc. Natl. Acad. Sci. U S A* 109, E1963–E1971. doi: 10.1073/pnas.1204023109

Ma, Z., Tanis, J. E., Taruno, A., and Foskett, J. K. (2016). Calcium homeostasis modulator (CALHM) ion channels. *Pflugers Arch.* 468, 395–403. doi: 10.1007/s00424-015-1757-6

Makani, S., and Chesler, M. (2010). Rapid rise of extracellular pH evoked by neural activity is generated by the plasma membrane calcium ATPase. *J. Neurophysiol.* 103, 667–676. doi: 10.1152/jn.00948.2009

Mori, K., Miyazaki, M., Iwase, H., and Maeda, M. (2002). Temporal profile of changes in brain tissue extracellular space and extracellular ion (Na^+, K^+) concentrations after cerebral ischemia and the effects of mild cerebral hypothermia. *J. Neurotrauma* 19, 1261–1270. doi: 10.1089/08977150260338047

Mutch, W. A., and Hansen, A. J. (1984). Extracellular pH changes during spreading depression and cerebral ischemia: mechanisms of brain pH regulation. *J. Cerebral Blood Flow Metabol.* 4, 17–27. doi: 10.1038/jcbfm.1984.3

Paukert, M., Babini, E., Pusch, M., and Grunder, S. (2004). Identification of the Ca^{2+} blocking site of acid-sensing ion channel (ASIC) 1: implications for channel gating. *J. Gen. Physiol.* 124, 383–394.

Pignataro, G., Simon, R. P., and Xiong, Z. G. (2007). Prolonged activation of ASIC1a and the time window for neuroprotection in cerebral ischaemia. *Brain* 130, 151–158. doi: 10.1093/brain/awl325

Raimondo, J. V., Burman, R. J., Katz, A. A., and Akerman, C. J. (2015). Ion dynamics during seizures. *Front. Cell. Neurosci.* 9:419. doi: 10.3389/fncel.2015.00419

Rash, L. D. (2017). Acid-sensing ion channel pharmacology, past, present, and future. *Adv. Pharmacol.* 79, 35–66. doi: 10.1016/bs.apha.2017.02.001

Rook, M. L., Musgaard, M., and MacLean, D. M. (2021). Coupling structure with function in acid-sensing ion channels: challenges in pursuit of proton sensors. *J. Physiol.* 599, 417–430. doi: 10.1113/JP278707

Rook, M. L., Williamson, A., Lueck, J. D., Musgaard, M., and Maclean, D. M. (2020). β11-12 linker isomerization governs acid-sensing ion channel desensitization and recovery. *Elife* 9:e51111. doi: 10.7554/eLife.51111

Schuhmacher, L. N., Srivats, S., and Smith, E. S. (2015). Structural domains underlying the activation of acid-sensing ion channel 2a. *Mol. Pharmacol.* 87, 561–571. doi: 10.1124/mol.114.096909

Sherwood, T. W., and Askwith, C. C. (2009). Dynorphin opioid peptides enhance acid-sensing ion channel 1a activity and acidosis-induced neuronal death. *J. Neurosci.* 29, 14371–14380. doi: 10.1523/JNEUROSCI.2186-09.2009

Sibille, J., Dao Duc, K., Holcman, D., and Rouach, N. (2015). The neuroglial potassium cycle during neurotransmission: role of Kir4.1 channels. *PLoS Comput. Biol.* 11:e1004137. doi: 10.1371/journal.pcbi.1004137

Siesjö, B. K., von Hanwehr, R., Nergelius, G., Nevander, G., and Ingvar, M. (1985). Extra- and intracellular pH in the brain during seizures and in the recovery period following the arrest of seizure activity. *J. Cerebral Blood Flow Metabol.* 5, 47–57. doi: 10.1038/jcbfm.1985.7

Sluka, K. A., and Gregory, N. S. (2015). The dichotomized role for acid sensing ion channels in musculoskeletal pain and inflammation. *Neuropharmacology* 94, 58–63. doi: 10.1016/j.neuropharm.2014.12.013

Soto, E., Ortega-Ramirez, A., and Vega, R. (2018). Protons as messengers of intercellular communication in the nervous system. *Front. Cell. Neurosci.* 12:342. doi: 10.3389/fncel.2018.00342

Syková, E., and Svoboda, J. (1990). Extracellular alkaline-acid-alkaline transients in the rat spinal cord evoked by peripheral stimulation. *Brain Res.* 512, 181–189. doi: 10.1016/0006-8993(90)90625-L

Tombaugh, G. C., and Somjen, G. G. (1996). Effects of extracellular pH on voltage-gated Na^+, K^+ and Ca^{2+} currents in isolated rat CA1 neurons. *J. Physiol.* 493, 719–732.

Tominaga, M., Caterina, M. J., Malmberg, A. B., Rosen, T. A., Gilbert, H., Skinner, K., et al. (1998). The cloned capsaicin receptor integrates multiple pain-producing stimuli. *Neuron* 21, 531–543.

Vessey, J. P., Stratis, A. K., Daniels, B. A., Da Silva, N., Jonz, M. G., Lalonde, M. R., et al. (2005). Proton-mediated feedback inhibition of presynaptic calcium channels at the cone photoreceptor synapse. *J. Neurosci.* 25, 4108–4117. doi: 10.1523/JNEUROSCI.5253-04.2005

Vick, J. S., and Askwith, C. C. (2015). ASICs and neuropeptides. *Neuropharmacology* 94, 36–41. doi: 10.1016/j.neuropharm.2014.12.012

Vilin, Y. Y., Peters, C. H., and Ruben, P. C. (2012). Acidosis differentially modulates inactivation in $Na_V1.2$, $Na_V1.4$, and $Na_V1.5$ channels. *Front. Pharmacol.* 3:109. doi: 10.3389/fphar.2012.00109

Na_V

Vukicevic, M., and Kellenberger, S. (2004). Modulatory effects of acid-sensing ion channels on action potential generation in hippocampal neurons. *Am. J. Physiol. Cell. Physiol.* 287, C682–C690. doi: 10.1152/ajpcell.00127.2004

Wemmie, J. A., Askwith, C. C., Lamani, E., Cassell, M. D., Freeman, J. H. Jr., and Welsh, M. J. (2003). Acid-sensing ion channel 1 is localized in brain regions with high synaptic density and contributes to fear conditioning. *J. Neurosci.* 23, 5496–5502.

Wemmie, J. A., Taugher, R. J., and Kreple, C. J. (2013). Acid-sensing ion channels in pain and disease. *Nat. Rev. Neurosci.* 14, 461–471. doi: 10.1038/nrn3529

Xiong, Z. G., Zhu, X. M., Chu, X. P., Minami, M., Hey, J., Wei, W. L., et al. (2004). Neuroprotection in ischemia: Blocking calcium-permeable acid- sensing ion channels. *Cell* 118, 687–698.

Yang, L., and Palmer, L. G. (2014). Ion conduction and selectivity in acid-sensing ion channel 1. *J. Gen. Physiol.* 144, 245–255. doi: 10.1085/jgp.201411220

Conflict of Interest: The authors declare that the research was conducted in the absence of any commercial or financial relationships that could be construed as a potential conflict of interest.

The reviewer, LR, declared a shared committee with one of the authors, SK, at the time of review.

Publisher's Note: All claims expressed in this article are solely those of the authors and do not necessarily represent those of their affiliated organizations, or those of the publisher, the editors and the reviewers. Any product that may be evaluated in this article, or claim that may be made by its manufacturer, is not guaranteed or endorsed by the publisher.

frontiers in Physiology

ORIGINAL RESEARCH
published: 15 October 2021
doi: 10.3389/fphys.2021.750696

Paradoxical Potentiation of Acid-Sensing Ion Channel 3 (ASIC3) by Amiloride *via* Multiple Mechanisms and Sites Within the Channel

*Daniel S. Matasic[1,2], Nicholas Holland[1,3], Mamta Gautam[1,4], David D. Gibbons[1,4], Nobuyoshi Kusama[1,4], Anne M. S. Harding[1,4], Viral S. Shah[2], Peter M. Snyder[1,2,4] and Christopher J. Benson[1,3,4]**

[1] Division of Cardiovascular Medicine, Department of Internal Medicine, University of Iowa, Iowa City, IA, United States, [2] Department of Molecular Physiology and Biophysics, University of Iowa, Iowa City, IA, United States, [3] Department of Neuroscience and Pharmacology, University of Iowa, Iowa City, IA, United States, [4] Iowa City VA Healthcare System, Iowa City, IA, United States

OPEN ACCESS

Edited by:
Enrique Soto,
Meritorious Autonomous University of Puebla, Mexico

Reviewed by:
Laura Bianchi,
University of Miami, United States
Shaohu Sheng,
University of Pittsburgh, United States

***Correspondence:**
Christopher J. Benson
chris-benson@uiowa.edu

Specialty section:
This article was submitted to Membrane Physiology and Membrane Biophysics, a section of the journal Frontiers in Physiology

Received: 31 July 2021
Accepted: 20 September 2021
Published: 15 October 2021

Citation:
Matasic DS, Holland N, Gautam M, Gibbons DD, Kusama N, Harding AMS, Shah VS, Snyder PM and Benson CJ (2021) Paradoxical Potentiation of Acid-Sensing Ion Channel 3 (ASIC3) by Amiloride via Multiple Mechanisms and Sites Within the Channel.
Front. Physiol. 12:750696.
doi: 10.3389/fphys.2021.750696

Acid-Sensing Ion Channels (ASICs) are proton-gated sodium-selective cation channels that have emerged as metabolic and pain sensors in peripheral sensory neurons and contribute to neurotransmission in the CNS. These channels and their related degenerin/epithelial sodium channel (DEG/ENaC) family are often characterized by their sensitivity to amiloride inhibition. However, amiloride can also cause paradoxical potentiation of ASIC currents under certain conditions. Here we characterized and investigated the determinants of paradoxical potentiation by amiloride on ASIC3 channels. While inhibiting currents induced by acidic pH, amiloride potentiated sustained currents at neutral pH activation. These effects were accompanied by alterations in gating properties including (1) an alkaline shift of pH-dependent activation, (2) inhibition of pH-dependent steady-state desensitization (SSD), (3) prolongation of desensitization kinetics, and (4) speeding of recovery from desensitization. Interestingly, extracellular Ca^{2+} was required for paradoxical potentiation and it diminishes the amiloride-induced inhibition of SSD. Site-directed mutagenesis within the extracellular non-proton ligand-sensing domain (E79A, E423A) demonstrated that these residues were critical in mediating the amiloride-induced inhibition of SSD. However, disruption of the purported amiloride binding site (G445C) within the channel pore blunted both the inhibition and potentiation of amiloride. Together, our results suggest that the myriad of modulatory and blocking effects of amiloride are the result of a complex competitive interaction between amiloride, Ca^{2+}, and protons at probably more than one site in the channel.

Keywords: acid-sensing ion channels, channel gating, proton sensing, amiloride, whole-cell patch clamp

INTRODUCTION

Acid-sensing Ion Channels (ASICs) are H^+-gated cation channels within the degenerin/epithelial sodium channel (DEG/ENaC) family (Waldmann et al., 1997b). Primarily expressed in neurons of the central and peripheral nervous systems, ASICs have emerged as important mediators in a variety of physiological processes including pain sensation (Sluka et al., 2009), learning behaviors

(Wemmie et al., 2002), and fear conditioning (Wemmie et al., 2003, 2004). In general, ASICs exhibit a rapid inward sodium current when activated by extracellular protons that subsequently desensitizes over the course of milliseconds to seconds in the continued presence of protons. Of the six homologous subunits identified (*ASIC*1a, -1b, -2a, -2b, -3, -4), ASIC3 is the key component in the peripheral nervous system, governing the excitability of a variety of sensory neurons (Waldmann et al., 1997a; Benson et al., 2002; Hattori et al., 2009; Khataei et al., 2020). In addition to its expression profile, ASIC3-containing channels are unique by generating sustained currents from incomplete desensitization of channels in the continued presence of protons. This sustained current occurs around pH 7 via an overlap between pH-dependent activation and desensitization dose-response curves to generate a "window" current (Yagi et al., 2006).

Amiloride is the established and historical non-selective inhibitor of ASIC channels and thought to block current by physical occlusion at a binding site within the pore. Previous studies established that amiloride block was dependent on the potential difference across the membrane (Adams et al., 1999). As a weak base (pKa = 8.7), the cationic amiloride is thought to gravitate toward the electrical field within the pore, resulting in the block of Na^+ current (Kellenberger and Schild, 2002). At more positive membrane potentials, the positively charged amiloride is driven out of the pore and amiloride-mediated inhibition is diminished. However, in addition to blocking ASIC currents, amiloride was found to paradoxically potentiate sustained currents in both ASIC3-containing channels and "Deg"-mutant ASIC2a-containing channels (Adams et al., 1999; Yagi et al., 2006). Interestingly, this potentiation by amiloride was not influenced by the transmembrane potential difference and therefore amiloride was speculated to be acting at a different site, likely on the extracellular face (Adams et al., 1999). Insights into the potential structural binding sites of amiloride were advanced with the crystallization of the chicken ASIC1 trimeric complex which demonstrated complexity of extracellular subdomains and labeled akin to its "hand" appearance: palm, thumb, finger, β-ball, and knuckle (Jasti et al., 2007; Gonzales et al., 2009). However, the structural-functional relationship of the paradoxical potentiation of amiloride on ASIC3 remains unclear.

Investigation into the underlying mechanisms of amiloride-induced potentiation has been aided by the discovery of synthetic compounds such as 2-guanidine-4-methylquinazoline (GMQ) that have emerged as activators of ASIC3 at neutral pH (Yu et al., 2010; Li et al., 2011). GMQ activates ASIC3 sustained currents by inducing an acidic shift in the pH-dependence of inactivation while provoking an alkaline shift in the pH-dependence of activation (Alijevic and Kellenberger, 2012). These effects, like amiloride-induced potentiation, increase overlap between the pH-dependent curves and thereby generate a larger sustained window current. It is evident amiloride-induced activation shares similarities to the complexities seen with GMQ-induced activation.

Characterization of GMQ on ASIC3 led to the identification of a non-proton ligand-sensing domain involving residues within the lower "palm" extracellular subdomain, E79 and E423, that were critical for amiloride-induced and GMQ-induced sustained currents (Yu et al., 2010; Li et al., 2011). However, subsequent studies found that disruption of these residues did not completely abolish the effect of GMQ to alter pH-dependent gating of ASICs (Alijevic and Kellenberger, 2012). Together, these studies suggest that the purported non-proton ligand-sensing domain may not be the sole site underlying these modulatory effects. As further evidence of a more complex mechanism, studies involving chimeras of ASIC1a and ASIC3 demonstrated involvement of both extracellular and transmembrane/cytosolic domains in amiloride-induced activation of ASIC3 (Besson et al., 2017). Here in these studies, we further characterize the paradoxical potentiation of ASIC3 by amiloride and investigate its determinants.

MATERIALS AND METHODS

DNA Constructs

Rat ASIC3 in pMT3 vectors were cloned as previously described (Eshcol et al., 2008). Point mutations were generated by site-directed mutagenesis using the QuikChange kit (Stratagene, La Jolla, CA) and sequenced at the Iowa Institute of Human Genomics facility at the University of Iowa. Green fluorescent protein (GFP; pGreen Lantern) was obtained from Life Technologies (Thermo Fisher Scientific, Carlsbad, CA).

Cell Culture and Transfection

Chinese Hamster Ovarian (CHO-K1) cells (ATCC, Manassas, Virginia) were cultured in F12 medium (GIBCO, Carlsbad, CA) containing 10% fetal bovine serum (FBS) and 1% penicillin-streptomycin. Cells were cultured at 37°C, 5% CO_2, and plated at approximately 10% confluency into 35 mm dishes for electrophysiological studies. Cells were transfected using the lipid transfection reagent Transfast (Promega, Madison, WI) following manufacturer's instructions. Wildtype rASIC3 cDNA (0.18 μg/1.5 ml) was transfected with rASIC3 G445C (0.162 μg/1.5 ml) at a 1:10 ratio. All cells were transfected with GFP (0.330 μg/1.5 ml) to assist with identification of transfected cells.

Whole-Cell Patch Clamp Electrophysiology

Whole-cell patch clamp (−70 mV) recordings in CHO-K1 cells were performed at room temperature with an Axopatch 200B amplifier (Axon Instruments, Foster City, CA). Traces were acquired and analyzed with PatchMaster/FitMaster (HEKA Electronics, Lambrecht, Germany) or pClamp8 (Molecular Devices, San Jose, CA) and Prism (GraphPad Software, La Jolla, CA). Capacitive currents were compensated for and recorded for normalization of peak current amplitudes. Glass electrophysiology pipettes (2–4 MΩ) for most experiments contained 100 KCl, 10 EGTA, 40 HEPES, and 5 $MgCl_2$ (mM), pH 7.4 with KOH. For experiments involving positive voltages, NaCl was used in place of KCl. External solutions typically contained 120 NaCl, 5 KCl, 1 $MgCl_2$, 2 $CaCl_2$, 10

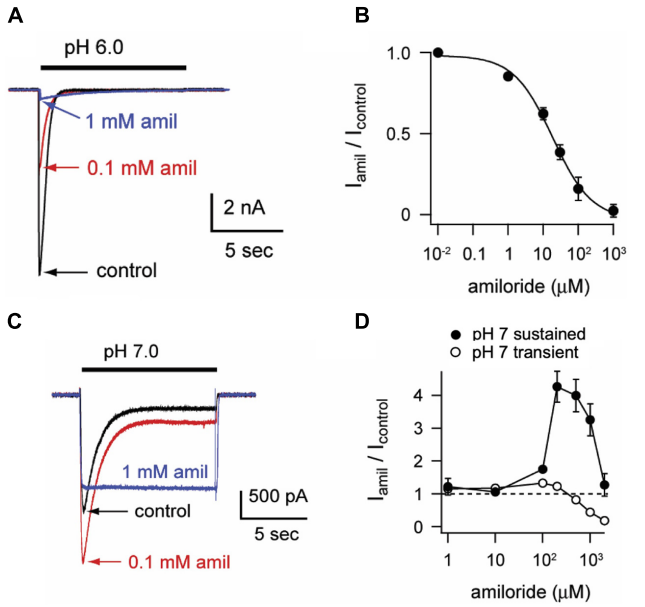

FIGURE 1 | Amiloride paradoxically inhibits or potentiates ASIC3. **(A)** Overlay of representative currents recorded from CHO cells transfected with ASIC3 evoked by stepping from pH 8 (containing no amiloride) to pH 6 in the absence (control) or presence of 100 μM or 1 mM amiloride. **(B)** Dose-response curve for amiloride inhibition of pH 6-evoked currents. Line is fit of Hill equation (IC_{50} = 18.6 μM; n = 5–8 for each data point). **(C)** Overlay of pH-7 evoked currents in absence or presence of indicated amiloride concentrations. **(D)** Dose-responses of amiloride on the peak (transient) and sustained (measured at the end of 10 s pH 7 application) components of pH 7-evoked currents (n = 8–11 for each data point). Note that data points above the dashed line represent amiloride potentiation and those below represent inhibition.

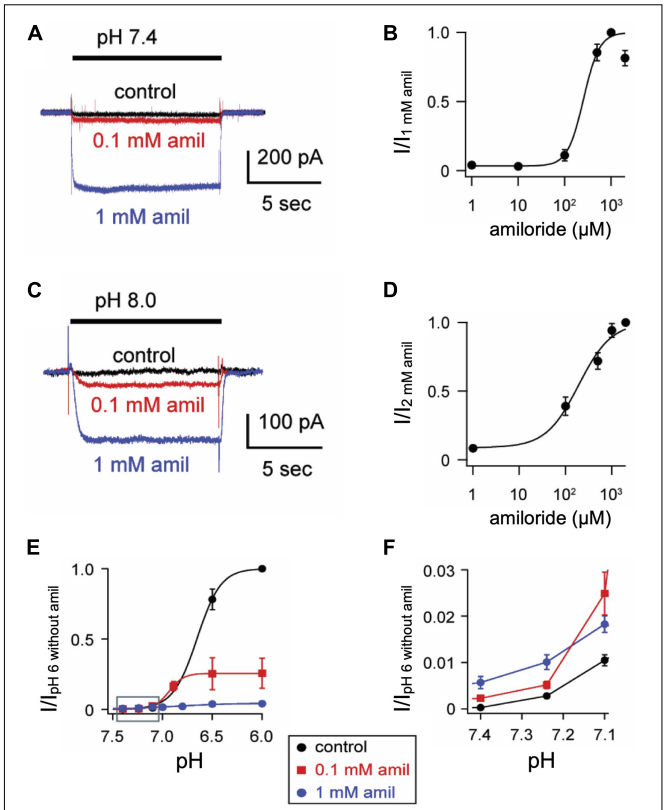

FIGURE 2 | Amiloride increases the pH sensitivity of activation of ASIC3. **(A)** Representative superimposed ASIC3 currents evoked from a control solution of pH 8.0 (no amiloride) to pH 7.4 (containing the indicated amiloride concentrations at 0, 0.1 mM, and 1 mM). **(B)** Dose-response curve for amiloride on pH 7.4-evoked currents (n = 7–11 for each data point). Line is fit of Hill equation (EC_{50} = 255 μM). **(C)** Representative superimposed currents from a control solution of pH 8.0 (no amiloride) to pH 8.0 (containing the indicated amiloride concentrations). **(D)** Dose-response curve for amiloride on pH 8.0-evoked currents (n = 8). Line is fit of Hill equation (EC_{50} = 193 μM). **(E)** pH dose-response curves for activation in 0 mM (control), 0.1, and 1 mM amiloride. Data are acquired by stepping from pH 8.0 (with 0 mM amiloride) to the indicated test solutions (containing the indicated amiloride concentrations) and are normalized to the peak currents evoked by pH 6.0 in no amiloride (n = 4–9 for each data point). Lines are fits of Hill equations (pH_{50} = 6.7, 6.9, and 6.8 for 0, 0.1, and 1 mM amiloride, respectively). Note the error bars are often smaller than the markers. **(F)** A graph of the boxed area in **(E)** with expanded axes demonstrating the potentiating effect of amiloride at the foot of the pH dose-response curves (one-way ANOVAs at pH 7.40 and 7.24 found differences between groups ($p < 0.01$), with Dunnit's multiple comparisons showing $p < 0.01$ for amiloride 1 mM vs. control at pH 7.40 and 7.24).

HEPES, and 10 MES (mM), pH adjusted to target by TMA-OH and osmolarity was balanced with TMA-Cl. Ca^{2+} levels in external solutions were modified for some experiments as noted in results. Nominal divalent solutions contained no added Ca^{2+} or Mg^{2+}. Rapid extracellular solution exchanges were made using a computer-driven solenoid valve system. Kinetics of desensitization were fit with single exponential equations, and time constants (τ) reported. pH-dependent activation and steady-state desensitization (SSD) curves were fit to the Hill equation using GraphPad Prism. Data are means ± SEM. Statistical differences were assessed as described in figure legends using GraphPad Prism.

RESULTS

Inhibition and Potentiation of Acid-Sensing Ion Channel 3 Currents by Amiloride

To characterize the paradoxical effects of amiloride, we studied pH-evoked currents from ASIC3 channels expressed in CHO cells. At a maximally activating pH 6, amiloride caused a classic dose-dependent block (IC_{50} = 18.6 μM, **Figures 1A,B**). However, at a more modest pH 7 activation, a dose-dependent paradoxical stimulatory effect was observed (**Figure 1C**). The pH 7-evoked currents demonstrate two components: a transient component that undergoes desensitization (like the pH 6-evoked currents) and a sustained component due to an overlap of the activation and SSD pH-dependent dose-response curves in the pH 7 range (Yagi et al., 2006). Paradoxical potentiation of both the transient ($p < 0.02$ by paired student's t-test) and sustained ($p < 0.02$ by paired student's t-test) pH 7-evoked currents is seen with 0.1 mM amiloride. However, at higher doses

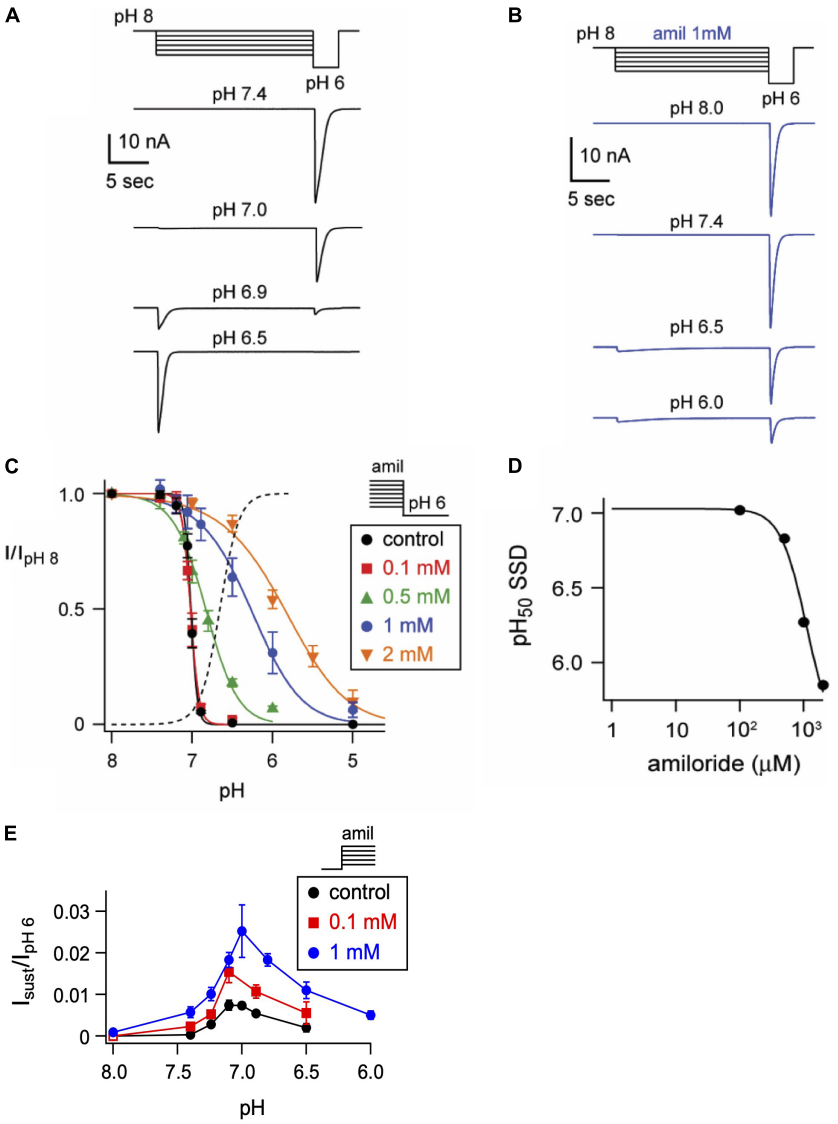

FIGURE 3 | Amiloride inhibits the pH-dependent steady-state desensitization of ASIC3. **(A)** Representative ASIC3 currents evoked by stepping from pH 8 to the indicated desensitizing pH application for 20 s, following by a pH 6 test application. **(B)** Currents were recorded as in *A*, except the desensitizing 20 s pH solutions contained 1 mM amiloride. **(C)** pH dose-response curves for steady-state desensitization (SSD) recorded as in *A,* in control (no amiloride) and the indicated amiloride concentration solutions normalized to the currents evoked by stepping from pH 8 to pH 6 (n = 3–10 per data point). Lines are fits of the Hill equation (pH_{50} = 7.0, 7.0, 6.8, 6.3, and 5.9 for 0, 0.1, 0.5, 1, and 2 mM amiloride, respectively). Dashed line is fit of Hill equation for dose-response of pH activation in absence of amiloride from **Figure 2E**. **(D)** A plot of the amiloride dose-response on the pH_{50} values of steady-state desensitization measured from data in *C*. Line is fit of Hill equation (EC_{50} = 1.1 mM). **(E)** pH dose-response for activation of sustained currents (measured at the end of 10 s pH application) in 0 mM (control), 0.1, and 1 mM amiloride. Data are acquired by stepping from pH 8.0 (with 0 mM amiloride) to the indicated test solutions (containing the indicated amiloride concentrations) and are normalized to the peak currents (transient) evoked by pH 6.0 in no amiloride (n = 4–10 per data point).

of amiloride (1 mM), the transient component is blocked but the sustained component is potentiated. Interestingly, amiloride increasingly potentiated the pH 7.0-evoked sustained current up to a concentration of 200 μM, but current was diminished at higher doses of amiloride (**Figure 1D**). Even at neutral pH (7.4) and more alkaline pH (8.0), amiloride stimulates a sustained current in a dose-dependent manner (**Figures 2A–D**). However, at pH 9.0 amiloride was unable to evoke current (data not shown), implying that amiloride potentiates pH-evoked currents, rather than functioning as a channel activator on its own. Note that the doses of amiloride required for potentiation (**Figures 1D**, **2B,D**) all indicate an IC_{50} of greater than 100 μM, which is higher than the dose of amiloride required to block current (IC_{50} = 18.6 μM, **Figure 1B**). pH activation curves in the absence and presence of amiloride further demonstrate these paradoxical effects (**Figure 2E**); at more acidic pH values that maximally activate ASIC3, amiloride blocks current. However, at the foot of the activation curve, there is

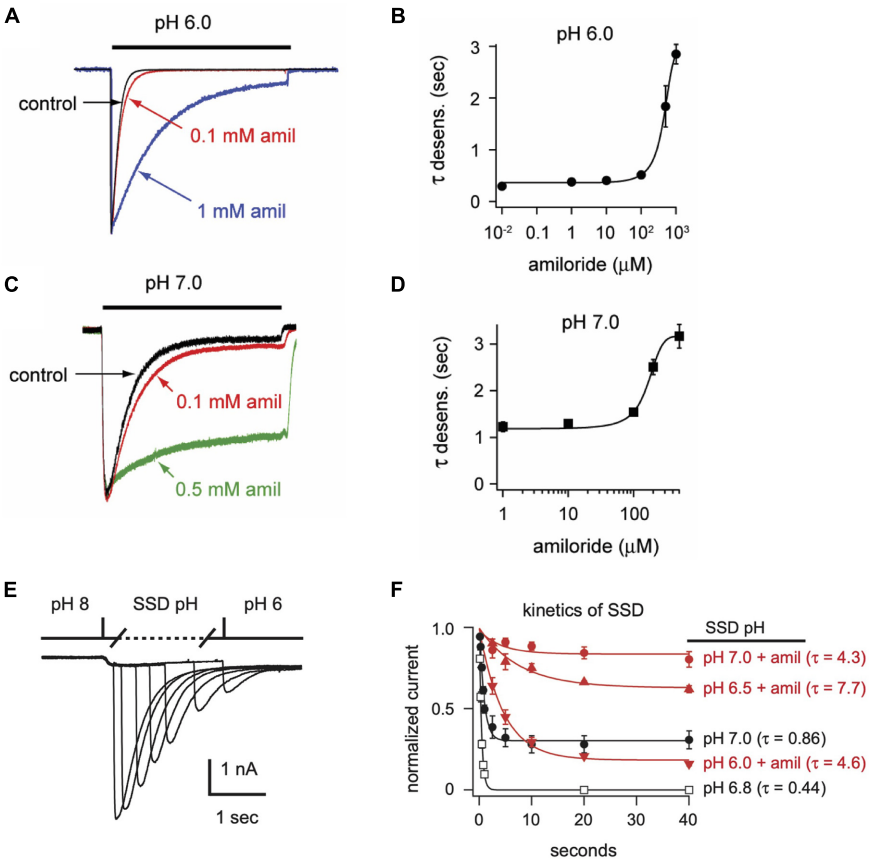

FIGURE 4 | Amiloride slows the rate of desensitization of ASIC3. Overlays of **(A)** pH 6- or **(C)** pH 7-evoked normalized currents in the absence (control) or presence of amiloride at the indicated concentrations. Acidic pH was applied for 10 s. Amplitudes of pH 6-evoked currents (nA): control 18.6, 0.1 mM 5.66, 1 mM 0.70; pH 7-evoked currents (nA): control 1.05, 0.1 mM 1.40, 0.5 mM 0.78. **(B,D)** Are the mean time constants of desensitization (τ) as measured from single exponential fits to the falling phase of pH 6- **(B)** and pH 7-evoked currents **(D)** in varying concentrations of amiloride (n = 4–8 per data point). Lines are sigmoid fits. **(E)** An overlay of currents evoked by stepping from pH 8 to pH 7 solution for variable time periods (see X axis of *F*), following by a pH 6 test application. This protocol measures the time to steady-state desensitization (SSD). **(F)** Mean data of the time to SSD as collected in *E* for currents that underwent SSD in the indicated pH solutions labeled at the right of each curve (n = 3–10 per data point). Solutions with amiloride (red) contained 1 mM amiloride. Lines are fits of single exponentials of the means and time constants (τ) are shown.

a shift to the left such that pH-evoked currents are potentiated (**Figure 2F**). In summary, as previously described (Yagi et al., 2006; Li et al., 2011), amiloride either blocks or potentiates ASIC3 current dependent on both the activating pH and the dose of amiloride.

Amiloride Alters pH-Dependent Steady-State Desensitization

One mechanism by which amiloride potentiates ASIC acid-evoked currents is by inhibiting pH-dependent SSD (Besson et al., 2017). To further explore the effect of amiloride on SSD, cells were conditioned with extracellular solutions at desensitizing pH values (8.0–5.0) for 20 s, followed by a pH 6 test application (**Figures 3A,B**). When added to the conditioning solution, SSD was shifted to the right by amiloride at doses greater than 0.1 mM (**Figure 2C**) in a dose-dependent manner (pH_{50} values of SSD in varying doses of amiloride show a $IC_{50} \geq 1.1$ mM amiloride; **Figure 3D**).

ASIC3 is unique among ASIC channels in that there exists an overlap between the pH range of activation and SSD, thus creating a sustained "window current" whereby channels are activated, but incompletely desensitized. Consistent with the shift to the left at the foot of the activation curves (**Figure 2F**), and the shift to right of the SSD curves (**Figure 3C**), we found that amiloride generated larger sustained currents in this pH range (**Figure 3E**).

Amiloride Slows the Rate of Desensitization and Facilitates Recovery From Desensitization

In addition to differentially influencing current amplitudes, amiloride dose-dependently prolongs the desensitization of ASIC3 channels. Overlaying of pH 6-evoked currents

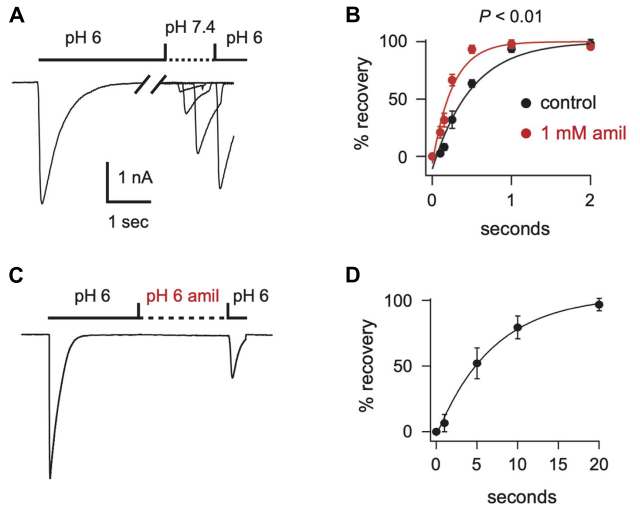

FIGURE 5 | Amiloride increases the rate of recovery from desensitization of ASIC3. **(A)** Overlay of current traces showing recovery from desensitization. Current was desensitized with a 7 s application of pH 6 (only the first 2.5 s is shown). Cells were then exposed to pH 7.4 solution (containing 0 or 1 mM amiloride) for the indicated times (see *x* axis in **B**) before they were stimulated again with pH 6. Recovery is the percentage of current evoked by the second pH 6 application compared with the first. **(B)** Mean recovery data as collected with either no amiloride (control) or 1 mM amiloride in the pH 7.4 solution (n = 3–6 for each point). Lines are fits of single exponentials of the means. Students t-test of the τ's calculated from the fits of the individual cells reveals that amiloride increased the rate of recovery ($p < 0.01$; n = 6). **(C)** Current evoked by a 10 s application of pH 6 without amiloride, followed by an exposure to a pH 6 solution containing 1 mM amiloride for variable times (see *x* axis in **D**), followed by a second pH 6 application without amiloride. After a 20 s exposure to the pH 6 solution with amiloride the ratio of the current evoked by the second pH 6 application compared to the first pH 6 application was 0.23 ± 0.04 (n = 8). **(D)** Mean normalized recovery data as collected in **(C)**. Data was normalized to the percentage of recovery at 20 s (n = 3–6). Line is fit of single exponential of the means (τ = 6.98 s).

with normalized amplitudes (**Figure 4A**) demonstrates slowing of the rate of desensitization in a dose-dependent manner (**Figure 4B**). Similar slowing of desensitization by amiloride was also observed with pH-7 evoked currents (**Figures 4C,D**).

We also tested if amiloride affects the kinetics of SSD. To measure time to SSD, we stepped from pH 8 to a desensitizing pH (6.0–7.0) for varying times, followed by a pH 6 test application (**Figure 4E**). Time to SSD was pH-dependent (faster at lower pH) and was significantly prolonged in the presence of 1 mM amiloride at all pH values tested (**Figure 4F**).

After acid-evoked desensitization, ASIC channels require exposure to a more alkaline pH for some time before they can again be activated by acidic solution. We found that amiloride significantly increased the rate of recovery from desensitization of ASIC3 currents (**Figures 5A,B**). Moreover, amiloride caused ASIC3 channels to recover from desensitization even in the absence of exposure to an alkaline pH. The addition of amiloride at pH 6 to a completely desensitized pH 6-evoked current caused 23% recovery from desensitization within 20 s (**Figures 5C,D**).

Extracellular Ca^{2+} Is Required for Amiloride Potentiation, While Inhibiting the Effects of Amiloride on Steady-State Desensitization

Divalent cations such as Ca^{2+} have previously been shown to stabilize ASIC channels in the closed state and that removal of extracellular Ca^{2+} opens ASIC3 channels (Immke and McCleskey, 2001; Babini et al., 2002; Immke and McCleskey, 2003). Similarly, we found that extracellular solutions without added Ca^{2+} or Mg^{2+} (nominal divalents) generated large ASIC3 currents at neutral and even alkaline pH solutions (**Figure 6A**). However, whereas amiloride potentiated currents evoked at pH 7.4 and 8.0 in the standard extracellular solution containing 2 mM Ca^{2+} and 1 mM Mg^{2+} (**Figures 2C–F**), amiloride inhibited currents in the absence of added divalents (**Figure 6A**), implying that extracellular divalent cations are required for amiloride potentiation.

Next, we tested if extracellular Ca^{2+} alters the effect of amiloride to inhibit ASIC3 pH-dependent SSD. By reducing extracellular Ca^{2+} to 100 μM, we found a significant shift to the left in the pH-dependence of SSD (**Figure 6B**). However, the addition of 1 mM amiloride to the 100 μM Ca^{2+} solution caused an even greater shift to the right than in the presence of 2 mM Ca^{2+}. Conversely, increasing extracellular Ca^{2+} to 10 mM caused a shift to the right in SSD compared to that in 2 mM Ca^{2+}, and the addition of 1 mM amiloride produced only a slight further shift to the right. Thus, these data indicate that extracellular Ca^{2+} inhibits, and possibly competes, with the effect of amiloride to inhibit SSD of ASIC3.

Amiloride Effects Are Voltage-Dependent and Others Are Voltage-Independent

Previous research on mutant ASIC2 channels showed that the blocking effects of amiloride were voltage-dependent, likely due to the influence of the membrane electrical field on the positively charged amiloride within the pore (Adams et al., 1999). We further tested the voltage-dependence of amiloride blocking and modulatory effects on ASIC3 (**Figure 7**). On pH 6-evoked currents, amiloride has a significant blocking effect at negative membrane potentials that lessens with increasing positive membrane potentials (**Figures 7A–C**). Although the blocking effect of amiloride was voltage-dependent, the prolongation of desensitization of ASIC3 by amiloride was not affected by voltage (**Figures 7D,E**). To assess the voltage-dependence of amiloride-mediated potentiation, the ratio of pH 7- to pH 6-evoked currents in the presence and absence of amiloride (1 mM) was examined to normalize against the blocking effects of amiloride (**Figures 7F,G**). Amiloride increased the pH 7- to pH 6-evoked current ratio equally across the voltage-gradient by approximately twenty-fold. This implies that the

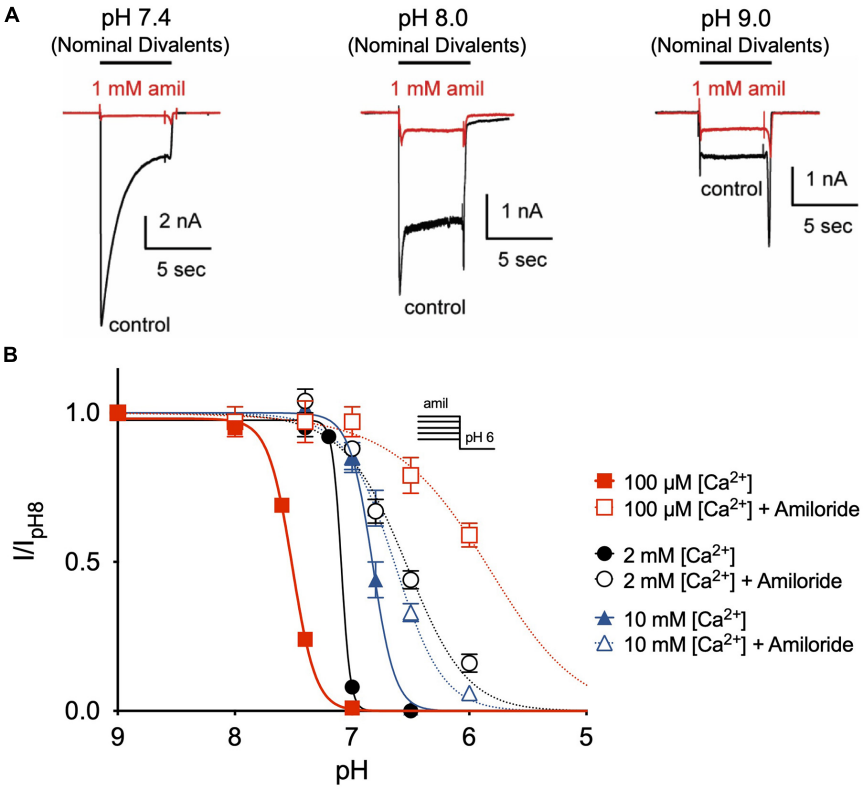

FIGURE 6 | Amiloride potentiation requires divalent cations. **(A)** Overlay of representative ASIC3 currents evoked by stepping from pH 8 (containing 2 mM Ca^{2+} and 1 mM Mg^{2+} and no amiloride) to solutions without added Ca^{2+} and Mg^{2+} (nominal divalents) at pH 7.4, 8.0, and 9.0 in the absence (control) or presence of 1 mM amiloride. **(B)** pH dose-response curves for steady-state desensitization (SSD) recorded in either 100 µM, 2 mM, or 10 mM extracellular Ca^{2+} (no added Mg^{2+}) in the desensitizing solutions in the absence of amiloride (pH_{50} = 7.51, 7.09, and 6.82, respectively) and in the presence of 1 mM amiloride (pH_{50} = 5.86, 6.57, and 6.64, respectively; *n* = 3–8 for each data point).

potentiating effects of amiloride to increase pH 7-evoked current is independent of voltage.

The Non-proton Ligand Sensing Domain Is Required for Shifts in Steady-State Desensitization by Amiloride

Disruption of a purported non-proton ligand sensing domain (E79 and E423) was previously shown to significantly blunt the stimulatory effect of amiloride on ASIC3 currents (Li et al., 2011). Similarly, we found that both E79A and E423A ASIC3 mutants shifted the pH-dependence of SSD toward more alkaline pH (E79A pH_{50} = 7.95, E423A pH_{50} = 7.53) when compared to wildtype (pH_{50} = 7.01), and completely mitigated the effect of amiloride on SSD (**Figure 8A**). Both E79A and E423A ASIC3 mutants displayed the same degree of potency of amiloride block of pH 6-evoked currents (data not shown). On the other hand, E79A did not fully abolish potentiation by amiloride. Due to a significant alkaline shift in the activation curve (Alijevic and Kellenberger, 2012), E79A channels generated small transient currents at pH 7.4, and current amplitude was increased in the presence of 1 mM amiloride (**Figures 8B,C**).

Disruption of the Amiloride Pore Binding Site Diminishes Potentiating Effects

The capacity to fully characterize the potentiating effect of amiloride on ASIC3 is hindered by its simultaneous inhibition of the channel. Thus, we hypothesized that mutation of a purported amiloride blocking site within the second transmembrane-spanning domain that sits just above the pore (G445) would unmask the full potentiating effect of amiloride on ASIC3 (Schild et al., 1997; Alijevic and Kellenberger, 2012). Expressed alone, G445C generated only small currents requiring very acidic pH for activation (pH < 5.0). Therefore, we co-expressed G445C with wildtype ASIC3 at a 10:1 ratio, respectively, and found that the resultant pH-evoked currents had properties different than those generated when either G445C or wildtype ASIC3 were expressed alone, indicating the formation of heteromultimeric channels. As anticipated, G445C mutation partially blunted the inhibitory action of amiloride on ASIC3 currents when compared to wildtype ASIC3 channels (G445C IC_{50} = 17.3 µM vs. Wildtype IC_{50} = 9.47 µM, **Figure 9A**). Unexpectedly, G445C also blunted the potentiating effects of amiloride on sustained current observed at pH 6.8 (**Figure 9B**). Furthermore, G445C abrogated the effects of amiloride to slow the rate of desensitization (**Figure 9C**), and the shift in pH-dependent SSD

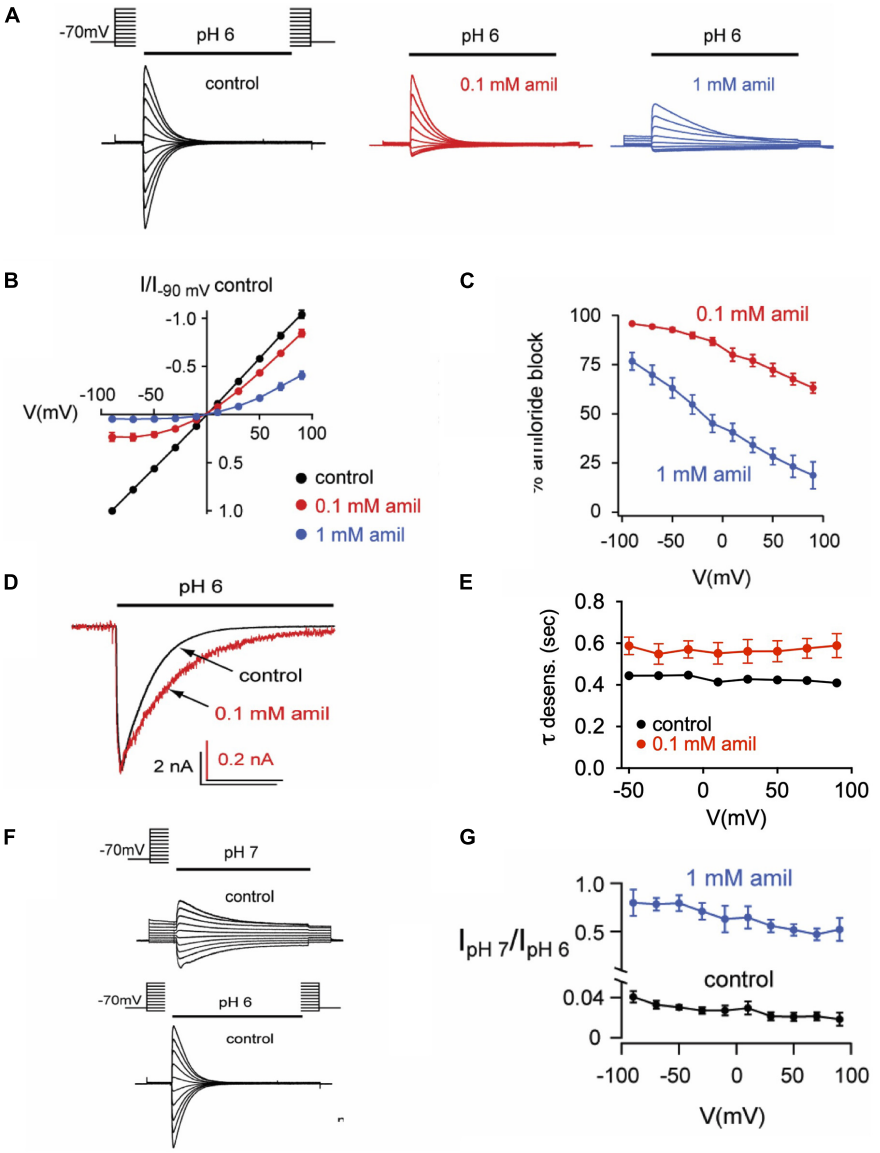

FIGURE 7 | Effects of amiloride on ASIC3 are voltage-dependent and voltage-independent. **(A)** Overlays of pH 6-evoked ASIC3 currents recorded during steps to various membrane potentials (−90 to + 90 mV). The test solution (pH 6) contained 0 (control), 0.1, or 1 mM amiloride. The intracellular (pipette) and extracellular solutions contained symmetrical NaCl concentrations. **(B)** Current vs. voltage curves for the data in *A*. Data are normalized to the currents evoked at -90 mV in no amiloride (n = 17) vs. 0.1 mM (n = 7) and 1 mM (n = 10) amiloride. **(C)** Mean percentage of pH 6-evoked current block by 0.1 mM (n = 10) and 1 mM (n = 6) amiloride at the indicated voltages. **(D)** Overlays of pH 6-evoked normalized currents in the absence (control) or presence of 0.1 mM amiloride. **(E)** Mean time constants of desensitization (τ) recorded in 0 (n = 21) or 0.1 mM (n = 7) amiloride at the indicated voltages. **(F)** Overlays of pH 7- and pH 6-evoked currents recorded during steps to various membrane potentials (−90 to + *90 mV*). **(G)** Mean ratios of pH 7- to pH 6-evoked current amplitudes recorded in test solutions containing 0 mM (n = 3) or 1 mM (n = 3) amiloride at the indicated voltages.

(**Figure 9D**). To further investigate the role of the pore binding site in mediating the effects of amiloride, SSD measurements were carried at a positive voltage (+50 mV) to generate outward pH-evoked currents. Interestingly, under positive voltage, the effect of amiloride on SSD was abrogated in both wildtype and G445C channels (**Figure 9E**), thereby suggesting that the shift in SSD requires an amiloride binding site within the pore that is exposed to changes in the membrane electrical field. Together, these data demonstrate that the purported amiloride binding site within the pore contributes to both inhibition and potentiation by amiloride.

DISCUSSION

Amiloride is the classic small-molecule blocker of ASICs. It has been used to probe the structure-function and gating mechanisms of ASICs and has served as a *in vivo* tool to explore

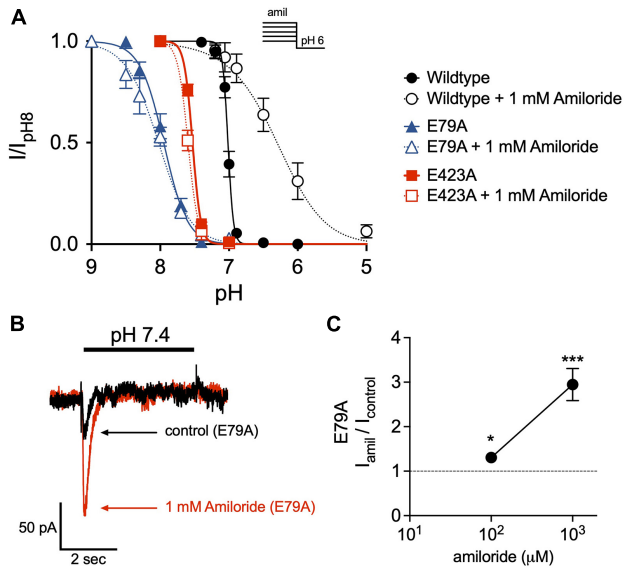

FIGURE 8 | The non-proton ligand-sensing domain is required for the amiloride-induced acidic shift in steady-state desensitization. **(A)** pH dose-response curves for steady-state desensitization (SSD) in ASIC3 wildtype, E79A, and E423A under control conditions (no amiloride) and with the 1 mM amiloride concentration solution normalized to the currents evoked by stepping from pH 8 to pH 6 (n = 4–8 for each point). Lines are fits of the Hill equation (pH_{50} = 7.01, 7.95, and 7.53 under control conditions for wildtype, E79A, E423A, respectively; with 1 mM amiloride pH_{50} = 6.31, 8.02, and 7.59) **(B)** Representative superimposed E79A pH 7.4-evoked currents in the absence and presence of 1 mM amiloride. **(C)** Dose-response effect of amiloride 0.1 and 1 mM on pH 7.4-evoked currents in ASIC3 E79A (n = 8; $^*p$ = 0.02 0.1 mM vs. control; $^{***}p < 0.001$ 1 mM vs. control, one-way ANOVA).

the physiological role of ASICs. And yet, recent studies have shown complex actions of amiloride on ASICs—including the capacity to potentiate pH-evoked current—which complicates our understanding of amiloride as a pure channel blocker. Here, we further explored the actions of amiloride on one of the ASIC isoforms, ASIC3. We confirmed that amiloride can both inhibit and potentiate ASIC3 pH-evoked current, dependent upon both the concentration of amiloride and the pH of activating solution. Much of the potentiating capacity of amiloride occurs *via* an alkaline shift in the pH dose-response of activation, and an acidic shift in the dose-response of SSD, which generates larger sustained "window" currents at the "foot" of the activation pH range. The variable effects of amiloride on ASIC3 occurred at varying potencies, varying voltage-dependency, and mutation of different sites within the channel variably disrupted the effects of amiloride—all suggesting that amiloride exerts its effects through multiple domains within the channel, and perhaps binds to multiple different sites. In particular, disruption of the purported blocking site within the pore not only abrogated inhibition, but also diminished the potentiating effects of amiloride. Moreover, we found the acidic shift of SSD induced by amiloride was voltage-dependent, suggesting a site with the transmembrane region is required for the potentiating effects of amiloride.

Amiloride Binds to Acid-Sensing Ion Channel 3 in Multiple Different Conformational States and Modulates Several Different Gating Transitions

In the simplest of gating models, ASICs transition from a closed to an open state upon exposure to H^+ (**Figure 10A**). From the open state, channels rapidly transition into a closed desensitized state depending on the pH of the activation solution. At less acidic non-activating H^+ concentrations, channels may also transition directly from a closed to a desensitized state, as measured with SSD protocols (**Figure 3**). While this scheme in **Figure 10A** does not account for multiple closed, open, and desensitized states, it serves our purpose to highlight the multiple effects of amiloride on ASIC3 gating. Much of the potentiating effects of amiloride on ASIC3 can be described by a destabilization of the desensitized state (**Figures 10A,B**). Amiloride inhibited the pH-dependence of SSD (**Figure 3**), slowed the rate of SSD (**Figures 4E,F**), and slowed the rate of desensitization from the open state (**Figures 4A–D**). Previous work did not find an effect of amiloride on the rate of ASIC3 open-channel desensitization (Besson et al., 2017)—the reason for the discrepancy could be due to different channel constructs or different cell expression systems. The effect of amiloride to destabilize the desensitized state is perhaps best illustrated by amiloride's effect on recovery from desensitization. Typically, this process requires exposure to an alkaline pH (presumably to remove H^+ bound to the channel), however recovery occurred in 1 mM amiloride even when pH remained at 6.0 (**Figures 5C,D**). Additionally, amiloride increased the rate of recovery from desensitization (**Figure 5B**).

The slowing of desensitization from either the open or closed states implies that amiloride causes an increase in the energy barrier to transition to the desensitized state (**Figure 10B**). The inhibition of pH-dependent SSD, and the potentiation of recovery from desensitization, imply that amiloride also generates an increase in the free energy (destabilization) of the desensitized state relative to the open and closed states.

As previously reported, amiloride also probably potentiates the pH-dependent activation of ASIC3 (Besson et al., 2017). We found that amiloride generated currents at pH solutions of pH 7.4 and 8.0 (ranges that do not generate ASIC3 current in the absence of amiloride), suggesting that amiloride caused an alkaline shift in pH activation. However, it should be noted that the pH dose-response of activation in the presence of amiloride cannot be accurately assessed due to: (1) amiloride inhibition of currents activated by more acidic pH solutions leads to an overestimation of pH sensitivity, and (2) depending on the rates of desensitization and activation, an alkaline shift in SSD could alone account for a shift in the foot of the pH-dose response of activation (Grunder and Pusch, 2015).

Amiloride likely binds to ASIC3 in all conformational states. Inhibition of SSD and slowing the rate of

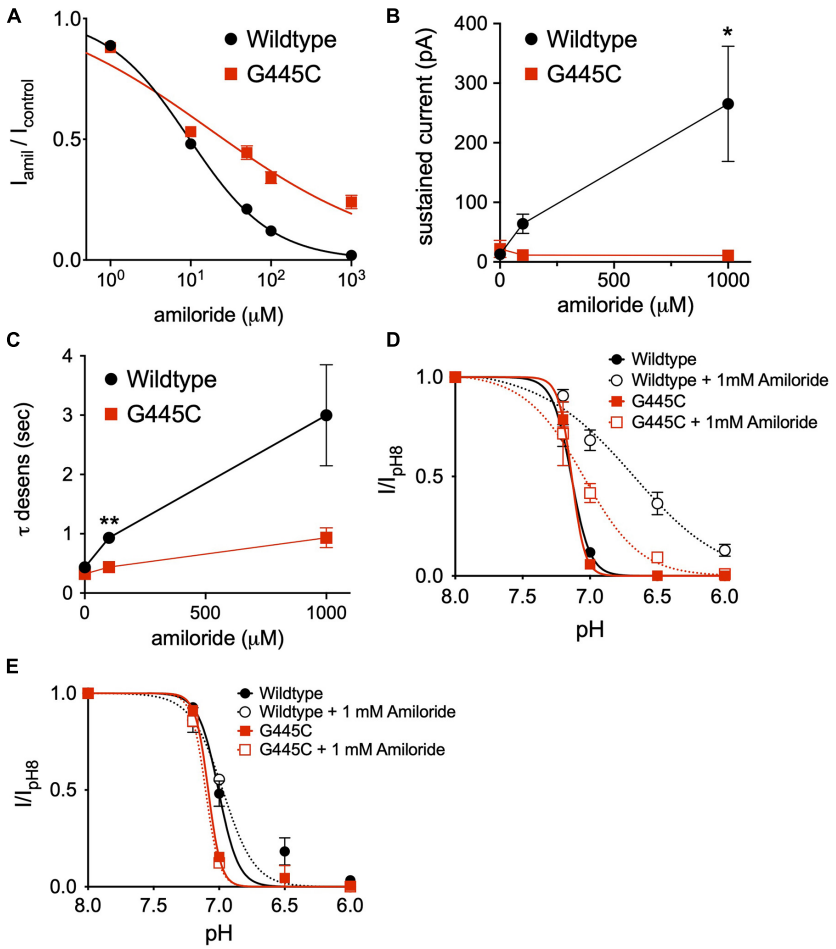

FIGURE 9 | An amiloride binding site within the pore of ASIC3 contributes to paradoxical block and potentiation. **(A)** Dose-response curves for amiloride inhibition of pH 6-evoked currents on ASIC3 wildtype and G445C mutant channels. Lines are fits of Hill equation (IC_{50} = 9.47 μM (wildtype, n = 10) and 17.3 μM (G445C, n = 9; $p < 0.001$ two-way ANOVA) **(B)** Mean pH 6.8-evoked sustained current amplitudes measured from ASIC3 wildtype (n = 14) or G445C mutant channels (n = 5) in 0, 0.1, 1 mM amiloride (p = 0.13 two-way ANOVA with multiple comparisons: *p = 0.03 wildtype vs. G445C at 1 mM amiloride). **(C)** Mean time constants of desensitization (τ) of pH 6.8-evoked currents measured from ASIC3 wildtype (n = 18) or G445C mutant channels (n = 14) in 0, 100, 1,000 μM amiloride ($p < 0.001$ two-way ANOVA with Bonferroni *post hoc* showing **$p < 0.001$ for wildtype vs. G445C at 100 **(D)** pH dose-response curves for steady-state desensitization (SSD) in ASIC3 wildtype (n = 10) or G445C mutant channels (n = 5–12) recorded at -70 mV holding potential. Lines are fits of the Hill equation [pH_{50} = 7.13 (wildtype), 6.70 (wildtype + 1 mM Amiloride), 7.13 (G445C), 7.05 (G445C + 1 mM Amiloride)] **(E)** pH dose-response curves for SSD in ASIC3 wildtype (n = 10) or G445C mutant channels (n = 2) recorded at + 50 mV holding potential. Lines are fits of the Hill equation [pH_{50} = 7.08 (wildtype), 7.00 (wildtype + 1 mM Amiloride), 7.10 (G445C), 6.97 (G445C + 1 mM Amiloride)].

open-channel desensitization implies that amiloride binds to both the closed and open states, respectively. Amiloride can also bind to the desensitized state since it facilitates recovery from desensitization. However, which sites within the channel that bind amiloride to generate these various functional effects is less clear.

Amiloride Competes With Extracellular Ca^{2+} to Modulate Acid-Sensing Ion Channel 3

Among ASIC isoforms, ASIC3 has the unique capacity to be activated at neutral pH by diminished extracellular Ca^{2+} (Immke and McCleskey, 2003; Paukert et al., 2004; Zhang et al., 2006). Changes in extracellular Ca^{2+} also cause significant shifts in pH-dependent activation and recovery from desensitization (Immke and McCleskey, 2001, 2003). Here we found that in the absence of extracellular Ca^{2+}, amiloride did not potentiate ASIC3 and only blocked current. Additionally, changes in extracellular Ca^{2+} also generated large shifts in the pH dose-response of SSD, demonstrating that Ca^{2+}, like amiloride, inhibits pH-dependent SSD. Moreover, we show that amiloride and Ca^{2+} compete to inhibit SSD, suggesting that they do so through a common mechanism, and perhaps a common binding site. Interestingly, Ca^{2+} also competes with the neuropeptide FMRFamide to inhibit pH-dependent SSD of ASIC1b/3 heteromeric channels (Chen et al., 2006). The Gründer group has characterized the blocking

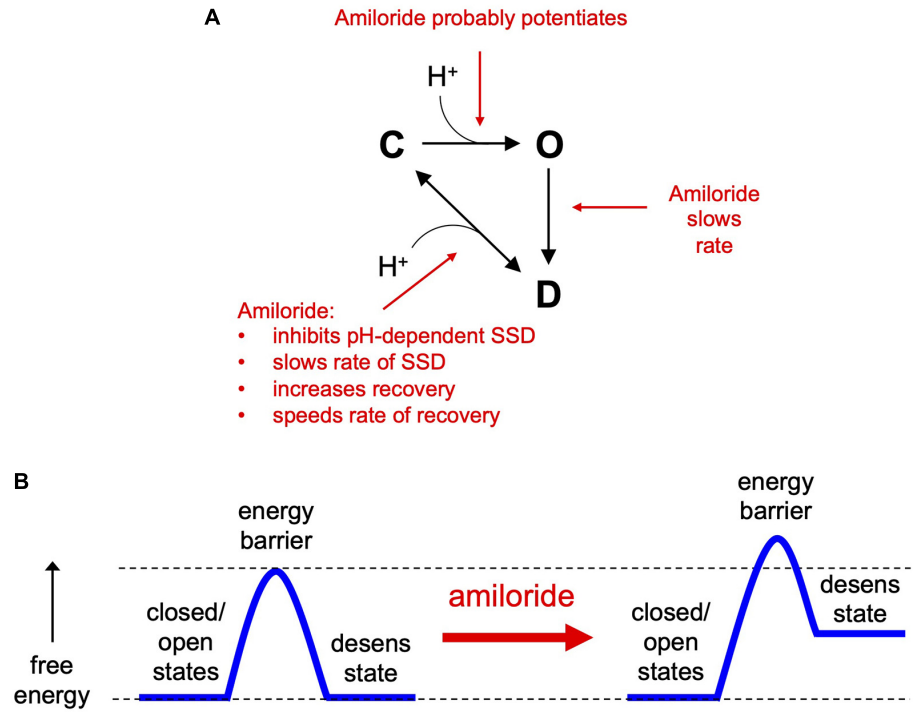

FIGURE 10 | The effects of amiloride on ASIC3 gating properties. **(A)** A simple state model highlighting the various effects of amiloride on ASIC3 gating [closed (C), open (O), and desensitized (D) states]. **(B)** An energy barrier model demonstrating how amiloride increases the barrier to the desensitized state and increases the free energy of the desensitized state.

and modulating effects of Ca^{2+} on ASIC1a and concluded that these varying effects occur *via* different Ca^{2+} binding sites in the channels that have different binding affinities—the blocking effect occurs with high-affinity (low micromolar range) (Immke and McCleskey, 2003), and the modulating effect occurs *via* a low-affinity site (~2 mM) (Babini et al., 2002). They found that Ca^{2+} competes for amiloride block of ASIC1a, and this competition was abolished with mutation of a purported Ca^{2+} binding site within the outer entrance of the pore (Paukert et al., 2004). Work to identify the Ca^{2+} modulating domains within ASICs have identified several different sites, dependent on the isoforms studied (Babini et al., 2002; Sherwood et al., 2009; Zuo et al., 2018). Further complicating the competitive interaction of Ca^{2+} with amiloride is that the presumed shared binding site(s) are undoubtedly protonated at lower pH (Immke and McCleskey, 2003; Paukert et al., 2004). Thus, we postulate that the myriad of modulatory and blocking effects of amiloride are the result of a complex competitive interaction between amiloride, Ca^{2+}, and H^+ at probably more than one site in the channel. In support of this idea, amiloride causes both the pH- activation and SSD dose-response curves to be less steep (**Figure 3C**; Besson et al., 2017), implying that amiloride disrupted the observed cooperativity of H^+-binding to the channel (Bonifacio et al., 2014). A competition between shared binding sites could very well explain the variable effects of amiloride to either block or potentiate, depending on both amiloride and H^+ concentrations.

Amiloride Likely Binds to Multiple Sites in Acid-Sensing Ion Channels and Modulates *via* Different Mechanisms

Previous work has demonstrated that amiloride has the capacity to bind to multiple sites within DEG/ENaC channels, including ASICs. The blocking effects of amiloride have been principally explored in ENaC, leading to identification of a purported binding site within the outer vestibule of the pore (McNicholas and Canessa, 1997), including a critical conserved Glycine residue (G445 in rat ASIC3) (Schild et al., 1997), although other sites may also contribute to ENaC block (Ismailov et al., 1997). However, amiloride is also known to inhibit other proteins including other sodium channels and Na^+/H^+ exchangers (Kellenberger and Schild, 2002), indicative of the non-specific binding properties of amiloride. Both molecular modeling of amiloride docking within human ASIC1 and crystallization of chicken ASIC1 in the presence of amiloride have demonstrated that amiloride has the potential to bind to multiple different sites within ASIC channels (Qadri et al., 2010; Baconguis et al., 2014).

Importantly, it should be noted that binding cannot necessarily be inferred from observed functional effects on the channel (Colquhoun, 1998, 2006). Ligand-induced changes in channel activity require binding of the ligand and then subsequent steps that typically involve conformational (gating) changes. Amiloride could bind to a particular site, and then

other domains are required for the subsequent conformational changes to a different state. For example, we confirmed that mutation of a purported non-proton ligand sensor (E79 and E423) largely abolished the effect of amiloride to inhibit pH-dependent SSD (Li et al., 2011; Besson et al., 2017). While amiloride could very well bind to this site (Yu et al., 2011), it is also possible that amiloride binds to a different site and that E79 and E423 are required for the subsequent conformation changes to the desensitized state, as these sites have proven to be critical for ASIC3 desensitization (Cushman et al., 2007). In fact, we found that mutation of E79 did not abolish amiloride potentiation of pH 7.4-evoked currents, suggesting that this site does not underlie the alkaline shift in the pH activation curve caused by amiloride. This is similar to that described with GMQ, whereby mutation of this site abolishes the amiloride shift of SSD, but not activation (Alijevic and Kellenberger, 2012). Thus, we conclude that the purported non-proton ligand sensing site does not account for all of the potentiating effects of amiloride or GMQ on ASIC channels.

On the other hand, our studies on the voltage-dependence of the various amiloride blocking and modulating effects lends direct insight as to where amiloride binds to produce these effects. Similar to studies in a mutant ASIC2a channel (Adams et al., 1999), we found that the blocking effect of amiloride on ASIC3 was voltage-dependent; holding the cell at positive voltages caused relief of amiloride block, presumably by electrostatically driving the positively charged amiloride from a binding site within the membrane-spanning domains. Conversely, the potentiation of pH 7-evoked current amplitude and the slowing of open-state desensitization were both voltage independent, implying that the amiloride binding site inducing these modulatory effects is outside of the membrane electrostatic field. Surprisingly, we also found amiloride inhibition of pH-dependent SSD was voltage-dependent; a finding supported by our results that mutation of a purported amiloride binding site on the second transmembrane-spanning domain (G445) largely mitigated the effect of amiloride on SSD. These results suggest that a binding site just above the pore contributes to both channel block and potentiation of pH-evoked currents. Such paradoxical effects could be explained by a "foot-in-the-door" phenomenon (Armstrong, 1971), whereby amiloride binds deeply near the entrance of the pore to block ion permeation and at the same time obstructs a conformational change to the desensitized state. It is interesting that amiloride potentiation of pH-7 evoked current amplitude was voltage-independent whereas its effect on SSD was voltage-dependent, suggesting that these modulatory effects occur through different amiloride binding sites. It is possible that the effects on SSD are mediated by an amiloride binding site within the transmembrane-spanning domains whereas the site(s) that leads to a shift in pH-dependent activation lies within the extracellular domains. It is also quite conceivable that amiloride binding to more than one site is required for a particular modulatory effect.

While much of our understanding of ASIC gating has focused on the extracellular domain sites where H^+ and other ligands bind and subsequently impart conformational changes that are transmitted to the transmembrane domains, it is interesting that mutations within the transmembrane domains can also have profound effects on pH-dependent activation and desensitization. Besson et al. (2017) found that replacing the transmembrane domains of ASIC3 with those of ASIC1a generated a channel that no longer generated window currents at the foot of the pH-activation dose response and in the presence of amiloride the window currents were ∼20 times diminished in amplitude compared to the effect of amiloride on wildtype ASIC3. Thus, there appears to be a complex interplay between the functional effects of ligand-binding sites within the extracellular domain and transmembrane domains that is not well understood.

CONCLUSION

The pharmaceutical industry is aware of the potential therapeutic benefits of ASIC modulation and has sought to engineer amiloride derivatives that have varying effects on channel function (Kuduk et al., 2009; Baron and Lingueglia, 2015). A better understanding of the modulatory mechanisms of amiloride on ASICs is critical to advancing this endeavor. Additionally, further insights into the modulation of ASICs by amiloride and other small-molecule derivatives will provide more context within studies utilizing these compounds to investigate the physiological role of ASICs *in vivo*. Here we report that amiloride can both block and modulate ASIC3 in a variety of ways and probably does so through multiple different binding sites. The mechanism underlying the modulatory effects of amiloride on ASICs is likely more complex than previously thought.

DATA AVAILABILITY STATEMENT

The raw data supporting the conclusions of this article will be made available by the authors, without undue reservation.

AUTHOR CONTRIBUTIONS

DM, NH, PS, and CB conceived and designed the studies. DM, NH, MG, DG, NK, AH, VS, and CB conducted the experiments and analyzed the data. DM, NH, and CB wrote the manuscript. All authors contributed to the article and approved the submitted version.

FUNDING

This study was supported by the Department of Veterans Affairs Merit Award (5I01BX000776).

REFERENCES

Adams, C. M., Snyder, P. M., and Welsh, M. J. (1999). Paradoxical stimulation of a DEG/ENaC channel by amiloride. *J. Biol. Chem.* 274, 15500–15504. doi: 10.1074/jbc.274.22.15500

Alijevic, O., and Kellenberger, S. (2012). Subtype-specific modulation of acid-sensing ion channel (ASIC) function by 2-guanidine-4-methylquinazoline. *J. Biol. Chem.* 287, 36059–36070. doi: 10.1074/jbc.M112.360487

Armstrong, C. M. (1971). Interaction of tetraethylammonium ion derivatives with the potassium channels of giant axons. *J. Gen. Physiol.* 58, 413–437. doi: 10.1085/jgp.58.4.413

Babini, E., Paukert, M., Geisler, H. S., and Grunder, S. (2002). Alternative splicing and interaction with di- and polyvalent cations control the dynamic range of acid-sensing ion channel 1 (ASIC1). *J. Biol. Chem.* 277, 41597–41603. doi: 10.1074/jbc.M205877200

Baconguis, I., Bohlen, C. J., Goehring, A., Julius, D., and Gouaux, E. (2014). X-ray structure of acid-sensing ion channel 1-snake toxin complex reveals open state of a Na(+)-selective channel. *Cell* 156, 717–729. doi: 10.1016/j.cell.2014.01.011

Baron, A., and Lingueglia, E. (2015). Pharmacology of acid-sensing ion channels - Physiological and therapeutical perspectives. *Neuropharmacology* 94, 19–35. doi: 10.1016/j.neuropharm.2015.01.005

Benson, C. J., Xie, J., Wemmie, J. A., Price, M. P., Henss, J. M., Welsh, M. J., et al. (2002). Heteromultimers of DEG/ENaC subunits form H+-gated channels in mouse sensory neurons. *Proc. Natl. Acad. Sci. U S A.* 99, 2338–2343. doi: 10.1073/pnas.032678399

Besson, T., Lingueglia, E., and Salinas, M. (2017). Pharmacological modulation of Acid-Sensing Ion Channels 1a and 3 by amiloride and 2-guanidine-4-methylquinazoline (GMQ). *Neuropharmacology* 125, 429–440. doi: 10.1016/j.neuropharm.2017.08.004

Bonifacio, G., Lelli, C. I., and Kellenberger, S. (2014). Protonation controls ASIC1a activity *via* coordinated movements in multiple domains. *J. Gen. Physiol.* 143, 105–118. doi: 10.1085/jgp.201311053

Chen, X., Paukert, M., Kadurin, I., Pusch, M., and Grunder, S. (2006). Strong modulation by RFamide neuropeptides of the ASIC1b/3 heteromer in competition with extracellular calcium. *Neuropharmacology* 50, 964–974. doi: 10.1016/j.neuropharm.2006.01.007

Colquhoun, D. (1998). Binding, gating, affinity and efficacy: the interpretation of structure-activity relationships for agonists and of the effects of mutating receptors. *Br. J. Pharmacol.* 125, 924–947. doi: 10.1038/sj.bjp.0702164

Colquhoun, D. (2006). Agonist-activated ion channels. *Br. J. Pharmacol.* 147(Suppl. 1), S17–S26. doi: 10.1038/sj.bjp.0706502

Cushman, K. A., Marsh-Haffner, J., Adelman, J. P., and McCleskey, E. W. (2007). A conformation change in the extracellular domain that accompanies desensitization of acid-sensing ion channel (ASIC) 3. *J. Gen. Physiol.* 129, 345–350. doi: 10.1085/jgp.200709757

Eshcol, J. O., Harding, A. M., Hattori, T., Costa, V., Welsh, M. J., and Benson, C. J. (2008). Acid-sensing ion channel 3 (ASIC3) cell surface expression is modulated by PSD-95 within lipid rafts. *Am. J. Physiol. Cell Physiol.* 295, C732–C739. doi: 10.1152/ajpcell.00514.2007

Gonzales, E. B., Kawate, T., and Gouaux, E. (2009). Pore architecture and ion sites in acid-sensing ion channels and P2X receptors. *Nature* 460, 599–604. doi: 10.1038/nature08218

Grunder, S., and Pusch, M. (2015). Biophysical properties of acid-sensing ion channels (ASICs). *Neuropharmacology* 94, 9–18. doi: 10.1016/j.neuropharm.2014.12.016

Hattori, T., Chen, J., Harding, A. M., Price, M. P., Lu, Y., Abboud, F. M., et al. (2009). ASIC2a and ASIC3 heteromultimerize to form pH-sensitive channels in mouse cardiac dorsal root ganglia neurons. *Circ. Res.* 105, 279–286. doi: 10.1161/CIRCRESAHA.109.202036

Immke, D. C., and McCleskey, E. W. (2001). Lactate enhances the acid-sensing Na+ channel on ischemia-sensing neurons. *Nat. Neurosci.* 4, 869–870. doi: 10.1038/nn0901-869

Immke, D. C., and McCleskey, E. W. (2003). Protons open acid-sensing ion channels by catalyzing relief of Ca2+ blockade. *Neuron* 37, 75–84. doi: 10.1016/S0896-6273(02)01130-3

Ismailov, I. I., Kieber-Emmons, T., Lin, C., Berdiev, B. K., Shlyonsky, V. G., Patton, H. K., et al. (1997). Identification of an amiloride binding domain within the alpha-subunit of the epithelial Na+ channel. *J. Biol. Chem.* 272, 21075–21083. doi: 10.1074/jbc.272.34.21075

Jasti, J., Furukawa, H., Gonzales, E. B., and Gouaux, E. (2007). Structure of acid-sensing ion channel 1 at 1.9 A resolution and low pH. *Nature* 449, 316–323. doi: 10.1038/nature06163

Kellenberger, S., and Schild, L. (2002). Epithelial sodium channel/degenerin family of ion channels: a variety of functions for a shared structure. *Physiol. Rev.* 82, 735–767. doi: 10.1152/physrev.00007.2002

Khataei, T., Harding, A. M. S., Janahmadi, M., El-Geneidy, M., Agha-Alinejad, H., Rajabi, H., et al. (2020). ASICs are required for immediate exercise-induced muscle pain and are downregulated in sensory neurons by exercise training. *J. Appl. Physiol.* 129, 17–26. doi: 10.1152/japplphysiol.00033.2020

Kuduk, S. D., Di Marco, C. N., Chang, R. K., Dipardo, R. M., Cook, S. P., Cato, M. J., et al. (2009). Amiloride derived inhibitors of acid-sensing ion channel-3 (ASIC3). *Bioorg. Med. Chem. Lett.* 19, 2514–2518. doi: 10.1016/j.bmcl.2009.03.029

Li, W. G., Yu, Y., Huang, C., Cao, H., and Xu, T. L. (2011). Nonproton ligand sensing domain is required for paradoxical stimulation of acid-sensing ion channel 3 (ASIC3) channels by amiloride. *J. Biol. Chem.* 286, 42635–42646. doi: 10.1074/jbc.M111.289058

McNicholas, C. M., and Canessa, C. M. (1997). Diversity of channels generated by different combinations of epithelial sodium channel subunits. *J. Gen. Physiol.* 109, 681–692. doi: 10.1085/jgp.109.6.681

Paukert, M., Babini, E., Pusch, M., and Grunder, S. (2004). Identification of the Ca2+ blocking site of acid-sensing ion channel (ASIC) 1: implications for channel gating. *J. Gen. Physiol.* 124, 383–394. doi: 10.1085/jgp.200308973

Qadri, Y. J., Song, Y., Fuller, C. M., and Benos, D. J. (2010). Amiloride docking to acid-sensing ion channel-1. *J. Biol. Chem.* 285, 9627–9635. doi: 10.1074/jbc.M109.082735

Schild, L., Schneeberger, E., Gautschi, I., and Firsov, D. (1997). Identification of amino acid residues in the alpha, beta, and gamma subunits of the epithelial sodium channel (ENaC) involved in amiloride block and ion permeation. *J. Gen. Physiol.* 109, 15–26. doi: 10.1085/jgp.109.1.15

Sherwood, T., Franke, R., Conneely, S., Joyner, J., Arumugan, P., and Askwith, C. (2009). Identification of protein domains that control proton and calcium sensitivity of ASIC1a. *J. Biol. Chem.* 284, 27899–27907. doi: 10.1074/jbc.M109.029009

Sluka, K. A., Winter, O. C., and Wemmie, J. A. (2009). Acid-sensing ion channels: A new target for pain and CNS diseases. *Curr. Opin. Drug Discov. Devel.* 12, 693–704.

Waldmann, R., Champigny, G., Bassilana, F., Heurteaux, C., and Lazdunski, M. A. (1997b). proton-gated cation channel involved in acid-sensing. *Nature* 386, 173–177. doi: 10.1038/386173a0

Waldmann, R., Bassilana, F., de Weille, J., Champigny, G., Heurteaux, C., and Lazdunski, M. (1997a). Molecular cloning of a non-inactivating proton-gated Na+ channel specific for sensory neurons. *J. Biol. Chem.* 272, 20975–20978. doi: 10.1074/jbc.272.34.20975

Wemmie, J. A., Askwith, C. C., Lamani, E., Cassell, M. D., Freeman, J. H. Jr., and Welsh, M. J. (2003). Acid-sensing ion channel 1 is localized in brain regions with high synaptic density and contributes to fear conditioning. *J. Neurosci.* 23, 5496–5502. doi: 10.1523/JNEUROSCI.23-13-05496.2003

Wemmie, J. A., Chen, J., Askwith, C. C., Hruska-Hageman, A. M., Price, M. P., Nolan, B. C., et al. (2002). The acid-activated ion channel ASIC contributes to synaptic plasticity, learning, and memory. *Neuron* 34, 463–477. doi: 10.1016/S0896-6273(02)00661-X

Wemmie, J. A., Coryell, M. W., Askwith, C. C., Lamani, E., Leonard, A. S., Sigmund, C. D., et al. (2004). Overexpression of acid-sensing ion channel 1a in transgenic mice increases acquired fear-related behavior. *Proc. Natl. Acad. Sci. U S A.* 101, 3621–3626. doi: 10.1073/pnas.0308753101

Yagi, J., Wenk, H. N., Naves, L. A., and McCleskey, E. W. (2006). Sustained currents through ASIC3 ion channels at the modest pH changes that occur during myocardial ischemia. *Circ. Res.* 99, 501–509. doi: 10.1161/01.RES.0000238388.79295.4c

Yu, Y., Chen, Z., Li, W. G., Cao, H., Feng, E. G., Yu, F., et al. (2010). A nonproton ligand sensor in the acid-sensing ion channel. *Neuron.* 68, 61–72. doi: 10.1016/j.neuron.2010.09.001

Yu, Y., Li, W. G., Chen, Z., Cao, H., Yang, H., Jiang, H., et al. (2011). Atomic level characterization of the nonproton ligand-sensing domain of ASIC3 channels. *J. Biol. Chem.* 286, 24996–25006. doi: 10.1074/jbc.M111.239558

Zhang, P., Sigworth, F. J., and Canessa, C. M. (2006). Gating of acid-sensitive ion channel-1: release of Ca2+ block vs. allosteric mechanism. *J. Gen. Physiol.* 127, 109–117. doi: 10.1085/jgp.200509396

Zuo, Z., Smith, R. N., Chen, Z., Agharkar, A. S., Snell, H. D., Huang, R., et al. (2018). Identification of a unique Ca(2+)-binding site in rat acid-sensing ion channel 3. *Nat. Commun.* 9:2082. doi: 10.1038/s41467-018-04424-0

Conflict of Interest: The authors declare that the research was conducted in the absence of any commercial or financial relationships that could be construed as a potential conflict of interest.

Publisher's Note: All claims expressed in this article are solely those of the authors and do not necessarily represent those of their affiliated organizations, or those of the publisher, the editors and the reviewers. Any product that may be evaluated in this article, or claim that may be made by its manufacturer, is not guaranteed or endorsed by the publisher.

frontiers in Physiology

REVIEW
published: 26 October 2021
doi: 10.3389/fphys.2021.733267

Properties and Differential Expression of H^+ Receptors in Dorsal Root Ganglia: Is a Labeled-Line Coding for Acid Nociception Possible?

*Omar Páez[1], Pedro Segura-Chama[1,2], Angélica Almanza[1], Francisco Pellicer[3] and Francisco Mercado[1]**

[1]*Laboratorio de Fisiología Celular, Dirección de Investigaciones en Nuerociencias, Instituto Nacional de Psiquiatría Ramón de la Fuente Muñiz, Ciudad de México, Mexico,* [2]*Cátedras CONACyT, Instituto Nacional de Psiquiatría Ramón de la Fuente Muñiz, Ciudad de México, Mexico,* [3]*Laboratorio de Neurofisiología Integrativa, Dirección de Investigaciones en Neurociencias, Instituto Nacional de Psiquiatría Ramón de la Fuente Muñiz, Ciudad de México, Mexico*

OPEN ACCESS

Edited by:
Candice Askwith, The Ohio State University, United States

Reviewed by:
Avi Priel, Hebrew University of Jerusalem, Israel
Linlin Ma, Griffith University, Australia

***Correspondence:**
Francisco Mercado
fmercado@imp.edu.mx

Specialty section:
This article was submitted to Membrane Physiology and Membrane Biophysics, a section of the journal Frontiers in Physiology

Received: *30 June 2021*
Accepted: *05 October 2021*
Published: *26 October 2021*

Citation:
Páez O, Segura-Chama P, Almanza A, Pellicer F and Mercado F (2021) Properties and Differential Expression of H^+ Receptors in Dorsal Root Ganglia: Is a Labeled-Line Coding for Acid Nociception Possible? Front. Physiol. 12:733267. doi: 10.3389/fphys.2021.733267

Pain by chemical irritants is one of the less well-described aspects of nociception. The acidic substance is the paradigm of the chemical noxious compound. An acidic insult on cutaneous, subcutaneous and muscle tissue results in pain sensation. Acid (or H^+) has at least two main receptor channels in dorsal root ganglia (DRG) nociceptors: the heat receptor transient receptor potential vanilloid 1 (TRPV1) and the acid-sensing ionic channels (ASICs). TRPV1 is a low-sensitivity H^+ receptor, whereas ASIC channels display a higher H^+ sensitivity of at least one order of magnitude. In this review, we first describe the functional and structural characteristics of these and other H^+-receptor candidates and the biophysics of their responses to low pH. Additionally, we compile reports of the expression of these H^+-receptors (and other possible complementary proteins) within the DRG and compare these data with mRNA expression profiles from single-cell sequencing datasets for ASIC3, ASIC1, transient receptor potential Ankiryn subtype 1 (TRPA1) and TRPV1. We show that few nociceptor subpopulations (discriminated by unbiased classifications) combine acid-sensitive channels. This comparative review is presented in light of the accumulating evidence for labeled-line coding for most noxious sensory stimuli.

Keywords: proton, nociceptor, pain, acid, ASIC, TRP channels, DRG

INTRODUCTION

Nociception is the nerve coding for noxious stimuli. In the last two decades, many advances have been made to understand how different nociceptive stimuli are transduced, which nociceptors are involved in their transduction, and how afferent neurons relay the information to second-order neurons in the dorsal horn of the spinal cord (Abrahamsen et al., 2008; Moehring et al., 2018; Emery and Wood, 2019; Emery and Ernfors, 2020). Nociceptors respond to a variety of stimuli that can be classified into three categories: (i) mechanical (high-threshold mechanical stimuli), (ii) chemical (pruritogenic compounds, acidic substances, etc.), and (iii) physical (high

or low temperature). Most nociceptors respond to a specific kind of nociceptive stimulus, remaining unresponsive to other noxious stimuli (Cavanaugh et al., 2009; Emery et al., 2016). This conclusion challenges a long-lasting dominant idea in which most nociceptors are considered polymodal (Perl, 1996), demonstrating that nociceptors transduce stimuli in a labeled line-code fashion. Using next-generation research techniques, it is now possible to identify most of the afferent neurons transducing distinct noxious stimuli.

Noxious-cold nociceptors are characterized by the expression of TRPM8 channels, corresponding to approximately 10–20% of nociceptors. TRPM8 is an ionic channel that is opened by cold temperatures (<10°C), allowing flow of a cationic current that depolarizes the neuron. There is still controversy about whether TRPM8 is the unique channel necessary for noxious cold transduction since, for example, transient receptor potential Ankiryn subtype 1 (TRPA1) could have a role in cold sensing (Story et al., 2003). TRPM8 knockout (KO) mice have an important behavioral deficit in sensing cold environments; they poorly discriminate a cold room from a warm room, but surprisingly, TRPM8 is not necessary for the detection of extreme cold temperatures (<0°C), which activate another subset of nociceptors lacking TRPM8 expression (Dhaka et al., 2007; Luiz et al., 2019).

In a similar way, it is known that heat-thermonociceptive neurons express transient receptor potential vanilloid 1 (TRPV1) channels and complementary TRPML3 and TRPA1 (Vandewauw et al., 2018). TRPV1 opens with temperatures above 42°C (Caterina et al., 1997; Tominaga et al., 1998), and in psychophysical experiments, it matches the temperature considered to produce the burning sensation. TRPV1 is coexpressed with the marker calcitonin gene-related peptide (CGRP; **Figure 1**). Excitotoxic elimination of TRPV1-expressing neurons with intrathecal infusion of capsaicin reduced the CGRP population by half, with other dorsal root ganglia (DRG) nociceptor populations remaining almost unaltered, such as IB4+ neurons (Cavanaugh et al., 2009, 2011). This means that heat-sensing neurons belong to the peptidergic (PEP) nociceptor population. The ablation of TRPV1-expressing neurons produces a profound deficit in the detection of noxious heat, highlighting the importance of that subset of neurons in this sensory modality.

The recently cloned ion channel TACAN, which transduces noxious mechanical stimuli, is expressed by a particular subset of nociceptors that do not express TRPV1, TRPM8, or TRPA1. In fact, TACAN is mainly expressed in nonpeptidergic nociceptors and colocalizes with the marker IB4, the purinergic ion channel P2X3, and the MrgprD receptor (**Figure 1**; Beaulieu-Laroche et al., 2020). These markers were previously related to the detection of mechanically noxious stimuli (Cavanaugh et al., 2009).

Therefore, cold-coding, heat-coding, and mechano-coding nociceptors are identifiable and experimentally corroborated *in vivo* whole-animal experiments. As many as 85% of nociceptors respond only to a specific kind of the abovementioned stimuli (Emery and Wood, 2019). However, chemonociception is less well-described because chemical sensitivity is infrequently tested (Emery and Wood, 2019).

Physiologically relevant chemical nociception is caused by acidic substances. The cutaneous and subcutaneous application of acid solutions in humans produces clearly recognizable pain, sometimes referred to as "acid burning" (Jones et al., 2004). Infusion of a pH 5.2 solution into the skin (Steen and Reeh, 1993) and hypodermic infusion of a pH 6.5 solution (and lower pH values; Ugawa et al., 2002) elicit pain in human subjects. Muscle pain can also be elicited with a pH 5.2 intramuscular infusion in humans (Law et al., 2008). In animal models, solutions of pH 6.9 and 6.6 are sufficient to elicit nocifensive behavior in rats (Deval et al., 2008). After two intramuscular injections of pH 4 saline, mice develop hyperalgesia without any tissue damage. After the second application of acid, this hyperalgesia becomes chronic (Sluka et al., 2001; Sharma et al., 2009).

In knockout mice for the different acid-sensing receptors, nociceptors continue responding to an acidic solution challenge, albeit with some deficit, and the KO mouse behavioral response resembles that of wild-type mice (Caterina et al., 2000; Price et al., 2000, 2001). The fact that no acid-insensitive phenotype could be obtained opens the possibility that a combination of H^+ receptors mediates the transduction of acidic stimuli. Moreover, if there is a subset of nociceptors best suited to transduce acidic solutions as noxious stimuli, it has not yet been studied.

In this review, we first summarize the biophysical, pharmacological, and physiological characteristics of ionic channels that act as H^+-activated receptors, mainly acid-sensing ionic channels (ASICs) and TRP channels. Then, for each H^+ receptor, we combine the evidence of its expression among neuronal populations in the DRG from rodents. We include reports of expression by both immunohistochemistry and the distribution of acid-induced currents in cultured DRG neurons. Finally, we contrast these data with mRNA expression profiles from the novel unbiased classifications of sensory neurons. We show that the concomitant expression of H^+-gated receptors (ASIC3, ASIC1, TRPV1, or TRPA1) in sensory neurons is notably subpopulation-specific, which is suggestive of a specialized sensory role for acid in these subpopulations.

ASIC CHANNELS

Acid sensing ion channels are homo- or heterotrimeric channels activated by low pH. They are part of the ENaC/degenerin family (Waldmann et al., 1997a,b). There are four ASIC genes that code for six subunits in rodents: ASIC1a, ASIC1b, ASIC2a, ASIC2b, ASIC3, and ASIC4. Each ASIC subunit consists of two transmembrane domains and an arm-shaped conformation. Accordingly, most of the ASIC subunit domains are extracellular, so-called wrist, palm, and thumb domains (**Figure 2**; Jasti et al., 2007).

Protons bind ASIC subunits *via* an acidic pocket rich in carboxylate groups spanning residues D238–D350, E239–D346, and E220–D408 (Jasti et al., 2007). Outside this pocket, there are also important protonation sites, such as the wrist domain and the first 87 residues after transmembrane domain 1 (Paukert

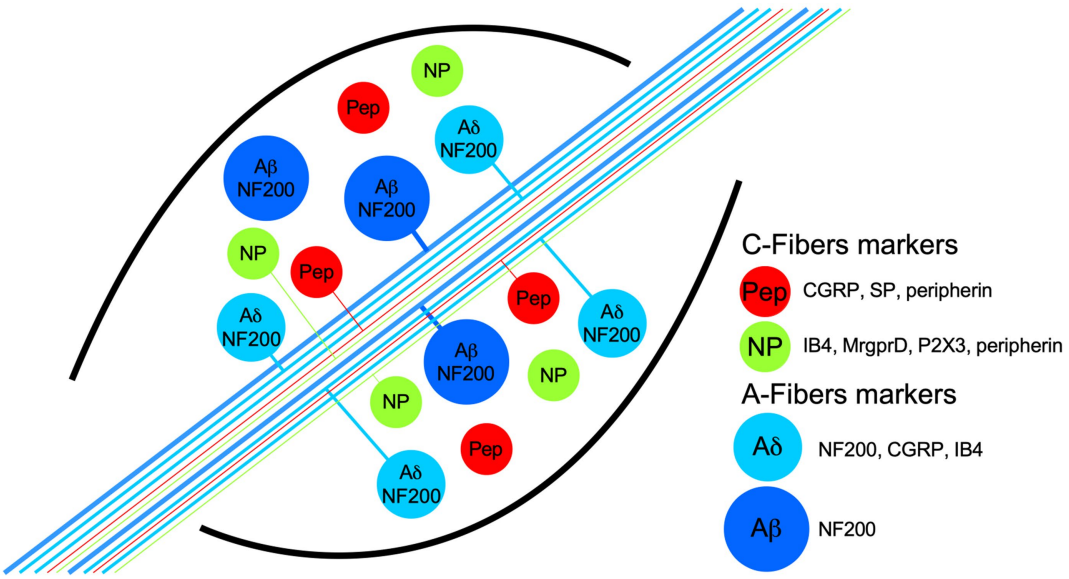

FIGURE 1 | Schematic representation of dorsal root ganglia (DRG) neuron populations classified by their biochemical markers and membrane topology of some proton receptors coupled to an ion channel. The neurons have pseudomonopolar shapes and vary in soma size and axon diameter. Thin, unmyelinated axons belong to small-diameter soma neurons and are called C-fibers (green and red somas), which are classified grossly in two populations by the expression, in some neurons, of the neuropeptides calcitonin-gene related peptide (CGRP) and substance P (SP), which are called peptidergic (red somas; PEP). Nonpeptidergic neurons (green somas; NP) characteristically bind lectin IB4 and express the MrgprD and P2X3 receptors. PEP and NP neurons are stained by the marker peripherin. C-fibers transduce high-threshold stimuli, and almost all are nociceptors. Myelinated axons belong to neurons with larger soma sizes and are called A-fibers. Because the axon conduction velocities are subclassified in α, β, and δ, only the last two are illustrated. Aβ neurons are light-touch neurons, and the axon conduction velocities are faster than Aδ. Meanwhile, a high proportion of Aδ neurons are nociceptors, and both share medium-weight filaments (NF200) as markers, but some Aδ neurons are also stained by CGRP and IB4.

et al., 2008; Li et al., 2009; Schuhmacher et al., 2015). Residues involved in the pH dependence of activation or desensitization are also located in multiple domains spanning the thumb and palm domains (Liechti et al., 2010; Krauson and Carattino, 2016). Activation by protons involves the closure of the thumb domain into the acidic pocket and the opening of the channel gate (Yoder et al., 2018).

When ASIC is activated, an inward Na^+ current sensitive to amiloride is generated through the channel. The inward Na^+ current is transient, with fast activation and desensitization kinetics. Desensitization is a nonconducting state that occurs after fractions of a second of prolonged low pH (Waldmann et al., 1997b; Gründer and Pusch, 2015). This desensitized state is controlled by the palm domain (Roy et al., 2013; Vullo et al., 2017). ASIC channels could then be found in closed, open, and desensitized states.

Most ASIC subunits sense pH changes within the physiological range and are activated if the extracellular pH falls below 7, reaching a maximal open probability at pH ~6.0 (Waldmann et al., 1997b; Gründer and Pusch, 2015).

The ASIC subunits (i.e., expressed in Xenopus oocytes) show different pH dependences for activation. Homomeric ASIC3 and ASIC1a channels are the most sensitive to protons. ASIC3 channels show a pH_{50} of 6.4–6.7, and ASIC1a channels show a pH_{50} of 6.4–6.6 (Benson et al., 2001; Sutherland et al., 2001; Babini et al., 2002; Hesselager et al., 2004; Chen et al., 2005; Yagi et al., 2006; Sherwood et al., 2011); moreover, ASIC2 subunits are the least sensitive to acidity (pH_{50} 4.5). ASIC subunits also differ in some other biophysical properties, notably their desensitization time constant, in which ASIC3 and ASIC1a and 1b show significantly faster desensitization kinetics than ASIC2; additionally, ASIC3 shows a significantly larger sustained current at low pH (Hesselager et al., 2004; Salinas et al., 2009; Delaunay et al., 2012). This pronounced sustained current along with its highest sensitivity to pH changes make ASIC3 a strong candidate to transduce tissue acidosis (Dulai et al., 2021). ASICs usually form heteromultimers when coexpressed, so the biophysical properties of heterotrimeric channels reflect their subunit composition (Benson et al., 2001; Hesselager et al., 2004; Gautam and Benson, 2013; Bartoi et al., 2014).

Distribution of ASIC Currents Among Small Unmyelinated DRG Neurons

The response of DRG neurons to protons has been extensively documented in the literature, and in many cases, the suspected ASIC subunit or combinations of them have been deduced from the current kinetics. In the DRG, nociceptors have been traditionally divided into myelinated medium diameter Aδ and unmyelinated small-diameter C types. Here, we will focus on reports making an explicit distinction between PEP and nonpeptidergic small DRG neurons (**Table 1**). The common neuronal marker used in these studies is the binding of the IB4 lectin. Most of the neurons not binding IB4 are peptidergic

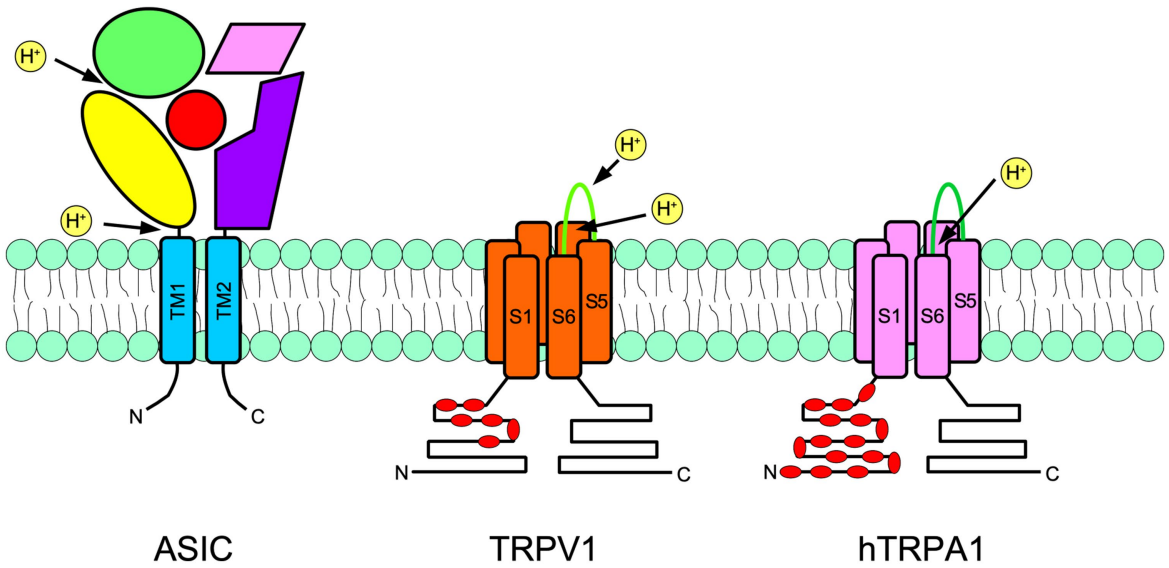

FIGURE 2 | Schematic representation of a subunit of an acid-sensing ion channel (ASIC; left), transient receptor potential vanilloid 1 (TRPV1; center), and transient receptor potential ankyrin 1 (TRPA1; right) are shown. ASIC are trimers, meanwhile TRPs are tetramers. The approximate localization of proton receptors within the protein of each channel is shown with arrows. The ASIC large extracellular portion is arranged in an arm shape, as has been suggested by crystallographic studies. The thumb is in yellow, the palm is in purple, the fingers are in green, beta-balls are in red and knuckles are in pink. In TRPs, red indicates the intracellular ankyrin repeats. N indicates the amino terminus and C indicates the carboxy terminus.

(i.e., they express CRGP), and most of those binding IB4 are nonpeptidergic (**Figure 1**). These neuronal subpopulations show different currents and action potential characteristics (Stucky and Lewin, 1999; Fang et al., 2006). More importantly, as will be discussed further, these two major groups of nociceptors fulfil different sensory roles within the DRG.

When exposed to low pH, some small-diameter rat DRG neurons respond with nondesensitizing, sustained ionic currents, while others respond with desensitizing or mixed currents (Petruska et al., 2000). Consistent with the presence of ASIC subunits, amiloride blocks the transient current and the transient part of mixed currents, whereas sustained currents are insensitive to amiloride. The latter currents are attributed to TRPV1 channels and are observed at lower pH (appearing at pH 6.1); in contrast, the transient currents are attributed to ASIC channels (appearing at pH 6.8; Petruska et al., 2000).

Approximately 90% of all rat DRG small neurons respond to pH 5 with inward currents (Liu et al., 2004). These currents were classified by their desensitization rate into three types: transient, sustained, or mixed. The frequency and waveform of these currents were different between the IB4+ and IB4− subpopulations. The IB4+ population produced most of the sustained (63%) currents, whereas IB4- neurons produced the most mixed currents (69%; Liu et al., 2004). Transient-only currents were not prevalent in any of the two subpopulations (<20% of total observed currents). These transient inward currents begin to activate at pH 7 and are maximal at pH 5. ASICs likely mediate these transient currents since they were sensitive to amiloride. The activation profile of mixed currents results from transient plus sustained currents. Based on these results, it was suggested that small IB4− rather than IB4+ neurons could play an essential role in acid sensing (Liu et al., 2004). Accordingly, ASIC currents (transient and mixed) are exclusive to small IB4- neurons (Drew et al., 2004).

In mouse DRG neurons, specifically unmyelinated nociceptors, it was reported that ASIC currents are also exclusive to the IB4− peptidergic subgroup and largely absent from IB4+ neurons. Transient-only currents were not detected; only (1) mixed and (2) sustained-only currents were detected, and both types were inhibited by amiloride (Dirajlal et al., 2003). DRG neurons from rats and mice generate ASIC currents mostly in IB4- neurons, and this predominance is seen across a wide acidic pH range (pH 6, 5, and 4; Leffler et al., 2006). These reports indicate that within unmyelinated DRG neurons from both rats and mice, ASIC-like currents can be detected almost exclusively within the peptidergic subgroup.

Poirot et al. (2006) provided a more relevant description of ASIC responses in rat DRG small neurons. Only currents that are initially activated within pH values of 6 and higher were investigated. Small sensory neurons produce a slowly inactivating current (Type 1) and two rapidly inactivating currents (Types 2 and 3). Type 1 current is the most prevalent current, the most sensitive to pH (pH_{50} 6.6) and might be mediated by ASIC1a homomers. Type 2 is the less frequent current and is mediated by heteromers containing ASIC2. Type 3 also shows high proton sensitivity (pH_{50} 6.5) and may be mediated by ASIC1a/ASIC3 heteromers (Poirot et al., 2006). Independent of the type, 91% of IB4− but only 36% of IB4+ neurons expressed an ASIC current. The distribution

TABLE 1 | Distribution of transient ASIC-like currents in small/unmyelinated DRG neurons in culture: peptidergic vs. nonpeptidergic neurons.

Reference	Criteria for cell selection/ species	Major division presented here according to	Candidate channel; antagonist used for validation	Peptidergic, IB4−	Non-peptidergic, IB4+
pH down to 5.2–5.0					
Liu et al., 2004	Small (15–30 μm); rat DRG neurons	IB4-binding	Transient: ASIC channels; blocked by amiloride Sustained: TRPV1 channels; blocked by capsazepine	pH 5.0: 69% mixed currents (transient + sustained)	pH 5.0: 27% mixed currents (transient + sustained)
Drew et al., 2004	Small (<30 μm); rat DRG neurons	Wild-type (WT) neurons by IB4-binding	Validated by comparison to ASIC2/3 KO mouse DRG neurons	pH 5.3: 50% transient currents	pH 5.3: 0% transient or mixed currents.
Dirajlal et al., 2003	Mouse DRG neurons that are N52(–) (e.g., unmyelinated) and that have an AP inflection (e.g., nociceptors)	IB4-binding	Transient: ASIC channels; blocked by amiloride Sustained: TRPV1 or ASIC3 channels; also blocked by amiloride at pH 5	pH 5: 33% mixed currents (transient + sustained)	pH 5: 0% transient or mixed currents
Leffler et al., 2006	Small (average 20–24 μm); DRG neurons from both mouse and rat	IB4-binding and according to species (WT neurons only)	Transient: ASIC channels; blocked by amiloride	Transient currents: Rat> pH 6.0: 91%; pH 5.0: 78% Mouse> pH 6.0: 25%; pH 5.0: 19%	Rat> pH 6.0: 40%; pH 5.0: 33% Mouse>pH 6.0: 8%; pH 5.0: 3%
pH down to 6.0					
Poirot et al., 2006	Small (<30 μm); rat DRG neurons	Current type (most to least frequent) and IB4-binding	ASIC1a heteromers according to inhibition by *Psalmopoeus c.* venom and time of course recovery τ Likely heteromers containing ASIC1a/3 according to the pH dependence of activation Likely heteromers containing ASIC2 according to Zn^{2+} positive modulation. Additionally, TRPV1; blocked by capsazepine	Type 1 current: $pH_{0.5}$ 6.6 ~52% Type 3 current: $pH_{0.5}$ 6.5 ~28% Type 2 current: $pH_{0.5}$ 6.0 ~8%	~6% ~16% ~10%

of type 1 and type 3 currents is heterogeneous among small DRG neurons. Type 1 current is expressed at higher levels in IB4− neurons than in IB4+ neurons (6-fold). Type 3 current is also more common in IB4− than IB4+ neurons (Poirot et al., 2006). These results suggest that within small, likely unmyelinated neurons, ASIC1, and ASIC3 might play specific roles in the IB4− peptidergic subpopulation, in which transient proton-gated currents are highly expressed. In addition to the detailed biophysical characterization of ASIC currents in the work by Poirot et al. (2006), this study provided two important demonstrations: (1) activation of ASICs in small DRG neurons can induce action potentials, and the probability of this induction increases with lower extracellular pH, in the pH 6.8–6.0 range; and (2) most H^+-gated currents in small DRG neurons are mediated by ASICs, with the notable exception of a small fraction of neurons (approximately 15%) expressing the type 2 current, in which there is a high current component mediated by TRPV1 channels (i.e., blocked by capsazepine).

Expression of ASIC3 and ASIC1 Channels Among Subpopulations of DRG Neurons

In DRG neurons from mice, ASIC3 is the most abundant subunit, whereas ASIC1b is the least abundant subunit (Schuhmacher and Smith, 2016). Regarding its distribution, ASIC subunits, especially ASIC3, do not show heterogeneous expression in immunohistochemistry studies. ASIC3 is more abundant in large-diameter neurons (Alvarez de la Rosa et al., 2002). ASIC3 is expressed mainly in TrkA+ neurons (Molliver et al., 2005), which is the receptor for nerve growth factor (NGF) and a marker of most peptidergic neurons, with medium Aδ and small C fibers. Small sensory neurons that innervate skeletal muscle express more ASIC3 than those that innervate the skin. Moreover, most ASIC3+ muscle afferents (80%) also express CGRP (Molliver et al., 2005). Another study analyzed the expression of ASIC3 in the DRG of eGFP knock-in mice (Lin et al., 2016). One-third of neurons expressed the ASIC3 subunit. ASIC3 localizes to 50% of large-diameter N52+ neurons and 39% of small-diameter peripherin+ neurons. Small peptidergic CGRP+ and IB4+ neurons show lower ASIC3 expression (27 and 23%; Lin et al., 2016). Thus, the expression of the ASIC3 subunit is higher in myelinated Aβ and Aδ fibers.

Analysis of mRNA levels shows that ASIC3 and ASIC1a/b subunits are the most abundant in the complete DRG (Poirot et al., 2006). In a recent work, Papalampropoulou-Tsiridou et al. (2020) analyzed the distribution of ASIC channels in the mouse DRG using RNAscope probes. This tool is a variant of *in situ* hybridization with higher sensitivity. Neurons were classified by the markers NF200 (marker of medium- to large-diameter myelinated neurons), IB4, and CGRP. None of the five ASIC subunits showed a similar distribution among the three different groups of DRG neurons (Papalampropoulou-Tsiridou et al., 2020). IB4+ neurons showed low expression of ASIC3 (~10% of total neurons) and the highest levels of ASIC2a expression (~70% of total neurons), while ASIC1a and 1b were not detected. This is contrasting to the IB4− subpopulation, in which more than 60% express the ASIC3 subunit and approximately 25% express ASIC1a and ASIC1b.

Finally, NF200+ myelinated neurons showed the highest levels of ASIC3 subunit expression.

These differences in mRNA levels agree with the conclusions of the electrophysiological studies previously mentioned. First, they corroborate that ASIC3 is mostly expressed in medium to large NF200+ neurons (Alvarez de la Rosa et al., 2002; Lin et al., 2016). This population corresponds to myelinated Aβ and Aδ fibers. In this population, ASIC1 and ASIC1b are expressed at considerably higher levels (>70%) than in small sensory neurons. In fact, in large-diameter DRG neurons, two slowly and two rapidly inactivating H^+-gated currents have been detected (Poirot et al., 2006). At least two of these currents have a pH dependence of activation (pH_{50} 6.6) similar to that of the more prevalent type 1 current in small neurons (Poirot et al., 2006). Second, the lack of ASIC1 and the lowest expression of ASIC3 subunits in IB4+ neurons explain the scarcity of transient ASIC currents in IB4+ neurons (Dirajlal et al., 2003; Liu et al., 2004; Leffler et al., 2006). Finally, the coexpression of three ASIC subunit mRNAs per single neuron was also analyzed. The three neuron subpopulations (NF200+, IB4+, and CGRP+) show different combinations of ASIC subunits, indicating that heterotrimeric ASIC channels are the dominant form present in most primary sensory neurons. The asymmetric distribution of ASIC subunits in DRG neurons suggests a specialized response to acidification from specific DRG neuronal groups (Papalampropoulou-Tsiridou et al., 2020).

TRPV1 CHANNELS

Transient receptor potential vanilloid 1 is the most studied member of the TRP family of ion channels. The main agonist of TRPV1 channels is capsaicin, the pungent compound in chili peppers that evokes the burning pain sensation (Caterina et al., 1997). TRPV1 is also a receptor for endovanilloids, lipids, heat, and protons. Each TRPV1 subunit is formed by a TRP domain and six transmembrane domains, and four subunits form a functional channel (**Figure 2**). The C and N terminals are located at the intracellular side of the channel, where an ankyrin repeat domain is also located (Liao et al., 2013; Rosasco and Gordon, 2017). TRP channels have cationic unspecific pores, in which Ca^{2+} ions are highly permeable, but significant Na^+ and K^+ conductance could be detected (Tominaga et al., 1998; Garcia-Sanz, 2004).

Compared to ASIC channels, TRPV1 channels respond differently to low pH. TRPV1 channels show two responses to protons: (1) sensitization and (2) direct activation. Sensitization occurs at extracellular pH > 6 and is observed upon activation by capsaicin and heat (Tominaga et al., 1998; Baumann and Martenson, 2000; Jordt et al., 2000; Neelands et al., 2005; Ryu et al., 2007). Direct activation occurs at lower pH (<6) and results in a sustained current at physiological temperature (Caterina et al., 1997; Tominaga et al., 1998). Protons behave as partial agonists of TRPV1 in comparison to capsaicin (20–30% of the current magnitude at saturating doses; Tominaga et al., 1998). TRPV1 H^+-gated currents show similar kinetics to those induced by capsaicin. Both presented similar desensitization profiles and are sensitive to the antagonist capsazepine (Tominaga et al., 1998).

Different extracellular residues are responsible for TRPV1 activation and potentiation by protons. For example, Glu600 participates in setting the pH sensitivity of the H^+-potentiation effect on TRPV1, and Glu648 is involved in direct activation by protons (Jordt et al., 2000). In rat TRPV1, two domains were identified in direct activation by extracellular protons. These domains are the pore helix, especially Thr366, and in the linker (TM3–TM4) region, the residue Val538 (Ryu et al., 2007). In the human TRPV1 channel, Glu536 in the TM3 to TM4 linker is required for the proton potentiation effect of capsaicin at high doses (Wang et al., 2010a). All these residues are different from the capsaicin-binding site, which is located intracellularly between the second and third transmembrane helices (Welch et al., 2000; Jordt and Julius, 2002).

Distribution of Acid-Induced TRPV1 Currents in Cultured DRG Neurons

Transient receptor potential vanilloid 1 colocalizes with ASIC1a and ASIC3 within single small sensory neurons to a considerable extent (Ugawa et al., 2005). Indeed, several reports of ASIC-like currents in cultured DRG neurons have simultaneously detected H^+-gated TRPV1-like currents (Neelands et al., 2010; Blanchard and Kellenberger, 2011). In response to protons, mouse DRG neurons produce a sustained inward current that inactivates slowly (>20 s; Dirajlal et al., 2003). Small C-type neurons show an unequal distribution of these TRPV1-like H^+-activated currents. At pH 5, 86% of small IB4− neurons generate sustained and, to a lesser extent, sustained and transient currents. Only 33% of IB4+ neurons responded in a similar way. However, not all neurons generating a sustained TRPV1-like H^+-gated current are capsaicin-responsive (Dirajlal et al., 2003). In another study, only a quarter of small IB4+ neurons showed sustained currents in response to pH 5.3, and half of IB4− neurons showed either sustained or mixed currents (Drew et al., 2004). As expected, in DRG neurons from double-knockout ASIC2/3 mice, the distribution of these sustained currents is not affected (Drew et al., 2004). This heterogeneous distribution of low pH sustained currents was not observed in cultured DRG neurons from rats (Liu et al., 2004).

Rat DRG neurons are more responsive to capsaicin than mouse DRG neurons and have a higher prevalence and magnitude of H^+-activated currents. When DRG neurons from TRPV1(−/−) mice were analyzed, there was a high reduction in proton responses. In comparison to WT neurons, TRPV1(−/−) neurons show significantly smaller currents at pH 5 and 4 (Leffler et al., 2006). As expected, transient ASIC-like currents remained unaltered in TRPV1(−/−) neurons. Moreover, in a skin nerve preparation *in vitro*, the response of myelinated Aδ fibers to pH 5 and 4 was unaffected in TRPV1(−/−) neurons in comparison to WT neurons. This suggests that the observed TRPV1 responses

to low pH are predominantly generated by small unmyelinated neurons (Leffler et al., 2006).

Expression of TRPV1 Across the DRG

Cavanaugh et al. (2011) used two lines of knock-in mice to study the distribution of TRPV1 in the DRG. During development, a wide variety of DRG neurons, both peptidergic and nonpeptidergic, express TRPV1 (Cavanaugh et al., 2011). In adult mice, however, TRPV1 expression is more restricted to the peptidergic population. Of the total TRPV1-expressing neurons, 64% were peptidergic, and only 11% were nonpeptidergic IB4+ neurons. Of all SP+ neurons in the DRG, 82% are TRPV1+, and of all CGRP+ neurons, 49% are TRPV1+ (Cavanaugh et al., 2011). Substance P (SP) is a marker of unmyelinated peptidergic neurons, while CGRP marks all peptidergic neurons (Aδ and C fibers). Previous studies reported a predominant expression of TRPV1 in the peptidergic subpopulation (Tominaga et al., 1998; Zwick et al., 2002). Since the detection of reporter genes is a more sensitive tool than immunostaining, the study of Cavanaugh et al. (2011) overcame the underestimation of TRPV1 expression in previous studies (Breese et al., 2005; Hjerling-Leffler et al., 2007). Interestingly, 20% of all TRPV1+ neurons are neither IB4+ nor CGRP+ (Cavanaugh et al., 2011).

Patil et al. (2018) classified DRG neurons based on their electrophysiological properties. The authors assessed DRG neurons in culture from several transgenic mouse lines carrying reporter genes for Nav1.8, TRPV1, and CGRP. They compared these against those of transgenic mice expressing well-established neuronal markers. Four of the resulting groups of neurons expressed TRPV1. The four TRPV1+ groups are small-diameter neurons. Three of those subpopulations are indeed peptidergic (CGRP+), and only one is nonpeptidergic (CGRP-; Patil et al., 2018).

Dorsal root ganglia neurons reveal a gradient of expression of TRPV1. Small neuronal bodies and a range of lightly stained neurons of various sizes are densely stained (Goswami et al., 2014). In the rat DRG, colocalization of TRPV1 with the NF200 marker was reported to occur in 11% of the total TRPV1+ neurons (Mitchell et al., 2014). In the mouse, however, TRPV1-induced reporter genes marked approximately 5% of myelinated NF200+ neurons. Thus, within the peptidergic population, there is one small group of myelinated TRPV1+ neurons (Cavanaugh et al., 2011).

TRANSIENT RECEPTOR POTENTIAL ANKIRYN SUBTYPE 1

Transient receptor potential Ankiryn subtype 1 channel also plays a role in H^+ detection in intra- and extracellular compartments. TRPA1 is activated for compounds considered irritants such as mustard oil (MO), acrolein, formaldehyde, and cinnamaldehyde (Jordt et al., 2004; Bautista et al., 2005). Extracellular H^+ elicits ionic current opening in human TRPA1 in channels but not in rodent orthologs (de la Roche et al., 2013). The response to extracellular pH of hTRPA1 has a pH_{50} of 6.5, which is intermediate between the proton sensitivity of most ASICs and TRPV1. Residues V942 and S943 (in the human channel sequence but substituted by an isoleucine and an alanine in the rodent channel) are important for extracellular H^+-sensing. The ionic current evoked by H^+ is similar to those evoked by MO or any other agonist of TRPA1 and is a calcium-permeable current with slow kinetics (de la Roche et al., 2013).

The contribution of TRPA1 to the response to acidic substances at the physiological level has also been proposed. In experiments in rodents, TRPA1 contributes significantly to the detection of weak acids and CO_2 in trigeminal ganglia, and the response is highly specific to neurons expressing TRPA1 (Wang et al., 2010b, 2011). CO_2 or weak acid application also acidifies the cytosol, so intracellular protons bind TRPA1, activating it, which depolarizes neurons. Similar results have been obtained by blocking Na^+-H^+ exchanger 1 (NHE1), which is the main proton pump expressed by DRG neurons and is important for maintaining intracellular pH homeostasis. NHE1 extrudes H^+ to the extracellular space, increasing the pH in the intracellular compartment. Intracellular acidification induced by zoniporide (a specific blocker of NHE1) directly activates TRPA1 and inhibits its desensitization, increasing calcium entry during intracellular acidosis in TRPA1-expressing neurons (Martínez-Rojas et al., 2021). In painful conditions, such as inflammatory pain, NHE1 expression is downregulated; consequently, intracellular pH acidification produces sensitization of DRG neurons and hyperalgesia, which is in part prevented by TRPA1 blockers.

Expression of TRPA1 Across the DRG

Transient receptor potential Ankiryn subtype 1 is expressed by small-DRG neurons. Neurons expressing TRPA1 almost always express TRPV1 channels, and approximately half of the neurons that respond to capsaicin also respond to mustard oil or some other TRPA1 agonist (Bautista et al., 2005). Additionally, TRPA1 has a high degree of colocalization with CRGP, SP, and IB4 (Bautista et al., 2005; Kim et al., 2010). The expression of TRPA1 in medium- or large-diameter DRG neurons was almost absent (less than 6% of large neurons). TRPA1 was found to be functionally expressed by a significant proportion of nonpeptidergic neurons (NP; 80% of TRPA1-responsive neurons to MO bind IB4) but not in a great proportion of CRGP+ neurons (only 20% of CRGP+ neurons responded to MO; Barabas et al., 2012). This last is supported by transcriptomic studies in DRGs, where higher TRPA1 expression was detected in nonpeptidergic neurons than in peptidergic nociceptors (Usoskin et al., 2015; Zeisel et al., 2018).

BIOCHEMICAL MARKERS IN DRG SUBPOPULATIONS AND SINGLE-CELL TRANSCRIPTOMIC ANALYSIS

Almost every neuronal marker shows some degree of overlap between neuronal subgroups. The lectin IB4, used for dividing

nociceptors in most of the reports of acid-induced currents we have reviewed, is not 100 % accurate. Some subpopulations of nonpeptidergic (CGRP-) but IB4− C fibers exist in the mouse DRG (Patil et al., 2018), and approximately 10% of CGRP+ neurons bind IB4 (McCoy et al., 2013). Furthermore, Price et al. (2000) showed that there are a substantial number of peptidergic (CGRP+) neurons that bind IB4 in rats. This overlap between CGRP and IB4 occurs to a lesser extent in mice (Price and Flores, 2007). The relationship between soma diameter and fiber type, despite reflecting normal distributions, is also overlapping (Lawson et al., 2019).

Neuropeptide expression is another example of overlapping between subtypes. Labeling nociceptors as "nonpeptidergic" does not mean they do not express neuropeptides (i.e., Calca and Tac1 genes). New classifications of mouse DRG neurons have emerged based on single-cell mRNA sequencing overcoming these inherent biases (Usoskin et al., 2015; Zeisel et al., 2018). A combination of markers is encouraged for successful identification of a subtype. Combinations of classical/new markers have already been validated *in vivo*, and a handful of other markers have been proposed (Usoskin et al., 2015).

Extensive evidence has shown that peptidergic C nociceptors are responsible for thermal sensation and pain in response to noxious heat or capsaicin. These heat nociceptors can release neuropeptides and other agents involved in cutaneous inflammation. In contrast, nonpeptidergic nociceptors sense noxious mechanical pain, and some produce itch by chemical irritants (Crawford and Caterina, 2020). This major division of nociceptors in peptidergic and NPs was confirmed in the emerging classifications based on transcriptional profiles. Usoskin et al. (2015) identified 11 groups of neurons: five myelinated A-fiber neurons, of which three are likely LTMRs (NF1, NF2 and NF3) and two are likely proprioceptive (NF4 and NF5). Peptidergic neurons are classified into two groups: unmyelinated C-fibers (PEP1) and lightly myelinated Aδ-type (PEP2; Usoskin et al., 2015). Three groups of nonpeptidergic neurons (NP1, NP2 and NP3) were identified. The clustering of C nociceptors, however, was more comprehensive in the study by Zeisel et al. (2018), which was possible because of the much larger number of neurons sequenced. In the nonpeptidergic population, two subgroups within each of the NP1 and NP2 clusters were identified. In the peptidergic population, PEP1 neurons are classified into four different groups (PSEP2 to PSEP5; Zeisel et al., 2018; **Figure 3**). That said, there are at least 18 types of neurons in the DRG, and there is a strong correlation between subtype and function (Emery and Ernfors, 2020).

It is worth noting that although this unbiased classification has many advantages, such as the lack of overlapping populations, it is still a picture of the DRG that requires functional validation for most of the resulting clusters; hence, it has opened many opportunities for hypothesis testing regarding the coding of sensory stimuli. Additionally, the conclusions obtained from the search of acid-sensing receptor expression data are complementary to the conclusions obtained with the evidence presented to date.

EXPRESSION OF ASIC1, ASIC3, TRPV1, AND TRPA1 IN SINGLE-CELL TRANSCRIPTOMIC ANALYSIS

Data on differentially expressed genes in the DRG (Usoskin et al., 2015) and the whole nervous system transcriptome (Zeisel et al., 2018) are publicly available in online datasets.[1] The contrast between the two clustering systems shows consistency of expression for all genes among groups, despite clustering differences. Here, we collected and compared the expression levels of the most acid-sensitive ASIC subunits, ASIC1 and ASIC3, for TRPV1 and the emerging acid-sensitive TRPA1 channel (**Figure 2**).

ASIC1 and ASIC3 Are Not Expressed by Nonpeptidergic Nociceptors

ASIC1 and ASIC3 expression is abundant in two clusters of DRG neurons: NF and PEP. The highest expression of ASIC1 channels is reported in large myelinated Aβ neurons (NF4/5). ASIC1 is also expressed in PEP1 and TRPM8+ cells but is absent from NP neurons. Large myelinated Aβ neurons (NF4/5) also express high levels of ASIC3, which has been linked to proprioceptive mechanotransduction in this population (Lin et al., 2016). However, the highest expression of ASIC3 was found in Aδ nociceptors (PEP2), and similar to ASIC1, ASIC3 was also absent from NP neurons (**Figure 3**). This largely coincides with the results of mRNA detection showing that neither of the two ASIC1 isoforms, ASIC1a or ASIC1b, can be detected in IB4+ neurons and that ASIC3 expression is lowest in this group (Papalampropoulou-Tsiridou et al., 2020). Contrary to the ASIC1 and ASIC3 subunits, the expression of the least sensitive ASIC2 subunit is almost homogenous across the DRG. Thus, ASIC1 and ASIC3 are not expressed by nonpeptidergic nociceptors, which agrees with electrophysiological, immunohistochemical, and *in situ* hybridization studies.

TRPV1 Is Characteristic of All Peptidergic Subpopulations, but TRPA1 Is Expressed in Higher Amounts by Nonpeptidergic Neurons

Transient receptor potential vanilloid 1 expression is a feature of all PEP neurons, including C-type nociceptors, Aδ nociceptors, and TRPM8+ neurons. Additionally, TRPV1 was also present in the two groups of NP nociceptors. This pattern of TRPV1 largely coincides with the expected results of electrophysiological (Patil et al., 2018) and reporter gene studies (Cavanaugh et al., 2011). The expression of TRPA1 is very restricted: it is found in specific subpopulations of PEP but mostly in NP neurons. The expression of both TRP channels is negligible in Aβ myelinated neurons. Thus, TRPV1 is characteristic of all peptidergic populations, whereas TRPA1 expression is more restricted (**Figure 3**).

[1]http://linnarssonlab.org/data/

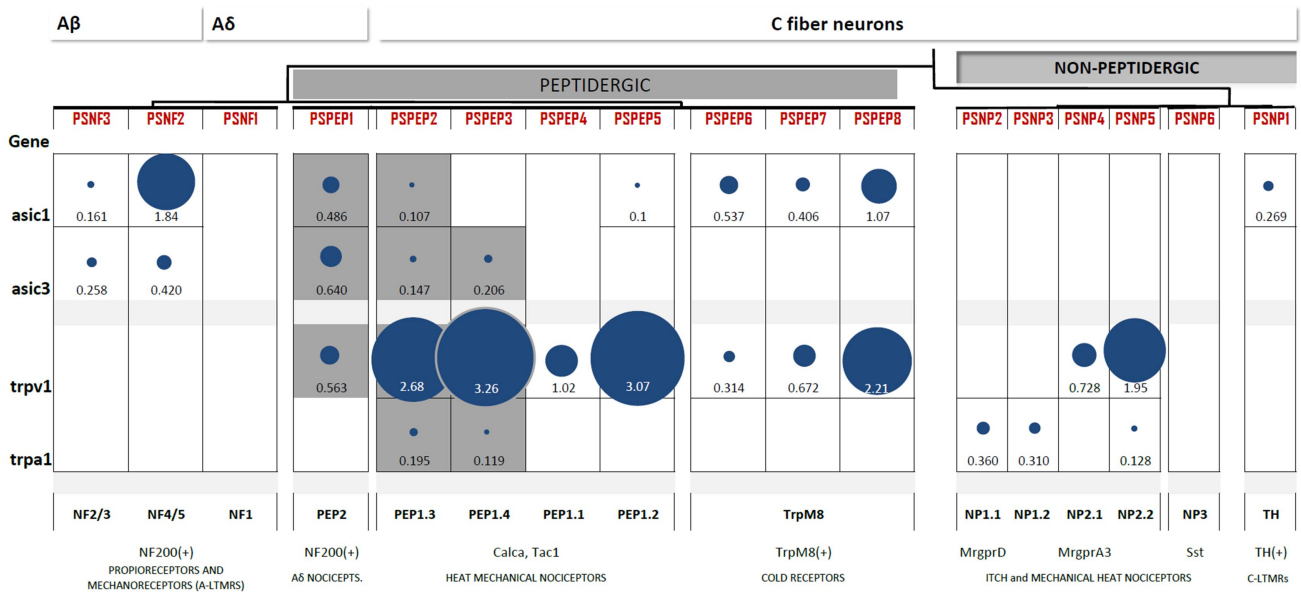

FIGURE 3 | Heterogeneous expression of ASIC1, ASIC3, TRPV1, and TRPA1 channels among subpopulations of DRG neurons. Differential gene expression data generated by Zeisel et al. (2018) available at http://mousebrain.org/genesearch.html. For each gene, numbers are normalized expression levels, and circle size represents relative expression among all clusters. Only those clusters with expression levels above 0.1 for the corresponding gene are shown. Equivalence to clusters reported in Usoskin et al. (2015) is described below, along with some important markers and likely functions per cluster. The subpopulations of nociceptors expressing both TRP and ASIC channels are highlighted in grey.

Some Peptidergic Subpopulations Combine Acid-Sensitive ASIC and TRP Channels

Only three subpopulations of PEP neurons combine acid-sensitive ASIC and TRP channel expression: PSPEP1 (Aδ nociceptors), PSEP2, and PSEP3 (both mechano-heat noxious neurons; **Figure 3**). This observation agrees with the findings of the distribution of acid-induced currents, we reviewed in the previous section, in which we concluded that there is a prevalence of acid-induced currents in the peptidergic C-nociceptor population. Thus, based on these two lines of evidence, we hypothesize that peptidergic nociceptors are better suited to transduce H^+ stimuli than nonpeptidergic nociceptors.

At the Subpopulation Level, PEP1 Neurons Have Not Been Attributed Specific Sensory Roles

For clarity, in all sections ahead, we will exclude the PSNP6–8 TRPM8+ cluster of cold-related neurons, which are unrelated to acid nociception, and the PSNP1 TH+ cluster of C-LTMRs, as that population does not sense noxious stimuli.

PEP2 (PSEP1) neurons are lightly myelinated Aδ nociceptors. This cluster of Aδ fibers is different from the Aδ-LTMRs innervating longitudinal lanceolate endings (Zimmerman et al., 2014), which are likely represented by the PSNF1 cluster (**Figure 3**). In addition to the myelin marker NF200, they also express CGRP and the TrkA receptor (Fang, 2005), the latter of which do not stain Aβ myelinated neurons. Aδ nociceptors have some degree of overlap with Aβ fibers with respect to diameter and conduction velocities, and they constitute less than 4% of total DRG neurons (Djouhri and Lawson, 2004; Lawson et al., 2019). Additionally, Aδ nociceptors are considered to be sensors of the "first pain" to noxious heat (which humans perceive as a cold sensation; Treede et al., 1998). Cutaneous Aδ nociceptors sensitize to mechanical stimuli after inflammation, similar to their C-fiber counterparts (Andrew and Greenspan, 1999; Potenzieri et al., 2008). Thus, Aδ nociceptors have a mechano-heat-noxious role as PEP1 C fibers do but with faster conduction velocities.

PEP1 (PSPEP2–5) neurons are unmyelinated nociceptors. As a group, they are defined by the expression of the marker Tac1. This nociceptor group is formed by classical mechano-heat noxious neurons (Emery and Ernfors, 2020). Notably, the subpopulations PSPEP2 and PSPEP3 combine TRPV1 and TRPA1 expression and could represent the main thermal nociceptors (i.e., C-type heat nociceptors) given that the triple deletion of TRPV1 + TRPA1 + TRMP3 abolishes noxious heat perception (Vandewauw et al., 2018). In addition, it is possible that the so-called "silent nociceptors" could correspond to some subpopulation of the PEP1 cluster. These unresponsive neurons are likely represented by mechanical-insensitive and heat-insensitive type C-neurons (cMiHis) and are present in both PEP and NP nociceptors (Lawson et al., 2019). Silent nociceptors are a group of peptidergic (CGRP+, IB4−, and TrkA+) C neurons expressing CHRNA3 and are sensitized to mechanical stimuli upon inflammation (Prato et al., 2017). Interestingly, the inflammation mediator PGE2 sensitizes C-type mechanically insensitive nociceptors (CMi). Whether thermal and/or silent

nociceptors are indeed represented by discrete subpopulations of the PEP1 cluster remains to be demonstrated.

Another possibility is that PEP1 subpopulations could represent different transcriptional states of the same neuronal group, as was considered by Usoskin et al. (2015), to reconcile the evidence for polymodality with the evidence for neuronal diversity. A recent study described the stimulus responsiveness (i.e., mechanical, heat, mechanical-heat, etc.) of DRG neurons innervating cutaneous tissue, in which neurons were clustered based on single-cell transcriptional profiling of 28 selected genes (Adelman et al., 2019). Cutaneous PEP neurons include two main types of nociceptors: C-type heat nociceptors (CHs) and polymodal C-type mechanical and heat nociceptors (CMHs), whereas NP neurons mainly include C-type mechanical nociceptors (CMs) and polymodal CMHs (Adelman et al., 2019).

Both groups of cutaneous nociceptors, PEP and NP, include CMHs, which are the most common type of C-type polymodal nociceptors (cPMNs) in the DRG (Dubin and Patapoutian, 2010; Lawson et al., 2019). Since the majority of CMHs and cPMNs in general are nonpeptidergic IB4+ nociceptors (Rau et al., 2009; Adelman et al., 2019), the role of PEP1 neurons as polymodal nociceptors seems less likely. Previous reports in cutaneous peptidergic neurons (SP+) of mice showed that CMHs also responded to the application of acid (pH 5) *via* ASIC3 (Price et al., 2001).

There are important differences between peptidergic nociceptors innervating muscle and cutaneous tissue. Unlike cutaneous DRG neurons, neurons innervating muscle appear to be clustered in different subpopulations; in particular, the PEP cluster of nociceptors displays more transcriptional variation, suggesting different subtypes in comparison to skin-innervating peptidergic neurons (Adelman et al., 2019). Importantly, more than 50% of Aδ or C muscle afferents (groups III and IV) are chemosensitive, with a very low percentage being polymodal and only 18% of the muscle afferents being silent nociceptors (Jankowski et al., 2013). Chemosensitive neurons innervating muscle are classified into two groups: (1) metaboreceptors, which sense a slight decrease in acidity (pH 7.0), low levels of lactic acid and ATP (Light et al., 2008), and (2) metabonociceptors, which respond to higher levels of lactic acid and ATP and higher acidity (pH 6.6). Both Aδ and C muscle-innervating metabonociceptors were found to be TRPV1+ and ASIC3+, whereas nonnociceptive metaboreceptors were TRPV1− and ASIC3− (Jankowski et al., 2013). This suggests that acid-sensitive Aδ and C muscle nociceptors are likely to be PEP neurons, the only cluster containing subpopulations expressing TRPV1 and ASIC3 together.

Thus, the assignment of distinct functional roles among PEP subpopulations is further complicated by the different innervated target tissues. It is more frequent for peptidergic (CGRP+) fibers to terminate in deeper tissues than nonpeptidergic (IB4+ or MrgprD+) fibers (Zylka et al., 2005). Accordingly, the majority of visceral afferents are peptidergic (CGRP+; Robinson and Gebhart, 2008), and the majority of silent nociceptors also innervate deep tissues (Prato et al., 2017). In fact, it has been argued that the PSPEP2 subpopulation might innervate cutaneous tissue, and the PSPEP3 subpopulation innervates deeper tissues (Emery and Ernfors, 2020).

ASIC3 and TRPV1 were coexpressed in only three peptidergic subpopulations of DRG neurons. PSEP1 neurons have a defined role as myelinated nociceptors and are susceptible to sensitization by inflammation. PSEP2 and PSPEP3 neurons likely represent heat nociceptors but, since they are part of the PEP1 cluster, may include mechanical-heat polymodal fibers, especially in the case of cutaneous afferents. In muscle afferents, it is possible that the PSEP2 subpopulation senses noxious acidosis.

CONCLUSION

In this work, we reviewed the characteristics of proton-gated ion channels, which once exposed to low pH increase the neuronal excitability in DRG nociceptors. ASICs and TRP (particularly V1 and A1 subtypes) are strong candidates for proton sensing in the somatosensory system. Experimental evidence about the nocifensive response against acid insult showed that most of these proteins participate in acid sensing, but as previously mentioned, abolishing only one of them does not produce an acid insult-insensitive phenotype.

The pattern and high titers of expression of proton-gated channels are restricted to a subset of PEP small-diameter neurons. This is intriguing since it suggests that acid sensing in nociceptors might be coded in a labeled-line fashion. Whichever the case, the selective ablation of some peptidergic subpopulations could give us a phenotype unresponsive to acidic insults.

Since chemical nociception is the less well-described nociceptive modality, it is important to complete the picture of how nociceptors are activated. It is not documented that the population responsible for activation by an acidic insult is worth finding. It will be interesting to determine whether acid detection by nociceptors obeys labeled-line coding, as occurs for noxious-mechanical or noxious-heat stimuli. Once identified, the physiology of acid-activated nociceptors could be better studied during nociceptive pain and better characterized during the genesis or maintenance of pathologically painful conditions.

AUTHOR CONTRIBUTIONS

OP collected the bibliographic information, elaborated the figure, and conceived and wrote the manuscript. PS-C reviewed the bibliographic information and the manuscript. AA conceived and reviewed the final version of the manuscript. FP reviewed the manuscript. FM supervised the work, collected bibliographic information, and conceived, wrote, and reviewed the final version of the manuscript. All authors contributed to the article and approved the submitted version.

FUNDING

This work was supported by an INPRFM grant (NC12165994.0) to FM.

REFERENCES

Abrahamsen, B., Zhao, J., Asante, C. O., Cendan, C. M., Marsh, S., Martinez-Barbera, J. P., et al. (2008). The cell and molecular basis of mechanical, cold, and inflammatory pain. *Science* 321, 702–705. doi: 10.1126/science.1156916

Adelman, P. C., Baumbauer, K. M., Friedman, R., Shah, M., Wright, M., Young, E., et al. (2019). Single-cell q-PCR derived expression profiles of identified sensory neurons. *Mol. Pain* 15:1744806919884496. doi: 10.1177/1744806919884496

Alvarez de la Rosa, D., Zhang, P., Shao, D., White, F., and Canessa, C. M. (2002). Functional implications of the localization and activity of acid-sensitive channels in rat peripheral nervous system. *Proc. Natl. Acad. Sci. U. S. A.* 99, 2326–2331. doi: 10.1073/pnas.042688199

Andrew, D., and Greenspan, J. D. (1999). Mechanical and heat sensitization of cutaneous nociceptors after peripheral inflammation in the rat. *J. Neurophysiol.* 82, 2649–2656. doi: 10.1152/jn.1999.82.5.2649

Babini, E., Paukert, M., Geisler, H. S., and Gründer, S. (2002). Alternative splicing and interaction with di- and polyvalent cations control the dynamic range of acid-sensing ion channel 1 (ASIC1). *J. Biol. Chem.* 277, 41597–41603. doi: 10.1074/jbc.M205877200

Barabas, M. E., Kossyreva, E. A., and Stucky, C. L. (2012). TRPA1 is functionally expressed primarily by IB4-binding, non-peptidergic mouse and rat sensory neurons. *PLoS One* 7:e47988. doi: 10.1371/journal.pone.0047988

Bartoi, T., Augustinowski, K., Polleichtner, G., Grunder, S., and Ulbrich, M. H. (2014). Acid-sensing ion channel (ASIC) 1a/2a heteromers have a flexible 2:1/1:2 stoichiometry. *Proc. Natl. Acad. Sci. U. S. A.* 111, 8281–8286. doi: 10.1073/pnas.1324060111

Baumann, T. K., and Martenson, M. E. (2000). Extracellular protons both increase the activity and reduce the conductance of capsaicin-gated channels. *J. Neurosci.* 20:RC80. doi: 10.1523/JNEUROSCI.20-11-j0004.2000

Bautista, D. M., Movahed, P., Hinman, A., Axelsson, H. E., Sterner, O., Högestätt, E. D., et al. (2005). Pungent products from garlic activate the sensory ion channel TRPA1. *Proc. Natl. Acad. Sci. U. S. A.* 102, 12248–12252. doi: 10.1073/pnas.0505356102

Beaulieu-Laroche, L., Christin, M., Donoghue, A., Agosti, F., Yousefpour, N., Petitjean, H., et al. (2020). TACAN is an ion channel involved in sensing mechanical pain. *Cell* 180, 956.e17–967.e17. doi: 10.1016/j.cell.2020.01.033

Benson, C. J., Xie, J., Wemmie, J. A., Price, M. P., Henss, J. M., Welsh, M. J., et al. (2001). Heteromultimers of DEGENaC subunits form H-gated channels in mouse sensory neurons. *Proc. Natl. Acad. Sci. U. S. A.* 99, 2338–2343. doi: 10.1073/pnas.032678399

Blanchard, M. G., and Kellenberger, S. (2011). Effect of a temperature increase in the non-noxious range on proton-evoked ASIC and TRPV1 activity. *Pflugers Arch.* 461, 123–139. doi: 10.1007/s00424-010-0884-3

Breese, N. M., George, A. C., Pauers, L. E., and Stucky, C. L. (2005). Peripheral inflammation selectively increases TRPV1 function in IB4-positive sensory neurons from adult mouse. *Pain* 115, 37–49. doi: 10.1016/j.pain.2005.02.010

Caterina, M. J., Leffler, A., Malmberg, A. B., Martin, W. J., Trafton, J., Petersen-Zeitz, K. R., et al. (2000). Impaired nociception and pain sensation in mice lacking the capsaicin receptor. *Science* 288, 306–313. doi: 10.1126/science.288.5464.306

Caterina, M. J., Schumacher, M. A., Tominaga, M., Rosen, T. A., Levine, J. D., and Julius, D. (1997). The capsaicin receptor: a heat-activated ion channel in the pain pathway. *Nature* 389, 816–824. doi: 10.1038/39807

Cavanaugh, D. J., Chesler, A. T., Bráz, J. M., Shah, N. M., Julius, D., and Basbaum, A. I. (2011). Restriction of transient receptor potential vanilloid-1 to the peptidergic subset of primary afferent neurons follows its developmental downregulation in nonpeptidergic neurons. *J. Neurosci.* 31, 10119–10127. doi: 10.1523/JNEUROSCI.1299-11.2011

Cavanaugh, D. J., Lee, H., Lo, L., Shields, S. D., Zylka, M. J., Basbaum, A. I., et al. (2009). Distinct subsets of unmyelinated primary sensory fibers mediate behavioral responses to noxious thermal and mechanical stimuli. *Proc. Natl. Acad. Sci. U. S. A.* 106, 9075–9080. doi: 10.1073/pnas.0901507106

Chen, X., Kalbacher, H., and Gründer, S. (2005). The tarantula toxin psalmotoxin 1 inhibits acid-sensing ion channel (ASIC) 1a by increasing its apparent H+ affinity. *J. Gen. Physiol.* 126, 71–79. doi: 10.1085/jgp.200509303

Crawford, L. K., and Caterina, M. J. (2020). Functional anatomy of the sensory nervous system: updates from the neuroscience bench. *Toxicol. Pathol.* 48, 174–189. doi: 10.1177/0192623319869011

de la Roche, J., Eberhardt, M. J., Klinger, A. B., Stanslowsky, N., Wegner, F., Koppert, W., et al. (2013). The molecular basis for species-specific activation of human TRPA1 protein by protons involves poorly conserved residues within transmembrane domains 5 and 6. *J. Biol. Chem.* 288, 20280–20292. doi: 10.1074/jbc.M113.479337

Delaunay, A., Gasull, X., Salinas, M., Noedl, J., Friend, V., Lingueglia, E., et al. (2012). Human ASIC3 channel dynamically adapts its activity to sense the extracellular pH in both acidic and alkaline directions. *Proc. Natl. Acad. Sci. U. S. A.* 109, 13124–13129. doi: 10.1073/pnas.1120350109

Deval, E., Noël, J., Lay, N., Alloui, A., Diochot, S., Friend, V., et al. (2008). ASIC3, a sensor of acidic and primary inflammatory pain. *EMBO J.* 27, 3047–3055. doi: 10.1038/emboj.2008.213

Dhaka, A., Murray, A. N., Mathur, J., Earley, T. J., Petrus, M. J., and Patapoutian, A. (2007). TRPM8 is required for cold sensation in mice. *Neuron* 54, 371–378. doi: 10.1016/j.neuron.2007.02.024

Dirajlal, S., Pauers, L. E., and Stucky, C. L. (2003). Differential response properties of IB 4-positive and-negative unmyelinated sensory neurons to protons and capsaicin. *J. Neurophysiol.* 89, 513–524. doi: 10.1152/jn.00371.00371.2002

Djouhri, L., and Lawson, S. N. (2004). Aβ-fiber nociceptive primary afferent neurons: a review of incidence and properties in relation to other afferent A-fiber neurons in mammals. *Brain Res. Rev.* 46, 131–145. doi: 10.1016/j.brainresrev.2004.07.015

Drew, L. J., Rohrer, D. K., Price, M. P., Blaver, K. E., Cockayne, D. A., Cesare, P., et al. (2004). Acid-sensing ion channels ASIC2 and ASIC3 do not contribute to mechanically activated currents in mammalian sensory neurones. *J. Physiol.* 556, 691–710. doi: 10.1113/jphysiol.2003.058693

Dubin, A. E., and Patapoutian, A. (2010). Nociceptors: the sensors of the pain pathway. *J. Clin. Invest.* 120, 3760–3772. doi: 10.1172/JCI42843

Dulai, J. S., Smith, E. S. J., and Rahman, T. (2021). Acid-sensing ion channel 3: an analgesic target. *Channels* 15, 94–127. doi: 10.1080/19336950.2020.1852831

Emery, E. C., and Ernfors, P. (2020). "Dorsal root ganglion neuron types and their functional specialization," in *The Oxford Handbook of the Neurobiology of Pain*. ed. J. N. Wood (Oxford, United Kingdom: Oxford University Press).

Emery, E. C., Luiz, A. P., Sikandar, S., Magnúsdóttir, R., Dong, X., and Wood, J. N. (2016). In vivo characterization of distinct modality-specific subsets of somatosensory neurons using GCaMP. *Sci. Adv.* 2:e1600990. doi: 10.1126/sciadv.1600990

Emery, E. C., and Wood, J. N. (2019). Somatosensation a la mode: plasticity and polymodality in sensory neurons. *Curr. Opin. Physiol.* 11, 29–34. doi: 10.1016/j.cophys.2019.04.014

Fang, X. (2005). trkA is expressed in nociceptive neurons and influences electrophysiological properties via Nav1.8 expression in rapidly conducting nociceptors. *J. Neurosci.* 25, 4868–4878. doi: 10.1523/JNEUROSCI.0249-05.2005

Fang, X., Djouhri, L., McMullan, S., Berry, C., Waxman, S. G., Okuse, K., et al. (2006). Intense isolectin-B4 binding in rat dorsal root ganglion neurons distinguishes C-fiber nociceptors with broad action potentials and high Nav1.9 expression. *J. Neurosci.* 26, 7281–7292. doi: 10.1523/JNEUROSCI.1072-06.2006

Garcia-Sanz, N. (2004). Identification of a tetramerization domain in the C terminus of the vanilloid receptor. *J. Neurosci.* 24, 5307–5314. doi: 10.1523/JNEUROSCI.0202-04.2004

Gautam, M., and Benson, C. J. (2013). Acid-sensing ion channels (ASICs) in mouse skeletal muscle afferents are heteromers composed of ASIC1a, ASIC2, and ASIC3 subunits. *FASEB J.* 27, 793–802. doi: 10.1096/fj.12-220400

Goswami, S. C., Mishra, S. K., Maric, D., Kaszas, K., Gonnella, G. L., Clokie, S. J., et al. (2014). Molecular signatures of mouse TRPV1-lineage neurons revealed by RNA-seq transcriptome analysis. *J. Pain* 15, 1338–1359. doi: 10.1016/j.jpain.2014.09.010

Gründer, S., and Pusch, M. (2015). Biophysical properties of acid-sensing ion channels (ASICs). *Neuropharmacology* 94, 9–18. doi: 10.1016/j.neuropharm.2014.12.016

Hesselager, M., Timmermann, D. B., and Ahring, P. K. (2004). pH dependency and desensitization kinetics of heterologously expressed combinations of acid-sensing ion channel subunits. *J. Biol. Chem.* 279, 11006–11015. doi: 10.1074/jbc.M313507200

Hjerling-Leffler, J., AlQatari, M., Ernfors, P., and Koltzenburg, M. (2007). Emergence of functional sensory subtypes as defined by transient receptor potential channel expression. *J. Neurosci.* 27, 2435–2443. doi: 10.1523/JNEUROSCI.5614-06.2007

Jankowski, M. P., Rau, K. K., Ekmann, K. M., Anderson, C. E., and Koerber, H. R. (2013). Comprehensive phenotyping of group III and IV muscle afferents in mouse. *J. Neurophysiol.* 109, 2374–2381. doi: 10.1152/jn.01067.2012

Jasti, J., Furukawa, H., Gonzales, E. B., and Gouaux, E. (2007). Structure of acid-sensing ion channel 1 at 1.9Å resolution and low pH. *Nature* 449, 316–323. doi: 10.1038/nature06163

Jones, N. G., Slater, R., Cadiou, H., McNaughton, P., and McMahon, S. B. (2004). Acid-induced pain and its modulation in humans. *J. Neurosci.* 24, 10974–10979. doi: 10.1523/JNEUROSCI.2619-04.2004

Jordt, S.-E., Bautista, D. M., Chuang, H.-H., McKemy, D. D., Zygmunt, P. M., Högestätt, E. D., et al. (2004). Mustard oils and cannabinoids excite sensory nerve fibres through the TRP channel ANKTM1. *Nature* 427, 260–265. doi: 10.1038/nature02282

Jordt, S.-E., and Julius, D. (2002). Molecular basis for species-specific sensitivity to "hot" chili peppers. *Cell* 108, 421–430. doi: 10.1016/S0092-8674(02)00637-2

Jordt, S.-E., Tominaga, M., and Julius, D. (2000). Acid potentiation of the capsaicin receptor determined by a key extracellular site. *Proc. Natl. Acad. Sci. U. S. A.* 97, 8134–8139. doi: 10.1073/pnas.100129497

Kim, Y. S., Son, J. Y., Kim, T. H., Paik, S. K., Dai, Y., Noguchi, K., et al. (2010). Expression of transient receptor potential ankyrin 1 (TRPA1) in the rat trigeminal sensory afferents and spinal dorsal horn. *J. Comp. Neurol.* 518, 687–698. doi: 10.1002/cne.22238

Krauson, A. J., and Carattino, M. D. (2016). The thumb domain mediates acid-sensing ion channel desensitization. *J. Biol. Chem.* 291, 11407–11419. doi: 10.1074/jbc.M115.702316

Law, L. A. F., Sluka, K. A., McMullen, T., Lee, J., Arendt-Nielsen, L., and Graven-Nielsen, T. (2008). Acidic buffer induced muscle pain evokes referred pain and mechanical hyperalgesia in humans. *Pain* 140, 254–264. doi: 10.1016/j.pain.2008.08.014

Lawson, S. N., Fang, X., and Djouhri, L. (2019). Nociceptor subtypes and their incidence in rat lumbar dorsal root ganglia (DRGs): focusing on C-polymodal nociceptors, Aβ-nociceptors, moderate pressure receptors and their receptive field depths. *Curr. Opin. Physiol.* 11, 125–146. doi: 10.1016/j.cophys.2019.10.005

Leffler, A., Mönter, B., and Koltzenburg, M. (2006). The role of the capsaicin receptor TRPV1 and acid-sensing ion channels (ASICS) in proton sensitivity of subpopulations of primary nociceptive neurons in rats and mice. *Neuroscience* 139, 699–709. doi: 10.1016/j.neuroscience.2005.12.020

Li, T., Yang, Y., and Canessa, C. M. (2009). Interaction of the aromatics Tyr-72/Trp-288 in the interface of the extracellular and transmembrane domains is essential for proton gating of acid-sensing ion channels. *J. Biol. Chem.* 284, 4689–4694. doi: 10.1074/jbc.M805302200

Liao, M., Cao, E., Julius, D., and Cheng, Y. (2013). Structure of the TRPV1 ion channel determined by electron cryo-microscopy. *Nature* 504, 107–112. doi: 10.1038/nature12822

Liechti, L. A., Bernèche, S., Bargeton, B., Iwaszkiewicz, J., Roy, S., Michielin, O., et al. (2010). A combined computational and functional approach identifies new residues involved in pH-dependent gating of ASIC1a. *J. Biol. Chem.* 285, 16315–16329. doi: 10.1074/jbc.M109.092015

Light, A. R., Hughen, R. W., Zhang, J., Rainier, J., Liu, Z., and Lee, J. (2008). Dorsal root ganglion neurons innervating skeletal muscle respond to physiological combinations of protons, ATP, and lactate mediated by ASIC, P2X, and TRPV1. *J. Neurophysiol.* 100, 1184–1201. doi: 10.1152/jn.01344.2007

Lin, S.-H., Cheng, Y.-R., Banks, R. W., Min, M.-Y., Bewick, G. S., and Chen, C.-C. (2016). Evidence for the involvement of ASIC3 in sensory mechanotransduction in proprioceptors. *Nat. Commun.* 7:11460. doi: 10.1038/ncomms11460

Liu, M., Willmott, N. J., Michael, G. J., and Priestley, J. V. (2004). Differential pH and capsaicin responses of *Griffonia simplicifolia* IB4 (IB4)-positive and IB4-negative small sensory neurons. *Neuroscience* 127, 659–672. doi: 10.1016/j.neuroscience.2004.05.041

Luiz, A. P., MacDonald, D. I., Santana-Varela, S., Millet, Q., Sikandar, S., Wood, J. N., et al. (2019). Cold sensing by Na V 1.8-positive and Na V 1.8-negative sensory neurons. *Proc. Natl. Acad. Sci. U. S. A.* 116, 3811–3816. doi: 10.1073/pnas.1814545116

Martínez-Rojas, V. A., Salinas-Abarca, A. B., Gómez-Víquez, N. L., Granados-Soto, V., Mercado, F., and Murbartián, J. (2021). Interaction of NHE1 and TRPA1 activity in DRG neurons isolated from adult rats and its role in inflammatory nociception. *Neuroscience* 465, 154–165. doi: 10.1016/j.neuroscience.2021.04.025

McCoy, E. S., Taylor-Blake, B., Street, S. E., Pribisko, A. L., Zheng, J., and Zylka, M. J. (2013). Peptidergic CGRPα primary sensory neurons encode heat and itch and tonically suppress sensitivity to cold. *Neuron* 78, 138–151. doi: 10.1016/j.neuron.2013.01.030

Mitchell, K., Lebovitz, E. E., Keller, J. M., Mannes, A. J., Nemenov, M. I., and Iadarola, M. J. (2014). Nociception and inflammatory hyperalgesia evaluated in rodents using infrared laser stimulation after Trpv1 gene knockout or resiniferatoxin lesion. *Pain* 155, 733–745. doi: 10.1016/j.pain.2014.01.007

Moehring, F., Halder, P., Seal, R. P., and Stucky, C. L. (2018). Uncovering the cells and circuits of touch in normal and pathological settings. *Neuron* 100, 349–360. doi: 10.1016/j.neuron.2018.10.019

Molliver, D. C., Immke, D. C., Fierro, L., Paré, M., Rice, F. L., and McCleskey, E. W. (2005). ASIC3, an acid-sensing ion channel, is expressed in metaboreceptive sensory neurons. *Mol. Pain* 1:35. doi: 10.1186/1744-8069-1-35

Neelands, T. R., Jarvis, M. F., Han, P., Faltynek, C. R., and Surowy, C. S. (2005). Acidification of rat TRPV1 alters the kinetics of capsaicin responses. *Mol. Pain* 1:28. doi: 10.1186/1744-8069-1-28

Neelands, T. R., Zhang, X.-F., McDonald, H., and Puttfarcken, P. (2010). Differential effects of temperature on acid-activated currents mediated by TRPV1 and ASIC channels in rat dorsal root ganglion neurons. *Brain Res.* 1329, 55–66. doi: 10.1016/j.brainres.2010.02.064

Papalampropoulou-Tsiridou, M., Labrecque, S., Godin, A. G., De Koninck, Y., and Wang, F. (2020). Differential expression of acid—sensing ion channels in mouse primary afferents in naïve and injured conditions. *Front. Cell. Neurosci.* 14:103. doi: 10.3389/fncel.2020.00103

Patil, M. J., Hovhannisyan, A. H., and Akopian, A. N. (2018). Characteristics of sensory neuronal groups in CGRP-cre-ER reporter mice: comparison to Nav1.8-cre, TRPV1-cre and TRPV1-GFP mouse lines. *PLoS One* 13:e0198601. doi: 10.1371/journal.pone.0198601

Paukert, M., Chen, X., Polleichtner, G., Schindelin, H., and Gründer, S. (2008). Candidate amino acids involved in H+ gating of acid-sensing ion channel 1a. *J. Biol. Chem.* 283, 572–581. doi: 10.1074/jbc.M706811200

Perl, E. R. (1996). Cutaneous polymodal receptors: characteristics and plasticity. *Prog. Brain Res.* 113, 21–37. doi: 10.1016/s0079-6123(08)61079-1

Petruska, J. C., Napaporn, J., Johnson, R. D., Gu, J. G., and Cooper, B. Y. (2000). Subclassified acutely dissociated cells of rat DRG: histochemistry and patterns of capsaicin-, proton-, and ATP-activated currents. *J. Neurophysiol.* 84, 2365–2379. doi: 10.1152/jn.2000.84.5.2365

Poirot, O., Berta, T., Decosterd, I., and Kellenberger, S. (2006). Distinct ASIC currents are expressed in rat putative nociceptors and are modulated by nerve injury. *J. Physiol.* 576, 215–234. doi: 10.1113/jphysiol.2006.113035

Potenzieri, C., Brink, T. S., Pacharinsak, C., and Simone, D. A. (2008). Cannabinoid modulation of cutaneous Aδ nociceptors during inflammation. *J. Neurophysiol.* 100, 2794–2806. doi: 10.1152/jn.90809.2008

Prato, V., Taberner, F. J., Hockley, J. R. F., Callejo, G., Arcourt, A., Tazir, B., et al. (2017). Functional and molecular characterization of mechanoinsensitive "silent" nociceptors. *Cell Rep.* 21, 3102–3115. doi: 10.1016/j.celrep.2017.11.066

Price, T. J., and Flores, C. M. (2007). Critical evaluation of the colocalization between calcitonin gene-related peptide, substance P, transient receptor potential vanilloid subfamily type 1 immunoreactivities, and isolectin B4 binding in primary afferent neurons of the rat and mouse. *J. Pain* 8, 263–272. doi: 10.1016/j.jpain.2006.09.005

Price, M. P., Lewin, G. R., McIlwrath, S. L., Cheng, C., Xie, J., Heppenstall, P. A., et al. (2000). The mammalian sodium channel BNC1 is required for normal touch sensation. *Nature* 407, 1007–1011. doi: 10.1038/35039512

Price, M. P., McIlwrath, S. L., Xie, J., Cheng, C., Qiao, J., Tarr, D. E., et al. (2001). The DRASIC cation channel contributes to the detection of cutaneous touch and acid stimuli in mice. *Neuron* 32, 1071–1083. doi: 10.1016/S0896-6273(01)00547-5

Rau, K. K., McIlwrath, S. L., Wang, H., Lawson, J. J., Jankowski, M. P., Zylka, M. J., et al. (2009). Mrgprd enhances excitability in specific populations of cutaneous murine polymodal nociceptors. *J. Neurosci.* 29, 8612–8619. doi: 10.1523/JNEUROSCI.1057-09.2009

Robinson, D. R., and Gebhart, G. F. (2008). Inside information: the unique features of visceral sensation. *Mol. Interv.* 8, 242–253. doi: 10.1124/mi.8.5.9

Rosasco, M. G., and Gordon, S. E. (2017). "TRP channels," in *Neurobiology of TRP Channels*. ed. T. L. Rosembaum (Boca Raton: CRC Press).

Roy, S., Boiteux, C., Alijevic, O., Liang, C., Bernèche, S., and Kellenberger, S. (2013). Molecular determinants of desensitization in an ENaC/degenerin channel. *FASEB J.* 27, 5034–5045. doi: 10.1096/fj.13-230680

Ryu, S., Liu, B., Yao, J., Fu, Q., and Qin, F. (2007). Uncoupling proton activation of vanilloid receptor TRPV1. *J. Neurosci.* 27, 12797–12807. doi: 10.1523/JNEUROSCI.2324-07.2007

Salinas, M., Lazdunski, M., and Lingueglia, E. (2009). Structural elements for the generation of sustained currents by the acid pain sensor ASIC3. *J. Biol. Chem.* 284, 31851–31859. doi: 10.1074/jbc.M109.043984

Schuhmacher, L.-N., and Smith, E. S. J. (2016). Expression of acid-sensing ion channels and selection of reference genes in mouse and naked mole rat. *Mol. Brain* 9:97. doi: 10.1186/s13041-016-0279-2

Schuhmacher, L. N., Srivats, S., and St. Smith, E. J. (2015). Structural domains underlying the activation of acid-sensing ion channel 2a. *Mol. Pharmacol.* 87, 561–571. doi: 10.1124/mol.114.096909

Sharma, N. K., Ryals, J. M., Liu, H., Liu, W., and Wright, D. E. (2009). Acidic saline-induced primary and secondary mechanical hyperalgesia in mice. *J. Pain* 10, 1231–1241. doi: 10.1016/j.jpain.2009.04.014

Sherwood, T. W., Lee, K. G., Gormley, M. G., and Askwith, C. C. (2011). Heteromeric acid-sensing ion channels (ASICs) composed of ASIC2b and ASIC1a display novel channel properties and contribute to acidosis-induced neuronal death. *J. Neurosci.* 31, 9723–9734. doi: 10.1523/JNEUROSCI.1665-11.2011

Sluka, K. A., Kalra, A., and Moore, S. A. (2001). Unilateral intramuscular injections of acidic saline produce a bilateral, long-lasting hyperalgesia. *Muscle Nerve* 24, 37–46. doi: 10.1002/1097-4598(200101)24:1<37::AID-MUS4>3.0.CO;2-8

Steen, K. H., and Reeh, P. W. (1993). Sustained graded pain and hyperalgesia from harmless experimental tissue acidosis in human skin. *Neurosci. Lett.* 154, 113–116. doi: 10.1016/0304-3940(93)90184-M

Story, G. M., Peier, A. M., Reeve, A. J., Eid, S. R., Mosbacher, J., Hricik, T. R., et al. (2003). ANKTM1, a TRP-like channel expressed in nociceptive neurons, is activated by cold temperatures. *Cell* 112, 819–829. doi: 10.1016/S0092-8674(03)00158-2

Stucky, C. L., and Lewin, G. R. (1999). Isolectin B 4-positive and-negative nociceptors are functionally distinct. *J. Neurosci.* 19, 6497–6505. doi: 10.1523/JNEUROSCI.19-15-06497.1999

Sutherland, S. P., Benson, C. J., Adelman, J. P., Mccleskey, E. W., and Baylor, D. (2001). Acid-sensing ion channel 3 matches the acid-gated current in cardiac ischemia-sensing neurons. *Proc. Natl. Acad. Sci. U. S. A.* 98, 711–716. doi: 10.1073/pnas.011404498

Tominaga, M., Caterina, M. J., Malmberg, A. B., Rosen, T. A., Gilbert, H., Skinner, K., et al. (1998). The cloned capsaicin receptor integrates multiple pain-producing stimuli. *Neuron* 21, 531–543. doi: 10.1016/S0896-6273(00)80564-4

Treede, R.-D., Meyer, R. A., and Campbell, J. N. (1998). Myelinated mechanically insensitive afferents from monkey hairy skin: heat-response properties. *J. Neurophysiol.* 80, 1082–1093. doi: 10.1152/jn.1998.80.3.1082

Ugawa, S., Ueda, T., Ishida, Y., Nishigaki, M., Shibata, Y., and Shimada, S. (2002). Amiloride-blockable acid-sensing ion channels are leading acid sensors expressed in human nociceptors. *J. Clin. Invest.* 110, 1185–1190. doi: 10.1172/JCI200215709

Ugawa, S., Ueda, T., Yamamura, H., and Shimada, S. (2005). In situ hybridization evidence for the coexistence of ASIC and TRPV1 within rat single sensory neurons. *Mol. Brain Res.* 136, 125–133. doi: 10.1016/j.molbrainres.2005.01.010

Usoskin, D., Furlan, A., Islam, S., Abdo, H., Lönnerberg, P., Lou, D., et al. (2015). Unbiased classification of sensory neuron types by large-scale single-cell RNA sequencing. *Nat. Neurosci.* 18, 145–153. doi: 10.1038/nn.3881

Vandewauw, I., De Clercq, K., Mulier, M., Held, K., Pinto, S., Van Ranst, N., et al. (2018). A TRP channel trio mediates acute noxious heat sensing. *Nature* 555, 662–666. doi: 10.1038/nature26137

Vullo, S., Bonifacio, G., Roy, S., Johner, N., Bernèche, S., and Kellenberger, S. (2017). Conformational dynamics and role of the acidic pocket in ASIC pH-dependent gating. *Proc. Natl. Acad. Sci. U. S. A.* 114, 3768–3773. doi: 10.1073/pnas.1620560114

Waldmann, R., Bassilana, F., de Weille, J., Champigny, G., Heurteaux, C., and Lazdunski, M. (1997a). Molecular cloning of a non-inactivating proton-gated Na+ channel specific for sensory neurons. *J. Biol. Chem.* 272, 20975–20978. doi: 10.1074/jbc.272.34.20975

Waldmann, R., Champigny, G., Bassilana, F., Heurteaux, C., and Lazdunski, M. (1997b). A proton-gated cation channel involved in acid-sensing. *Nature* 386, 173–177. doi: 10.1038/386173a0

Wang, Y. Y., Chang, R. B., Allgood, S. D., Silver, W. L., and Liman, E. R. (2011). A TRPA1-dependent mechanism for the pungent sensation of weak acids. *J. Gen. Physiol.* 137, 493–505. doi: 10.1085/jgp.201110615

Wang, Y. Y., Chang, R. B., and Liman, E. R. (2010b). TRPA1 is a component of the nociceptive response to CO_2. *J. Neurosci.* 30, 12958–12963. doi: 10.1523/JNEUROSCI.2715-10.2010

Wang, S., Poon, K., Oswald, R. E., and Chuang, H. (2010a). Distinct modulations of human capsaicin receptor by protons and magnesium through different domains. *J. Biol. Chem.* 285, 11547–11556. doi: 10.1074/jbc.M109.058727

Welch, J. M., Simon, S. A., and Reinhart, P. H. (2000). The activation mechanism of rat vanilloid receptor 1 by capsaicin involves the pore domain and differs from the activation by either acid or heat. *Proc. Natl. Acad. Sci. U. S. A.* 97, 13889–13894. doi: 10.1073/pnas.230146497

Yagi, J., Wenk, H. N., Naves, L. A., and McCleskey, E. W. (2006). Sustained currents through ASIC3 ion channels at the modest pH changes that occur during myocardial ischemia. *Circ. Res.* 99, 501–509. doi: 10.1161/01.RES.0000238388.79295.4c

Yoder, N., Yoshioka, C., and Gouaux, E. (2018). Gating mechanisms of acid-sensing ion channels. *Nature* 555, 397–401. doi: 10.1038/nature25782

Zeisel, A., Hochgerner, H., Lönnerberg, P., Johnsson, A., Memic, F., van der Zwan, J., et al. (2018). Molecular architecture of the mouse nervous system. *Cell* 174, 999.e22–1014.e22. doi: 10.1016/j.cell.2018.06.021

Zimmerman, A., Bai, L., and Ginty, D. D. (2014). The gentle touch receptors of mammalian skin. *Science* 346, 950–954. doi: 10.1126/science.1254229

Zwick, M., Davis, B. M., Woodbury, C. J., Burkett, J. N., Koerber, H. R., Simpson, J. F., et al. (2002). Glial cell line-derived neurotrophic factor is a survival factor for isolectin B4-positive, but not vanilloid receptor 1-positive, neurons in the mouse. *J. Neurosci.* 22, 4057–4065. doi: 10.1523/JNEUROSCI.22-10-04057.2002

Zylka, M. J., Rice, F. L., and Anderson, D. J. (2005). Topographically distinct epidermal nociceptive circuits revealed by axonal tracers targeted to Mrgprd. *Neuron* 45, 17–25. doi: 10.1016/j.neuron.2004.12.015

Conflict of Interest: The authors declare that the research was conducted in the absence of any commercial or financial relationships that could be construed as a potential conflict of interest.

Publisher's Note: All claims expressed in this article are solely those of the authors and do not necessarily represent those of their affiliated organizations, or those of the publisher, the editors and the reviewers. Any product that may be evaluated in this article, or claim that may be made by its manufacturer, is not guaranteed or endorsed by the publisher.

frontiers in Behavioral Neuroscience

ORIGINAL RESEARCH
published: 29 October 2021
doi: 10.3389/fnbeh.2021.767426

Post-acquisition CO_2 Inhalation Enhances Fear Memory and Depends on ASIC1A

Rebecca J. Taugher[1,2†], Amanda M. Wunsch[1,2†], Grace Z. Wang[1,2], Aubrey C. Chan[1,2,3,4,5], Brian J. Dlouhy[3,4,6] and John A. Wemmie[1,2,3,4,6,7,8]*

[1] Department of Psychiatry, University of Iowa, Iowa City, IA, United States, [2] Department of Veterans Affairs Medical Center, Iowa City, IA, United States, [3] Pappajohn Biomedical Institute, University of Iowa, Iowa City, IA, United States, [4] Iowa Neuroscience Institute, University of Iowa, Iowa City, IA, United States, [5] Department of Internal Medicine, University of Iowa, Iowa City, IA, United States, [6] Department of Neurosurgery, University of Iowa, Iowa City, IA, United States, [7] Department of Molecular Physiology and Biophysics, University of Iowa, Iowa City, IA, United States, [8] Roy J. Carver Chair of Psychiatry and Neuroscience, University of Iowa, Iowa City, IA, United States

OPEN ACCESS

Edited by:
Enrique Soto, Meritorious Autonomous University of Puebla, Mexico

Reviewed by:
Xiangping Chu, University of Missouri–Kansas City, United States
Timothy Lynagh, University of Bergen, Norway

***Correspondence:**
John A. Wemmie
john-wemmie@uiowa.edu

[†]These authors share first authorship

Specialty section:
This article was submitted to Learning and Memory, a section of the journal Frontiers in Behavioral Neuroscience

Received: *01 September 2021*
Accepted: *04 October 2021*
Published: *29 October 2021*

Citation:
Taugher RJ, Wunsch AM, Wang GZ, Chan AC, Dlouhy BJ and Wemmie JA (2021) Post-acquisition CO_2 Inhalation Enhances Fear Memory and Depends on ASIC1A. Front. Behav. Neurosci. 15:767426. doi: 10.3389/fnbeh.2021.767426

A growing body of evidence suggests that memories of fearful events may be altered after initial acquisition or learning. Although much of this work has been done in rodents using Pavlovian fear conditioning, it may have important implications for fear memories in humans such as in post-traumatic stress disorder (PTSD). A recent study suggested that cued fear memories, made labile by memory retrieval, were made additionally labile and thus more vulnerable to subsequent modification when mice inhaled 10% carbon dioxide (CO_2) during retrieval. In light of this finding, we hypothesized that 10% CO_2 inhalation soon after fear acquisition might affect memory recall 24 h later. We found that both cue and context fear memory were increased by CO_2 exposure after fear acquisition. The effect of CO_2 was time-dependent, as CO_2 inhalation administered 1 or 4 h after cued fear acquisition increased fear memory, whereas CO_2 inhalation 4 h before or 24 h after cued fear acquisition did not increase fear memory. The ability of CO_2 exposure following acquisition to enhance fear memory was not a general consequence of stress, as restraining mice after acquisition did not alter cued fear memory. The memory-enhancing action of CO_2 may be relatively specific to fear conditioning as novel object recognition was impaired by post-training CO_2 inhalation. To explore the molecular underpinnings of these effects, we tested if they depended on the acid-sensing ion channel-1a (ASIC1A), a proton-gated cation channel that mediates other effects of CO_2, likely via its ability to sense acidosis induced during CO_2 inhalation. We found that CO_2 inhalation did not alter cued or context fear memory in *Asic1a*$^{-/-}$ mice, suggesting that this phenomenon critically depends on ASIC1A. These results suggest that brain acidosis around the time of a traumatic event may enhance memory of the trauma, and may thus constitute an important risk factor for developing PTSD. Moreover, preventing peritraumatic acidosis might reduce risk of PTSD.

Keywords: carbon dioxide, pH, fear memory, acid-sensing ion channel, ASIC1a, novel object recognition (NOR)

INTRODUCTION

Dysregulated fear memories can be extremely maladaptive, such as in post-traumatic stress disorder (PTSD; Kessler et al., 2017; Watson, 2019). Recent studies suggest that altering fear memories might be an effective treatment strategy (Nader, 2015; Kida, 2019; Uniyal et al., 2020). Much of this work has relied on rodent models of fear memory, such as Pavlovian fear conditioning in which an aversive unconditioned stimulus such as a foot shock is paired with a neutral conditioned stimulus such as a tone or context (Fenster et al., 2018). Several strategies have been employed to attenuate memory after fear conditioning. For example, inhibiting the conversion of a short-term memory to a long-term memory (Schafe and LeDoux, 2000; Duvarci et al., 2008) or developing an inhibitory extinction memory (Myers and Davis, 2007) reduces conditioned freezing. Others have decreased or erased memory by using retrieval to render the memory labile and inhibiting reconsolidation (Nader et al., 2000) or facilitating erasure via extinction (Monfils et al., 2009; Clem and Huganir, 2010).

A recent study found that if mice inhaled 10% carbon dioxide (CO_2) during retrieval, cued fear memory was made more labile than with retrieval alone, making it more susceptible to modification via subsequent extinction or reconditioning. CO_2 inhalation during cued retrieval facilitated insertion of Ca2 + -permeable AMPA receptors (CP-AMPARs), increased cAMP-response element binding protein (CREB) phosphorylation and re-activated a greater percentage of neurons in the memory trace as compared to retrieval alone (Du et al., 2017). In addition to being labile after a retrieval event, fear memories are labile for a period of time immediately following acquisition during which they are vulnerable to disruption (Schafe and LeDoux, 2000; Duvarci et al., 2008). Thus, we wondered if CO_2 inhalation during this labile period following acquisition might similarly alter fear memory.

Moreover, Du et al. found that the CO_2 effect on cued retrieval depended on the acid-sensing ion channel-1 (ASIC1A; Du et al., 2017). ASIC1A is a synaptic cation channel that is activated when extracellular pH drops (Waldmann et al., 1997; Wemmie et al., 2002, 2013; Zha et al., 2006). It is abundantly expressed in the brain, but is particularly abundant in fear circuit structures such as the amygdala (Wemmie et al., 2003; Coryell et al., 2007; Price et al., 2014), where it has been implicated in synaptic transmission and plasticity (Du et al., 2014; Chiang et al., 2015). Several CO_2-induced behaviors depend on ASIC1A, likely because of its ability to sense CO_2-induced acidosis, including acid- and CO_2-evoked freezing, CO_2 aversion, CO_2 conditioned place avoidance, and CO_2-enhanced center avoidance (Ziemann et al., 2009; Taugher et al., 2014). Therefore, we hypothesized that any effects of post-acquisition CO_2 inhalation would critically depend on ASIC1A.

MATERIALS AND METHODS

Mice

Asic1a$^{-/-}$ mice, in which *Asic1a* but not *Asic1b* transcription is disrupted, were generated as previously described (Wemmie et al., 2002). Mice were maintained on a congenic C57BL/6J background. Mice had *ad libitum* access to water and chow (Teklab) and all mice were group housed. Mice were kept on a 12 h light/dark cycle; all experiments were conducted during the light phase. Both male and female mice were used in these studies and experimental groups were sex- and age-matched (10–20 weeks of age). Separate groups of mice were used for each experiment. All experiments were approved by the University of Iowa Animal Care and Use Committee and animal care met National Institutes of Health Standards.

Cued Fear Conditioning

On the acquisition day, mice were placed in a near-infrared video fear conditioning chamber (Med Associates, Inc.) for a total of 14 min. During the first 3 min mice explored the chamber, and then a series of 5 tones (3 kHz, 80 dB, 20 s) were played each co-terminating with a shock (0.75 mA, 1 s) administered via the floor rods. There was a 120 s intertrial interval between tone/shock presentations. 24 h later, cue-evoked responses were assessed in a novel context in which lighting, odor, and floor texture had been altered. Mice were in this context for a total of 10 min with the tone continuously presented during minutes 4–6. A no-shock control group was performed with identical methods as described above except that foot shocks were omitted. VideoFreeze software (Med Associates, Inc.) was used to quantify freezing during acquisition and testing. Freezing is quantified during the entirety of acquisition and during the time that the tone is played during the cued test, with freezing normalized to the air-treated condition. Freezing in seconds (mean ± SEM) for each group is reported in **Supplementary Table 1**.

Gas Exposure

Mice were exposed to 10% CO_2 or air in an airtight clear Plexiglas container (20.3 cm × 20.3 cm × 16.5 cm) into which gas was infused at a rate of 5 L/min for 30 min. In order to avoid context generalization, gases were administered in a different room than fear conditioning and different cleaning products were used in the fear conditioning and gas contexts to give the chambers distinct odors.

Context Fear Conditioning

On the acquisition day, mice were placed in a near-infrared video fear conditioning chamber (Med Associates, Inc.) for a total of 8 min. During the first 3 min mice explored the chamber, and then a series of 5 shocks (0.75 mA, 1 s) were administered via the floor rods with a 60 s intertrial interval. 24 h later, mice were returned to the acquisition context for 6 min in the absence of foot shocks. As with cued conditioning, freezing was quantified during acquisition and testing using VideoFreeze software (Med Associates, Inc.) and normalized to the freezing in the air-treated condition. Freezing in seconds (mean ± SEM) for each group is reported in **Supplementary Table 1**.

Restraint Stress

Mice were placed in a plastic restraint tube fashioned from a 50 mL conical tube for 30 min. Non-stressed control mice remained in the home cage during this time.

Novel Object Recognition

On days 1–3, mice were habituated to the open field apparatus (40.6 cm × 40.6 cm × 36.8 cm; ViewPoint) for 30 min per day. On the day 4, mice underwent an object recognition acquisition session in which they explored two identical objects (inverted beaker or media bottle placed in the back left and front right corners) in the open field apparatus for 15 min. On day 5, novel object recognition (NOR) was tested by replacing one of the familiar objects with a novel object (inverted beaker or media bottle) and allowing the mice to explore both objects in the open field for 10 min. The order in which objects were presented was counterbalanced. Mice were videotaped during acquisition (day 4) the object recognition test (day 5) and an experimenter blinded to genotype and condition assessed the amount of time the animal spent exploring each object (defined as having been within 2 cm of the object and their nose oriented toward the object). The discrimination ratio on the acquisition day was calculated by dividing the time spent exploring the left object by the total time spent exploring either object, and on the test day was calculated by dividing the time spent exploring the novel object by the total time spent exploring either object.

Statistical Analysis

An unpaired Student's *t*-test was used to test for statistical significance between 2 groups. Welch's correction was applied when an *F* test revealed a significant difference in variance between groups. A one sample *t* test was used to test if the mean of a group differed from random chance. A two-way ANOVA was used to test for statistical significance where a 2 × 2 experimental design was used. Outliers were identified using ROUT (Motulsky and Brown, 2006), $Q = 1\%$. 3 outliers were removed from the 10% CO_2 group in **Figures 2B,C**, 1 outlier was removed from the air group in **Figures 2E,F**, 2 outliers were removed from the air group and 1 outlier was removed from the 10% CO_2 group in **Figures 4E,F**, and 1 outlier was removed from the air group in **Figures 4H,I**. $p < 0.05$ was considered significant. All statistical analyses were performed in Graphpad Prism.

RESULTS

Because inhaling 10% CO_2 during the labile period induced by cued fear retrieval further enhanced memory lability (Du et al., 2017), we hypothesized that exposing mice to 10% CO_2 1 h after acquisition, during the time period in which new memories are thought to be labile (Mednick et al., 2011), would also alter fear memory. Thus, we trained mice in a cued fear conditioning paradigm in which we paired an auditory cue with a foot shock and 1 h later mice were placed in a different context and exposed mice to air or 10% CO_2. 24 h after acquisition, mice underwent cued testing in which they were presented with the auditory tone in a novel context in the absence of foot shocks and conditioned freezing was assessed (**Figure 1A**). Prior to gas exposure, the air and 10% CO_2-treated groups exhibited similar levels of freezing during cued fear acquisition (**Figure 1B**). Interestingly, the mice that had been exposed to 10% CO_2 displayed a marked increase in freezing during cued testing as compared to air-exposed controls (**Figure 1C**). This suggests that CO_2 exposure during the time period following acquisition can potentiate fear memory.

To rule out the possibility that CO_2 exposure might have an effect on freezing that was independent of cued fear conditioning, we performed a no shock control experiment. The same cued fear acquisition paradigm (**Figure 1A**) was used, except that foot shocks were omitted from the protocol. This resulted in minimal freezing during both acquisition and cued fear testing, with 10% CO_2 treatment having no effect on freezing (**Figures 1B,C**). This suggests that the effect of CO_2 on cued fear memory depends on cued fear conditioning, rather than being a non-specific effect of CO_2 exposure.

Because exposure to 10% CO_2 is aversive and may induce stress (Ziemann et al., 2009; Taugher et al., 2014; Spiacci et al., 2018), we next sought to test if exposing mice to a different stressor would recapitulate the effects of CO_2 inhalation on cued fear memory. We chose restraint stress given its widespread use as a method for inducing stress in mice (Stewart et al., 2008; Roper et al., 2010). We trained mice in a cued fear conditioning paradigm and 1 h later mice were either placed in a restraint tube for 30 min or left in the home cage (**Figure 1D**). Both treatment groups displayed a similar level of freezing during acquisition (**Figure 1E**), and restraint stress did not alter cued fear memory (**Figure 1F**). This suggests that the effects of 10% CO_2 exposure might not be the result of its ability to induce stress, but instead the result of its other attributes, such as its ability to induce acidosis.

Next, we sought to determine if this effect of 10% CO_2 on cued fear memory was time-dependent. First, we administered air or 10% CO_2 4 h after cued fear conditioning (**Figure 2A**). Prior to gas exposure, the air and 10% CO_2-treated groups exhibited similar levels of freezing during acquisition (**Figure 2B**). Mice treated with CO_2 4 h after acquisition displayed much more freezing during cued testing than air-treated controls (**Figure 2C**), similar to when CO_2 was given 1 h after acquisition (**Figure 1C**). To determine if this effect would extend to later time points, we administered air or 10% CO_2 24 h after cued fear conditioning and tested cued fear memory 48 h after acquisition (**Figure 2D**). Prior to gas exposure, the air and 10% CO_2-treated groups exhibited similar levels of freezing during acquisition (**Figure 2E**). No effect of gas exposure was seen during cued testing (**Figure 2F**), suggesting that there is a critical time period after acquisition for 10% CO_2 inhalation to affect cued fear memory. Next, we sought to determine if CO_2 exposure prior to acquisition would have a similar effect on cued fear memory as CO_2 exposure after acquisition. Thus, we administered air or 10% CO_2 4 h before cued fear conditioning and assessed cued fear memory 24 h later (**Figure 2G**). 10% CO_2 pre-treatment did not affect freezing during acquisition (**Figure 2H**) or cued testing (**Figure 2I**), suggesting that it might be necessary for 10% CO_2 exposure to occur after acquisition in order to potentiate fear memory.

We next sought to determine if the effect CO_2 on fear memory was specific to cued fear conditioning. Thus, we performed context fear conditioning, a form of Pavlovian conditioning in which an association is made between a neutral context and a series of foot shocks. 4 h after context fear acquisition, we

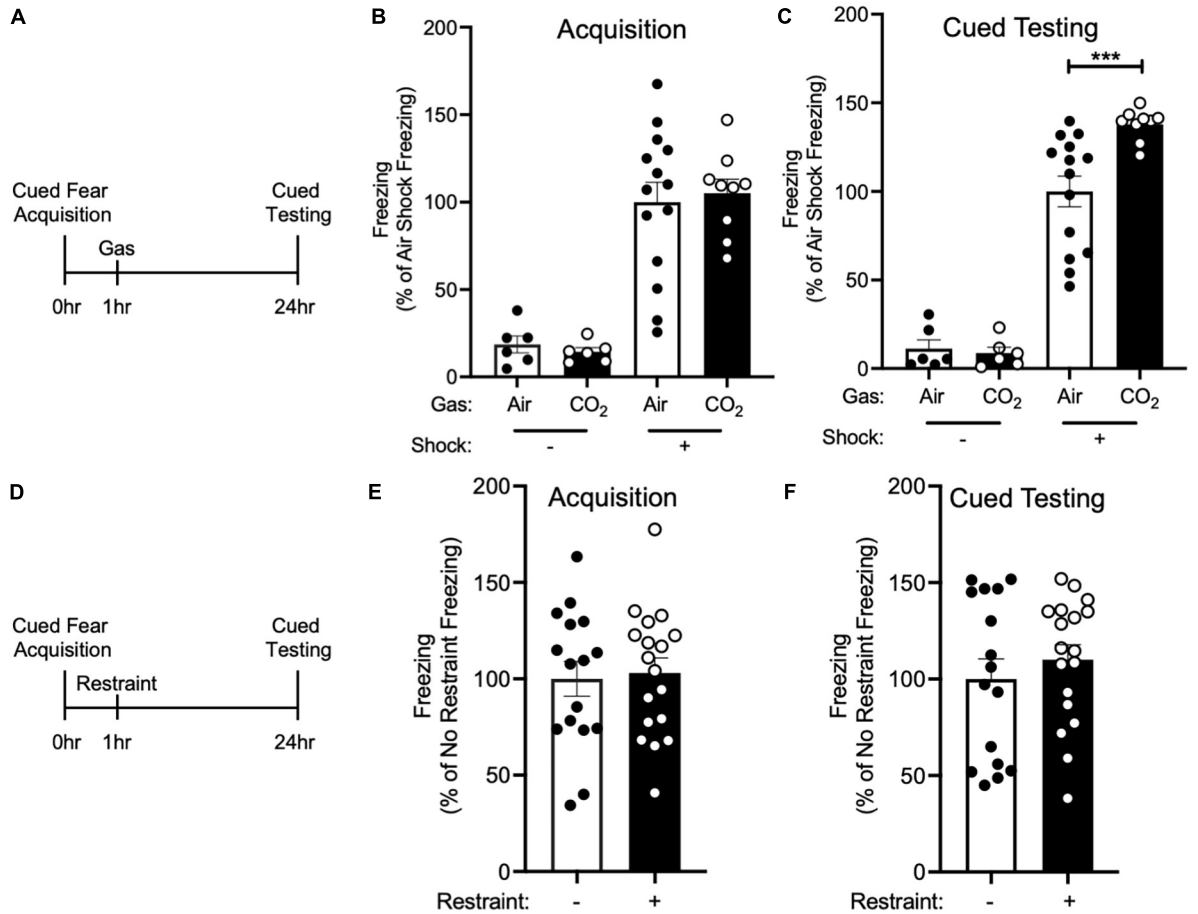

FIGURE 1 | CO_2 Inhalation after cued fear conditioning enhances fear memory. **(A)** Experimental timeline. 1 h after cued fear acquisition, mice were exposed to air or 10% CO_2 for 30 min. 24 h after acquisition, cued fear memory was assessed. **(B)** During acquisition, much less freezing was observed when foot shocks were omitted from the training protocol [effect of shock, two-way ANOVA $F(1, 31) = 61.22$, $p < 0.0001$, $n = 6–14$]. Freezing in mice assigned to Air and CO_2 treatment was similar in both the no shock ($p = 0.8135$) and shock groups ($p = 0.6957$). **(C)** On the cued fear test day, robust freezing to the tone was observed in mice who had received foot shocks during acquisition and this freezing was enhanced by CO_2 treatment [gas by shock interaction, two-way ANOVA $F(1,31) = 6.389$, $p = 0.0168$]. Planned contrast testing revealed a robust effect of CO_2 treatment in mice that had received foot shocks during acquisition (***$p = 0.0004$), whereas in contrast, CO_2 treatment had no effect on freezing in the no shock control group ($p = 0.8453$). **(D)** Experimental timeline. 1 h after cued fear acquisition, mice were placed in a restraint tube for 30 min or left in the home cage. 24 h after acquisition, cued fear memory was assessed. **(E)** Freezing during acquisition was similar in both treatment groups [$t(32) = 0.2560$, $p = 0.7996$]. **(F)** Freezing during cued fear testing was not altered by restraint stress [$t(32) = 0.7850$, $p = 0.4382$].

administered air or 10% CO_2, and 24 h after acquisition, we returned mice to the acquisition context and assessed conditioned freezing responses (**Figure 3A**). Prior to gas exposure, the air and 10% CO_2-treated groups exhibited similar levels of freezing during acquisition (**Figure 3B**). Similar to cued fear conditioning (**Figure 2C**), mice treated with 10% CO_2 4 h after context fear acquisition exhibited more freezing during context testing than air-treated controls (**Figure 3C**). This suggests that CO_2 following acquisition has similar effects on cued and context fear memory.

To test if CO_2 could also potentiate other types of memory, we tested its effects on NOR. Mice acquired a memory of the familiar object by exploring two identical objects. 4 h later, we exposed mice to air or 10% CO_2. 24 h after acquisition, we assessed NOR by replacing one of the familiar objects with a novel object and assessing the amount of time that mice spent interacting with the novel and familiar objects (**Figure 3D**). During acquisition, mice exhibited similar levels of interaction with each object, and no difference between treatment groups was observed (**Figure 3E**). Surprisingly, when NOR was assessed 24 h later, we found that 10% CO_2 treatment had decreased NOR as compared to air-treated controls and also caused a failure to discriminate between the novel and familiar objects (**Figure 3F**). This suggests that CO_2 may affect different types of memory in distinct ways.

To explore the molecular underpinnings of these effects, we tested if they depended on ASIC1A. ASIC1A is a proton-gated cation channel that is known to mediate other effects of CO_2, likely via its ability to sense acidosis induced by CO_2 inhalation (Ziemann et al., 2009; Taugher et al., 2014). Thus, we tested the effects of 10% CO_2 exposure on memory in *Asic1a*$^{-/-}$ mice under the same conditions in which CO_2 enhanced fear memory in wild-type mice. Neither administering 10% CO_2 1 h

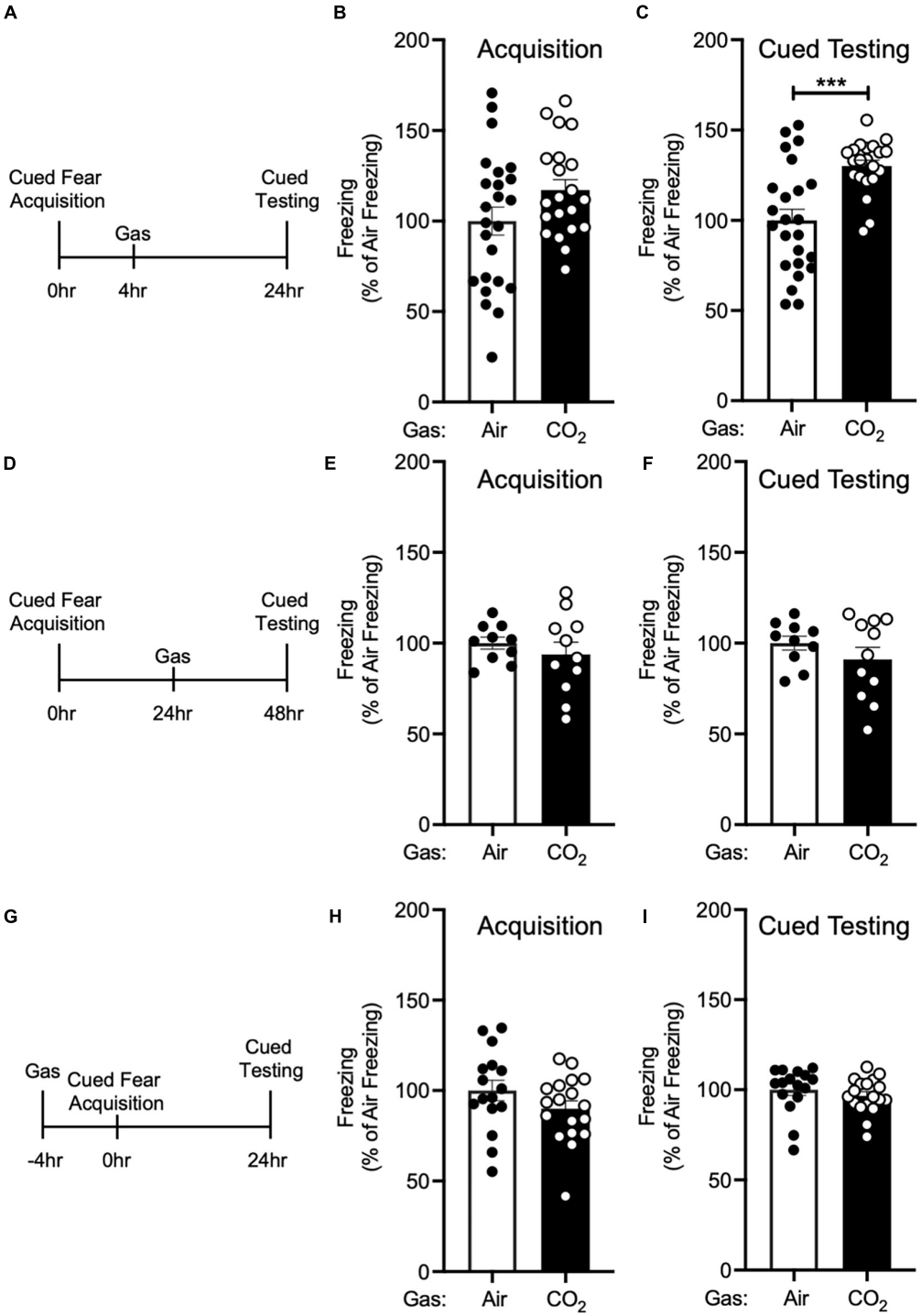

FIGURE 2 | The enhancing effect of CO_2 inhalation on cued fear memory is time-dependent. **(A)** Experimental timeline. 4 h after cued fear acquisition, mice were exposed to air or 10% CO_2 for 30 min. 24 h after acquisition, cued fear memory was assessed. **(B)** Freezing during acquisition prior to gas exposure did not differ significantly between air and 10% CO_2-treated groups [$t(43) = 1.748$, $p = 0.0876$, $n = 24, 21$]. **(C)** Exposure to 10% CO_2 4 h after acquisition increased freezing during the cued fear test [$t(34.49) = 4.359$, $^{***}p = 0.0001$]. **(D)** Experimental timeline. 24 h after cued fear acquisition, mice were exposed to air or 10% CO_2 for 30 min. 24 h after gas exposure, cued fear memory was assessed. **(E,F)** In mice exposed to gas 24 h after acquisition, freezing during acquisition prior to gas exposure did not differ between air and 10% CO_2-treated groups **(E)** [$t(14.49) = 0.8350$, $p = 0.4173$, $n = 10, 11$] nor did freezing during the cued fear test **(F)** [$t(19) = 1.129$, $p = 0.2731$]. **(G)** Experimental timeline. 4 h before cued fear acquisition, mice were exposed to air or 10% CO_2 for 30 min. 24 h after acquisition, cued fear memory was assessed. **(H,I)** When acquisition occurred 4 h after gas exposure, CO_2 treatment had no effect on freezing during acquisition **(H)** [$t(32) = 1.435$, $p = 0.1610$, $n = 16, 18$] or freezing during the cued fear test was observed **(I)** [$t(32) = 0.8642$, $p = 0.3939$].

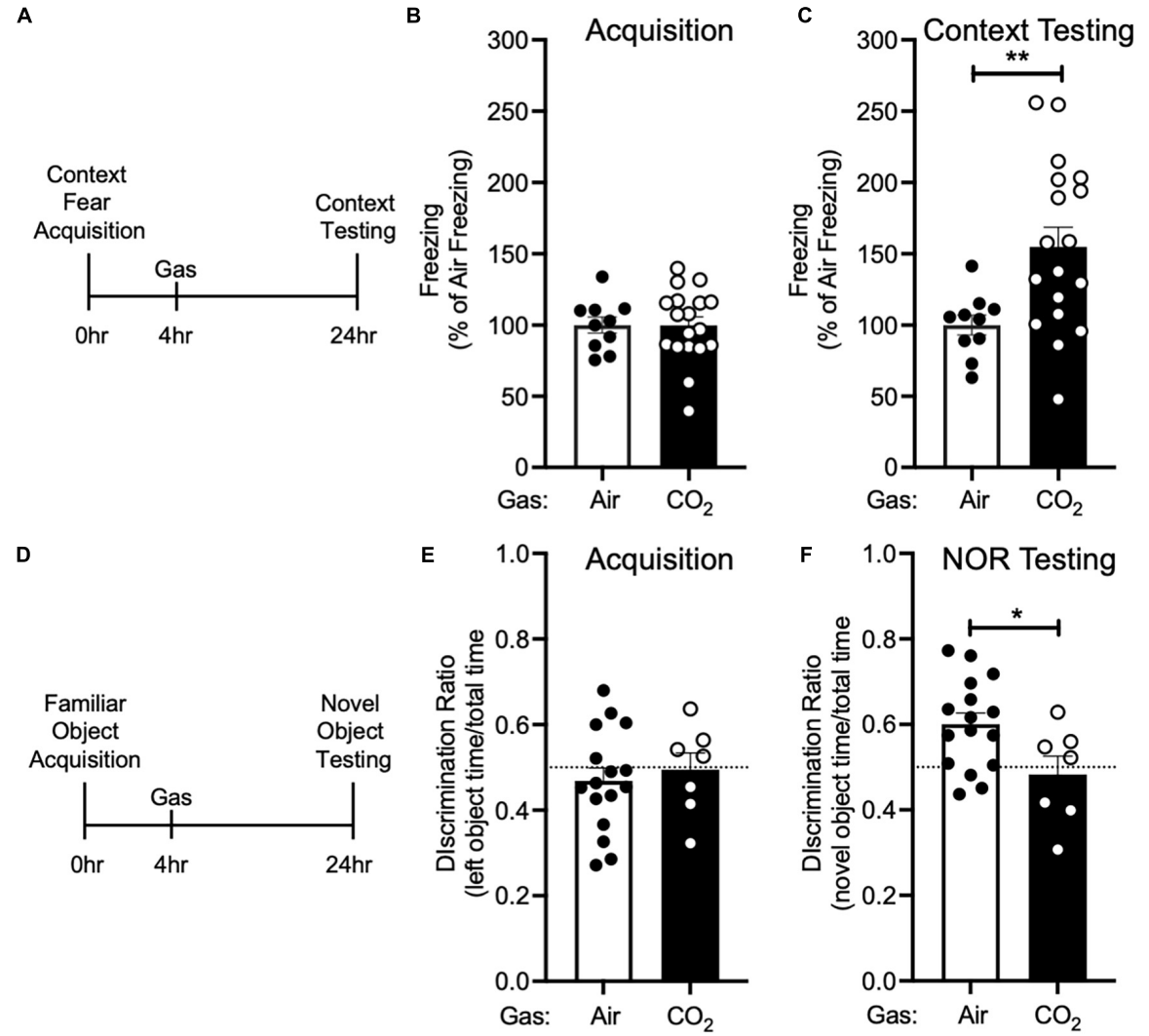

FIGURE 3 | CO_2 Inhalation after acquisition enhances context fear memory, but decreases novel object recognition **(A)** Experimental timeline. 4 h after context fear acquisition, mice were exposed to air or 10% CO_2 for 30 min. 24 h after acquisition, context fear memory was assessed. **(B)** Freezing during acquisition prior to gas exposure did not differ between air and 10% CO_2-treated groups [$t(26) = 0.01532$, $p = 0.9879$, $n = 10, 18$]. **(C)** Exposure to 10% CO_2 4 h after acquisition increased freezing during the context fear test [$t(23.95) = 3.531$, $^{**}p = 0.0017$]. **(D)** Experimental timeline. 4 h after novel object acquisition, mice were exposed to air or 10% CO_2 for 30 min. **(E)** Prior to gas exposure, object preference during acquisition did not differ between air and 10% CO_2-treated groups [$t(21) = 0.4902$, $p = 0.6290$, $n = 16, 7$] and neither air [$t(15) = 1.050$, $p = 0.3104$] nor 10% CO_2-treated [$t(6) = 0.1454$, $p = 0.8891$] groups preferred the left or right objects. **(F)** Exposure to 10% CO_2 4 h after acquisition decreased discrimination between the novel and familiar objects [$t(21) = 2.409$, $^{*}p = 0.0253$]. Novel object preference was observed in the air group [$t(15) = 3.805$, $p = 0.0017$], but not the 10% CO_2-treated group [$t(6) = 0.7037$, $p = 0.7037$].

after (**Figures 4A–C**) nor 4 h after (**Figures 4D–F**) cued fear acquisition altered freezing during cued testing in *Asic1a*$^{-/-}$ mice. Similarly, we found no effect of 10% CO_2 administered 4 h after context fear acquisition on freezing in *Asic1a*$^{-/-}$ mice during context testing (**Figures 4G–I**). Together, these observations suggest that ASIC1A is critical for the effects of CO_2 exposure on fear memory observed in wild-type mice.

Next, we tested whether the reduction in NOR induced by CO_2 exposure similarly depended on ASIC1A (**Figure 4J**). Prior to gas exposure, *Asic1a*$^{-/-}$ mice exhibited similar levels of interaction with each object (**Figure 4K**). When gas was administered 4 h after acquisition, novel object preference was intact in air-treated *Asic1a*$^{-/-}$ mice, but not in those exposed to 10% CO_2 (**Figure 4L**). However, the difference between air versus CO_2-exposed *Asic1a*$^{-/-}$ mice did not reach significance ($p = 0.07$). These results are similar to those seen in wild-type mice, and suggest that in contrast to fear memory, the effects of CO_2 exposure on NOR may be independent of ASIC1A.

DISCUSSION

Our results identify a novel effect of post-acquisition CO_2 exposure on both cued and context fear memory. We found that

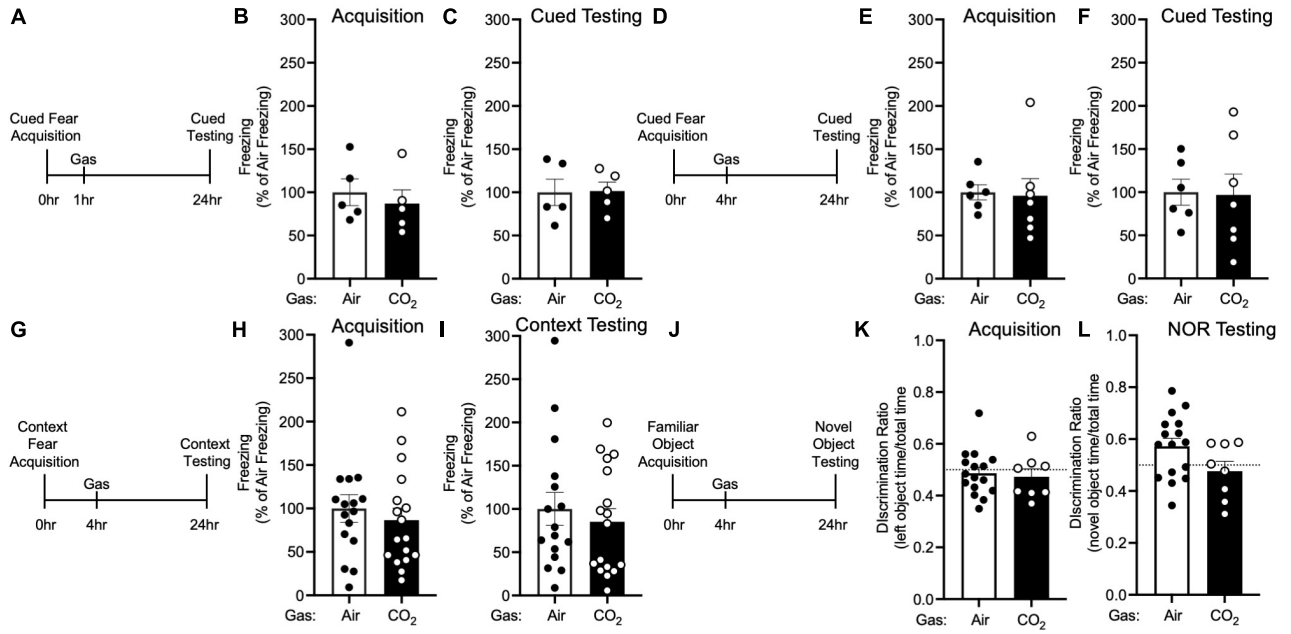

FIGURE 4 | The effects of CO_2 Inhalation on fear memory depend on ASIC1A. **(A)** Experimental timeline. 1 h after cued fear acquisition, *Asic1a*$^{-/-}$ mice were exposed to air or 10% CO_2 for 30 min. 24 h after acquisition, cued fear memory was assessed. **(B,C)** Prior to gas exposure, freezing during acquisition prior to gas exposure did not differ between air and 10% CO_2-treated groups **(B)** [$t(8) = 0.5867$, $p = 0.5736$, $n = 5$/group] nor did freezing after gas exposure during the cued fear test **(C)** [$t(8) = 0.07644$, $p = 0.9409$]. **(D)** Experimental timeline. 4 h after cued fear acquisition, mice were exposed to air or 10% CO_2 for 30 min. 24 h after acquisition, cued fear memory was assessed. **(E,F)** Freezing during acquisition prior to gas exposure did not differ between air and 10% CO_2-treated groups **(E)** [$t(11) = 0.1697$, $p = 0.8683$, $n = 6, 7$] nor did freezing during the cued fear test **(F)** [$t(11) = 0.1077$, $p = 0.9162$]. **(G)** Experimental timeline. 4 h after context fear acquisition, mice were exposed to air or 10% CO_2 for 30 min. 24 h after acquisition, context fear memory was assessed. **(H,I)** Freezing during acquisition did not differ between air and 10% CO_2-treated groups **(H)** [$t(31) = 0.6410$, $p = 0.5262$, $n = 16, 17$] nor did freezing during the context fear test **(I)** [$t(31) = 0.5469$, $p = 0.6091$]. **(J)** Experimental timeline. 4 h after novel object acquisition, mice were exposed to air or 10% CO_2 for 30 min. **(K)** Prior to gas exposure, object preference during acquisition prior to gas exposure did not differ between air and 10% CO_2-treated groups [$t(22) = 0.3543$, $p = 0.7265$, $n = 16, 8$] and neither air [$t(15) = 0.6143$, $p = 0.5482$] nor 10% CO_2-treated [$t(7) = 0.8899$, $p = 0.4031$] groups preferred the left or right objects. **(L)** A trend toward a reduction in discrimination between the novel and familiar objects was observed in 10% CO_2-treated mice [$t(22) = 1.878$, $p = 0.0737$]. Novel object preference was observed in the air group [$t(15) = 2.367$, $p = 0.0318$], but not the 10% CO_2-treated group [$t(7) = 0.6167$, $p = 0.5570$].

during a discrete time period, including 1 and 4 h after fear acquisition, but not 24 h after, 10% CO_2 inhalation increased fear memory. In contrast, there was no effect of CO_2 exposure under the same conditions in *Asic1a*$^{-/-}$ mice, suggesting that ASIC1A is critical for this effect. Moreover, CO_2 may affect distinct types of memory in different ways, as in contrast to these enhancements in fear memory, NOR was decreased by post-training CO_2 inhalation.

These observations raise questions about where and how CO_2 and ASIC1A act to produce their effects on fear memory. The amygdala is a likely site of ASIC1A action. ASIC1A is abundantly expressed in the amygdala (Wemmie et al., 2003; Coryell et al., 2007; Price et al., 2014; Chiang et al., 2015), and manipulating ASIC1A in the amygdala alters cued and context fear memory (Coryell et al., 2008; Chiang et al., 2015), as well as CO_2-evoked freezing (Ziemann et al., 2009). Likewise, localized acidosis in the amygdala promotes freezing (Ziemann et al., 2009) and plasticity (Du et al., 2017). However, ASIC1A is also expressed in several other fear circuit structures in which it could influence fear memory, such as the bed nucleus of the stria terminalis, periaqueductal gray, hippocampus, prefrontal, and cingulate cortices (Wemmie et al., 2003; Coryell et al., 2007; Price et al., 2014). On the cellular level, these effects are likely due to ASIC1A in neurons. Neurons are a critical site of ASIC1A action in cued and context fear memory and CO_2-induced freezing (Taugher et al., 2017), though it is possible that ASIC1A in non-neuronal cells could also be involved.

The acidosis caused by CO_2 inhalation may activate ASIC1A directly (Ziemann et al., 2009). CO_2 may also influence the activation of ASIC1A by protons released during neurotransmission (Du et al., 2014; Kreple et al., 2014; Gonzalez-Inchauspe et al., 2017). Either or both of these mechanisms might contribute to the effects of CO_2 and ASIC1A observed here. Interestingly, acidosis not only activates these channels, it also inhibits them through inactivation and steady-state desensitization (Waldmann et al., 1997; Sherwood et al., 2012). These inhibitory effects of acid exposure have been demonstrated *in vitro*, although it is not clear to what degree they occur *in vivo*. Steady-state desensitization can be limited by endogenous peptides such as dynorphins and RF-amides (Sherwood and Askwith, 2008, 2009), raising the possibility that densitization *in vivo* may be less pronounced. It is also conceivable that the ASIC1A effects observed here may not require sustained channel activity.

The mechanisms downstream of ASIC1A are not yet clear. We speculate that the effects of CO_2 and ASIC1A on fear memory may depend on CP-AMPARs in the postsynaptic membrane of lateral amygdala neurons, and or CREB-mediated transcriptional regulation. Conversion of short term fear memory to long lasting memory (i.e., consolidation) has been previously found to require both CP-AMPAR insertion (Rumpel et al., 2005; Nedelescu et al., 2010), and CREB phosphorylation and subsequent changes in gene transcription (Alberini, 2009). Previously, it was shown that when coupled with memory reactivation, CO_2 exposure also increased both insertion of CP-AMPARs and CREB phosphorylation, which may be critical for promoting susceptibility of the fear memory to subsequent modification (Du et al., 2017). The potential role of ASIC1A in CREB phosphorylation has not been tested. However, the increase in CP-AMPAR insertion critically depended on the presence of ASIC1A (Du et al., 2017). Thus, CP-AMPAR insertion and CREB dependent transcription would seem good candidates for mediating the fear memory effects of CO_2 and ASIC1A reported here.

Besides potentiating fear memory, our results suggests that CO_2 may decrease other types of memory. 10% CO_2 administered 4 h after acquisition attenuated NOR memory (**Figure 4F**). This may reflect the partially overlapping circuitry of these behaviors (Kim and Jung, 2006; Warburton and Brown, 2015; Fenster et al., 2018) or distinct molecular mechanisms being at play. Interestingly, whereas 10% CO_2 had no effect on cued and context fear memory in *Asic1a*$^{-/-}$ mice, there was a strong trend toward a decrease in NOR in *Asic1a*$^{-/-}$ mice, suggesting that ASIC1A might mediate the fear conditioning, but not object recognition memory. Although additional work will be needed to identify the pH-sensitive molecules involved in the CO_2 effect on novel object recognition, there are numerous pH-sensitive ion channels and receptors at synapses that could potentially be involved (Wemmie, 2011). Additional investigation will be needed to explore the effects of CO_2 inhalation on other types of memory and other receptors.

Together, these observations suggest that brain pH around the time of a traumatic event may impact the associated fear memory, potentially altering the risk of developing PTSD. Consistent with this others have observed elevated levels of PTSD in patients with conditions that may result in a chronic respiratory acidosis such as asthma (O'Toole and Catts, 2008; Allgire et al., 2021), chronic obstructive pulmonary disease (Teixeira et al., 2015), obstructive sleep apnea (Colvonen et al., 2015), COVID-19 (Mertz Schou et al., 2021), and patients who are mechanically ventilated for a prolonged period of time (Wade et al., 2013). This suggests that pH alterations such as respiratory or metabolic acidosis or changes in acid-base equilibrium might contribute to PTSD risk and raises the exciting possibility that preventing acidosis or inducing alkalosis after a traumatic event could attenuate the associated fear memory.

DATA AVAILABILITY STATEMENT

The raw data supporting the conclusions of this article will be made available by the authors, without undue reservation.

ETHICS STATEMENT

The animal study was reviewed and approved by The University of Iowa Animal Care and Use Committee.

AUTHOR CONTRIBUTIONS

RT conceptualized experiments, collected and analyzed data, and wrote the manuscript. AW conceptualized experiments, collected and analyzed data, and revised the manuscript. GW collected data. AC, BD, and JW conceptualized experiments and revised the manuscript. All authors contributed to the article and approved the submitted version.

FUNDING

This work was funded by the National Institutes of Health (MH-113325) and the Department of Veterans Affairs (BX004440). AC was supported by MH-019113. BD was supported by NS-112573.

ACKNOWLEDGMENTS

We thank Rong Fan, Collin Kreple, Kaitlyn Zenner, and Jason Allen for their recommendations and assistance.

SUPPLEMENTARY MATERIAL

The Supplementary Material for this article can be found online at: https://www.frontiersin.org/articles/10.3389/fnbeh.2021.767426/full#supplementary-material

REFERENCES

Alberini, C. M. (2009). Transcription factors in long-term memory and synaptic plasticity. *Physiol. Rev.* 89, 121–145. doi: 10.1152/physrev.00017.2008

Allgire, E., Mcalees, J. W., Lewkowich, I. P., and Sah, R. (2021). Asthma and posttraumatic stress disorder (PTSD): emerging links, potential models and mechanisms. *Brain Behav. Immun.* 97, 275–285. doi: 10.1016/j.bbi.2021.06.001

Chiang, P. H., Chien, T. C., Chen, C. C., Yanagawa, Y., and Lien, C. C. (2015). ASIC-dependent LTP at multiple glutamatergic synapses in amygdala network is required for fear memory. *Sci. Rep.* 5:10143. doi: 10.1038/srep10143

Clem, R. L., and Huganir, R. L. (2010). Calcium-permeable AMPA receptor dynamics mediate fear memory erasure. *Science* 330, 1108–1112. doi: 10.1126/science.1195298

Colvonen, P. J., Masino, T., Drummond, S. P., Myers, U. S., Angkaw, A. C., and Norman, S. B. (2015). Obstructive sleep apnea and posttraumatic stress

disorder among OEF/OIF/OND Veterans. *J. Clin. Sleep Med.* 11, 513–518. doi: 10.5664/jcsm.4692

Coryell, M., Ziemann, A. E., Westmoreland, P. J., Haenfler, J. M., Kurjakovic, Z., Zha, X. M., et al. (2007). Targeting ASIC1a reduces innate fear and alters neuronal activity in the fear circuit. *Biol. Psychiatry* 62, 1140–1148. doi: 10.1016/j.biopsych.2007.05.008

Coryell, M. W., Wunsch, A. M., Haenfler, J. M., Allen, J. E., Mcbride, J. L., Davidson, B. L., et al. (2008). Restoring Acid-sensing ion channel-1a in the amygdala of knock-out mice rescues fear memory but not unconditioned fear responses. *J. Neurosci.* 28, 13738–13741. doi: 10.1523/JNEUROSCI.3907-08.2008

Du, J., Price, M. P., Taugher, R. J., Grigsby, D., Ash, J. J., Stark, A. C., et al. (2017). Transient acidosis while retrieving a fear-related memory enhances its lability. *Elife* 6:e22564. doi: 10.7554/eLife.22564.018

Du, J., Reznikov, L. R., Price, M. P., Zha, X. M., Lu, Y., Moninger, T. O., et al. (2014). Protons are a neurotransmitter that regulates synaptic plasticity in the lateral amygdala. *Proc. Natl. Acad. Sci. U. S. A.* 111, 8961–8966. doi: 10.1073/pnas.1407018111

Duvarci, S., Nader, K., and Ledoux, J. E. (2008). De novo mRNA synthesis is required for both consolidation and reconsolidation of fear memories in the amygdala. *Learn Mem.* 15, 747–755. doi: 10.1101/lm.1027208

Fenster, R. J., Lebois, L. A. M., Ressler, K. J., and Suh, J. (2018). Brain circuit dysfunction in post-traumatic stress disorder: from mouse to man. *Nat. Rev. Neurosci.* 19, 535–551. doi: 10.1038/s41583-018-0039-7

Gonzalez-Inchauspe, C., Urbano, F. J., Di Guilmi, M. N., and Uchitel, O. D. (2017). Acid-sensing ion channels activated by evoked released protons modulate synaptic transmission at the mouse calyx of held synapse. *J. Neurosci.* 37, 2589–2599. doi: 10.1523/JNEUROSCI.2566-16.2017

Kessler, R. C., Aguilar-Gaxiola, S., Alonso, J., Benjet, C., Bromet, E. J., Cardoso, G., et al. (2017). Trauma and PTSD in the WHO world mental health surveys. *Eur. J. Psychotraumatol.* 8:1353383. doi: 10.1080/20008198.2017.1353383

Kida, S. (2019). Reconsolidation/destabilization, extinction and forgetting of fear memory as therapeutic targets for PTSD. *Psychopharmacology (Berl)* 236, 49–57. doi: 10.1007/s00213-018-5086-2

Kim, J. J., and Jung, M. W. (2006). Neural circuits and mechanisms involved in Pavlovian fear conditioning: a critical review. *Neurosci. Biobehav. Rev.* 30, 188–202. doi: 10.1016/j.neubiorev.2005.06.005

Kreple, C. J., Lu, Y., Taugher, R. J., Schwager-Gutman, A. L., Du, J., Stump, M., et al. (2014). Acid-sensing ion channels contribute to synaptic transmission and inhibit cocaine-evoked plasticity. *Nat. Neurosci.* 17, 1083–1091. doi: 10.1038/nn.3750

Mednick, S. C., Cai, D. J., Shuman, T., Anagnostaras, S., and Wixted, J. T. (2011). An opportunistic theory of cellular and systems consolidation. *Trends Neurosci.* 34, 504–514. doi: 10.1016/j.tins.2011.06.003

Mertz Schou, T., Joca, S., Wegener, G., and Bay-Richter, C. (2021). Psychiatric and neuropsychiatric sequelae of COVID-19 - a systematic review. *Brain Behav. Immun.* 97, 328–348. doi: 10.1016/j.bbi.2021.07.018

Monfils, M. H., Cowansage, K. K., Klann, E., and Ledoux, J. E. (2009). Extinction-reconsolidation boundaries: key to persistent attenuation of fear memories. *Science* 324, 951–955. doi: 10.1126/science.1167975

Motulsky, H. J., and Brown, R. E. (2006). Detecting outliers when fitting data with nonlinear regression - a new method based on robust nonlinear regression and the false discovery rate. *BMC Bioinformatics* 7:123. doi: 10.1186/1471-2105-7-123

Myers, K. M., and Davis, M. (2007). Mechanisms of fear extinction. *Mol. Psychiatry* 12, 120–150. doi: 10.1038/sj.mp.4001939

Nader, K. (2015). Reconsolidation and the Dynamic Nature of Memory. *Cold Spring Harb. Perspect. Biol.* 7, a021782. doi: 10.1101/cshperspect.a021782

Nader, K., Schafe, G. E., and Le Doux, J. E. (2000). Fear memories require protein synthesis in the amygdala for reconsolidation after retrieval. *Nature* 406, 722–726. doi: 10.1038/35021052

Nedelescu, H., Kelso, C. M., Lázaro-Muñoz, G., Purpura, M., Cain, C. K., Ledoux, J. E., et al. (2010). Endogenous GluR1-containing AMPA receptors translocate to asymmetric synapses in the lateral amygdala during the early phase of fear memory formation: an electron microscopic immunocytochemical study. *J. Comp. Neurol.* 518, 4723–4739. doi: 10.1002/cne.22472

O'Toole, B. I., and Catts, S. V. (2008). Trauma, PTSD, and physical health: an epidemiological study of Australian Vietnam veterans. *J. Psychosom. Res.* 64, 33–40. doi: 10.1016/j.jpsychores.2007.07.006

Price, M. P., Gong, H., Parsons, M. G., Kundert, J. R., Reznikov, L. R., Bernardinelli, L., et al. (2014). Localization and behaviors in null mice suggest that ASIC1 and ASIC2 modulate responses to aversive stimuli. *Genes Brain Behav.* 13, 179–194. doi: 10.1111/gbb.12108

Roper, J. A., Craighead, M., O'carroll, A. M., and Lolait, S. J. (2010). Attenuated stress response to acute restraint and forced swimming stress in arginine vasopressin 1b receptor subtype (Avpr1b) receptor knockout mice and wild-type mice treated with a novel Avpr1b receptor antagonist. *J. Neuroendocrinol.* 22, 1173–1180. doi: 10.1111/j.1365-2826.2010.02070.x

Rumpel, S., Ledoux, J., Zador, A., and Malinow, R. (2005). Postsynaptic receptor trafficking underlying a form of associative learning. *Science* 308, 83–88. doi: 10.1126/science.1103944

Schafe, G. E., and LeDoux, J. E. (2000). Memory consolidation of auditory pavlovian fear conditioning requires protein synthesis and protein kinase A in the amygdala. *J. Neurosci.* 20:RC96. doi: 10.1523/JNEUROSCI.20-18-j0003.2000

Sherwood, T. W., and Askwith, C. C. (2008). Endogenous arginine-phenylalanine-amide-related peptides alter steady-state desensitization of ASIC1a. *J. Biol. Chem.* 283, 1818–1830. doi: 10.1074/jbc.M705118200

Sherwood, T. W., and Askwith, C. C. (2009). Dynorphin opioid peptides enhance acid-sensing ion channel 1a activity and acidosis-induced neuronal death. *J. Neurosci.* 29, 14371–14380. doi: 10.1523/JNEUROSCI.2186-09.2009

Sherwood, T. W., Frey, E. N., and Askwith, C. C. (2012). Structure and activity of the acid-sensing ion channels. *Am. J. Physiol. Cell Physiol.* 303, C699–C710. doi: 10.1152/ajpcell.00188.2012

Spiacci, A. Jr., Vilela-Costa, H. H., Sant'ana, A. B., Fernandes, G. G., Frias, A. T., Da Silva, G. S. F., et al. (2018). Panic-like escape response elicited in mice by exposure to CO(2), but not hypoxia. *Prog. Neuropsychopharmacol. Biol. Psychiatry* 81, 178–186. doi: 10.1016/j.pnpbp.2017.10.018

Stewart, L. Q., Roper, J. A., Young, W. S. III., O'carroll, A. M., and Lolait, S. J. (2008). Pituitary-adrenal response to acute and repeated mild restraint, forced swim and change in environment stress in arginine vasopressin receptor 1b knockout mice. *J. Neuroendocrinol.* 20, 597–605. doi: 10.1111/j.1365-2826.2008.01704.x

Taugher, R. J., Lu, Y., Fan, R., Ghobbeh, A., Kreple, C. J., Faraci, F. M., et al. (2017). ASIC1A in neurons is critical for fear-related behaviors. *Genes Brain Behav.* 16, 745–755. doi: 10.1111/gbb.12398

Taugher, R. J., Lu, Y., Wang, Y., Kreple, C. J., Ghobbeh, A., Fan, R., et al. (2014). The bed nucleus of the stria terminalis is critical for anxiety-related behavior evoked by CO2 and acidosis. *J. Neurosci.* 34, 10247–10255. doi: 10.1523/JNEUROSCI.1680-14.2014

Teixeira, P. J., Porto, L., Kristensen, C. H., Santos, A. H., Menna-Barreto, S. S., and Do Prado-Lima, P. A. (2015). Post-traumatic stress symptoms and exacerbations in COPD patients. *COPD* 12, 90–95. doi: 10.3109/15412555.2014.922063

Uniyal, A., Singh, R., Akhtar, A., Dhaliwal, J., Kuhad, A., and Sah, S. P. (2020). Pharmacological rewriting of fear memories: a beacon for post-traumatic stress disorder. *Eur. J. Pharmacol.* 870:172824. doi: 10.1016/j.ejphar.2019.172824

Wade, D., Hardy, R., Howell, D., and Mythen, M. (2013). Identifying clinical and acute psychological risk factors for PTSD after critical care: a systematic review. *Minerva Anestesiol.* 79, 944–963.

Waldmann, R., Champigny, G., Bassilana, F., Heurteaux, C., and Lazdunski, M. (1997). A proton-gated cation channel involved in acid-sensing. *Nature* 386, 173–177. doi: 10.1038/386173a0

Warburton, E. C., and Brown, M. W. (2015). Neural circuitry for rat recognition memory. *Behav. Brain Res.* 285, 131–139. doi: 10.1016/j.bbr.2014.09.050

Watson, P. (2019). PTSD as a public mental health priority. *Curr. Psychiatry Rep.* 21:61. doi: 10.1007/s11920-019-1032-1

Wemmie, J. A. (2011). Neurobiology of panic and pH chemosensation in the brain. *Dialogues Clin. Neurosci.* 13, 475–483. doi: 10.31887/DCNS.2011.13.4/jwemmie

Wemmie, J. A., Askwith, C. C., Lamani, E., Cassell, M. D., Freeman, J. H. Jr., and Welsh, M. J. (2003). Acid-sensing ion channel 1 is localized in brain regions

with high synaptic density and contributes to fear conditioning. *J. Neurosci.* 23, 5496–5502. doi: 10.1523/JNEUROSCI.23-13-05496.2003

Wemmie, J. A., Chen, J., Askwith, C. C., Hruska-Hageman, A. M., Price, M. P., Nolan, B. C., et al. (2002). The acid-activated ion channel ASIC contributes to synaptic plasticity, learning, and memory. *Neuron* 34, 463–477. doi: 10.1016/S0896-6273(02)00661-X

Wemmie, J. A., Taugher, R. J., and Kreple, C. J. (2013). Acid-sensing ion channels in pain and disease. *Nat. Rev. Neurosci.* 14, 461–471. doi: 10.1038/nrn3529

Zha, X. M., Wemmie, J. A., Green, S. H., and Welsh, M. J. (2006). Acid-sensing ion channel 1a is a postsynaptic proton receptor that affects the density of dendritic spines. *Proc. Natl. Acad. Sci. U. S. A.* 103, 16556–16561. doi: 10.1073/pnas.0608018103

Ziemann, A. E., Allen, J. E., Dahdaleh, N. S., Drebot, I. I., Coryell, M. W., Wunsch, A. M., et al. (2009). The amygdala is a chemosensor that detects carbon dioxide and acidosis to elicit fear behavior. *Cell* 139, 1012–1021. doi: 10.1016/j.cell.2009.10.029

Conflict of Interest: The authors declare that the research was conducted in the absence of any commercial or financial relationships that could be construed as a potential conflict of interest.

frontiers in Cellular Neuroscience

ORIGINAL RESEARCH
published: 24 November 2021
doi: 10.3389/fncel.2021.761813

Molecular Investigation of Chicken Acid-Sensing Ion Channel 1 β11-12 Linker Isomerization and Channel Kinetics

Matthew L. Rook[1†], Anna Ananchenko[2†], Maria Musgaard[2‡] and David M. MacLean[3*]*

[1] Graduate Program in Cellular and Molecular Pharmacology and Physiology, University of Rochester Medical Center, Rochester, NY, United States, [2] Department of Chemistry and Biomolecular Sciences, University of Ottawa, Ottawa, ON, Canada, [3] Department of Pharmacology and Physiology, University of Rochester Medical Center, Rochester, NY, United States

OPEN ACCESS

Edited by:
Haruyuki Kamiya,
Hokkaido University, Japan

Reviewed by:
Lachlan Rash,
The University of Queensland, Australia
Andreas Reiner,
Ruhr University Bochum, Germany

***Correspondence:**
Maria Musgaard
mariamusgaard@gmail.com
David M. MacLean
david_maclean@urmc.rochester.edu

[†] These authors have contributed equally to this work

[‡] **Present address:**
Maria Musgaard,
OMass Therapeutics, Oxford, United Kingdom

Specialty section:
This article was submitted to Cellular Neurophysiology, a section of the journal Frontiers in Cellular Neuroscience

Received: 20 August 2021
Accepted: 05 November 2021
Published: 24 November 2021

Citation:
Rook ML, Ananchenko A, Musgaard M and MacLean DM (2021) Molecular Investigation of Chicken Acid-Sensing Ion Channel 1 β11-12 Linker Isomerization and Channel Kinetics. Front. Cell. Neurosci. 15:761813. doi: 10.3389/fncel.2021.761813

Structures of the trimeric acid-sensing ion channel have been solved in the resting, toxin-bound open and desensitized states. Within the extracellular domain, there is little difference between the toxin-bound open state and the desensitized state. The main exception is that a loop connecting the 11th and 12th β-strand, just two amino acid residues long, undergoes a significant and functionally critical re-orientation or flipping between the open and desensitized conformations. Here we investigate how specific interactions within the surrounding area influence linker stability in the "flipped" desensitized state using all-atom molecular dynamics simulations. An inherent challenge is bringing the relatively slow channel desensitization and recovery processes (in the milliseconds to seconds) within the time window of all-atom simulations (hundreds of nanoseconds). To accelerate channel behavior, we first identified the channel mutations at either the Leu414 or Asn415 position with the fastest recovery kinetics followed by molecular dynamics simulations of these mutants in a deprotonated state, accelerating recovery. By mutating one residue in the loop and examining the evolution of interactions in the neighbor, we identified a novel electrostatic interaction and validated prior important interactions. Subsequent functional analysis corroborates these findings, shedding light on the molecular factors controlling proton-mediated transitions between functional states of the channel. Together, these data suggest that the flipped loop in the desensitized state is stabilized by interactions from surrounding regions keeping both L414 and N415 in place. Interestingly, very few mutations in the loop allow for equivalent channel kinetics and desensitized state stability. The high degree of sequence conservation in this region therefore indicates that the stability of the ASIC desensitized state is under strong selective pressure and underlines the physiological importance of desensitization.

Keywords: gating, desensitization, acid-sensing ion channels, ASICs, molecular dynamics

INTRODUCTION

The majority of ligand-gated ion channels (LGICs) undergo a process of desensitization wherein channels enter a long-lived non-conducting state in the continued presence of agonist (Katz and Thesleff, 1957). Thus, desensitization shapes the time course of ion flux and may also play a protective role when ligand clearance is compromised (Jones and Westbrook, 1996; Christie et al., 2010). Desensitized channels must ultimately recover from this non-conducting state before they can be activated again, and, like desensitization, the recovery time course also influences the physiological roles of LGICs (Chen et al., 2018). The era of structural biology has provided many insights and hypotheses regarding the molecular basis of desensitization for numerous LGICs (Plested, 2016; Noviello et al., 2021; Yu et al., 2021) including acid-sensing ion channels (ASICs) (Gonzales et al., 2009; Baconguis and Gouaux, 2012; Baconguis et al., 2014; Yoder et al., 2018; Yoder and Gouaux, 2020).

Acid-sensing ion channels are trimeric sodium-selective channels found throughout the brain and body (Boscardin et al., 2016). In response to a rapid drop in extracellular pH, ASICs activate and subsequently desensitize nearly completely with time constants ranging from 100 ms to 2 s, depending on the species, subunit and pH stimulus (Grunder and Pusch, 2015; Rook et al., 2021b). Recent structures of the resting, toxin-stabilized open and desensitized states of chicken ASIC1 (cASIC1) showed that the main difference in the ASIC extracellular domains of desensitized channels, relative to resting and open channels, is the isomerization of two amino acid residues linking the 11th and 12th β-strands (Yoder et al., 2018; Rook et al., 2021b). In the resting and toxin-stabilized open state, the first amino acid in this linker (Leu414) points up and away from the middle of the channel while the second amino acid (Asn415) points downward (**Figures 1A,B**). In the desensitized structures, this linker has isomerized or flipped such that Leu414 now points inward and Asn415 outward (**Figure 1B**). This was hypothesized to reflect a "molecular clutch" (Yoder et al., 2018). When the clutch is engaged, conformational changes in the extracellular domain can propagate to the pore and drive activation. However, once the clutch disengages (i.e., the linker flips), conformational changes are no longer effectively coupled to the pore. This enables the extracellular domain to remain in an "active" state while the pore can close, preventing continued ion influx under acidic conditions (Yoder et al., 2018). This elegant mechanism explains earlier functional data and was recently supported by additional mutations, simulations and state-dependent crosslinking (Rook et al., 2020). The goal of the present work was to further probe the molecular determinants of linker flipping using molecular dynamics simulations in conjunction with fast-perfusion electrophysiology.

To do this, we measured the kinetics of desensitization and recovery for a panel of mutations at both the Leu414 and Asn415 positions. We reasoned that the fastest mutations would have an increased propensity for motion of the β11-12 linker, thus potentially allowing us to observe linker dynamics within the timeframe of MD. Thus, the fastest mutants were used for subsequent all-atom molecular dynamics simulations to study the behavior of the β11-12 linker. Our simulations identified previously characterized electrostatic interactions as well as a novel hydrogen bond interaction that controls the stability of the ASIC desensitized state. Taken together, these data deepen our understanding of the molecular determinants of ASIC desensitization while advancing new metrics for the analysis of these transitions.

MATERIALS AND METHODS

Cell Culture, Mutagenesis and Transfection

Human Embryonic Kidney 293 ASIC1 knockout (KO) cells (Rook et al., 2021a) were maintained in Dulbecco's Modification of Eagle's Medium (DMEM) with 4.5 g/L glucose, L-glutamine and sodium pyruvate (Corning/Mediatech, Inc.) or Minimum Essential Medium (MEM) with Glutamax and Earle's Salts (Gibco), supplemented with 10% FBS (Atlas Biologicals) and penicillin/streptomycin (Invitrogen). Cells were passaged every 2–3 days when approximately 90% confluence was achieved. Cells were plated on tissue culture treated 35 mm dishes, transfected 24–48 h later and recorded from 24 to 48 h post-transfection. Cells were transiently transfected with wild type or mutations of full length cASIC1 (in pcDNA3.1(+)) along with eGFP using an ASIC:eGFP ratio of 2.5:1 μg of cDNA per 10 mL of media. Transfections were performed using polyethylenimine 25k (PEI 25k, Polysciences, Inc.) following manufacturer's instructions, with media change at 6–8 h. Mutations were introduced using site-directed mutagenesis PCR and confirmed by sequencing (Fisher Scientific/Eurofins Genomics).

Electrophysiology and Fast Perfusion

Culture dishes were visualized using a 20× objective mounted on a Nikon Ti2 microscope with phase contrast. A 470 nm LED (Thorlabs) and dichroic filter cube were used to excite GFP and detect transfected HEK cells. Outside-out patches were excised using heat-polished, thick-walled borosilicate glass pipettes of 3–8 MΩ resistance. The pipette internal solution contained (in mM) 135 CsF, 33 CsOH, 11 EGTA, 10 HEPES, 2 $MgCl_2$, and 1 $CaCl_2$ (pH 7.4). External solutions with a pH greater than 7 were composed of (in mM) 150 NaCl, 20 HEPES, 1 $CaCl_2$, and 1 $MgCl_2$ with pH values adjusted to their respective values using NaOH. For solutions with a pH lower than 7, HEPES was replaced with MES at the same concentration (20 mM). All recordings were performed at room temperature with a holding potential of −60 mV using an Axopatch 200B amplifier (Molecular Devices). Data were acquired using AxoGraph software (AxoGraph) at 20 kHz, filtered at 10 kHz and digitized using a USB-6343 DAQ (National Instruments). Series resistance was routinely compensated by 90–95% where the peak amplitude exceeded 100 pA. Rapid perfusion was performed using home-built, triple-barrel application pipettes (Vitrocom), manufactured following an established protocol (MacLean, 2015). Translation of application pipettes was achieved using a piezo translator (P601.40 or P212.80, PI) mounted to a manual manipulator and driven by a voltage power supply (E505.00 or E-471.20, PI).

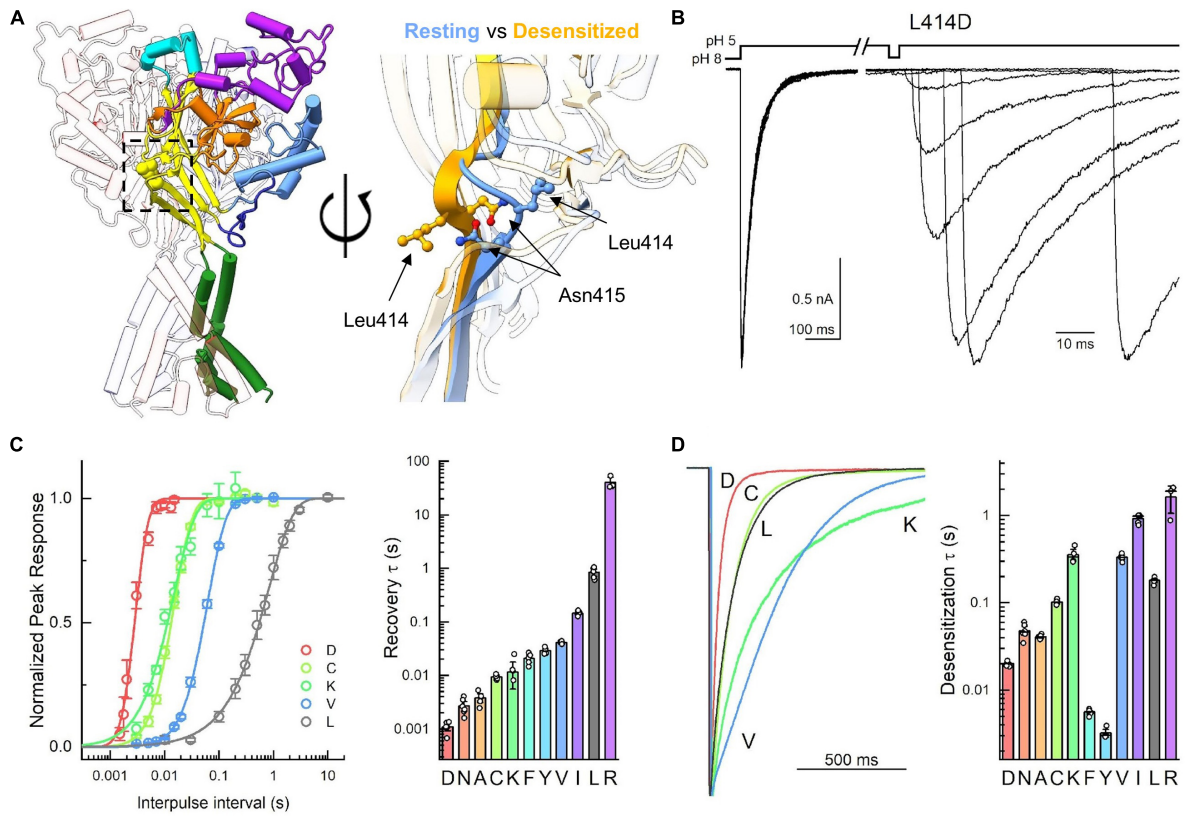

FIGURE 1 | Mutations to Leu414 have substantial impact on channel kinetics. (**A**, left) Trimeric structure of the resting state with individual domains colored (PDB: 6VTL). (**A**, right) Zoom in of the β11-12 linker in overlay of resting (6VTL, blue) and desensitized states (6VTK, orange). **(B)** Example outside-out patch recordings of L414D during recovery from desensitization protocol. Note the change in time scale in the example traces. **(C)** Summary recovery time course (left) and time constants (right) for Leu414 mutant panel from this and previous work. **(D)** Example traces (left) and summary of time constants (right) for desensitization decays of Leu414 mutant panel. Symbols represent individual patches and error bars are SEM. Differences in both desensitization and recovery kinetics for all mutations were statistically significant from wild type. Some data reproduced from Rook et al. (2020) under Creative Commons Attribution License (https://creativecommons.org/licenses/by/4.0/).

Voltage commands to the piezo were first low-pass filtered (eight-pole Bessel; Frequency Devices) at 50–100 Hz. Solution exchange was routinely measured at the end of each patch recording using open tip currents with exchange times ranging from 250 to 500 μs.

Molecular Dynamics Simulations

Molecular dynamics simulations were performed using a cASIC1 structure solved at 3 Å resolution in a proposed desensitized state (PDB ID: 4NYK) (Gonzales et al., 2009). In this crystal structure, residues 42–455 were resolved, of which 23 residues had missing atoms, which were modeled using MODELLER 9v20 (Sali and Blundell, 1993). Missing residues at the N- and C-termini were disregarded. Bound chloride ions and crystallographically resolved water molecules were retained. The orientation of the structure for placement in the lipid bilayer was obtained from the Orientations of Proteins in Membranes (OPM) database (Lomize et al., 2012). Disulfide bonds for each chain were maintained between the following cysteine pairs: C94-C195, C173-C180, C291-C366, C309-C362, C313-C360, C322-C344, and C324-C336. All residues were kept in their standard ionization state. To construct the simulation system, the protein was embedded in a 120 × 120 Å POPC bilayer using the CHARMM-GUI membrane builder (Jo et al., 2008), with a box length of 147 Å. The system was solvated with TIP3P water molecules and a NaCl concentration of 150 mM.

The L414D and N415G mutant systems were constructed in the same way, with mutations selected in the CHARMM-GUI interface.

The simulations were performed using GROMACS 2019.4 (Abraham et al., 2015) and the CHARMM36m forcefield was applied (Huang and MacKerell, 2013). All system constructs were minimized for 5000 steps or until a maximum force of 1000 kJ mol^{-1} nm^{-1} on any atom was reached. As per the default CHARMM-GUI method, the systems were then equilibrated in six steps. The first three steps were 125 ps long with a timestep of 1 fs. The final three steps were 500 ps long with a timestep of 2 fs. Following the default CHARMM-GUI equilibration, position restraints were gradually lifted with each equilibration step. The final production run had a timestep of 2 fs and was performed for 5 × 500 ns for each system, with the starting velocities of each repeat randomized prior to equilibration. Periodic boundary

conditions were applied and all systems were simulated in the NPT ensemble. The Verlet cut-off scheme was used throughout all steps with a force-switch modifier starting at 10 Å and a cut-off of 12 Å. The particle mesh Ewald (PME) method (Darden et al., 1993; Essmann et al., 1995) was used for long-range electrostatics and a cut-off of 12 Å was used for short-range electrostatics. For the equilibration steps, a temperature of 310 K was maintained using the Berendsen thermostat (Berendsen et al., 1984). The Berendsen barostat (Berendsen et al., 1984) was used to maintain a pressure of one bar for the last four steps of equilibration using semi-isotropic pressure coupling. For the production run, the Nose-Hoover thermostat (Nose, 1984; Hoover, 1985) was used to maintain temperature at 310 K and the Parrinello-Rahman barostat (Parrinello and Rahman, 1981) was used to maintain pressure at one bar using semi-isotropic pressure coupling. Covalent bonds including hydrogen atoms were constrained using the LINCS algorithm (Hess, 2008).

Analysis was performed using MDAnalysis tools (Michaud-Agrawal et al., 2011; Gowers et al., 2016) as well as in-house scripts. Structural figures prepared using VMD (Humphrey et al., 1996) and Chimera (Pettersen et al., 2004).

Sequence Alignments

Amino acid sequences for ASICs from evolutionarily distant organisms (Lynagh et al., 2018) were obtained directly from Dr. Lynagh. Sequences for mammalian, avian, amphibian and fish were obtained from NCBI. Sequences were aligned using Muscle (Edgar, 2004) with default settings. The percent conservation, logo plot and consensus sequence was calculated using Jalview (Waterhouse et al., 2009) and illustrated using Chimera (Meng et al., 2006).

Statistics and Data Analysis

Current desensitization decays were fitted using exponential decay functions in Clampfit (Molecular Devices). For recovery from desensitization experiments, the piezo command voltage was split and re-directed as an input signal. The resulting piezo "mirror" signal was used to define conditioning and test pulse epochs. A custom script in Matlab (Mathworks) was used to detect peaks within each epoch and normalize the test pulse peak to the conditioning pulse. OriginLab (OriginLab Corp.) was used to fit the normalized responses to:

$$I_t = \left(1 - e^{\left(\frac{-t}{\tau}\right)}\right)^m \quad (1)$$

where I_t is the fraction of the test peak at an interpulse interval of t compared to the conditioning peak, τ is the time constant of recovery and m is the slope of the recovery curve. Each protocol was performed between 1 and 3 times on a single patch, with the resulting test peak/conditioning peak ratios averaged together. For steady-state desensitization (SSD) curves, peak currents within a patch were normalized to the peak response evoked by pH 5.5 and fit to:

$$I_x = {}^{1}\Big/\left(1 + 10^{((pH_{50} - pH_x)n_H)}\right) \quad (2)$$

where I_x is the current obtained using a given conditioning pH value X, pH_{50} is the pH yielding half maximal response and n_H is the Hill slope. For recovery experiments and SSD, patches were individually fit and averages for the fits were reported in the text. For all experiments, N was taken to be a single patch and error is reported as SEM. Unless otherwise state, non-parametric two-tailed, unpaired randomization tests with 100,000 iterations were implemented in Python to assess statistical significance. Bonferroni-Holm corrections for multiple comparisons were used and the adjusted *P*-values are reported in either text, figure legend or **Table 1**. Statistical comparisons of recovery from desensitization and SSD were based on differences in recovery time constant and pH_{50}, respectively.

To assess statistical differences in side chain angles from molecular dynamics simulations, we measured the median side chain angle from all three chains within each simulation as median is less sensitive to outliers (or multiple populations) than mean. To compare side chains angles between conditions (e.g., N415 angles for wild type vs. L414D), we compared the median side chain angles for each simulation in each group using a Mann–Whitney *U* test where n is the number of simulations.

RESULTS

Kinetics of Desensitization and Recovery Are Strongly Influenced by Mutations to the β11-12 Linker

With the exception of the acidic pocket, the most salient difference between the resting and desensitized states of cASIC1 is the isomerization of the linker connecting the 11th and 12th beta strands. This is illustrated in **Figure 1A** where the side chains of the linker residues are shown within the palm domain as well as superimposed in the resting and desensitized states [PDB: 6VTL and 6VTK (Yoder and Gouaux, 2020)]. In the resting state, Leu414 points outward from the central axis of the channel and slightly up. However, in the desensitized state, the Leu414 side chain swings inward and down, toward a hydrophobic cleft (Rook et al., 2020). In parallel, Asn415 rotates from a down and inward position in the resting state to an upward and out position in the desensitized state. This swivel was proposed to act as a molecular clutch, uncoupling the proton sensing extracellular domain from the channel pore and thereby allowing the extracellular domain to adopt an "active-like" protonated conformation while the pore shuts closed (Yoder et al., 2018). Consistent with this, using non-canonical amino acid trapping, we recently demonstrated that local motion of this area is critical for desensitization to occur (Rook et al., 2020). We also found that slight mutations to the Leu414 position (i.e., L414A) result in dramatic changes in channel desensitization and recovery (Rook et al., 2020). The goal of the present study was to further probe the molecular determinants of this linker isomerization using molecular dynamics simulations.

A challenge in using molecular dynamics simulations to explore functional transitions of ion channels is the discrepant time scales of molecular dynamics simulations ($\sim 10^{-7}$ s) vs. patch clamp experiments ($\sim 10^{-3}$ s). In this case, the

TABLE 1 | Time constants of desensitization and recovery.

Mutation	τ_{des} (ms)	$\tau_{des,fast}$ (ms) [% area]	$\tau_{des,slow}$ (ms) [% area]	Adj. *P*-value vs. wt	τ_{rec} (ms)	m_{rec}	Adj. *P*-value vs. wt	*n*
WT	180 ± 6	–	–		840 ± 90	0.96 ± 0.05	–	5
A83G	31 ± 2	–	–	0.00025	210 ± 30	1.2 ± 0.05	0.00014	5
L414C	100 ± 3	–	–	0.01773	9.6 ± 0.5	2.5 ± 0.2	0.0008	5
L414D	20 ± 0.6	–	–	0.00618	1.1 ± 0.1	9.7 ± 1.7	0.001	5
L414K	370 ± 60*	120 ± 32 [45 ± 5]	590 ± 140 [55 ± 5]	0.0234	21 ± 2	3.5 ± 0.5	0.0022	4
L414V	330 ± 10	–	–	0.0009	41 ± 1	2.09 ± 0.07	0.00125	5
L414N	47 ± 4	–	–	0.0126	2.7 ± 0.4	12 ± 4	0.0009	6
L414A	41 ± 1	–	–	0.01228	3.8 ± 0.5	9 ± 3	0.00087	5
L414F	56 ± 2	–	–	0.0236	21 ± 2	3.5 ± 0.5	0.00112	5
L414Y	32 ± 2	–	–	0.02805	29 ± 2	2.7 ± 0.2	0.00076	4
L414I	920 ± 50	–	–	0.00408	145 ± 6	1.40 ± 0.04	0.00108	5
L414R	1600 ± 400	–	–	0.001	40000 ± 6000	0.30 ± 0.03	0.0007	3
N415A	38 ± 2	–	–	0.0082	13 ± 1	1.9 ± 0.2	0.0014	5
N415D	110 ± 5	–	–	0.00522	46 ± 1	1.6 ± 0.04	0.00098	5
N415E	2000 ± 70	–	–	0.0012	3.2 ± 0.07	3.6 ± 0.2	0.00096	4
N415F	1500 ± 50	–	–	0.0011	22 ± 2	2.1 ± 0.3	0.0008	4
N415G	3.6 ± 0.4	–	–	0.00984	5.9 ± 0.4	1.9 ± 0.2	0.00154	5
N415I	18000 ± 400*	3000 ± 800 [42 ± 5]	30000 ± 2000 [58 ± 5]	0.00605	290000 ± 80000	0.3 ± 0.6	0.0012	3
N415K	9900 ± 600	–	–	0.00938	35 ± 4	2.8 ± 0.2	0.00032	4
N415L	7800 ± 600	–	–	0.001	860 ± 90	0.99 ± 0.05	0.85608	2
N415Q	1900 ± 100	–	–	0.00736	29 ± 5	2.2 ± 0.2	0.00048	4
N415R	4700 ± 400	–	–	0.00594	18 ± 0.5	3.3 ± 0.1	0.00126	5
N415S	53 ± 3	–	–	0.00744	45 ± 6	1.4 ± 0.04	0.00112	5
N415W	3400 ± 70	–	–	0.00848	25 ± 0.6	1.1 ± 0.1	0.00064	4

**Indicates weighted time constant.*
Desensitization decays measured in pH 5. Recovery measured in pH 8.

functional transitions of interest are desensitization and recovery, respectively. To partially bridge the timescale gap, we have previously taken advantage of the pH-dependence of recovery from desensitization (Rook et al., 2020). ASICs recover faster from desensitization when incubated in more alkaline solutions. This effect is quite strong in cASIC1, which recovers with a time constant of 840 ± 90 ms at pH 8 but accelerates to 7.5 ± 0.4 ms at pH 10 (Rook et al., 2020). By starting simulations from the desensitized/protonated crystal structure and de-protonating acidic residues (i.e., approximating a functional transition from extracellular pH 5 to 9), we can provoke the beginning of the transition from desensitized to resting state. When this strategy is combined with mutations which accelerate recovery from desensitization, we have previously been able to observe the linker flipping behavior directly in molecular dynamics simulations (Rook et al., 2020). Hence, we again focused on capturing the recovery process in the simulations, rather than the desensitization process.

A second challenge or caveat in comparing molecular dynamics simulations with results from patch clamp experiments is that the measured macroscopic channel desensitization and recovery processes reflect a population of channels transitioning between resting, active, pre-active and desensitized states. Changes to one or more of these transitions may alter the macroscopic desensitization decays measured in the population without much influence on the microscopic desensitization transition itself (Jones and Westbrook, 1996; Daniels et al., 2013). Since molecular dynamics simulations more likely reflects the single channel state transitions, we must bear this caveat in mind.

We set out to extend our previous work by first characterizing a wide range of mutations at both the Leu414 and Asn415 positions. The fastest mutations uncovered would then be used for molecular dynamics simulations to better probe the interactions governing linker isomerization. As an added benefit, these experiments would further map the structure-function relationships in this critical region.

To do this, we made four additional mutations to Leu414 in cASIC1 (D, C, K, and V). This isoform was used to enable direct comparison with past work, due to the larger number of structures and because, in our hands, cASIC1 undergoes far less tachyphylaxis [long-lived inactivation or run-down (Chen and Grunder, 2007)], thus enabling longer recordings of recovery from desensitization. To measure recovery, we excised patches from transfected ASIC KO HEK cells (Rook et al., 2021a) and used piezo-driven fast perfusion to jump from pH 8 to 5. Recovery was mapped using a standard two-pulse protocol where channels were first exposed to a conditioning pulse of pH 5 to populate the desensitized state followed by jumping to pH 8 for variable intervals before a test pulse of pH 5 is applied. Conditioning pulse durations were chosen for each mutation

to achieve equilibrium desensitization. However, the test pulse was generally 500 ms in duration (although 50 ms was used for N415G). Strikingly, each mutation showed a statistically significant difference in recovery from desensitization compared to wild type (**Figure 1C** and **Table 1**). To our surprise, we found the L414D showed the fastest recovery from desensitization (τ = 1.1 ± 0.1 ms, m = 9.7 ± 1.7, n = 5) while the structurally smaller L414A and L414C were actually slower than L414D (**Figures 1B,C**). Even with this new expanded series, we could discern no clear pattern or structural feature that predicted fast recovery. The large and positively charged Arg side chain desensitized and recovered slowly (Rook et al., 2020), however, the smaller Lys side chain actually recovered faster than wild-type (τ = 21 ± 2 ms, m = 3.5 ± 0.5, n = 4). Moreover, the sizeable hydrophobic side chains of Tyr and Phe recovered faster.

In the course of this experiment, we also measured the rates of entry into desensitization of the mutant panel during the conditioning pulse (**Figure 1D**). As with recovery, all mutations showed statistically significant differences in desensitization kinetics compared to wild type (**Figure 1D** and **Table 1**). We found that L414D was the fastest of the new mutations, with a desensitization time constant of 20 ± 0.6 ms (n = 5). Taken together, our data suggest that L414D is a promising mutation with extraordinarily fast kinetics, both desensitization and recovery, and hence may be a suitable candidate for molecular dynamics simulations. Specifically, using L414D to provoke swiveling might enable us to study the trajectory of the unaltered partner N415. To identify a similar candidate in N415 (fast mutation which would allow us to study the interactions of L414), we mutated N415 to 12 different residues and mapped their recovery from desensitization (**Figures 2A,B**). Among these, N415E showed the fastest recovery from desensitization (3.0 ± 0.7 ms, m = 3.6 ± 0.2, n = 4). While N415E recovered very quickly, this clone underwent desensitization slower than wild type (**Figure 2**) with a time constant of 2 ± 0.07 s. In contrast, N415G both entered and exited the desensitized state quickly (**Figure 2**) and hence was selected for subsequent molecular dynamics simulations. We found that nearly all mutations accelerated recovery in a statistically significant manner, while some slowed and others accelerated desensitization. The sole exception was N415I, which showed nearly 100 fold slower desensitization and recovery compared to wild type (**Figure 2** and **Table 1**).

Two additional general observations emerge from this mutant panel. First, we have previously remarked that when the time course of ASIC recovery is accelerated (by mutation or pH), the slope of the recovery curve becomes steeper and when recovery is slowed, the slope becomes more shallow (Rook et al., 2020). This positive correlation between rate constant of recovery and slope is also found within this expanded dataset (to our knowledge the largest panel of recovery experiments for ASICs) (**Figure 3A**). Such behavior is not expected for a simple kinetic model (Rook et al., 2020). A precise molecular explanation for this robust feature is unclear but its persistence through the mutant series is an essential aspect of ASIC recovery. Second, any alteration to Leu414 or Asn415 produces very large changes in kinetics. This is seen in the scatter plots in **Figure 3B**, where the time constants for desensitization are plotted in the abscissa and the recovery in the ordinate. It is immediately apparent that Leu414 and Asn415 are relatively isolated. That is, any small changes to these side chains produce robust, often order of magnitude, effects in desensitization and recovery. In principle, the kinetics of desensitization and recovery reflect the stability of the desensitized state. If all other transitions remain constant, a mutation causing slower desensitization (or faster recovery) should also lead to a less stable desensitized state, requiring stronger stimuli to desensitize. This should manifest as a right shift or acidic shift in the SSD curve, the process where ASICs desensitize upon exposure to acidic conditions too mild to detectably activate the channel. To examine this, we measured an SSD curve for N415D that has faster recovery than wild type with a comparatively small change in desensitization (**Figure 3C**). As expected, this mutation produced a less stable desensitized state as evidenced by the significant right shift in the SSD curve (wild type: pH_{50} 7.31 ± 0.01, n_H 6.6 ± 0.3, n = 6; N415D: pH_{50} 7.048 ± 0.005, n_H 15.9 ± 0.4, n = 4, p = 0.0044, **Figure 3D**). We next examined N415K, a mutation with comparable recovery to N415D but roughly 100 fold slower desensitization kinetics (**Figure 3C**). This mutation should produce a further right shift in the SSD curve. Indeed, as predicted the pH_{50} for SSD of N415K was significantly more acidic than N414D (N415K: pH_{50} 6.827 ± 0.005, n_H 8.7 ± 0.4, n = 4, p = 0.018 vs. N415D, **Figure 3D**). Our kinetic data (**Figures 3A,B**) underscores the essential nature of the β11-12 in governing transitions to the desensitized state. Furthermore, the remarkable sensitivity of this region suggests that the interactions surrounding this linker have been exquisitely shaped by evolution to obtain exactly the desired kinetic behavior (**Figures 3A,B**) or desensitized state stability (**Figure 3D**). To explore what these interactions might be, we turned to all-atom molecular dynamics simulations.

Molecular Dynamics Simulations With Fast Recovering Mutations

To approximate the early phase of the desensitized to resting transition (i.e., the recovery process), we simulated either wild type, L414D or N415G desensitized state trimers in a bilayer. To accelerate conformational changes as illustrated previously (Rook et al., 2020), all acidic side chains were de-protonated in the simulations (approximating a pH of 8–9 based on pK_a estimates) and ensuing motions were examined. Each construct was simulated five times for 500 ns each. We used two main metrics to quantify changes observed during these simulations. First, we measured the phi and psi dihedral angles for residues 414 and 415 to quantify backbone conformational changes and flexibility (**Figure 4A**). However, since the phi/psi dihedral angles do not substantially change between resting and desensitized states for Leu414, we primarily used this metric for Asn415. Second, we measured the side chain angle, defined as the angle centered at the α carbon, between the channel center and the γ carbon atoms of Leu414 and Asn415 (**Figures 4B,C**). Examples of these metrics in wild type, one for a very stable simulation and one for a simulation showing some local instability, are shown in **Figures 4D–G**. In four

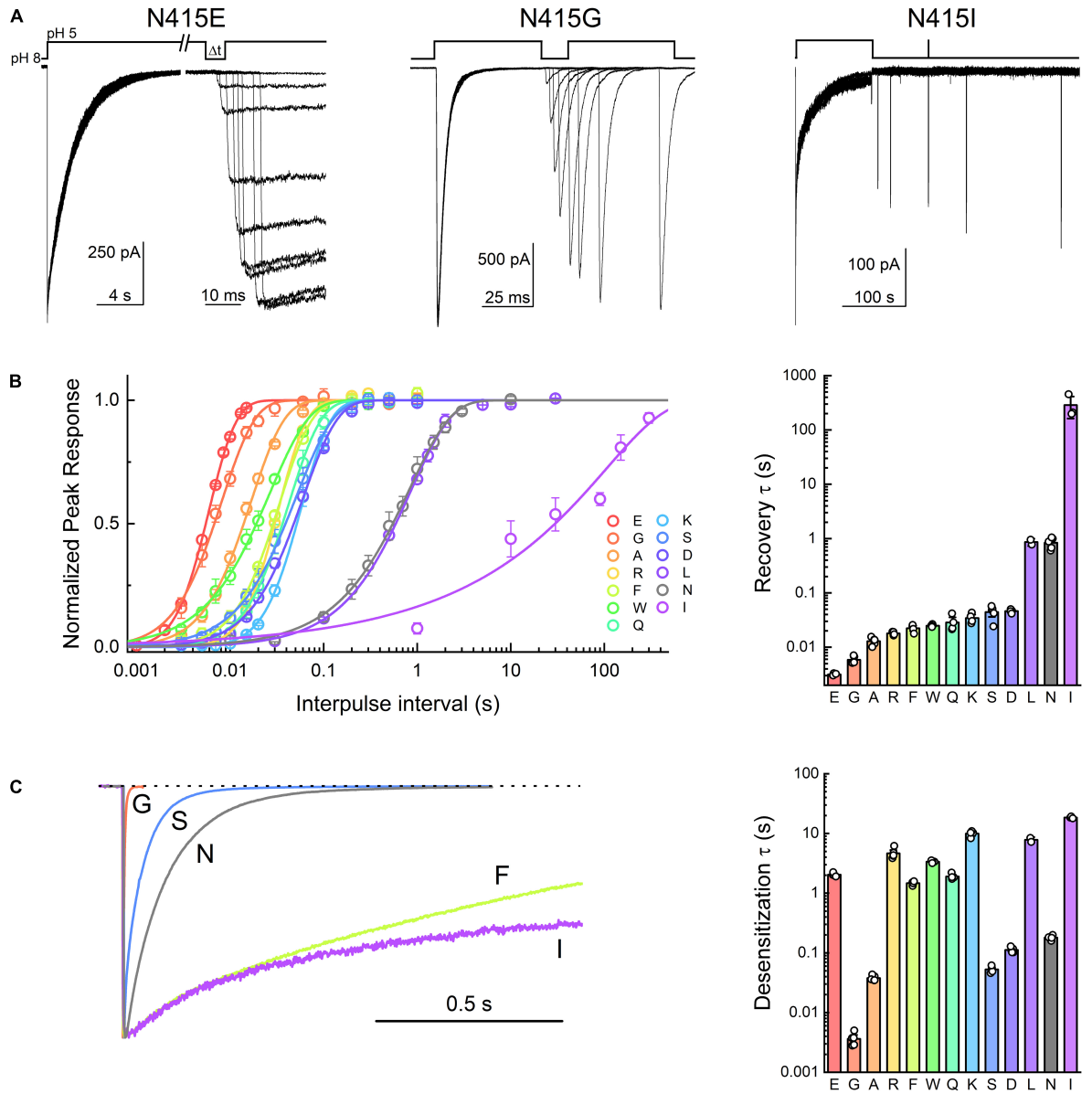

FIGURE 2 | Acid-sensing ion channel (ASIC) desensitization and recovery is altered by mutations to Asn415. **(A)** Example outside-out patch recordings of N415E, G, and I (left, middle, and right, respectively). Note the change in time scale in the N415E example. **(B)** Summary recovery time course (left) and time constants (right) for Asn415 mutant panel. **(C)** Example traces (left) and summary of time constants (right) for desensitization decays of Asn415 mutant panel. Symbols represent individual patches and error bars are SEM. Differences in both desensitization and recovery kinetics for all mutations were statistically significant from wild type, with the exception of N415L recovery that was not different.

out of five wild type simulations, there was minimal change in these metrics. **Figures 4D,E** shows an example of such a stable run where the side chain angles and the phi/psi plots for each chain remain close to that of the desensitized state (**Figure 4D**) and the side chain position does not move appreciably (**Figure 4E**). However, in run 5 Asn415 of chain B undergoes a significant conformational shift from a desensitized-like side chain angle and phi/psi plot to become closer to the resting state (**Figure 4F**). In this simulation, the Asn415 side chain is also far more mobile (**Figure 4G**). We therefore turned to analyzing our fast recovering mutants, expecting to see greater dynamics.

As expected of the fast recovering mutants, in all five L414D simulations we observed a much greater degree of Asn415 motion and a tendency for side chain angles and phi/psi plots to approach those of the resting state. **Figure 5** shows one such example where at the start of the simulation, the Asn415 phi/psi plots of all three chains overlap with that expected of the desensitized structure (**Figure 5A**). Interestingly, the side chain angles begin to deviate quickly from that expected of the desensitized state. Around the

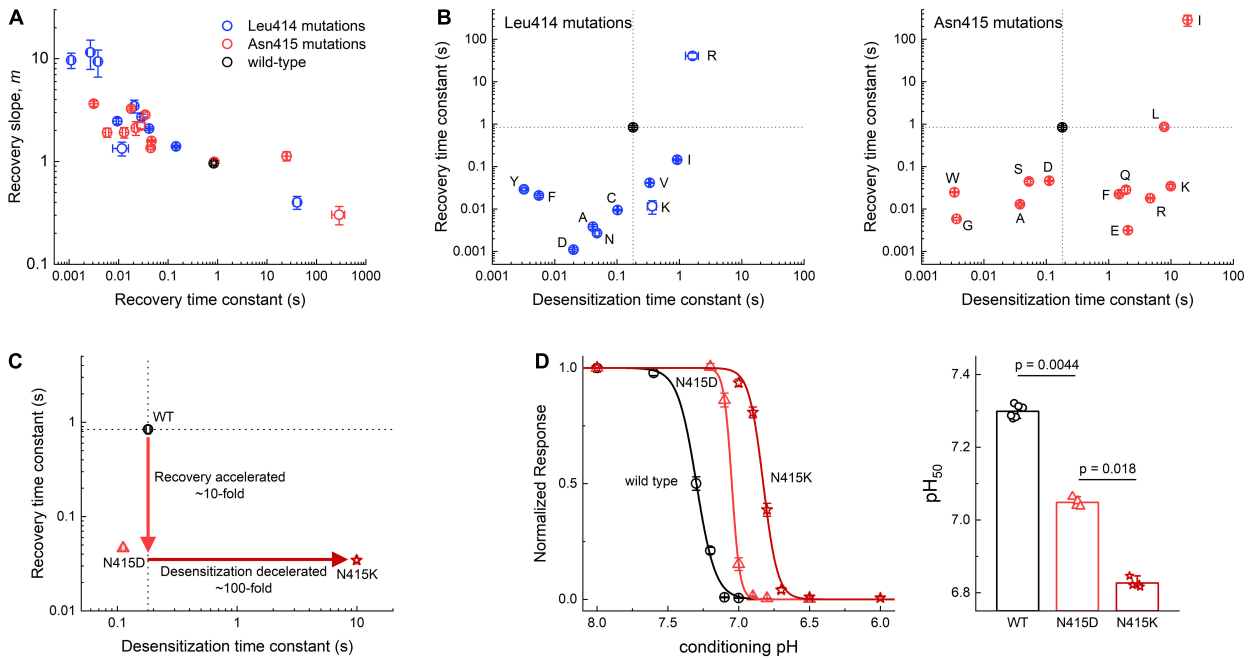

FIGURE 3 | Summary of Leu414 and Asn415 mutant kinetics. **(A)** Recovery slope (*m*) vs. time constant (τ) of the recovery curve for mutant series in Leu414 (blue) or Asn415 (red). **(B)** Summary of entry and exit time constants for each mutant in L414 (left) and Asn415 (right). Note that the wild type side chains (black) are relative isolated with any deviation producing order of magnitude changes in kinetics. **(C)** N415D has ∼10 fold faster recovery with comparable desensitization vs. wild type. N415K has ∼100 fold slower desensitization with comparable recovery as N415D. **(D)** Steady-state desensitization curves for wild type, N415D and N415K (left) and pH_{50}s from each patch. *P*-values are from randomization tests. All error bars are SEM.

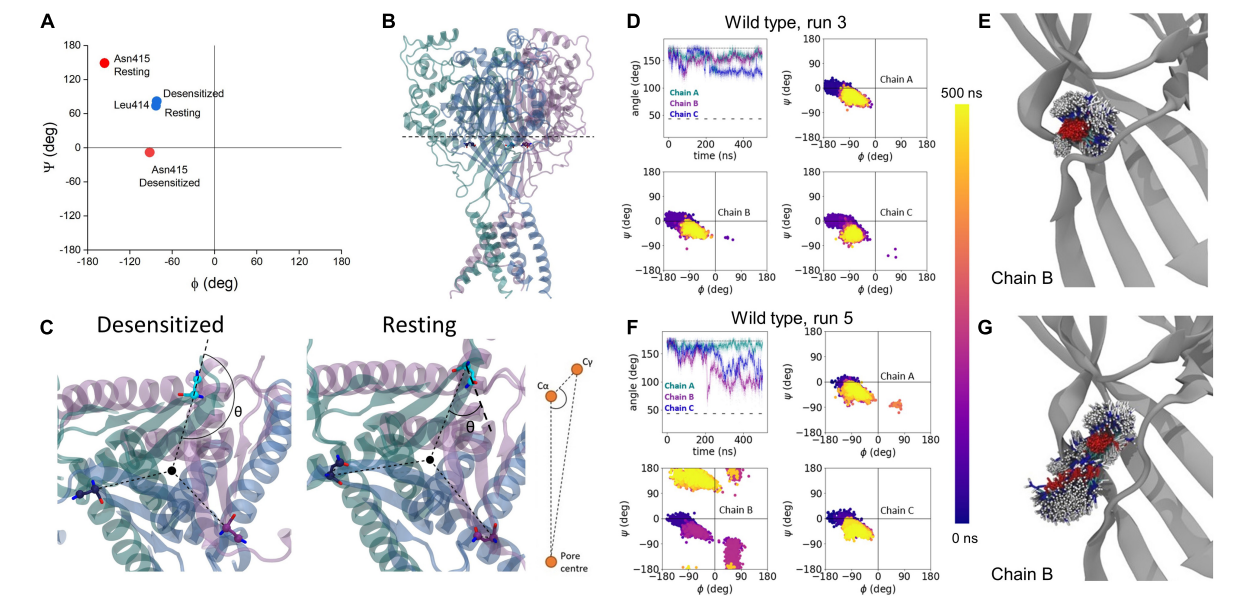

FIGURE 4 | Analysis of transitions to resting state using molecular dynamics simulations. **(A)** Phi/psi plots of Leu414 (blue) and Asn415 (red) in desensitized and resting states. **(B)** Slice-through of the desensitized state structure to show the plane of angle defined in panel **(C)**. **(C)** Illustration of change in side chain angle, with respect to Cγ and channel center in desensitized and resting states. **(D)** Example of wild type run where no substantial changes were seen in the side chain angle (upper left), or phi/psi plots in each chain (upper right, lower panels). The dotted line illustrates the side chain angle of N415 in the desensitized state structure while the dashed line illustrates the side chain angle in the resting state structure. **(E)** Overlay of 1000 Asn415 positions at regular intervals over the 500 ns simulation. **(F,G)** Same as panels **(D,E)** but for wild type run where motion toward a resting-like conformation was observed in chain B.

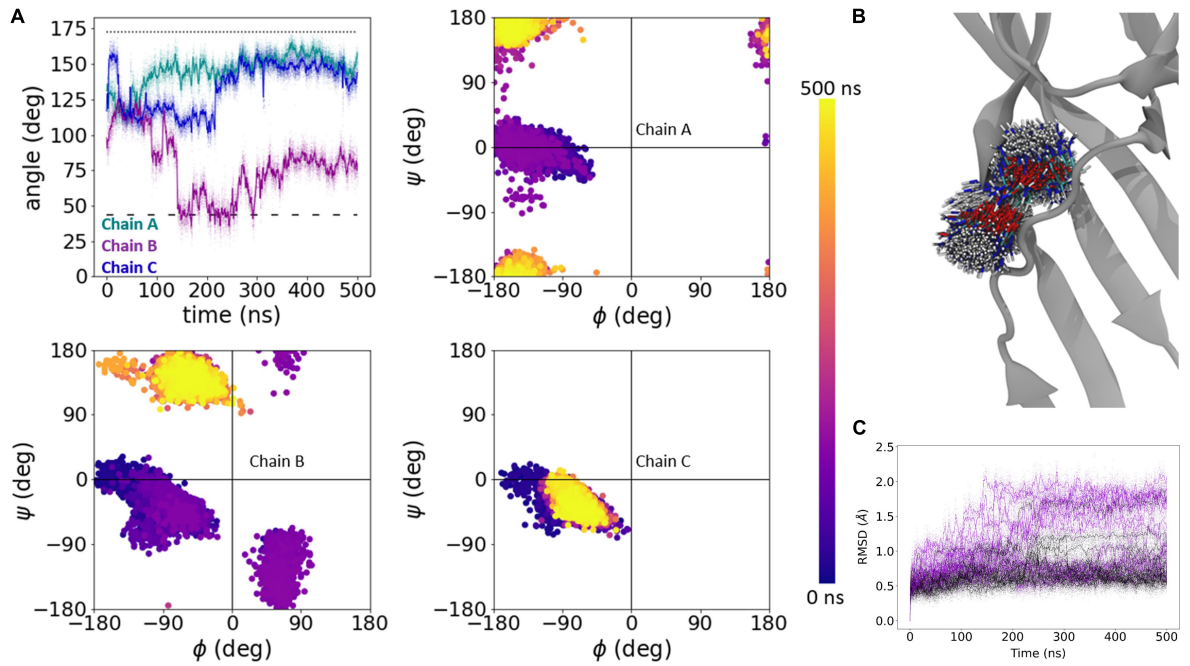

FIGURE 5 | Dynamics of Asn415 in L414D mutation. **(A)** Side chain angle (upper left) and phi/psi plots (upper right, lower) of Asn415 chains in L414D simulation, run 2. The dotted line illustrates the side chain angle of N415 in the desensitized state structure while the dashed line illustrates the side chain angle in the resting state structure. **(B)** 1000 snapshots from chain B, at regular intervals, from simulation in panel **(A)**. **(C)** Calculated RMSD of individual chains as a function of time for Cα atoms of amino acid residues 409–420 of wildtype (black) and L414D mutant (violet). Raw data is plotted in the background as transparent dots, smoothed data is plotted as a solid line.

140 ns time point, a major rearrangement of chain B's Asn415 side chain and backbone is evident both in the angle and phi/psi plots (**Figure 5A**). This change in conformation is further observed in a series of structural snapshots over the course of the simulation (**Figure 5B**). Comparing the root mean square deviation (RMSD) of the C_α -atoms of residues 409–420 for all simulated chains (three chains per protein times five repeats, i.e., 15 chains per system) moreover illustrates that while three to four chains in the wild type simulations undergo larger conformational changes (defined as reaching an RMSD > 1 Å), this is the case for 10 of the 15 chains for the L414D mutant (**Figure 5C**). Thus, looking at our full data set for wild type vs. the L414D mutant, it is also clear that the L414D point mutation provokes structural rearrangements to a larger degree than observed for the wild type.

We next conducted the same block of five 500 ns simulations of N415G (**Figure 2**) to examine the dynamics of Leu414 flipping. As with the L414D simulations, N415G resulted in an overall greater degree of motion of the Leu414 side chain as well as a highly increased backbone flexibility. This is illustrated with an example for a single chain in **Figures 6A,B**. As above, comparing the RMSD values for all chains for the β11-12 linker region, it is again clear that the mutation causes a much larger degree of structural change than observed for the wild type (14 out of 15 chains with an RMSD > 1 Å for the mutant vs. 3–4 chains for the wild type) (**Figure 6C**).

In addition to analyzing the individual simulations, we also examined the overall distributions for the side chain angles as well as the phi/psi backbone angles for our full data set (**Figure 7**). The median side chain angles of L414 were statistically different between wild type and the "fast mutant" N415G (median L414 side chain angles of wild type ranged from: 67.1–79.3°; N415G: 81.4–120.3°, $n = 5$, $p < 0.01$, Mann–Whitney U test). In particular, the L414 side chain angle only shows one population for the wild type simulations. The population peak overlaps with the side chain angle in the crystal structure of the desensitized state (**Figure 7A**). Interestingly, in the N415G mutant the L414 side chain angle measurements clearly form two populations. One of these is at an angle slightly higher than the angle in the crystal structure for the desensitized state, while the other population almost matches the side chain angle of L414 in the crystal structure of the resting state. In the case of N415, a similar pattern appears. The median side chain angles of N415 were different between wild type and L414D simulations (median N415 side chain angles of wild type ranged from: 153.6–161.3°; L414D: 95.7–128.7°, $n = 5$, $p < 0.01$, Mann–Whitney U test). But whereas the wild type simulations predominantly show side chain angles tightly grouped close to that of the desensitization state structure (**Figure 7B**), in the L414D simulations multiple populations arise, all of which are closer to the resting state angle (**Figure 7B**). This data again highlight that the mutations appear to push the structure of the β11-12 linker closer to the resting state structure. When plotting the backbone dihedral angles for all our simulation data, it is obvious that the wild type simulations show one overall population for both L414 (**Figure 7C**) and N415

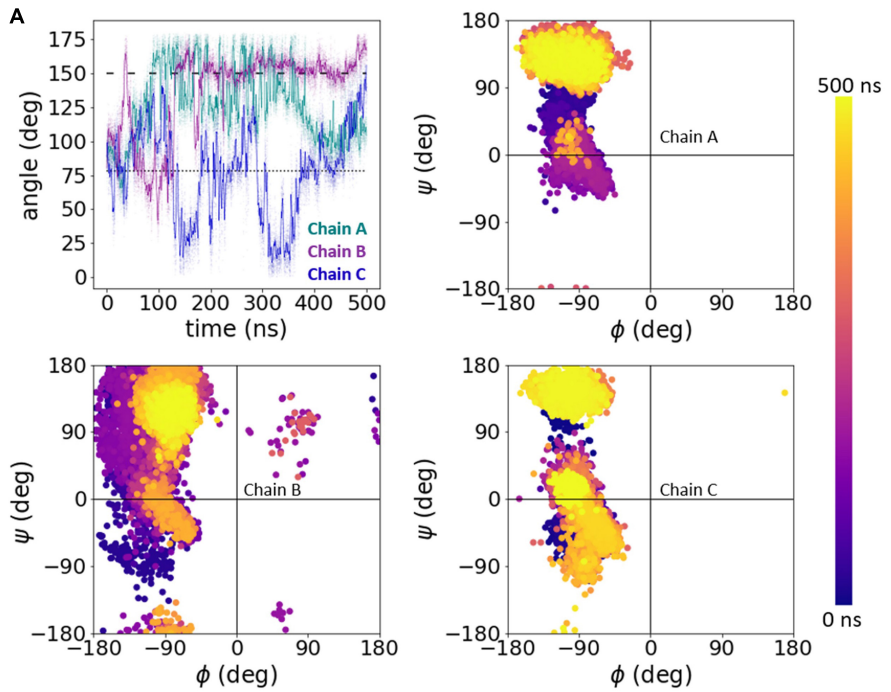

FIGURE 6 | Dynamics of Leu414 in N415G mutation. **(A)** Side chain bond angle (upper left) and phi/psi plots (upper right, lower) of Leu414 chains in N415G simulation, run 2. The dotted line illustrates the side chain angle of L414 in the desensitized state structure while the dashed line illustrates the side chain angle in the resting state structure. **(B)** 1000 snapshots from chain B, at regular intervals, from simulation in panel **(A)**. **(C)** Calculated RMSD of individual chains as a function of time for Cα atoms of amino acid residues 409–420 of wildtype (black) and N415G (teal). Raw data is plotted in the background as transparent dots, smoothed data is plotted as a solid line.

(**Figure 7D**), while for both of the mutants, the populations are less well defined, underlining the larger conformational flexibility caused by the point mutations.

We have previously described that the L414A mutation accelerates conformational changes and how L414 is nested in a hydrophobic pocket in the desensitized state (Rook et al., 2020). Thus, it is perhaps not surprising that the L414D mutation also increases the flexibility of the β11-12 linker. On the contrary, it is not immediately clear why the N415G mutant illustrates dramatically increased flexibility of the linker region. It is possible that these observed dynamics for the N415G mutant result from either the increased backbone flexibility expected with a Gly replacement or from the loss of some specific contacts of the Asn415 side chain when changing this position to N415G. To gain some insight into this question, and further analyze our wild type and L414D simulations, we examined this data set for candidate interactions, which may play roles in linker flipping. We observed that the backbone oxygen atom of Leu414 is frequently stabilized by a presumptive hydrogen bond interaction with the side chain of Gln277. This interaction has been reported in our prior simulations and plays a functional role in stabilizing the desensitized state (Rook et al., 2021a). We also observed a putative hydrogen bond between the side chain oxygen atom of Asn415 and the backbone amide N-H of Ala83 (**Figure 8A**). If this Asn415-Ala83 interaction has functional importance, one expects the interaction to be disrupted in simulations with faster recovering mutations. To test this, we measured the distance between the side chain oxygen atom of Asn415 and the backbone amide of Ala83 for all wild type and L414D simulations. As seen in **Figure 8A** (lower panel), simulations with the faster recovering mutation showed a substantial increase in the distance between these two atoms, well beyond the 3–3.5 Å of typical hydrogen bond interactions. We further examined the temporal dynamics of this interaction. As seen in **Figure 8B** with a stable wild type simulation, when the side chain angle and phi/psi plots remain at the desensitized state values, there is minimal change in the Asn415-Ala83 distance. However, when a fast recovering L414D trajectory is examined (**Figure 8C**), the Asn415-Ala83 distance increase is temporally correlated with the side chain angle and phi/psi dihedral angle changes. Thus, we hypothesized that the Asn415-Ala83 interaction is functionally important for stabilizing the desensitized state.

To test this experimentally, we substituted Ala83 for Gly. Standard mutagenesis cannot remove the Ala83 backbone amide, however, we reasoned that replacing the Ala with a Gly would impart additional flexibility, enabling the A83G position to move out of hydrogen bond distance from the Asn415, thereby weakening the interaction and accelerating recovery from desensitization. Consistent with this hypothesis, A83G resulted in marked acceleration of recovery (recovery τ of 210 ± 25 ms, $n = 5$, $p < 0.001$ vs. wild type, **Figure 8**). Taken together, these data support that the β11-12 linker flipping is critical for ASIC

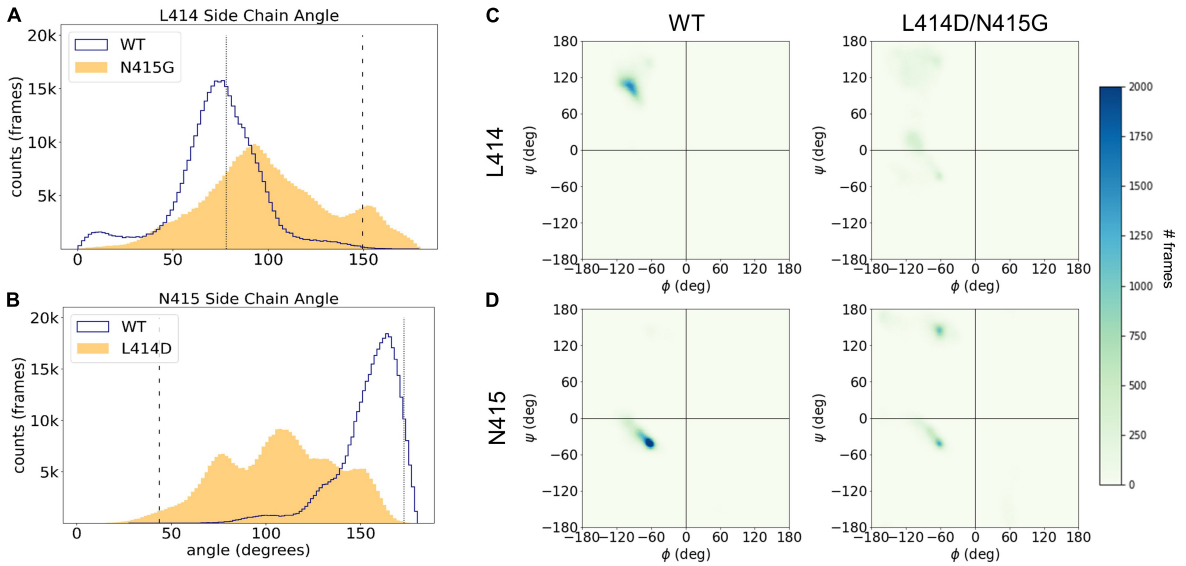

FIGURE 7 | Leu414 and Asn415 are more dynamic in mutant compared to WT simulations. **(A)** Histogram of side chain angle of Leu414 in all WT (blue trace) and N415G simulations (yellow area). The dotted line illustrates the side chain angle of L414 in the desensitized state structure while the dashed line illustrates the side chain angle in the resting state structure. **(B)** Same measurement as in panel **(A)** but comparing Asn415 sidechain angle in WT (blue trace) and L414D (yellow area) simulations. **(C)** Frequency of phi/psi pairs for Leu414 in WT simulations (left) or N415G simulations (right). **(D)** Frequency of phi/psi pairs Asn415 in WT simulations (left) or L414D simulations (right).

desensitization and highlight a new interaction between the Ala83 backbone and the side chain of Asn415. Our work also advances several metrics for analyzing ASIC simulations in the future.

DISCUSSION

Comparison With Past Work

There is considerable evidence indicating that the β11-12 linker is the essential structural determinant of pH-induced desensitization. Prior to the availability of ASIC structures, functional studies reported strong effects of mutations to the area surrounding the β11-12 linker (Coric et al., 2003). As structures of different states emerged, complimentary functional work supported the critical nature of the β11-12 linker in channel desensitization (Li et al., 2010a,b; Roy et al., 2013; Wu et al., 2019). Work from our own labs using UV-reactive non-canonical amino acid trapping has shown that desensitization can be nearly abolished by preventing the isomerization of the β11-12 linker (Rook et al., 2020), supporting the idea that linker swivel is necessary for desensitization. Here we examine a large panel of mutations to this linker and find that virtually every single mutation produces at least an order of magnitude shift in desensitization or recovery time constants (**Figures 1–3**). The marked sensitivity of this area to subtle perturbations is further evidence supporting the critical nature of this linker and the general "molecular clutch" model. However, is the β11-12 linker isomerization the only mechanism for channel desensitization?

Mutations in the thumb domain influence desensitization kinetics (Krauson et al., 2013; Krauson and Carattino, 2016; Braun et al., 2021) as does simple extracellular anion substitution (Kusama et al., 2010, 2013). How can these data be reconciled with a model where linker flipping is the crucial feature governing ASIC desensitization? Structural studies reveal an anion binding site physically proximal to the linker (15 Å from the Cl^- anion to the Cα of Leu414 in PDB 2QTS) (Jasti et al., 2007). This anion site is formed by Arg310 and Glu314 in the thumb domain and Lys212 from the adjacent subunit (cASIC1 numbering). Lys212 resides in a peptide loop immediately above the β11-12 linker. It is plausible that anion occupancy exerts an allosteric influence on linker flipping by stabilizing or destabilizing this upper loop through interactions between the anion and Lys212. Further, given that the base of the thumb forms the anion binding site, mutations to the thumb may impact desensitization kinetics by virtue of influencing anion occupancy. Clearly, further work is needed to test this hypothesis, however, it is certainly possible that the β11-12 linker represents a final common pathway for channel desensitization.

Physiological Role of Desensitization

The β11-12 linker is highly sensitive to mutation, as is the surrounding area (Coric et al., 2003; Wu et al., 2019; Rook et al., 2020, 2021b) with even conservative mutations producing log unit shifts in kinetics. This region is also highly conserved within ASICs. We aligned amino acid sequences of acid-responsive ASIC variants from mouse and human (ASIC1a and 3) as well as ASIC1a-like sequences from chicken, hummingbird, two amphibians, several fish, spiny dogfish (Springauf and Grunder, 2010) along with more distant sequences known to be pH-responsive (Lynagh et al., 2018). The percentwise conservation determined from this alignment was used to color the cASIC1

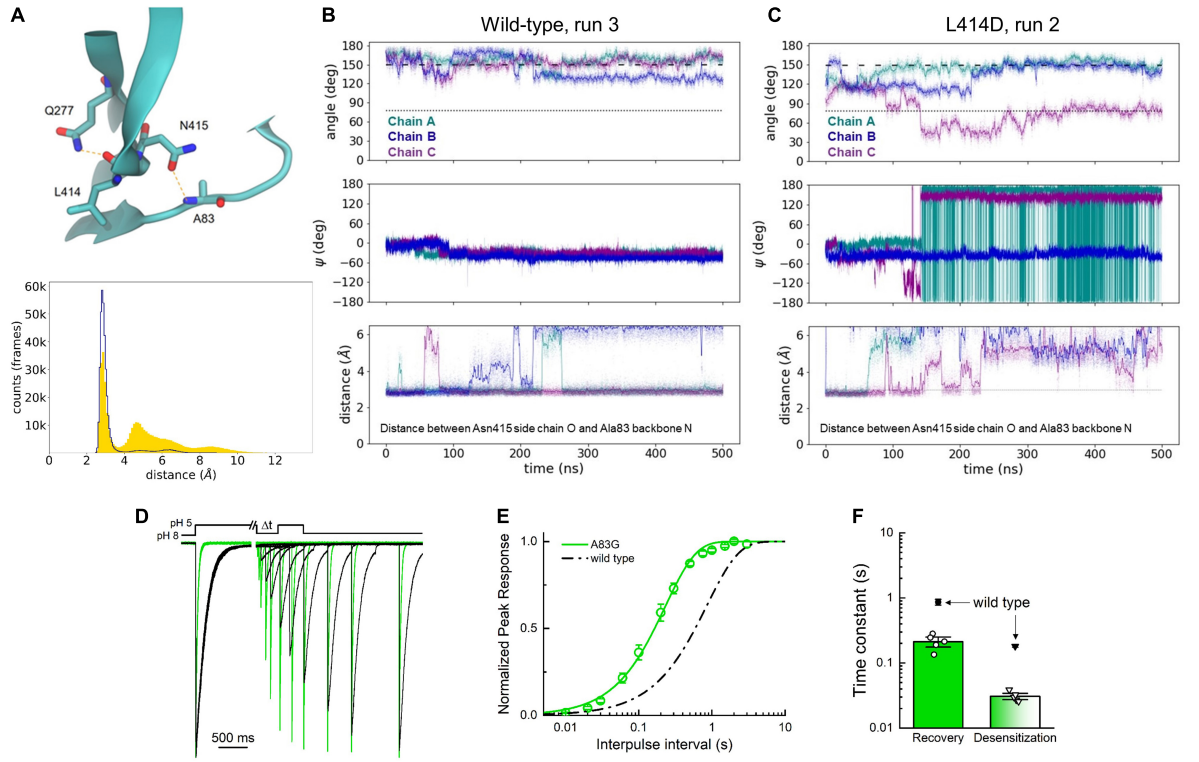

FIGURE 8 | Asn415 and Ala83 interaction may influence desensitized state stability. **(A)** Depiction of Asn415-Ala83 interaction in the desensitized state (upper) and histogram of distances in wild-type (blue trace) and L414D (yellow area) simulations (lower). **(B)** Side chain angle (upper), Asn415 psi angle (middle) and distance between Asn415 side chain oxygen atom and Ala83 backbone nitrogen atom (lower) in a stable wild-type simulation. The dotted line illustrates the side chain angle of L414 in the desensitized state structure while the dashed line illustrates the side chain angle in the resting state structure. **(C)** Same as panel **(A)** but for an L414D simulation. **(D)** Example recovery from desensitization experiments for wild-type (black) and A83G (green). **(E)** Recovery from desensitization curves for wild-type (black) and A83G (green). **(F)** Summary of recovery (circles) and desensitization (triangles) time constants. Open symbols represent individual patches. Filled symbols represent mean data from Rook et al. (2020). Error bars are SEM.

resting state subunit (**Figure 9A**). As seen in the expanded view of the structure (**Figure 9B**), and the alignment itself (**Figure 9C**), the Leu414 and Asn415 residues were completely conserved and the remaining positions in the β11-12 linker were highly conserved. The conservation of these critical positions suggest that the core mechanism of desensitization, or some related function, is physiologically important and has been preserved for hundreds of millions of years. However, the kinetics of ASIC desensitization vary considerably depending on the species and subunit variants under investigation. If the β11-12 linker is nearly completely conserved, what might be the source of species and subunit specific kinetics? Interestingly, the regions surrounding the β11-12 linker are not as well conserved. From the point of view in **Figure 9B**, the β11-12 linker is surrounded by the β1-2 and β4-5 linkers on the "front" and "top" faces, respectively, as well as the β9-α4 linker on the "right" side. Residues from the β9-α4 and α5-β10 linkers of the adjacent subunits surround the Leu414 and Asn415 on the "bottom" and "left" faces, respectively. Likewise, the α4 helix of the thumb domain of the adjacent subunit is near the β11-12 linker (**Figure 9B**). To further highlight the potential influence of these less conserved regions, we determined which side chains are within 5 Å of Leu414 and Asn415 in either resting or desensitized states (PDB:6VTL and 6VTK) and show these side chains in **Figure 9B**. These positions are also highlighted in the alignment in **Figure 9C**. Several of these highlighted positions have previously been shown to alter ASIC kinetics (Coric et al., 2003; Cushman et al., 2007; Li et al., 2010b; Roy et al., 2013). Therefore, we suggest that the main source of subunit or species specific kinetics is not the β11-12 linker itself but rather the surrounding amino acid residues which influence the β11-12 linker isomerization. Mutations to the surrounding area may lead to smaller changes in kinetics, more suitable for tuning receptor gating compared to the rather large shifts produced by mutating the β11-12 linker directly.

Our functional work focuses on the kinetics of desensitization and recovery, however, it is possible that the more physiologically important outcome is SSD. Acidic stimuli which are not strong enough to detectably activate the channel can still desensitize it (i.e., pH 7.1) (Grunder and Pusch, 2015). Thus, SSD is observed right near physiological pH values of 7.4, depending on the subunit and species. Moreover, the pH-dependence of SSD is modulated by numerous physiologically relevant signals such as extracellular Ca^{2+}, FMR amide-related

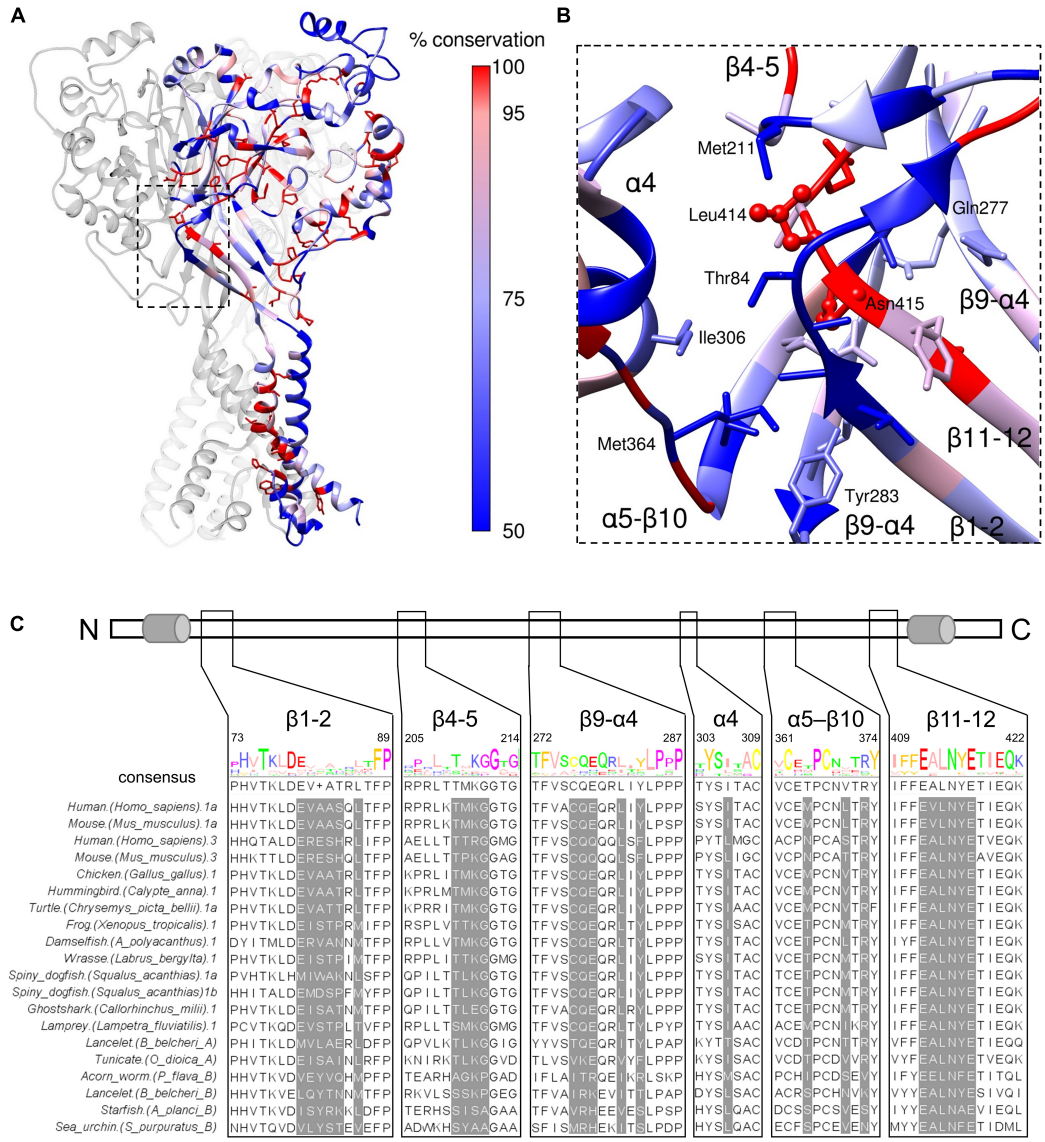

FIGURE 9 | β11-12 linker is highly conserved while the surrounding region is not. **(A)** Resting state structure (PDB: 6VTL) with one subunit colored based on sequence conservation using sequence alignment from ASIC sequences in panel **(C)**. Side chains of completely conserved positions are shown. **(B)** Close up view of the boxed region in panel **(A)** using the same coloring. Any amino acids within 5 Å of Leu414 or Asn415 have side chains depicted. **(C,** upper) Schematic of ASIC1 linear peptide with cylinders indicating transmembrane domains 1 and 2. (**C**, lower) Multi sequence alignment of the indicated ASICs. The amino acid regions shown from the alignment correspond to the segments in panel **(B)**. Positions highlighted in gray are within 5 Å of Leu414 or Asn415 and have side chains depicted in panel **(B)**.

peptides, Cl^- as well as by the heteromeric composition of the channel itself (Babini et al., 2002; Sherwood and Askwith, 2008; Kusama et al., 2013). The SSD process provides a powerful mechanism to control the magnitude of ASIC currents at any one time. A slightly alkaline or acidic extracellular solution will increase or decrease the maximum possible ASIC response. Furthermore, this effect can then be influenced by local Ca^{2+}, FMRF or Cl^- concentrations. Mutations that change desensitization or recovery kinetics will also alter the stability of the desensitized state, which in turn must impact the pH mid-point of the SSD curve (Rook et al., 2021a). This is seen in **Figure 3** where mutations which accelerate recovery (N415D) or both accelerate recovery and slow desensitization (N415K) produce increasingly more acidic pH_{50} values for SSD, consistent with a destabilized desensitized state. Thus, it is possible that the conservation of the β11-12 linker, and alterations of the surrounding areas, arose because of the physiological role of SSD rather than the precise timing of ASIC desensitization and recovery kinetics. It is also possible that the kinetics of channel desensitization and recovery are important, however, mainly in the context of slow changes in extracellular pH as have been recently examined (Alijevic et al., 2020) or

intracellular conformational changes which might be involved in signaling cascades (Wang et al., 2015, 2020; Couch et al., 2021). Understanding these issues will require a clearer accounting of the spatial-temporal dynamics of pH change *in situ* as well as introduction of ASICs with biophysically impactful mutations to appreciate the consequences.

DATA AVAILABILITY STATEMENT

The raw data supporting the conclusions of this article will be made available by the authors, without undue reservation.

AUTHOR CONTRIBUTIONS

MR, AA, MM, and DM designed and performed the experiments and simulations, analyzed the data, and interpreted the results. MM and DM obtained the funding. DM conceived the study and wrote the manuscript with input from all authors. All authors approved the final version of the manuscript.

FUNDING

Funding for this work was provided by NIH R35GM137951 to DM, NSERC Discovery Grant RGPIN 2019-06864 and the Canada Research Chairs Program 950-232154 to MM, and NIH T32GM068411-15 and F31NS120445 to MR. WestGrid and Compute Canada are acknowledged for providing the computing facilities.

ACKNOWLEDGMENTS

We thank Tim Lynagh for providing amino acid sequences for evolutionarily distant organisms. We also thank Lyndee Knowlton for technical assistance.

REFERENCES

Abraham, M. J., Murtola, T., Schulz, R., Pall, S., Smith, J. C., Hess, B., et al. (2015). GROMACS: High performance molecular simulations through multi-level parallelism from laptops to supercomputers. *SoftwareX* 1-2, 19–25.

Alijevic, O., Bignucolo, O., Hichri, E., Peng, Z., Kucera, J. P., and Kellenberger, S. (2020). Slowing of the Time Course of Acidification Decreases the Acid-Sensing Ion Channel 1a Current Amplitude and Modulates Action Potential Firing in Neurons. *Front. Cell. Neurosci.* 14:41. doi: 10.3389/fncel.2020.00041

Babini, E., Paukert, M., Geisler, H. S., and Grunder, S. (2002). Alternative splicing and interaction with di- and polyvalent cations control the dynamic range of acid-sensing ion channel 1 (ASIC1). *J. Biol. Chem.* 277, 41597–41603. doi: 10.1074/jbc.M205877200

Baconguis, I., and Gouaux, E. (2012). Structural plasticity and dynamic selectivity of acid-sensing ion channel-spider toxin complexes. *Nature* 489, 400–405. doi: 10.1038/nature11375

Baconguis, I., Bohlen, C. J., Goehring, A., Julius, D., and Gouaux, E. (2014). X-ray structure of acid-sensing ion channel 1-snake toxin complex reveals open state of a Na(+)-selective channel. *Cell* 156, 717–729. doi: 10.1016/j.cell.2014.01.011

Berendsen, H. J. C., Postma, J. P. M., Vangunsteren, W. F., Dinola, A., and Haak, J. R. (1984). Molecular-Dynamics with Coupling to an External Bath. *J. Chem. Phys.* 81, 3684–3690. doi: 10.1063/1.448118

Boscardin, E., Alijevic, O., Hummler, E., Frateschi, S., and Kellenberger, S. (2016). The function and regulation of acid-sensing ion channels (ASICs) and the epithelial Na(+) channel (ENaC): IUPHAR Review 19. *Br. J. Pharmacol.* 173, 2671–2701. doi: 10.1111/bph.13533

Braun, N., Friis, S., Ihling, C., Sinz, A., Andersen, J., and Pless, S. A. (2021). High-throughput characterization of photocrosslinker-bearing ion channel variants to map residues critical for function and pharmacology. *PLoS Biol.* 19:e3001321. doi: 10.1371/journal.pbio.3001321

Chen, X., and Grunder, S. (2007). Permeating protons contribute to tachyphylaxis of the acid-sensing ion channel (ASIC) 1a. *J. Physiol.* 579, 657–670. doi: 10.1113/jphysiol.2006.120733

Chen, X., Aslam, M., Gollisch, T., Allen, K., and von Engelhardt, J. (2018). CKAMP44 modulates integration of visual inputs in the lateral geniculate nucleus. *Nat. Commun.* 9:261. doi: 10.1038/s41467-017-02415-1

Christie, L. A., Russell, T. A., Xu, J., Wood, L., Shepherd, G. M., and Contractor, A. (2010). AMPA receptor desensitization mutation results in severe developmental phenotypes and early postnatal lethality. *Proc. Natl. Acad. Sci. U S A.* 107, 9412–9417. doi: 10.1073/pnas.0908206107

Coric, T., Zhang, P., Todorovic, N., and Canessa, C. M. (2003). The extracellular domain determines the kinetics of desensitization in acid-sensitive ion channel 1. *J. Biol. Chem.* 278, 45240–45247.

Couch, T., Berger, K., Kneisley, D. L., McCullock, T. W., Kammermeier, P., and Maclean, D. M. (2021). Topography and motion of acid-sensing ion channel intracellular domains. *Elife* 10:e68955. doi: 10.7554/eLife.68955

Cushman, K. A., Marsh-Haffner, J., Adelman, J. P., and McCleskey, E. W. (2007). A conformation change in the extracellular domain that accompanies desensitization of acid-sensing ion channel (ASIC) 3. *J. General Physiol.* 129, 345–350. doi: 10.1085/jgp.200709757

Daniels, B. A., Andrews, Aurousseau, M. R., Accardi, M. V., and Bowie, D. (2013). Crosslinking the ligand-binding domain dimer interface locks kainate receptors out of the main open state. *J. Physiol.* 591, 3873–3885. doi: 10.1113/jphysiol.2013.253666

Darden, T., York, D., and Pedersen, L. (1993). Particle mesh Ewald: An N log(N) method for Ewald sums in large systems. *J. Chem. Phys.* 98, 10089–10082. doi: 10.1063/1.464397

Edgar, R. C. (2004). MUSCLE: multiple sequence alignment with high accuracy and high throughput. *Nucleic Acids Res.* 32, 1792–1797. doi: 10.1093/nar/gkh340

Essmann, U., Perera, L., Berkowitz, M. L., Darden, T., Lee, H., and Pedersen, L. G. (1995). A Smooth Particle Mesh Ewald Method. *J. Chem. Phys.* 103, 8577–8593. doi: 10.1063/1.470117

Gonzales, E. B., Kawate, T., and Gouaux, E. (2009). Pore architecture and ion sites in acid-sensing ion channels and P2X receptors. *Nature* 460:599. doi: 10.1038/nature08218

Gowers, R. J., Linke, M., Barnoud, J., Reddy, T. J. E., Melo, M. N., Seyler, S. L., et al. (2016). MDAnalysis: A Python Package for the Rapid Analysis of Molecular Dynamics Simulations. *Proc. 15th Python Sci. Confer.* 2016, 98–105. doi: 10.1186/s12868-016-0283-6

Grunder, S., and Pusch, M. (2015). Biophysical properties of acid-sensing ion channels (ASICs). *Neuropharmacology* 94, 9–18. doi: 10.1016/j.neuropharm.2014.12.016

Hess, B. (2008). P-LINCS: A parallel linear constraint solver for molecular simulation. *J. Chem. Theory Comput.* 4, 116–122. doi: 10.1021/ct700200b

Hoover, W. G. (1985). Canonical Dynamics - Equilibrium Phase-Space Distributions. *Phys. Rev. A* 31, 1695–1697. doi: 10.1103/physreva.31.1695

Huang, J., and MacKerell, A. D. Jr. (2013). CHARMM36 all-atom additive protein force field: validation based on comparison to NMR data. *J. Comput. Chem.* 34, 2135–2145. doi: 10.1002/jcc.23354

Humphrey, W., Dalke, A., and Schulten, K. (1996). VMD: Visual molecular dynamics. *J. Mol. Graph Model.* 14, 33–38. doi: 10.1016/0263-7855(96)00018-5

Jasti, J., Furukawa, H., Gonzales, E. B., and Gouaux, E. (2007). Structure of acid-sensing ion channel 1 at 1.9 A resolution and low pH. *Nature* 449, 316–323. doi: 10.1038/nature06163

Jo, S., Kim, T., Iyer, V. G., and Im, W. (2008). CHARMM-GUI: a web-based graphical user interface for CHARMM. *J. Comput. Chem.* 29, 1859–1865. doi: 10.1002/jcc.20945

Jones, M. V., and Westbrook, G. L. (1996). The impact of receptor desensitization on fast synaptic transmission. *Trends Neurosci.* 19, 96–101. doi: 10.1016/s0166-2236(96)80037-3

Katz, B., and Thesleff, S. (1957). A study of the desensitization produced by acetylcholine at the motor end-plate. *J. Physiol.* 138, 63–80. doi: 10.1113/jphysiol.1957.sp005838

Krauson, A. J., and Carattino, M. D. (2016). The Thumb Domain Mediates Acid-sensing Ion Channel Desensitization. *J. Biol. Chem.* 291, 11407–11419. doi: 10.1074/jbc.m115.702316

Krauson, A. J., Rued, A. C., and Carattino, M. D. (2013). Independent contribution of extracellular proton binding sites to ASIC1a activation. *J. Biol. Chem.* 288, 34375–34383. doi: 10.1074/jbc.M113.504324

Kusama, N., Gautam, M., Harding, A. M., Snyder, P. M., and Benson, C. J. (2013). Acid-sensing ion channels (ASICs) are differentially modulated by anions dependent on their subunit composition. *Am. J. Physiol. Cell physiol.* 304, C89–C101. doi: 10.1152/ajpcell.00216.2012

Kusama, N., Harding, A. M., and Benson, C. J. (2010). Extracellular chloride modulates the desensitization kinetics of acid-sensing ion channel 1a (ASIC1a). *J. Biol. Chem.* 285, 17425–17431. doi: 10.1074/jbc.M109.091561

Li, T., Yang, Y., and Canessa, C. M. (2010a). Asn415 in the beta11-beta12 linker decreases proton-dependent desensitization of ASIC1. *J. Biol. Chem.* 285, 31285–31291. doi: 10.1074/jbc.M110.160382

Li, T., Yang, Y., and Canessa, C. M. (2010b). Leu85 in the beta1-beta2 linker of ASIC1 slows activation and decreases the apparent proton affinity by stabilizing a closed conformation. *J. Biol. Chem.* 285, 22706–22712. doi: 10.1074/jbc.M110.134114

Lomize, M. A., Pogozheva, I. D., Joo, H., Mosberg, H. I., and Lomize, A. L. (2012). OPM database and PPM web server: resources for positioning of proteins in membranes. *Nucleic Acids Res.* 40, D370–D376. doi: 10.1093/nar/gkr703

Lynagh, T., Mikhaleva, Y., Colding, J. M., Glover, J. C., and Pless, S. A. (2018). Acid-sensing ion channels emerged over 600 Mya and are conserved throughout the deuterostomes. *Proc. Natl. Acad. Sci. U S A.* 115, 8430–8435. doi: 10.1073/pnas.1806614115

MacLean, D. M. (2015). "Constructing a Rapid Solution Exchange System," in *Ionotropic Glutamate Receptor Technologies*, ed. G. K. Popescu (Berlin: Springer), 165–183. doi: 10.1007/978-1-4939-2812-5_12

Meng, E. C., Pettersen, E. F., Couch, G. S., Huang, C. C., and Ferrin, T. E. (2006). Tools for integrated sequence-structure analysis with UCSF Chimera. *BMC Bioinformatics* 7:339. doi: 10.1186/1471-2105-7-339

Michaud-Agrawal, N., Denning, E. J., Woolf, T. B., and Beckstein, O. (2011). MDAnalysis: a toolkit for the analysis of molecular dynamics simulations. *J. Comput. Chem.* 32, 2319–2327. doi: 10.1002/jcc.21787

Nose, S. (1984). A Molecular-Dynamics Method for Simulations in the Canonical Ensemble. *Mol. Phys.* 52, 255–268. doi: 10.1080/00268978400101201

Noviello, C. M., Gharpure, A., Mukhtasimova, N., Cabuco, R., Baxter, L., Borek, D., et al. (2021). Structure and gating mechanism of the alpha7 nicotinic acetylcholine receptor. *Cell* 184, 2121–2134e2113.

Parrinello, M., and Rahman, A. (1981). Polymorphic Transitions in Single-Crystals - a New Molecular-Dynamics Method. *J. Appl. Phys.* 52, 7182–7190. doi: 10.1063/1.328693

Pettersen, E. F., Goddard, T. D., Huang, C. C., Couch, G. S., Greenblatt, D. M., Meng, E. C., et al. (2004). UCSF Chimera–a visualization system for exploratory research and analysis. *J. Comput. Chem.* 25, 1605–1612. doi: 10.1002/jcc.20084

Plested, A. J. (2016). Structural mechanisms of activation and desensitization in neurotransmitter-gated ion channels. *Nat. Struct. Mol. Biol.* 23, 494–502. doi: 10.1038/nsmb.3214

Rook, M. L., Musgaard, M., and MacLean, D. M. (2021b). Coupling structure with function in acid-sensing ion channels: challenges in pursuit of proton sensors. *J. Physiol.* 599, 417–430. doi: 10.1113/JP278707

Rook, M. L., Miaro, M., Couch, T., Kneisley, D. L., Musgaard, M., and MacLean, D. M. (2021a). Mutation of a conserved glutamine residue does not abolish desensitization of acid-sensing ion channel 1. *J. General Physiol.* 153:e202012855.

Rook, M. L., Williamson, A., Lueck, J. D., Musgaard, M., and Maclean, D. M. (2020). beta11-12 linker isomerization governs Acid-sensing ion channel desensitization and recovery. *Elife* 9:e51111. doi: 10.7554/eLife.51111

Roy, S., Boiteux, C., Alijevic, O., Liang, C., Berneche, S., and Kellenberger, S. (2013). Molecular determinants of desensitization in an ENaC/degenerin channel. *FASEB J.* 27, 5034–5045. doi: 10.1096/fj.13-230680

Sali, A., and Blundell, T. L. (1993). Comparative protein modelling by satisfaction of spatial restraints. *J. Mol. Biol.* 234, 779–815. doi: 10.1006/jmbi.1993.1626

Sherwood, T. W., and Askwith, C. C. (2008). Endogenous arginine-phenylalanine-amide-related peptides alter steady-state desensitization of ASIC1a. *J. Biol. Chem.* 283, 1818–1830. doi: 10.1074/jbc.M705118200

Springauf, A., and Grunder, S. (2010). An acid-sensing ion channel from shark (Squalus acanthias) mediates transient and sustained responses to protons. *J. Physiol.* 588, 809–820. doi: 10.1113/jphysiol.2009.182931

Wang, J. J., Liu, F., Yang, F., Wang, Y. Z., Qi, X., Li, Y., et al. (2020). Disruption of auto-inhibition underlies conformational signaling of ASIC1a to induce neuronal necroptosis. *Nat. Commun.* 11:475. doi: 10.1038/s41467-019-13873-0

Wang, Y.-Z., Wang, J.-J., Huang, Y., Liu, F., Zeng, W.-Z., Li, Y., et al. (2015). Tissue acidosis induces neuronal necroptosis via ASIC1a channel independent of its ionic conduction. *eLife* 4:e05682.

Waterhouse, A. M., Procter, J. B., Martin, D. M., Clamp, M., and Barton, G. J. (2009). Jalview Version 2–a multiple sequence alignment editor and analysis workbench. *Bioinformatics* 25, 1189–1191. doi: 10.1093/bioinformatics/btp033

Wu, Y., Chen, Z., and Canessa, C. M. (2019). A valve-like mechanism controls desensitization of functional mammalian isoforms of acid-sensing ion channels. *eLife* 8:e45851. doi: 10.7554/eLife.45851

Yoder, N., and Gouaux, E. (2020). The His-Gly motif of acid-sensing ion channels resides in a reentrant 'loop' implicated in gating and ion selectivity. *Elife* 9:e56527. doi: 10.7554/eLife.56527

Yoder, N., Yoshioka, C., and Gouaux, E. (2018). Gating mechanisms of acid-sensing ion channels. *Nature* 555:397. doi: 10.1038/nature25782

Yu, J., Zhu, H., Lape, R., Greiner, T., Du, J., Lu, W., et al. (2021). Mechanism of gating and partial agonist action in the glycine receptor. *Cell* 184, 957–968e921.

Conflict of Interest: The authors declare that the research was conducted in the absence of any commercial or financial relationships that could be construed as a potential conflict of interest.

Publisher's Note: All claims expressed in this article are solely those of the authors and do not necessarily represent those of their affiliated organizations, or those of the publisher, the editors and the reviewers. Any product that may be evaluated in this article, or claim that may be made by its manufacturer, is not guaranteed or endorsed by the publisher.

Advantages of publishing in Frontiers

OPEN ACCESS
Articles are free to read for greatest visibility and readership

FAST PUBLICATION
Around 90 days from submission to decision

HIGH QUALITY PEER-REVIEW
Rigorous, collaborative, and constructive peer-review

TRANSPARENT PEER-REVIEW
Editors and reviewers acknowledged by name on published articles

Frontiers
Avenue du Tribunal-Fédéral 34
1005 Lausanne | Switzerland

Visit us: www.frontiersin.org
Contact us: frontiersin.org/about/contact

REPRODUCIBILITY OF RESEARCH
Support open data and methods to enhance research reproducibility

DIGITAL PUBLISHING
Articles designed for optimal readership across devices

FOLLOW US
@frontiersin

IMPACT METRICS
Advanced article metrics track visibility across digital media

EXTENSIVE PROMOTION
Marketing and promotion of impactful research

LOOP RESEARCH NETWORK
Our network increases your article's readership